10
I29A
No. 151

Copy

CIVIL ENGINEERING STUDIES

STRUCTURAL RESEARCH SERIES NO. 151

STUDIES OF THE STRAIN DISTRIBUTION IN WIDE PLATES DURING BRITTLE FRACTURE PROPAGATION

By
S. T. ROLFE
T. M. LYNAM
and
W. J. HALL

UNIVERSITY OF ILLINOIS

URBANA, ILLINOIS

STUDIES OF THE STRAIN DISTRIBUTION IN WIDE PLATES

DURING BRITTLE FRACTURE PROPAGATION

by

S. T. Rolfe

T. M. Lynam

and

W. J. Hall

A Technical Report

for the

SHIP STRUCTURE COMMITTEE

under the

BUREAU OF SHIPS, U. S. NAVY

Contract NObs 65790, Index No. NS-731-034

Subproject SR-137

Department of Civil Engineering

University of Illinois

Urbana, Illinois

April 1958

ABSTRACT

This report summarizes the results of a series of tests made as a part of the study of the propagation of brittle fractures in six-ft wide steel plates. All plates were tested under similar conditions of stress, temperature, and impact, which made it possible to superimpose the test data and obtain contours of strain on the surface of the plate for a propagating fracture. Contours of both the maximum principal strain and strain for vertically oriented gages for various lengths of crack are presented in this report. A study of all the applicable data from earlier tests made as a part of this program indicates that the strain contour data presented herein are representative of all the tests which have been conducted.

The strain contours reveal much about the nature of the strain field associated with a propagating brittle fracture. The studies indicate that for this particular specimen geometry and associated test conditions, the strain field associated with the tip of the advancing fracture remains essentially unchanged after traversing about one-third of the plate width.

TABLE OF CONTENTS

LIST OF TABLES

LIST OF FIGURES

LIST OF FIGURES (Continued)

LIST OF FIGURES (Continued)

I. INTRODUCTION

1. General

Brittle fractures in riveted and welded steel structures have been reported in the engineering literature for many years. These fractures generally are characterized by a lack of the ductility usually associated with failures of structural steel, and by a sudden occurrence with little or no previous warning.

The significance of the brittle fracture problem was not fully appreciated until World War II, when a large number of welded merchant vessels failed in this manner. Fortunately, through the use of improved geometrical layout, crack arrestors, and improved materials and fabrication procedures, it was possible to reduce greatly the number of major ship failures. In many cases provisions have been made to incorporate similar improvements or changes in the design of structures other than ships in order to minimize the possibility of the occurrence of brittle fractures. Nevertheless, in spite of these improvements in design which have resulted from the large amount of research completed during and since World War II, brittle fractures still occur, and further studies are required if a better understanding of the brittle fracture problem is to be obtained.

2. Object and Scope

The brittle fracture phenomenon is extremely complicated in that it involves a consideration of materials and their behavior in various environments. This particular program is concerned with a study of the propagation of brittle fractures in wide steel plates. The experimental approach followed in this investigation has consisted of measuring surface strains and crack speed as the fracture traverses a wide steel plate to obtain fundamental data that will be of assistance in arriving at a better understanding of the brittle fracture problem.

Until approximately one year ago it had been possible to obtain only a limited amount of data from any one test because a maximum of only nine channels of cathode ray oscilloscope recording equipment had been available. Nevertheless, the earlier work with both two-ft wide and six-ft wide plates produced much valuable information concerning expected fracture speed and the strain distribution at various points on the plate surface as recorded by single strain gages. The results of the work through the end of 1956 have been reported in a paper (1)[*], and in more detail in two technical reports (2, 3).

In 1957 an additional twenty-five channels of cathode ray oscilloscope recording equipment were made available to the program by the Naval Research Laboratory. Thus far, six major fracture tests of six-ft wide semi-killed steel plates have been completed in which 34 channels of cathode ray oscilloscope recording instrumentation have been utilized; in each test, 33 channels were used for eleven rectangular strain rosettes and one channel was used for speed detectors. The plates were tested at an average net applied stress of 19,000 psi, and at a temperature of about -10 deg. F. The fractures were initiated from one edge of the plate with the notch-wedge-impact method of fracture initiation. In conjunction with the crack arrestor program (Project SR-134), one additional set of records has been obtained for a plate tested at a higher stress level (28,000 psi) and at a lower temperature (-15 deg. F.).

The primary purpose of the latest tests and studies was to obtain sufficient data to establish representative strain contours on the plate surface during the time a brittle fracture is propagating. The results presented in this report are based on the tests reported herein for the first time, as well as all of the previous applicable data obtained as part of this program (2, 3, 4, 5).

---

[*] Numbers in parentheses refer to references listed in the Bibliography.

This is a research report consisting of a summary and preliminary analysis of the test data. More complete studies of these data, as well as subsequently obtained data, will be made as a part of this program.

Among the more important items presented in this report are the following:

(1) Strain gage traces from the component gages of the strain rosettes.

(2) The principal strain curves computed from the component gage strain traces.

(3) A discussion of the factors affecting the computed principal strain magnitudes and strain rates.

(4) Representative vertical and maximum principal strain contours for various crack lengths during the time the fracture is propagating.

(5) Typical sets of maximum principal strain contours, and vertical strain contours, associated with a crack in the central portion of the plate.

The strain contours should be of considerable value in correlating the test results and associated significant parameters with other experimental and analytical results, and with the analytical studies being conducted as a part of this program.

3. <u>Acknowledgment</u>

This investigation is a part of the Structural Research Program of the Department of Civil Engineering under the general direction of N. M. Newmark, Head, Department of Civil Engineering, and under the general supervision of W. H. Munse, Professor of Civil Engineering. The work was conducted by S. T. Rolfe and T. M. Lynam, Research Assistants in Civil Engineering, working under the immediate supervision of W. J. Hall, Associate Professor of Civil Engineering. The program is sponsored by the Ship Structure Committee through the Bureau of

4

Ships, U. S. Navy, Contract NObs 65790, Index No. NS-731-034 (Subproject SR-137).
The members of the Brittle Fracture Mechanics Advisory Committee to the Committee
on Ship Structural Design have acted in an advisory capacity in the planning of
this program.

V. J. McDonald, Associate Professor of Civil Engineering, supervised
the instrumentation and reduction of the test data from the photographic records.
M. P. Gaus, Research Associate in Civil Engineering, prepared the computer code
for the strain rosette computations, and F. W. Barton, Research Assistant in
Civil Engineering, helped with the tests and preparation of the figures for the
report.

4. Nomenclature

The following terms are used repeatedly throughout the text:

Dynamic strain gage -- SR-4 Type A7 (1/4 in. gage length) strain gage whose
    signal is monitored with respect to time on an oscilloscope during
    the fracture test.

Static strain gage -- SR-4 Type A7 (1/4 in. gage length) strain gage used to
    monitor the static strain level.

Component strain gage -- One of the three individual strain gages of the rectan-
    gular strain rosette.

Crack detector -- A single wire SR-4 Type A9 (6 in. gage length) strain gage
    located on the plate surface perpendicular to the expected fracture
    path. A rough measure of the fracture speed may be obtained from a
    knowledge of the distance between the detectors and the time interval
    corresponding to the breaking of adjacent detectors.

Initiation edge -- The edge of the specimen at which the brittle fracture is
    initiated.

Notch line -- An imaginary horizontal line connecting the fracture initiation

notches on opposite edges of the plate specimen.

Test load strain -- At any gage point, the strain corresponding to the applied

test load.

II. DESCRIPTION OF SPECIMENS AND INSTRUMENTATION

5. <u>Specimens and Material Properties</u>

The plate material for the six major fracture tests reported herein (Tests 33, 34 and 36 through 39) was a semi-killed steel, USS Heat Number 64M487, and was tested in the as-rolled condition. The specimens were 3/4 in. thick, 72 in. wide, and 20 in. long; the net width at the notch line was approximately 2-1/4 in. less than the gross width because of the notches on each edge. The specimen was welded with double-V butt welds made with E7016 electrodes on both ends to 1-in. thick pull-plates mounted in the testing machine; in welding the specimen to the pull-plates, care was taken to keep the warping and residual stresses to a minimum. A line diagram of the specimen and pull-plates, and two views of a typical test setup in the 3,000,000-lb hydraulic testing machine are shown in Fig. 1.

The composite plate specimen for the arrestor test (Test 35) was fabricated from, in order, a 36-in. fracture starter strake of rimmed steel (the plate on which the strain rosette gages were mounted), a 4-in. strake of T-1 steel, a 20-in. strake of rimmed steel, and a 12-in. strake of T-1 steel. Over all, the specimen was 3/4 in. thick, 72 in. wide, and 27 in. long.

Mechanical property tests were made on material taken from the central portion of the plate after the plate had been fractured. The check analyses and the tensile test data for each of the rimmed and semi-killed steel plates are presented in Tables 2 and 3. Charpy V-notch data are presented in Figs. 2, 3, and 4. The plate material used in these tests was from the same stock that was used in the earlier tests made as a part of this program and its properties, typical of A-7 structural steels, are in agreement with those reported earlier (1, 2).

6. Instrumentation

Baldwin SR-4 Type A-7 strain gages (1/4-in. gage length) were used to measure dynamic and static strains. The gages for dynamic measurements were connected in the customary manner in a Wheatstone bridge circuit. Three similar electrical strain gages, which were isolated from the specimen, were used as resistances to complete the bridge circuit. These bridges were excited by direct current and their outputs fed to the recording oscilloscope channels. A diagram of typical circuits is shown in Fig. 5.

The crack speed was measured with a system of six surface crack detectors which broke as the fracture traversed the plate; at each detector location in Tests 36 through 39 two 6-in. detectors (Baldwin SR-4 Type A-9 strain gages) were wired in series to give a 12-in. detector. The failure of a crack detector opened an electrical circuit and caused a stepped change in voltage. A diagram of a typical crack detector circuit is shown in Fig. 5. From a knowledge of the spacing between detectors and the elapsed time between successive interruptions of the circuit, the speed of the fracture could be computed. This system gives an average surface speed of the fracture since the crack front location is not known precisely at the time the detector breaks. Thus, all calculated speeds were rounded off to the nearest 50 fps. Crack detector calibration was obtained by successively opening switches arranged in series with the various detectors and recording the trace steps. The switch locations are indicated in the circuit shown in Fig. 5.

A triggering device, referred to as an external trigger because of its location, was utilized in these tests to activate the sweep and spot intensifying circuits in the recording equipment. This trigger consisted of a strip of aluminum foil which was broken as the piston device drove the wedge into the notch; thus, the circuits in the recording devices were energized just before the

fracture was initiated. To insure that the circuits would be energized in the event of failure of the external trigger, a plate surface trigger (A-9 strain gage) was connected in series with the external trigger. The trigger circuit is shown in Fig. 6.

The temperature of the specimen was continuously recorded during cooling by means of a Leeds and Northrup Type G "Speedomax" recorder and copper-constantan thermocouples located in 1/4-in. deep holes at various points across the specimen.

Twenty-five channels of the cathode-ray oscilloscope equipment were five-channel units manufactured by Franklin Electronics, and were made available to the program by the Naval Research Laboratory. The nine remaining channels consisted of two DuMont Type 333 and two DuMont Type 322 dual-beam cathode-ray oscilloscopes, and a Tektronix Type 512 single beam unit. The recording equipment, along with the calibrating oscillator that supplied the time signals, is shown in Fig. 7; the cameras for the DuMont equipment are not shown.

Six of the DuMont oscilloscope channels are sufficiently sensitive to allow at least 1-1/2 in. of trace deflection for 0.001 in./in. of strain. However, the deflection scale used to record the test data on these DuMont scopes was limited by the size of the scope face and the maximum value of expected strain. The other 28 channels had about one-third the aforementioned sensitivity, allowing about 1/2 in. of trace deflection for the same strain. Because of the smaller sensitivity of the Franklin units, the maximum possible trace deflection was used. In planning the recording of the test data, the equipment was arranged so that the strain gages that were expected to produce signals of lowest electrical magnitude were connected to the six oscilloscopes having the highest sensitivity. The frequency response of all oscilloscopes was flat up to at least 50 KC and adequate to record all strain signals from the strain gages. Portions of two typical strain records are presented in Fig. 8. The oscilloscope channels used

to measure and record strain were calibrated by shunting gages with a resistance whose equivalent strain value was known.

The time base for the records obtained from the DuMont and Franklin oscilloscopes was supplied by continuously moving 35 mm film. Timing marks on the traces from the Franklin units were energized by the oscillator and recorded as part of the strain traces; the DuMont units employed intensity modulation of the electron spot to define the time base. On all of the strain traces a simultaneous "blip" was produced by a synchronizing signal supplied from the Tektronix oscilloscope circuit, immediately before and after the test. This signal made it possible to synchronize accurately with each other all the strain traces from a particular test. The synchronizing "blip" is visible on the records shown in Fig. 8.

The crack detector trace on the Tektronix oscilloscope was recorded on a single frame of 35 mm film. The time axis was calibrated by putting a time signal of known frequency on the channel and photographing one sweep. This was done immediately after the test was completed.

A more complete description of the instrumentation may be found in reports and papers previously issued as a part of this program (1, 2, 3).

7. Data Reduction

Reduction of the strain data recorded on 35 mm strip film was facilitated with a decimal converter and the University of Illinois high speed digital computer, the ILLIAC.

A brief summary of the data reduction procedure is presented below. The 35 mm film strips were enlarged and the calibration and timing marks scaled on the enlargements. With the aid of the decimal converter, values of component gage strain versus time were simultaneously punched on IBM cards, plotted on an X-Y plotter, and typed in tabular form. The strain-time values were then

transferred from IBM cards to punched paper tape, and processed through the ILLIAC, to compute values of the principal strains. The ILLIAC results consisted of tabulated principal strain data, as well as scaled oscilloscope displays of component gage and principal strain traces which were photographed for later enlargement and processing. Drawings of the traces are presented as Figs. 25 through 89.

8. Apparatus and Test Procedure

In most respects the appartus and test procedure used for these tests was similar to that used in earlier tests made as a part of this program.

The notch-wedge-impact method of fracture initiation was used in these tests. A closeup view of the 1-1/8 in. deep notch and the wedge is shown in Fig. 9. A view of the gas operated piston device that provides the external impact is shown in Fig. 10. The theoretical output energy of the piston device was 1200 ft lb, but calibration tests indicate that the device actually delivered about 1000 ft lb.

Crushed dry ice was used to cool the plate specimen. Photographs of the dry ice containers, as well as a diagram showing the thermocouple locations for the specimens, are presented in Fig. 11. Typical cooling curves for Tests 33 through 39 are presented in Figs. 12 and 13.

After the instrumentation was mounted on the plate, and the plate spec-imen had been welded to the pull-heads, the specimen was stressed at room temper-ature to the test load to check the behavior of the strain gages; at the same time it was possible to ascertain the static strain distribution in the specimen and to obtain the test load strain values for each dynamic gage. Any gages that displayed faulty or questionable response were immediately replaced and the newly installed gages were checked by another test load cycle.

In Tests 36 through 39 wiring between gages and oscilloscopes was double checked by shunting each gage with a resistor and noting the direction of trace movement on the face of its respective oscilloscope. This gave a positive identification of the scope trace corresponding to each gage and the direction of the compression calibration for each gage.

At the time of test the cooling tanks were filled with crushed dry ice, and when the test temperature was approached, the plate was stressed to the test load. After loading, the recording equipment was calibrated, and the gas operated piston device pressurized. When the desired specimen temperature was obtained, the recording cameras were started, and the gas operated piston device was fired manually, driving the wedge into the edge notch to initiate the brittle fracture.

III. ANALYSIS OF TEST RESULTS

9. General

The results presented herein are based on all of the applicable data obtained as a part of this program. The extensive strain data obtained in Tests 33 through 39 are presented in this report for the first time. The use of strain rosettes in the latter tests permits the plotting of contours of maximum principal strain, as well as contours of vertical strain, on the surface of the plate as the fracture propagates across the plate. The data obtained in earlier tests (2, 3) support the results presented herein for the more recent tests; some of these earlier data are included in this report also.

The order of presentation of the results is as follows. The original strain-time traces from the component gages for Tests 33 through 39 are presented in Section 10. The principal strains computed from the component gage strain traces are presented and discussed in Section 11. Contours of maximum principal strain and contours of vertical strain, for various crack lengths, are presented and analyzed in Section 12. The principal strain contours were obtained by superimposing the data from Tests 33 through 39. The vertical strain contours were obtained in the same manner and are shown to be essentially the same as vertical strain contours based on data from earlier tests. Observations relating to the crack path and texture of the fractures are presented in Section 13.

10. Recorded Test Data

The primary objective of this particular series of tests was to obtain sufficient data to establish representative strain contours on the plate surface for various crack lengths during the time a brittle fracture is propagating across the plate. Since only thirty-four channels of strain recording equipment

were available (33 channels for eleven rectangular strain rosettes and one channel for crack speed detectors) and the exact location of the fracture path was unknown prior to each test, it was decided to concentrate the strain rosettes in three general areas with respect to width on three of the plate specimens, and thereafter superimpose the data to obtain the picture of the strain distribution associated with a propagating crack.

The instrumentation layouts and crack paths for Tests 33 through 39 are shown as Figs. 14 through 20. It should be noted that in general the rosettes were located on the opposite side of the plate shown in these drawings. The strain rosettes are located on only the first two-thirds of the plate since it was felt rosettes located in this region would yield the desired strain information. The strain rosettes were located at 7-in. intervals across the plate in order to obtain strain values at intervals of one-tenth the net plate width. Since a double fracture occurred in Test 36, a duplicate test (Test 39) was conducted.

The strain-time curves of the component gages from Tests 33 through 39 are presented in Figs. 25 through 89. All strain traces are plotted such that the strain at zero time is the initial test load strain.

The vertical and diagonal gage traces exhibit a general shape characterized by a fairly steady and rapid increase in strain to a maximum (peak) strain value as the fracture propagates past the gage; the peak strain is followed by a decrease to a strain level associated with the removal of external load. For gages located close to the fracture, the peak is very sharp; for gages located away from the fracture, the peak is of a lower magnitude and the pulse extends over a longer time.

The horizontal gage traces are characterized by three major changes in strain. The strain trace first exhibits an initial relaxation of compressive

strain, and this is followed by a compression pulse corresponding to the tension peak of the vertical gage. Finally, the trace exhibits another relaxation of compressive strain before leveling off at the final strain value.

Typical strain traces for component gages located at various distances from the fracture may be seen in Fig. 21; the three rosettes are from one plate and are mounted directly above one another at distances of 1.1 in., 4.1 in., and 7.1 in. from the fracture. The strain traces shown are representative of the strain-time curves obtained from all tests conducted as a part of this program. The decrease in maximum strain magnitude and the change in pulse shape as the distance between the gage and fracture changes may be clearly noted.

The second peak occurring in the component gage traces (and principal strain traces) in Figs. 47, 49, 51, and 54 was attributed to electrical effects associated with the recording equipment, (although there is still some question regarding this matter) and not the double fracture of the plate specimen in Test 36.

Static strain gages were located every seven inches along the notch line on both faces of the plate and three sets of back to back gages were placed 18 in. above the notch line. Strain readings showed that in each test there was a fairly uniform static strain distribution across the plate during application of the test load; in addition, bending strains were noted to be less than 0.0002 in./in. in all tests. To simplify the instrumentation drawings presented as Figs. 14 through 20, the positions of the static strain gages are not presented.

The crack speed detectors were used to measure the approximate surface fracture speed and to aid in determining the location of the surface fracture at any time during the brittle fracture test. The average surface speeds of propagation of the brittle fracture for Tests 33 through 39 are presented in Table 4.

It will be noted that these speeds ranged from 1850 to 4750 fps. These speeds are in the same range as those reported for earlier tests (2, 3).

11. Computed Principal Strains

Rectangular strain rosettes consisting of three SR-4 Type A-7 strain gages were used to determine the principal strains at various locations on the surface of each specimen. Since the component gages were of a finite size, it was obviously not possible to measure the strain in three directions precisely at a point; however, since the three component strain gages of the rosettes had a 1/4-in. gage length, it was possible to mount the three gage elements within a 0.7-in. diameter circle and this was considered to be satisfactory under the circumstances.

In the tests reported herein, two rosette layouts of the component gages were used. Photographs and drawings of both gage layouts are presented in Fig. 22. In layout A (used in Tests 33, 34, and 35) the diagonal gage was centered directly above the horizontal gage, and the vertical gage was mounted on the side near the initiation edge. In layout B (used in Tests 36 through 39) the vertical gage was centered directly above the horizontal gage, and the diagonal gage was mounted on the side away from the initiation edge.

In the case of strain records obtained with gage layout A, the vertical gage peaked ahead of, or at the same time as, the horizontal and diagonal gages for about 80 per cent of the rosettes. A detailed study of the component gage traces and the principal strain computations indicated that changes in the vertical and horizontal strain values had the greatest effect on the principal strain magnitudes; thus in Tests 36 through 39 it was decided to center the vertical and horizontal gages above one another, in the manner shown in layout B (Fig. 22). For records obtained with gage layout B, the vertical and horizontal gages peaked ahead of, or at the same time as, the diagonal gages for about 85

per cent of the rosettes. Typical component gage traces from both layouts are
shown in Fig. 23; the offset in peaking times may be noted clearly.

Initially, it was believed that a refinement in the results would be
obtained by shifting the recorded component gage traces to make the maximum
strain values occur at the same time. However, later studies showed that there
was only a small change in the principal strains as a result of shifting the
component gage traces. This is illustrated in Fig. 24, in which the principal
strains are computed for a typical rosette, in one case with the strain traces
as recorded and in the other case with the traces shifted to make the peaks
occur at the same time. It will be noted that shifting the trace does not
change the shape or magnitude of the maximum principal strain trace markedly.
For most rosettes it would be necessary to shift the trace less than 0.1 milli-
seconds to make the maximum strain values occur at the same time. This time
difference is of the same order of magnitude as the inherent time error asso-
ciated with matching of the trace times during a reduction of the original 35 mm
strip film record. It should be noted that many other factors also tend to
affect the strain traces, such as the discontinuous nature of the fracture, the
deviation of the crack path from the notch line, inherent variations in
instrumentation. etc. All of the foregoing factors and studies tend to justify
the decision not to shift the traces; therefore, all of the principal strains
have been computed from the "as recorded" component gage traces.

To obtain the computed principal strains from the rectangular strain
rosette equations it was necessary to first determine strain values from the
three component gage traces at selected times; the times were selected arbitrarily
at points corresponding to changes in strain in the component gage traces. The
data reduction procedure followed thereafter has been described in Section 7.

The rectangular strain rosette equations used in computing the principal strains and the direction of the maximum principal strain were as follows.

$$\epsilon_{max} = \frac{1}{2}\left[\epsilon_v + \epsilon_h + \sqrt{2(\epsilon_h - \epsilon_d)^2 + 2(\epsilon_d - \epsilon_v)^2}\right]$$

$$\epsilon_{min} = \frac{1}{2}\left[\epsilon_v + \epsilon_h - \sqrt{2(\epsilon_h - \epsilon_d)^2 + 2(\epsilon_d - \epsilon_v)^2}\right]$$

$$\theta = \frac{1}{2}\tan^{-1}\frac{2\epsilon_d - \epsilon_h - \epsilon_v}{\epsilon_h - \epsilon_v}$$

where: ϵ_{max} = maximum principal strain

ϵ_{min} = minimum principal strain

θ = angle between ϵ_{max} and the positive X-axis

ϵ_v = vertical (Y) component gage strain

ϵ_d = diagonal component gage strain

ϵ_h = horizontal (X) component gage strain

The resulting curves of the principal strains (ϵ_{max} and ϵ_{min}) and the direction of ϵ_{max} with respect to the positive X-axis (θ) for Tests 33 through 39 are presented in Figs. 25 through 89.

In general the maximum principal strain trace for each rosette is of essentially the same shape as the vertical component gage trace. Also for any rosette, the magnitudes of the peak strain for the vertical gage trace and for the principal strain trace are nearly equal. This is shown in Fig. 90 in which a comparison is made of the maximum principal and vertical peak strain magnitudes; it will be noted that there is nearly a one to one correspondence in strain values, irrespective of the distance from the fracture path. Almost all peak strain values fall in a range between 0.0008 in./in. and 0.0030 in./in.

The minimum principal strain traces are characterized by a shape which exhibits a slight peak in tension, followed by a fairly sharp compressive pulse occurring as the fracture propagates past the rosette; this compressive pulse

corresponds to the tension peak of the maximum principal strain. The traces then return to the final strain level of the rosette.

For the majority of the rosettes, as the fracture approaches the rosette, the direction of the maximum principal strain rotates slightly so that it points toward the approaching fracture, and then returns to a more or less vertical position as the peak value of the strain occurs. After the maximum strain value is reached, the direction of the maximum principal strain continues to rotate and in general continues to point toward the surface fracture tip. Values of θ plotted as short straight lines in the direction of ϵ_{max} on the principal strain contours show this behavior quite clearly. These contours are presented as Figs. 95 through 104 and are discussed in Section 12.

For rosettes located close to the fracture path, the magnitude of the strain peak is relatively large. As the distance between a rosette and fracture increases, the peak principal strain magnitude decreases rapidly. This may be seen clearly in Fig. 21, in which typical principal strain traces for rosettes located at various distances from the fracture are presented. When the distance between the rosette and the fracture exceeds about 2 in., the rate of decrease of the peak strain magnitudes is somewhat less. Figure 91 is a plot of all the peak maximum principal strains versus distance between the rosette and the fracture. This figure gives the impression that there is a wide scatter; however, if the curves are plotted for rosettes located at varying distances from the initiation edge (8 in., 15 in., etc.) the individual curves shift to the right with increasing distance as may be seen in Figs. 92 and 93. Thus, there is an increase in the peak maximum principal strain with increasing distance from the initiation edge; this increase is noticeable up to about 22 to 29 in. from the initiation edge after which there is no apparent change. Thus, the strain field associated

with the propagating fracture appears to reach a "steady state" condition at about 22 to 29 in. from the initiation edge.

Another characteristic of the strain-time curves that was studied was the variation of the maximum strain rate with vertical distance of the rosette from the fracture surface. The strain rate (in./in./sec) is difficult to determine accurately because of the very nature of the strain traces (Fig. 8); the computed strain rates presented in Fig. 94 should be considered to give only a qualitative picture. However, it is apparent that a general trend of strain rate versus distance between rosette and fracture does exist as might be expected. The sketch in the upper right corner of Fig. 93 illustrates the procedure by which the strain rates were determined. A "best fit" curve of all points is also shown on the plot. Strain rates ranging from 1 to 109 in./in./sec were computed; however the majority of the values fall in the range of 1 to 30 in./in./sec for gages located at 1/2 in. to 3 in. from the fracture.

Strain-time curves of the component gages and computed principal strains of the four rosettes for which records were obtained in Test 35 are presented as Figs. 42 to 45. This test was conducted at a higher stress (28,000 psi) and a lower temperature (-15° F) to determine the effect of a higher stress level on the strain pattern. The traces are essentially the same shape as those found in the plates tested at lower stresses although the peak maximum strains are slightly higher. However, the rosettes were located quite close to the fracture path and in view of the earlier discussion, it is to be expected that the strain magnitudes might be fairly high. The maximum principal peak strain magnitudes of rosettes from Test 35 are plotted on Fig. 91 and exhibit the same trend as peak strain magnitudes from the other tests. Thus, on the basis of one test only, it appears that there was no marked change in the strain behavior for a propagating crack at this somewhat higher stress level.

12. <u>Maximum Principal and Vertical Strain Contours</u>

In order to portray the strain distribution in a plate during the time a fracture is propagating, it was decided to plot contours of certain strain components for various crack lengths. The available data consists of strain-time traces for horizontal, diagonal, and vertical gages from this series of tests as well as from earlier tests; in addition, principal strain values have been computed for the rectangular rosettes formed with the component gages in the test series reported herein.

In view of the fact that this is a brittle fracture study and the maximum tensile strains are of interest, it was felt that plots of contours of maximum principal strains for various crack lengths would be particularly valuable. The maximum principal strains are of interest from another standpoint since they provide both the magnitude and direction of the maximum tensile strain. The maximum principal strain contours are presented as Figs. 95 through 105. As has been noted earlier, the magnitude of the maximum principal strain is essentially equal to that of the maximum vertical strain; one reason for this is that the principal strain direction does not rotate much from the vertical. Thus, as a matter of comparison, and because a plot of the vertical strain allows an incorporation of data from the earlier tests, it was decided to present contours for the vertical strains as well; the contours of vertical strain are presented in Figs. 106 through 117. Although contours of only the maximum principal strain and vertical strains are presented in this report, contours of the other strain components, namely the diagonal strain, horizontal strain, minimum principal strain, and shear strain, could be prepared from the strain data presented in Figs. 25 through 89.

In order to obtain strain contours, it was necessary to superimpose the results from a number of tests. The data were superimposed only from plates tested

under similar conditions of stress, temperature, and impact; the only major variable with respect to the individual tests was the location of the fracture path with respect to the notch line. In general, the fractures sloped upward from the point of initiation and then leveled off as they traveled across the plate. The excursions from the notch line were on the order of 2 to 8 in.; precise locations of the fracture paths are tabulated in Figs. 14 through 20. However, since these distances are small in relation to the plate width, the actual crack length was never more than a few per cent greater than the net plate width. The horizontal projection of the fracture was used as the common fracture path on the strain contour plots.

The procedure used in plotting the strain contours may be summarized as follows. It was first necessary to establish from the original strain-time curves the time corresponding to various selected crack lengths. At the same time, it was necessary to establish the position of the gage with respect to the fracture path. Then, at any particular time corresponding to a given crack length, the strain values were obtained from the test data and this strain data was used in plotting the contours. The contour lines were drawn in regions where data were available by joining points of equal strain. No contours were drawn in regions where there were no data, although, it is obvious that strain contours do exist in these regions.

Before strain values could be determined for any particular crack location, it was necessary to establish the respective times that corresponded to the desired crack positions in every test. These times were determined by a knowledge of the breaking times of the crack detectors and the peaking times of the vertical strain gages located closest to the fracture surface, and are tabulated in Table 5 for various crack lengths. It was assumed that the peak strain of a rosette occurs when the surface fracture is directly above or below the

rosette, although the exact position of the tip of the fracture cannot be determined at any precise time. At points where there was disagreement between detector breaking times and gage peaking times, the peaking times of the strain gages were selected as the more reliable indication of the surface fracture location because of the more sensitive response of the strain gage. As a general rule, the detector breaking times were used only as a guide to selecting times corresponding to selected crack lengths. At fracture positions where there were no strain gages or detectors, the corresponding time was approximated by a linear interpolation between any two known points.

Since the horizontal projection on the notch line of the actual fracture path was used as the common fracture path for all tests for purposes of superposition, it was important to locate accurately each gage or rosette with respect to this common fracture. Three different methods of determining the gage and rosette locations on the plate layout with the common fracture path were investigated. The first method consisted of measuring the vertical distance between the rosette and the actual fracture for particular tests and locating the rosettes on the plate layout accordingly. The second method consisted of measuring the perpendicular distance of each rosette or gage from a horizontal line projected across the plate from the tip of the surface fracture for the particular crack length under investigation. The third method consisted of measuring the perpendicular distance between a rosette and the fracture, or the extension of the fracture in the direction the fracture was traveling at that particular instant; the rosette was then located above or below the common fracture path by this amount. A study of the three methods of locating the gages and rosettes on the strain contour plots indicated that regardless of the method used, the final strain contours were essentially unchanged. Since, in general the fracture followed a horizontal path as it passed through the region where rosettes

were placed, it was obvious that in the majority of cases there would be no significant difference in the final rosette locations as determined by any of the three methods investigated. In tests where the fracture was not horizontal, there would be a change in rosette locations; however, in general, at some distance ahead of the tip of the fracture, the changes in strain were so small that the net result was that the strain contours were still not altered markedly. Therefore, it was decided to use the actual fracture path as the common reference line for location of the strain gages and rosettes.

With regard to the strain data which is plotted at any particular time for purposes of establishing the strain contours, there are several additional factors of importance which should be noted at this time. Because of the nature of the recording equipment, the component gage strain and the computed principal strains are accurate only to about the nearest 0.0001 in./in., and the recorded times are accurate only to about 0.05 milliseconds. For an average fracture speed of 2500 fps, this time error of 0.05 milliseconds would correspond to a fracture length of about 1-1/2 in.

Because of the slight bending of the plates caused by the welding of the specimens to the pull-plates, and the possible residual strains in the plates, the value of the test load strains varied somewhat for the tests. Because of this fact, and to minimize the effect of any other variables, the contour interval selected for the plots was 0.0002 to 0.0004 in./in. In the case of the maximum principal strain contours, all of the tests were made at about the same stress level; thus, it appeared desirable to plot the contours in terms of absolute strain, that is, with respect to the as-rolled condition.

The vertical strain contours could also have been plotted in terms of absolute strain. However, in order to incorporate the data from earlier tests in which the test load stress varied from 15,000 psi to 20,000 psi, it was

decided to subtract the test load strain from the absolute vertical strain and plot the relative strain values; in all cases the reference strain in the vertical strain contour plots is the test load strain.

In spite of the limitations discussed in this section, it is felt that the strain contours presented give a very representative picture of the effect of a propagating brittle crack on the strain distribution in a wide steel plate.

The maximum principal strain contours presented as Figs. 95 through 104, and the vertical strain contours presented as Figs. 106 through 115, are based on the data from Tests 33, 34, 37, 38, and 39. The data from Tests 35 and 36 were not used in the contour plots because Test 35 was conducted on an arrestor specimen at a higher applied stress level, and Test 36 resulted in a double fracture. A careful examination of the strain results from gages and rosettes of Tests 35 and 36 will show that the data from these two tests are similar to that of the other tests reported. In the contour plots, the magnitudes and directions of the maximum principal strain are shown at the respective locations on the plate layout. The directions of the maximum principal strain are shown as short straight lines. For ease in interpretation of the contours, all strain units are in./in. times 10^6.

For an 8-in. crack (Fig. 95), the shortest crack length for which contours have been plotted, it will be noted that the increase in strain directly above and below the surface fracture tip is small in comparison with strain changes for longer crack lengths. At points ahead of the 8-in. crack, the strain changes are negligible and the plotted strains correspond to the test load principal strains. The variation in test load principal strains for the rosettes and for the various tests accounts for the differences noted in the plotted strain values. The numbers in parentheses following the strain values refer to the test number and corresponding rosette from which the plotted strain values were

obtained. These two numbers are shown only on Fig. 95 but refer also to Figs. 95 through 104 as well. For an 8-in. crack length, the small changes in strain exhibited by the rosettes located only 8 in. from the initiation edge (Figs. 60 and 66) further attest to the fact that the notch-wedge-impact method of fracture initiation has little effect on the strain distribution in a wide plate.

The change in strain distribution as the crack length increases may be seen clearly by comparing Figs. 95, 96, and 97, in which the maximum principal strain contours are presented for crack lengths of 8 in., 15 in., and 18.5 in. As the crack length increases it will be noted that the magnitude and extent of the strain field associated with the crack tip have increased. At a crack length of 22 in., as is shown in Fig. 98, the strain pattern surrounding the moving crack tip ceases to change, and for crack lengths in excess of 22 in., the strain field surrounding the advancing crack tip remains essentially unchanged. This general effect was noted earlier in Section 11 in connection with Figs. 92 and 93 which show the results of a study of the peak strain magnitude versus distance of the rosette from the fracture, for rosettes located at various distances from the initiation edge. Figures 99 through 104, for crack lengths of 25-1/2 in. to 43 in., illustrate the fact that in the central one-third of the plate the strain field associated with the tip of the crack remains essentially unchanged. The extent of the strain contours directly ahead of the fracture increases only slightly with increasing crack length. Thus, for this particular specimen geometry, apparently the propagating brittle fracture does not reach a "steady state" condition until it has traversed a distance of about 22 in. This length is somewhat longer than that which earlier studies had suggested.

As may be seen in Fig. 98, the major portion of the strain field associated with the propagating brittle fracture extends only about 8 in. to 10 in. ahead of the fracture. In the region directly ahead of the cracks, the

strains decrease slightly as the fracture approaches. Possibly some of the strain variation observed directly ahead of the fracture is associated with the formation of fracture nuclei ahead of the main fracture.

The main changes in strain occur above and below the fracture tip and slightly ahead of it. Behind the fracture front the strains decrease more rapidly. Actually all strain contours appear to converge toward the fracture front. Although extensive strain measurements were not obtained at distances far above and below the fracture, the recorded strain data indicate that the contours are symmetrical about the fracture path.

A set of typical maximum principal strain contours is presented in Fig. 105; these contours are based on the results presented in Figs. 98 through 104, and for the geometry and test conditions used herein are considered to be representative of the strain field associated with the crack tip for a crack length in excess of 22 in.

Further information on the extent of the strain field associated with a propagating brittle fracture may be obtained by studying the strain traces presented in Figs. 48 and 50. These strain traces are for two rosettes (Numbers 3 and 5) located between the double fracture occurring in Test 36 (Fig. 17). Each rosette was located approximately 2 in. from one of the fractures and the strain traces of the rosettes are typical of strain curves for rosettes located 2 in. from a single fracture. A study of the strain data would seem to indicate that the strain field associated with either of the advancing fractures was affected little, if any, by the strain field associated with the other advancing fracture.

Vertical strain contours (in which the reference strain is the test load strain) are presented as Figs. 106 through 115. In Fig. 106, the numbers in parentheses following the strain values refer to the original test number and

corresponding vertical gage number respectively from which the plotted strain values were obtained. In general, these contours are similar in shape and magnitude (if the test load strain were added) to the maximum principal strain contours discussed previously. A typical set of vertical strain contours based on the results of Figs. 109 through 115 and for a crack length in excess of 22 in., is presented as Fig. 116.

Vertical strain contours for a crack length of 29 in., based on results from all earlier six-ft wide plate tests are presented in Fig. 117. A tabulation of the data used to plot the contours in Fig. 117 is presented in Table 6. These values are typical for the crack lengths in excess of 22 in. investigated for Tests 13 through 32. The strain values were superimposed in a manner described earlier; although a few exceptions may be noted, the strain values exhibit the same general pattern as shown in Fig. 116.

The contours of maximum principal strain and vertical strain are based on data obtained from all the six-ft wide plates tested as a part of this investigation, and are considered to be representative of the strain distribution recorded on the surface of the plates during brittle fracture propagation.

13. <u>Crack Path and Surface Texture</u>

Photographs of the fractured plate specimens are presented as Figs. 118 through 121. In general, the fractures slope upward from the point of initiation and then level off. A black string is stretched along the notch line in these figures. In most tests a secondary crack started from the notch cut at the far edge, propagated toward the approaching fracture, and ended in a submerged crack before reaching the main fracture. These secondary cracks may be seen in the figures.

The fracture in Test 36 branched near the center of the plate into two complete fractures. A close-up of the branch of the double fracture may be seen in Fig. 119.

Views of a typical fracture surface are presented in Fig. 121. The shear lip associated with the fractures was very small and almost imperceptible. Portions of the surface exhibit a coarse texture with the usual herringbone pattern while in other regions, usually near the initiation edge, the texture is quite smooth. Close-up views of both smooth and coarse fracture texture are presented in Fig. 122.

The reduction in plate thickness in the region of the fracture surface was one to two per cent; this reduction in thickness is of the same order of magnitude as that found in earlier fracture tests conducted as a part of this program.

IV. SUMMARY

This research report contains a summary and preliminary analysis of data primarily from Tests 33 through 39 conducted as a part of the current brittle fracture propagation study. More complete studies of these data, as well as data obtained subsequently, will be made as a part of the program.

The specimens were tested with a net stress of about 19,000 psi, at a temperature of about -10 deg F, and with a nominal impact of 1200 ft lb for fracture initiation. Thirty-three channels of instrumentation were used for each test; this is more than three times as many channels as had previously been available for any one test. The strain-time traces from the component gages, as well as the computed principal strains, are presented. Since the tests were conducted under similar conditions of stress, temperature, and impact, it was possible to superimpose the strain data to obtain a more complete picture of the strain distribution on the surface of the plate associated with the moving fracture.

The behavior exhibited by the component gages was similar to that observed in earlier tests. For example, in the case of a vertically oriented strain gage, as the distance between the gage and the fracture path decreased, the strain pulse became sharper and had a greater magnitude; as the distance between the gage and fracture increased, the strain pulse extended over a longer period of time, but the precise shape of the pulse depended on the distance from the fracture path. For gages oriented in the diagonal and horizontal directions, this same general trend was noted, but the shape of the strain trace, particularly in the case of the horizontal gage, was markedly different.

In the case of the principal strains computed from the component strain traces, the maximum principal strain was found to exhibit the same type

of behavior as observed for a vertically oriented gage, with the exception that the direction of the maximum principal strain was found to rotate slightly to either side of the vertical axis depending upon the location of the fracture.

Although the nature of the strain traces are such that only a rough picture of the strain rates may be obtained, the trend is of some interest. As would be expected, the maximum strain rate occurs for gages located quite close to the fracture. Strain rates ranging from 1 to 109 in./in./sec have been computed; however, the majority of the values fall in the range of 1 to 30 in./in./sec for gages located at 1/2 in. to 3 in. from the fracture.

Contours of maximum principal strain and vertical strain, for various crack lengths, are presented. The major portion of the strain field associated with the front of the propagating brittle fracture extends only about 8 to 10 in. ahead of the fracture; the regions most affected are above and below the fracture tip and slightly ahead of it. Although extensive strain measurements were not obtained at distances far above and below the fracture, the recorded strain data indicate that the contours are symmetrical about the fracture path.

A study of the data reveals that for crack lengths in excess of about 22 in., the extent, magnitude, and nature of the strain field associated with the advancing tip of the fracture remains essentially unchanged. Typical maximum principal strain contours and vertical strain contours based on all of the available data are presented for fractures propagating in the central one-third of the plate width.

BIBLIOGRAPHY

1. Hall, W. J., Mosborg, R. J., and McDonald, V. J., "Brittle Fracture
    Propagation in Wide Steel Plates," The Welding Journal, 36 (1), Research
    Supplement, pp. 1-s to 8-s (1957).

2. Hall, W. J., Godden, W. G., and Fettahlioglu, O. A., "Preliminary Studies
    of Brittle Fracture Propagation in Structural Steel," Civil Engineering
    Studies, Structural Research Series No. 123, University of Illinois, June
    1957.

3. Lazar, R. and Hall, W. J., "Studies of Brittle Fracture Propagation in
    Six-Foot Wide Structural Steel Plates," Civil Engineering Studies,
    Structural Research Series No. 136, University of Illinois, June 1957.

4. Lynam, T. M., "Strain Patterns During the Propagation of a Brittle Fracture
    in Steel Plates," M. S. Thesis submitted to the Graduate College, University
    of Illinois, (1957).

5. Rolfe, S. T., "Studies of the Strain Distribution in Wide Plates During
    Brittle Fracture Propagation," M. S. Thesis submitted to the Graduate
    College, University of Illinois, (1958).

TABLE 1

OUTLINE OF TESTS

Test No. (Plate No.) and Date of Test	Initial Load (kips)	Stress on Net Section (ksi)	Ave. Temp. (deg. F)	Remarks

With the exception of Test 35, all tests were conducted on 3/4 in. by 72 in. by 120 in. semi-killed steel plate specimens welded with E7016 electrodes to 1-in. thick pull-plates in the 3,000,000-lb Baldwin hydraulic testing machine. The brittle fractures were initiated by the notch-wedge-impact method with a nominal lateral impact of 1200 ft lb.

The notch was 1-1/8 in. long and consisted of a slot four hacksaw blades wide (~0.141 in.) for the first 1 in., one blade wide (~0.034 in.) for the next 1/16 in., and ended with a jewelers saw-cut (~0.012 in.) 1/16 in. long.

Test No. (Plate No.) and Date of Test	Initial Load (kips)	Stress on Net Section (ksi)	Ave. Temp. (deg. F)	Remarks
33 (XC-1) 28 Feb. 57	1000	19.0	0	Complete fracture -- good strain records obtained from 7 rosettes.
34 (XF-1) 12 Mar. 57	1000	19.0	0	Complete fracture -- good strain records obtained from 10 rosettes.
35 (RTRT-4) 16 April 57 (Tested in conjunction with Project SR-134)	1475	28.0	-15	Plate specimen composed of 36-in. starter strake of rimmed steel, 4-in. strake of T-1, 20-in. strake of rimmed steel, and a 12-in. strake of T-1 steel. Specimen was 27 in. long. Fracture arrested at leading edge of final T-1 strake. Final load -- 85 kips. Good strain records obtained from 4 rosettes.

TABLE 1 (Continued)

Test No. (Plate No.) and Date of Test	Initial Load (kips)	Stress on Net Section (ksi)	Ave. Temp. (deg. F)	Remarks
36 (X2B) 10 Oct. 57	997	19.0	-10	Complete fracture -- fair strain records obtained from 11 rosettes. Double fracture last two-thirds of plate width.
37 (X2F) 25 Oct. 57	997	19.0	-8	Complete fracture -- good strain records obtained from 11 rosettes.
38 (X1B) 1 Nov. 57	997	19.0	-9	Complete fracture -- good strain records obtained from 11 rosettes.
39 (X2E) 15 Nov. 57	997	19.0	-6	Complete fracture -- good strain records obtained from 11 rosettes.

TABLE 2

CHECK ANALYSES OF STEEL PLATE MATERIAL

Test No.	Material (Plate No.) Heat No.	Chemical Composition in Per Cent							
		C	Mn	P	S	Si	Cu	Ni	Al
33	Semi-killed Steel (XC-1) 64M487	0.17	0.71	0.019	0.028	0.058	0.02	0.0	0.03
34 and 37	Semi-killed Steel (XF) 64M487	0.20	0.76	0.019	0.028	0.052	0.02	Trace	0.03
35	Rimmed Steel (Z1A) 16445	0.18	0.42	0.013	0.031	0.02	0.23	0.14	0.003
36 and 38	Semi-killed Steel (XB) 64M487	0.21	0.82	0.018	0.030	0.058	0.02	0.0	0.03
39	Semi-killed Steel (XE) 64M487	0.20	0.76	0.019	0.040	0.03	0.04	0.16	0.002

TABLE 3

TENSILE TEST DATA FOR STEEL PLATE MATERIAL

(Standard ASTM 0.505-in. dia. specimens)

Test No.	Material (Plate No.) Heat No.	Lower Yield Strength (ksi)		Maximum Strength (ksi)	Per Cent Elongation in 2-in.	Per Cent Reduction of Area
33	Semi-Killed Steel (XC-1) 64M487	(L)*	32.9	59.3	40.5	66.5
		(T)	32.6	58.8	41.0	59.5
34	Semi-Killed Steel (XF-1) 64M487	(L)	32.9	61.8	40.7	66.3
		(T)	34.5	62.4	40.0	61.7
35	Rimmed Steel (Z1A) 16445	(L)	34.7	68.1	36.5	57.6
		(T)	35.2	68.7	31.2	51.6
36	Semi-Killed (X2B) 64M487	(L)	36.5	67.2	36.0	63.5
		(T)	35.2	67.8	34.5	58.8
37	Semi-Killed Steel (X2F) 64M487	(L)	35.5	64.4	41.0	67.8
		(T)	35.0	64.2	36.3	61.8
38	Semi-Killed Steel (X1B) 64M487	(L)	35.5	66.8	36.5	64.3
		(T)	35.6	66.4	36.8	59.8
39	Semi-Killed Steel (X2E) 64M487	(L)	34.3	61.6	39.5	65.3
		(T)	35.2	62.1	36.8	57.5

* (L) Average of two specimens taken parallel to the direction of rolling.
  (T) Average of two specimens taken transverse to the direction of rolling.

TABLE 4

FRACTURE SPEEDS

All distances are measured along the crack path.
Speeds are rounded off to nearest 50 fps.

Detector	Distance Between Detectors (in.)	Breaking Time	Time Interval	Speed
		(milliseconds)		(fps)

TEST 33

Detector	Distance Between Detectors (in.)	Breaking Time	Time Interval	Speed
A		.76		
	12.02		0.36	2800
B		1.12		
	13.16		0.37	2950
C		1.59		
	6.02		0.22	2300
D		1.71		
	6.05		0.25	2000
E		1.96		

TEST 34

Fracture Passed Above
Crack Detectors

TEST 35

Detector	Distance Between Detectors (in.)	Breaking Time	Time Interval	Speed
A		.77		
	8.00		0.23	2900
B		1.00		
	8.00		0.14	4750
C		1.14		
	8.00		0.24	2800
D		1.38		
	8.00		0.20	3350
E		1.58		

TEST 36

Detector	Distance Between Detectors (in.)	Breaking Time	Time Interval	Speed
A		0.31		
	7.10		0.13	3500
B		0.44		
	6.64		0.15	4150
C		0.59		
	7.32		0.23	3050
D		0.82		
	7.15		0.20	3000
E		1.02		
	14.47		0.52	2800
F		1.54		

TABLE 4 (Continued)

Detector	Distance Between Detectors (in.)	Breaking Time	Time Interval (milliseconds)	Speed (fps)
		TEST 37		
A		0.96		
	7.02		0.14	4200
B		1.10		
	7.10		0.18	3300
C		1.28		
	6.50		0.22	2450
D		1.50		
	6.97		0.28	2100
E		1.78		
	13.60		0.62	1850
F		2.40		
		TEST 38		
A		0.34		
	7.14		0.15	3950
B		0.49		
	7.16		0.16	3750
C		0.65		
	6.71		0.20	2800
D		0.85		
	6.94		0.22	2650
E		1.07		
	13.84		--	--
F		--		
		TEST 39		
A		0.06		
	6.73		0.19	2950
B		0.25		
	7.18		0.44	2700
C		--		
	7.18		--	--
D		0.69		
	7.24		0.26	2300
E		0.95		
	14.0		0.46	2550
F		1.41		

TABLE 5

TIMES CORRESPONDING TO VARIOUS CRACK LENGTHS

All times are in milliseconds and refer to the time base
of the strain-time curves presented in Figs. 25-89

Crack Length (in.)	Test No.				
	33	34	37	38	39
8	0.22	0.03	0.92	0.35	0.10
15	0.94	0.50	1.11	0.52	0.31
18.5	1.05	0.72	1.18	0.61	0.45
22	1.16	0.95	1.24	0.70	0.59
25.5	1.24	1.10	1.35	0.81	0.67
29	1.32	1.25	1.45	0.92	0.75
32.5	1.57	1.37	1.56	1.03	0.91
36	1.62	1.50	1.66	1.14	1.07
39.5	1.74	1.63	1.82	1.26	1.18
43	1.86	1.77	1.97	1.37	1.30

Note: These times, corresponding to various crack lengths, were used in
determining both the maximum principal strain contours (Figs. 95 through
104) and the vertical strain contours (Figs. 106 through 115).

TABLE 6

DATA OBTAINED FROM SRS-136 (TESTS 13-32)
(See Fig. 117)

Test No.	Vertical Gage No.	Distance of Gage from Init. Edge (in.)	Distance of Gage from Fracture (in.)	Time Corres. to 29-in. Crack (milliseconds)	Total Strain (in./in.)	Test Load Strain (in./in.)	Strain Referenced to Test Load Strain (in./in.)
13	1	12.0	-0.3	0.66	.00063	.00063	0
	2	35.5	-1.7	0.66	.00072	.00072	0
	3	60.0	-2.0	0.66	.00066	.00066	0
15	1	35.0	1.6	0.81	.00079	.00064	.00015
	2	36.0	1.6	0.81	.00071	.00049	.00022
	3	36.0	-3.4	0.81	.00090	.00078	.00012
19	2	36.5	-0.6	0.56	.00052	.00047	.00005
	4	61.0	0	0.56	.00055	.00055	0
22	1	37.0	-3.5	0.32	.00082	.00064	.00018
	4	61.0	-3.5	0.32	.00062	.00062	0
23	5	36.0	-3.0	0.82	.00067	.00067	0
	6	43.0	-3.4	0.82	.00067	.00067	0
	7	50.0	-3.5	0.82	.00064	.00064	0
	8	57.0	-3.5	0.82	.00063	.00063	0
	9	64.0	-3.5	0.82	.00052	.00062	-.00010
25	1	8.0	-0.5	0.92	-.00003	.00059	-.00062
	2	15.0	-0.8	0.92	-.00001	.00061	-.00062
	3	22.0	-0.7	0.92	-.00007	.00061	-.00068
	4	29.0	-0.7	0.92	.00231	.00056	.00175
	9	64.0	-0.8	0.92	.00061	.00061	0
32	1	15.0	-2.0	0.60	-.00011	.00057	-.00068
	2	36.0	-6.6	0.60	.00095	.00055	.00040
	3	50.0	-7.2	0.60	.00050	.00055	-.00005
	4	57.0	-7.1	0.60	.00054	.00054	0
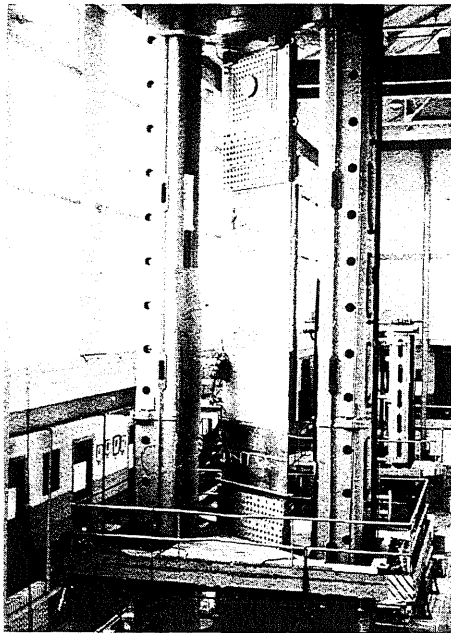
SPECIMEN IN 3,000,000—LB
TESTING   MACHINE
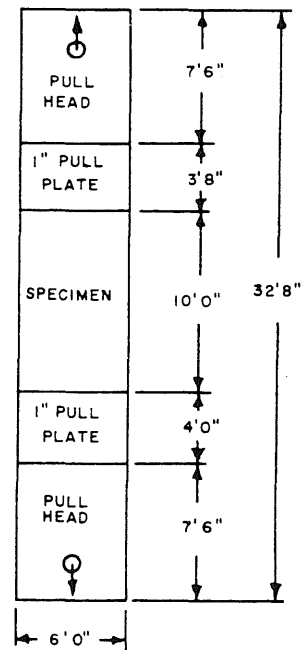
LINE DIAGRAM OF SPECIMEN

PULL HEAD	7'6"
1" PULL PLATE	3'8"
SPECIMEN	10'0" 32'8"
1" PULL PLATE	4'0"
PULL HEAD	7'6"

6'0"
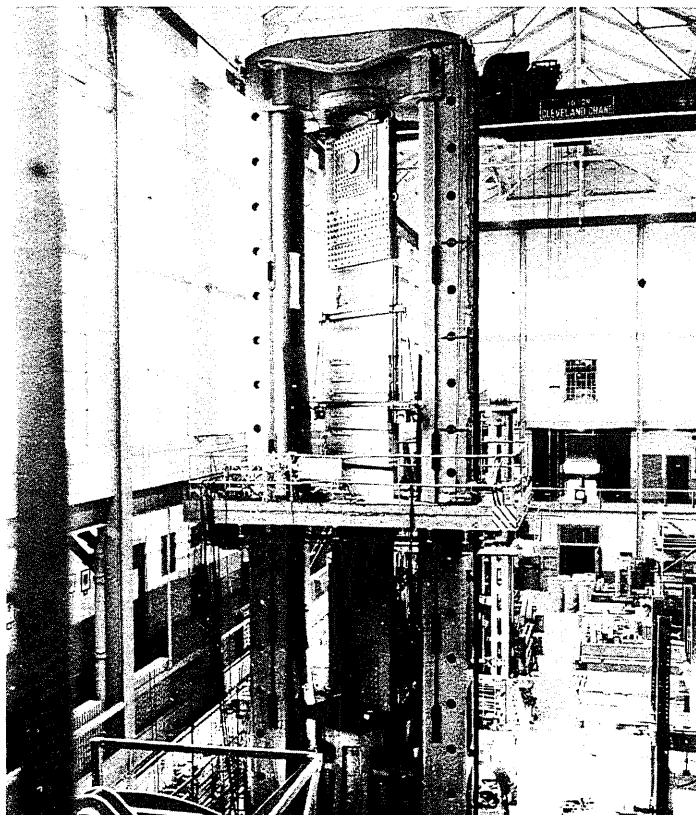
SPECIMEN   READY   FOR   TESTING

FIG. I   TYPICAL TEST SETUP
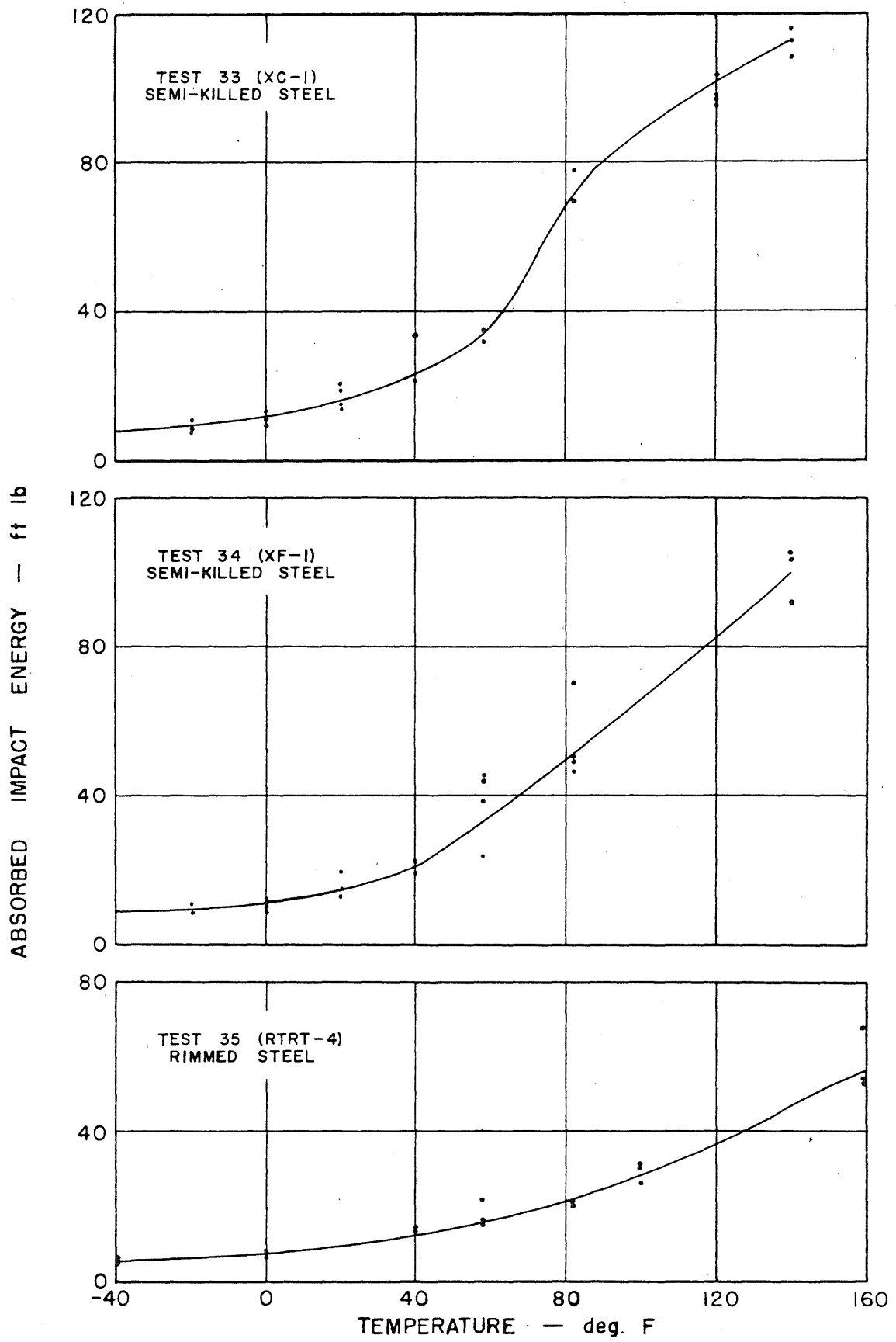
FIG. 2   CHARPY V-NOTCH CURVES — TESTS 33, 34, AND 35
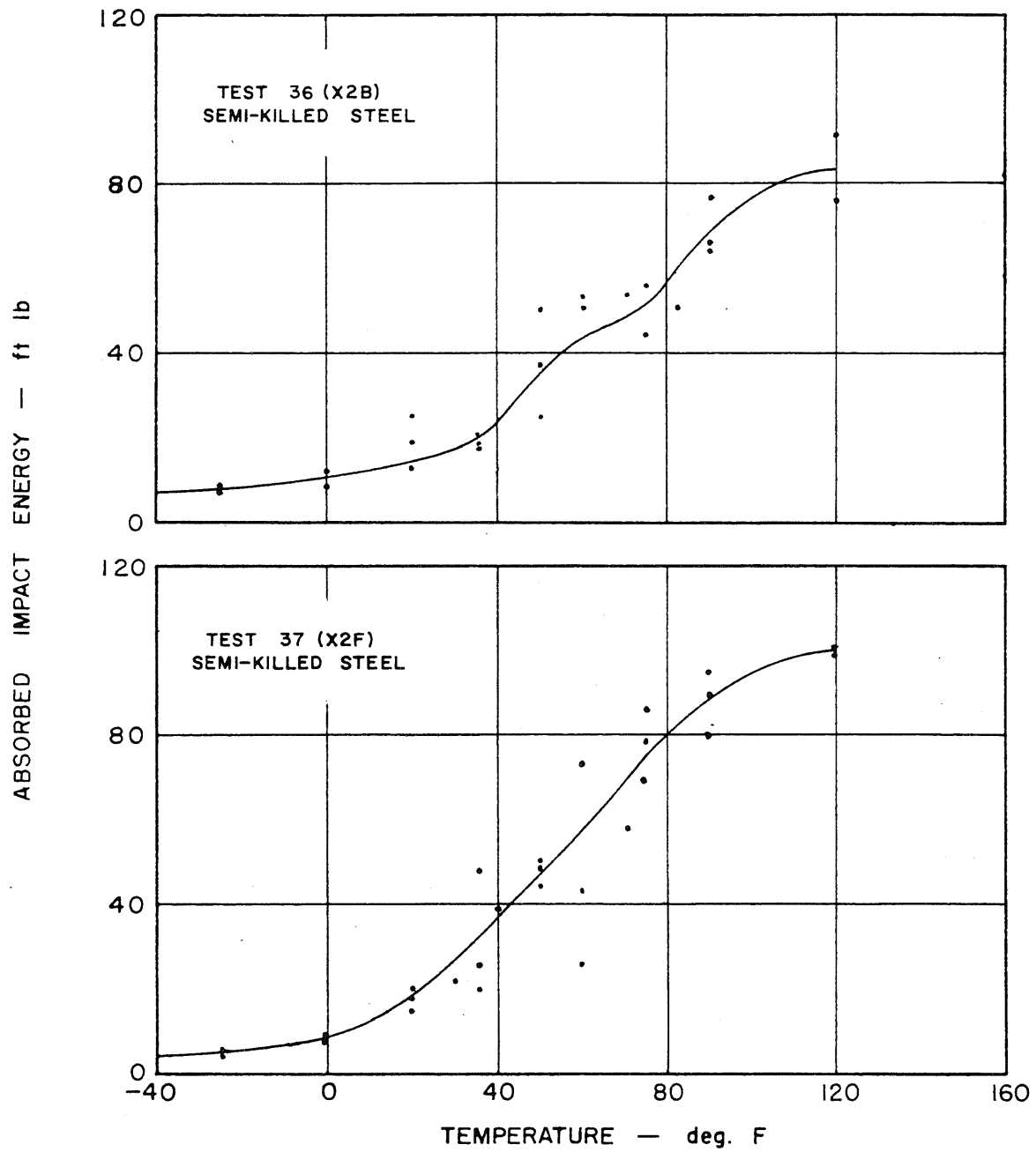
FIG. 3   CHARPY   V-NOTCH   CURVES   —   TESTS   36 AND 37
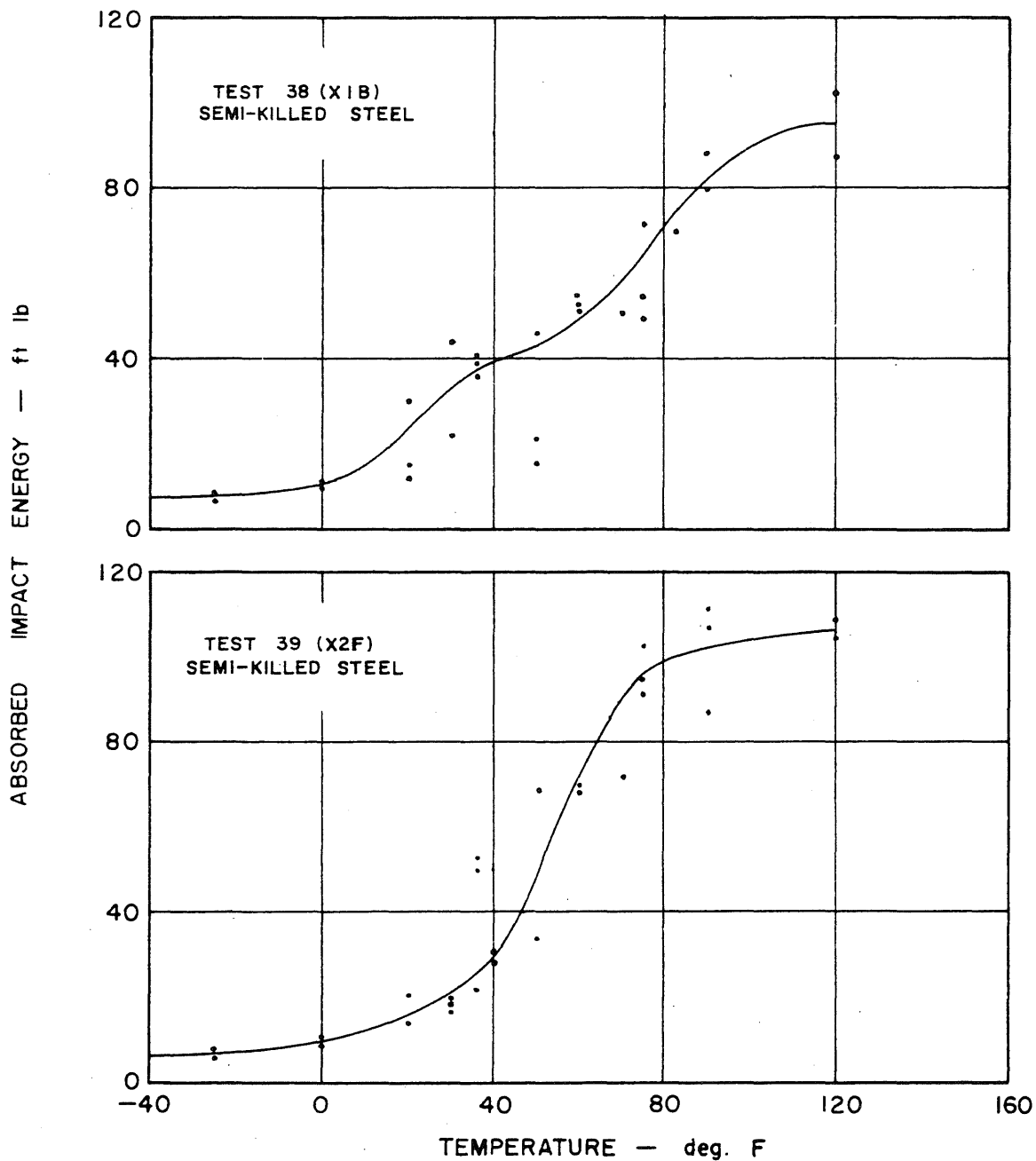
FIG. 4   CHARPY   V-NOTCH   CURVES   —   TESTS   38   AND   39

OUTPUTS

COMMON

6v

6v

6v

CALIBRATION
RESISTOR

STRAIN GAGE CIRCUITS

A   B   C   D CRACK DETECTOR

CALIBRATION SWITCHES

3v

OUTPUT

CRACK DETECTOR CIRCUITS
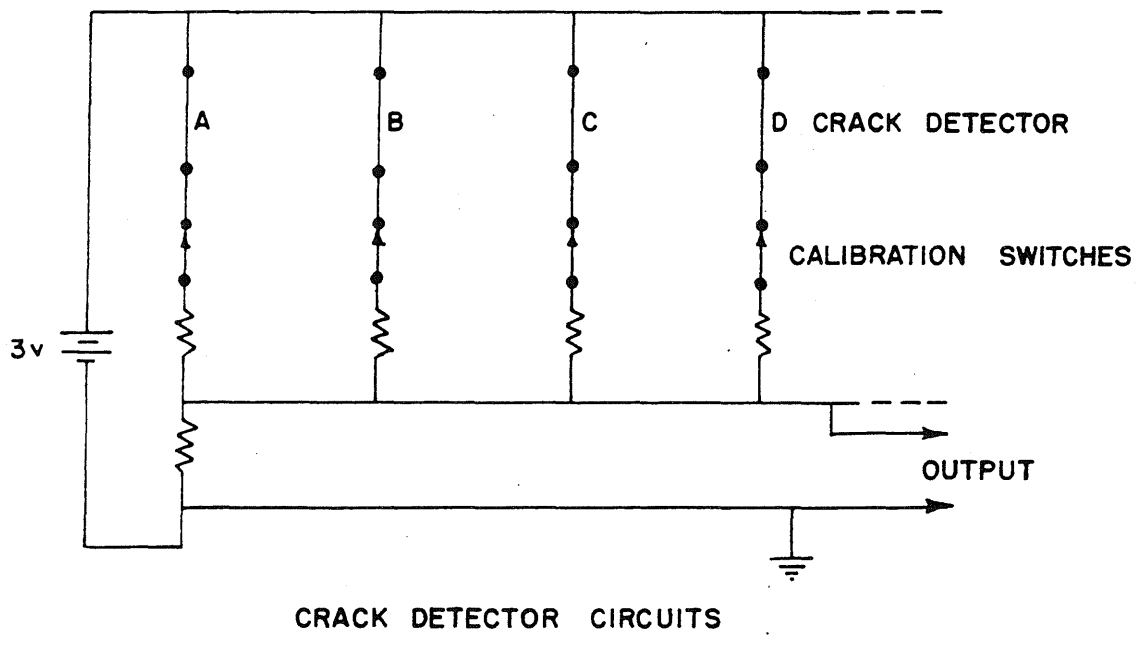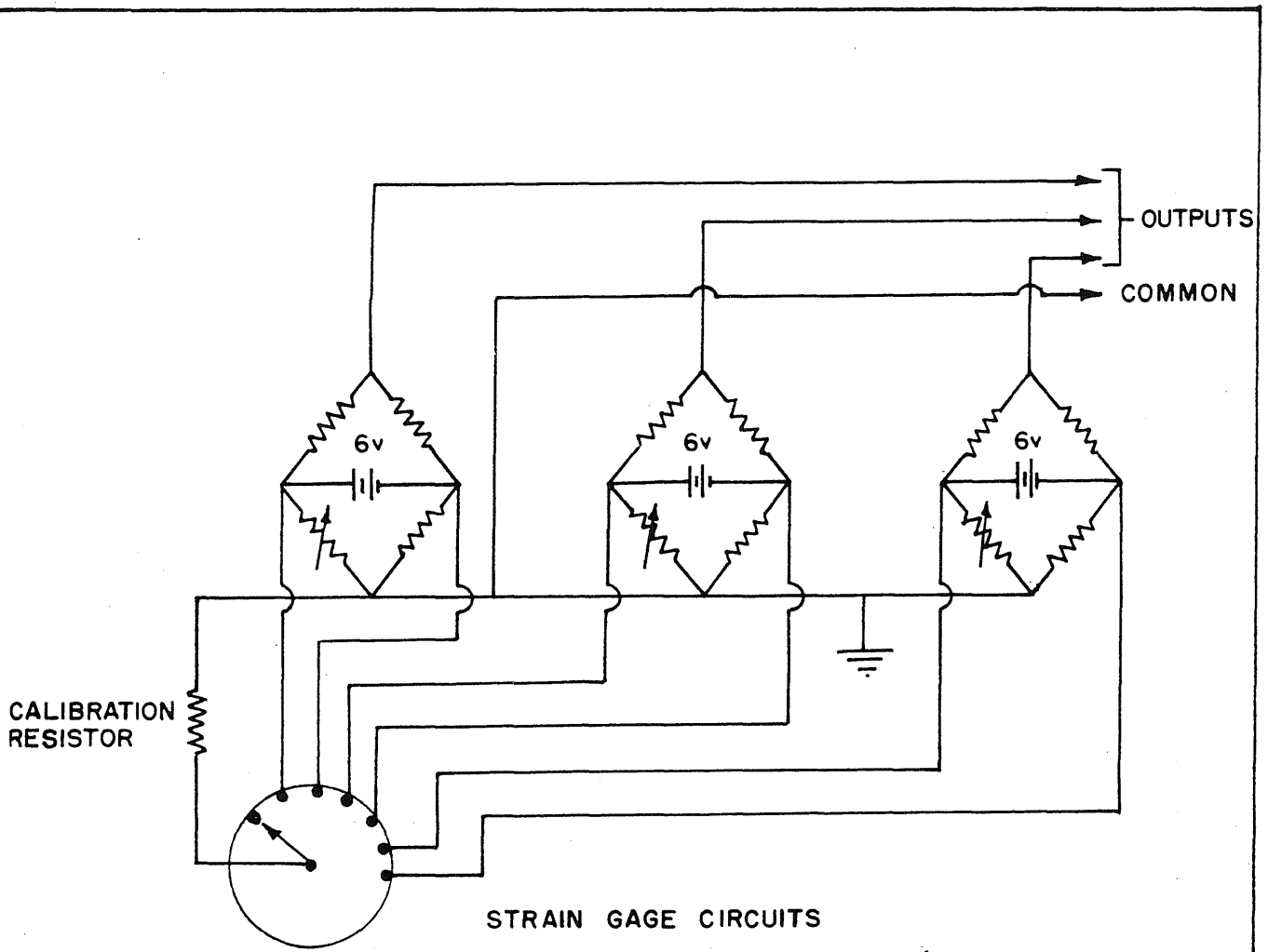
FIG. 5   INSTRUMENTATION   CIRCUITS

FIG. 6　　TRIGGER CIRCUIT

SPEEDOMAX

CALIBRATING OSCILLATORS

FRANKLIN OSCILLOSCOPES

DUMONT OSCILLOSCOPES

TEKTRONIX OSCILLOSCOPE
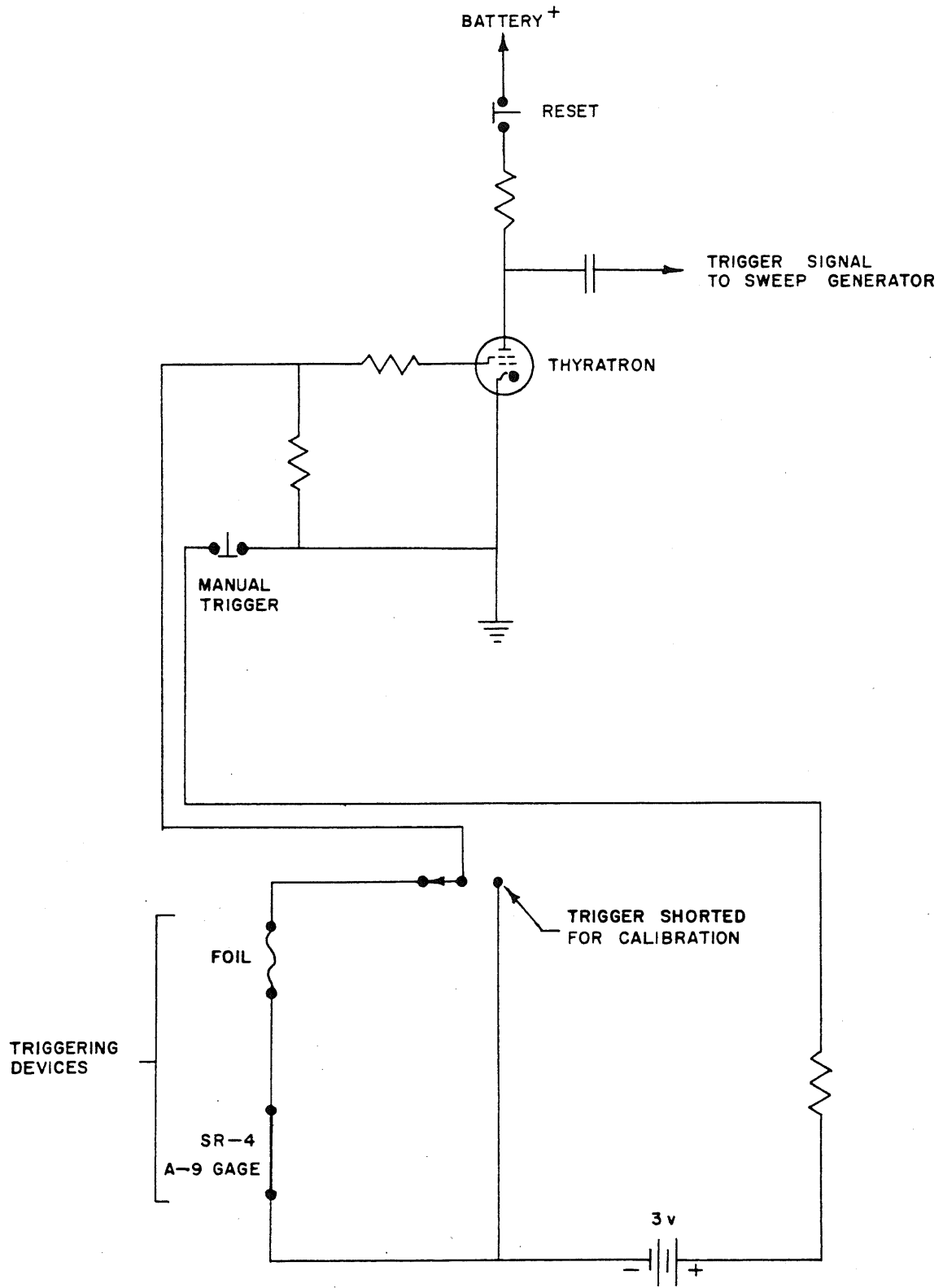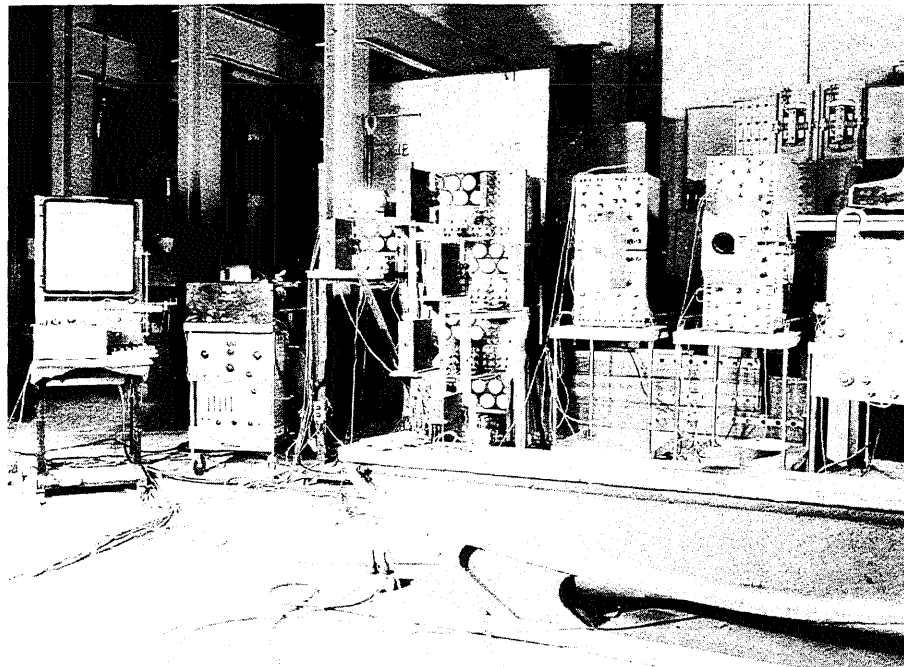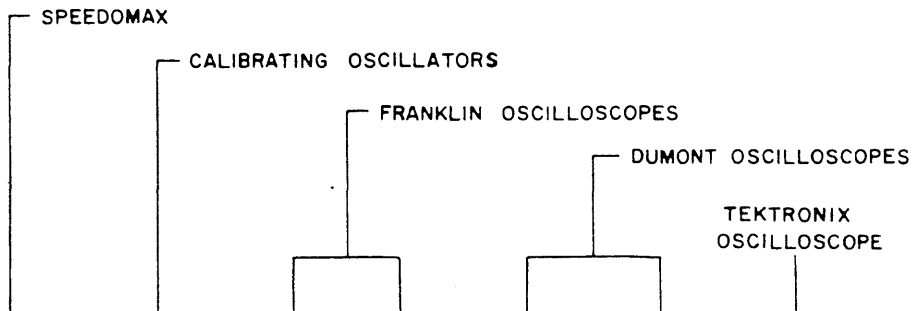
FIG. 7   RECORDING EQUIPMENT
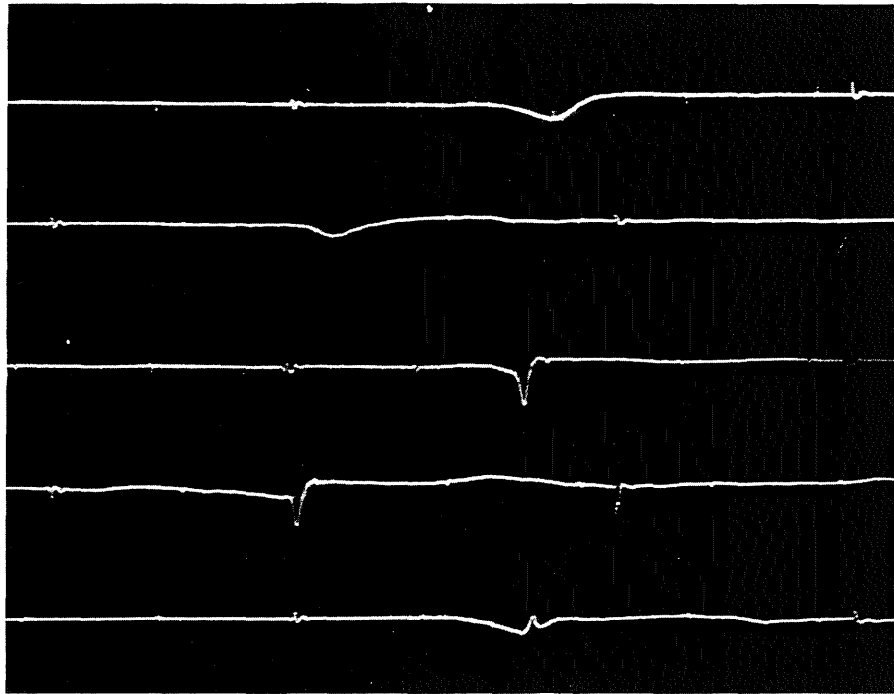
FRANKLIN   OSCILLOSCOPE   RECORD
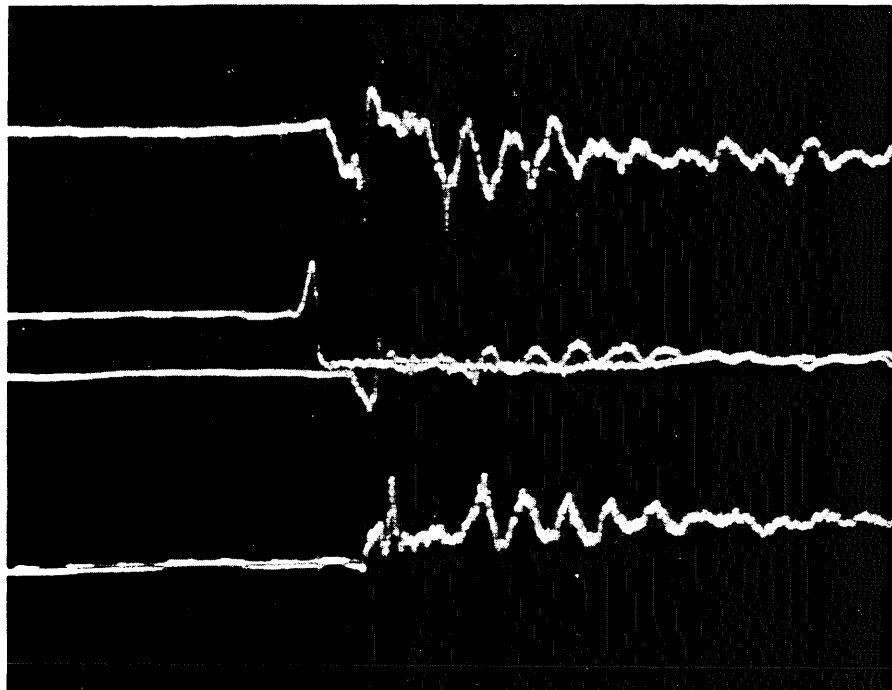
DUMONT   OSCILLOSCOPE   RECORD

FIG.   8   TYPICAL   STRAIN   RECORDS
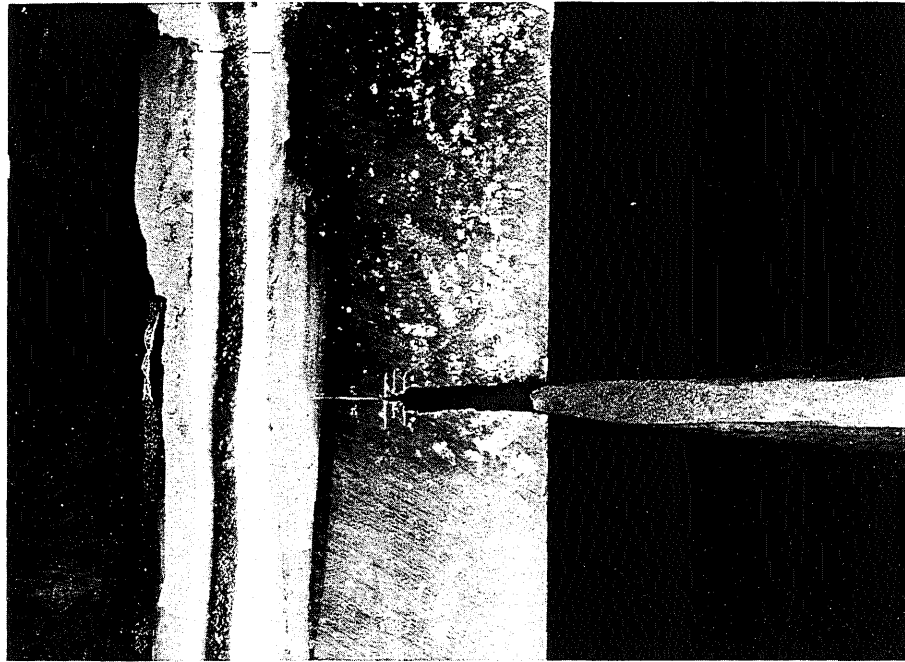
FIG. 9   CLOSEUP   OF   NOTCH   AND   TIP   OF   WEDGE
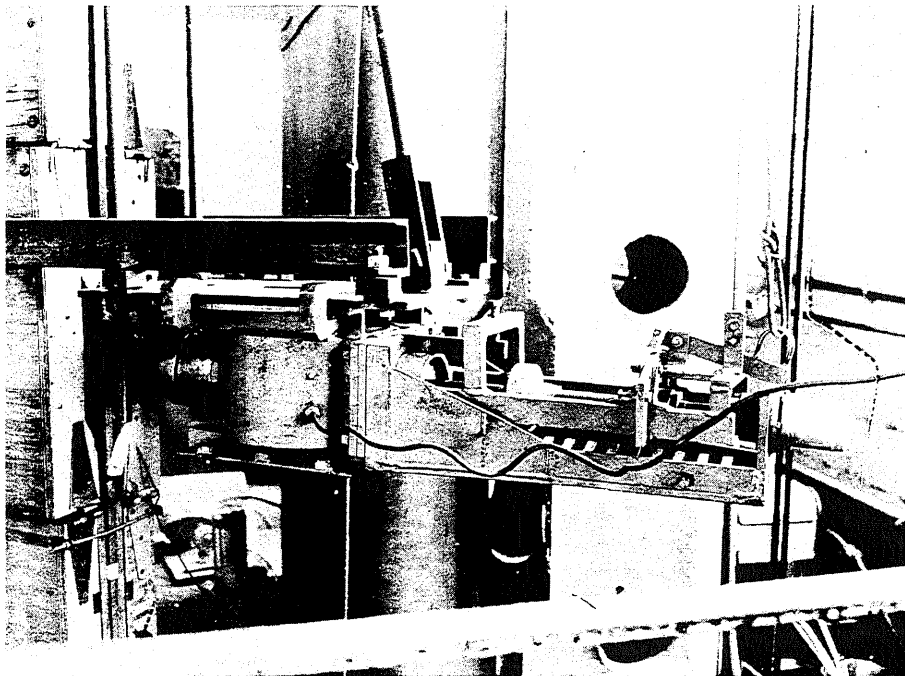
FIG. 10   PISTON   DEVICE   USED   FOR   FRACTURE   INITIATION
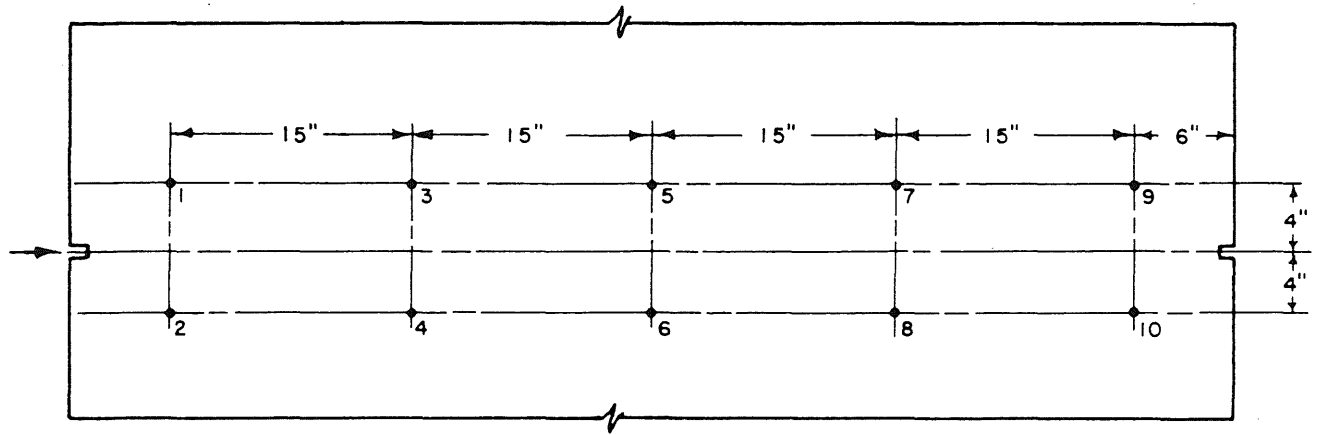
THERMOCOUPLE   LOCATIONS
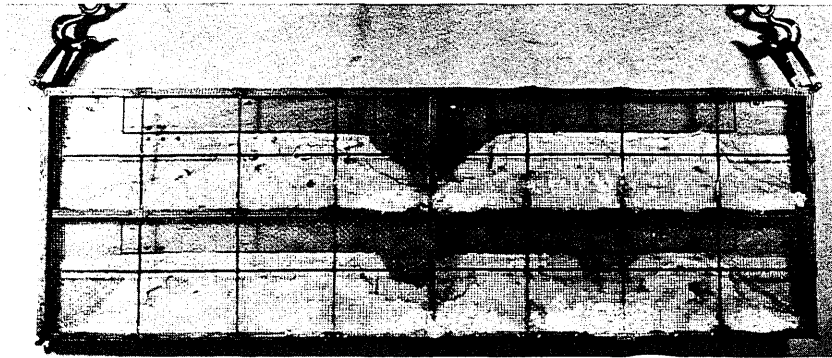
INDIVIDUAL   COOLING   TANK
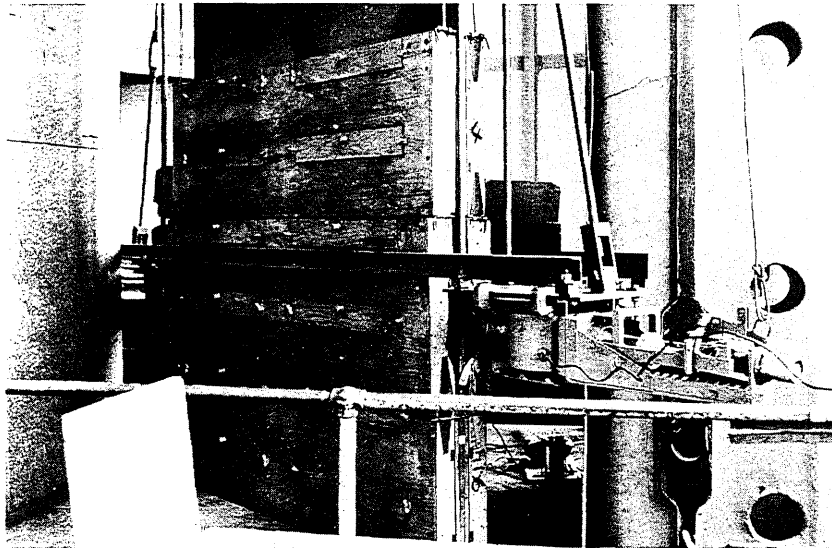
COOLING   TANKS   MOUNTED   PRIOR   TO   TESTING

FIG. 11   THERMOCOUPLE   LOCATIONS   AND   COOLING   APPARATUS
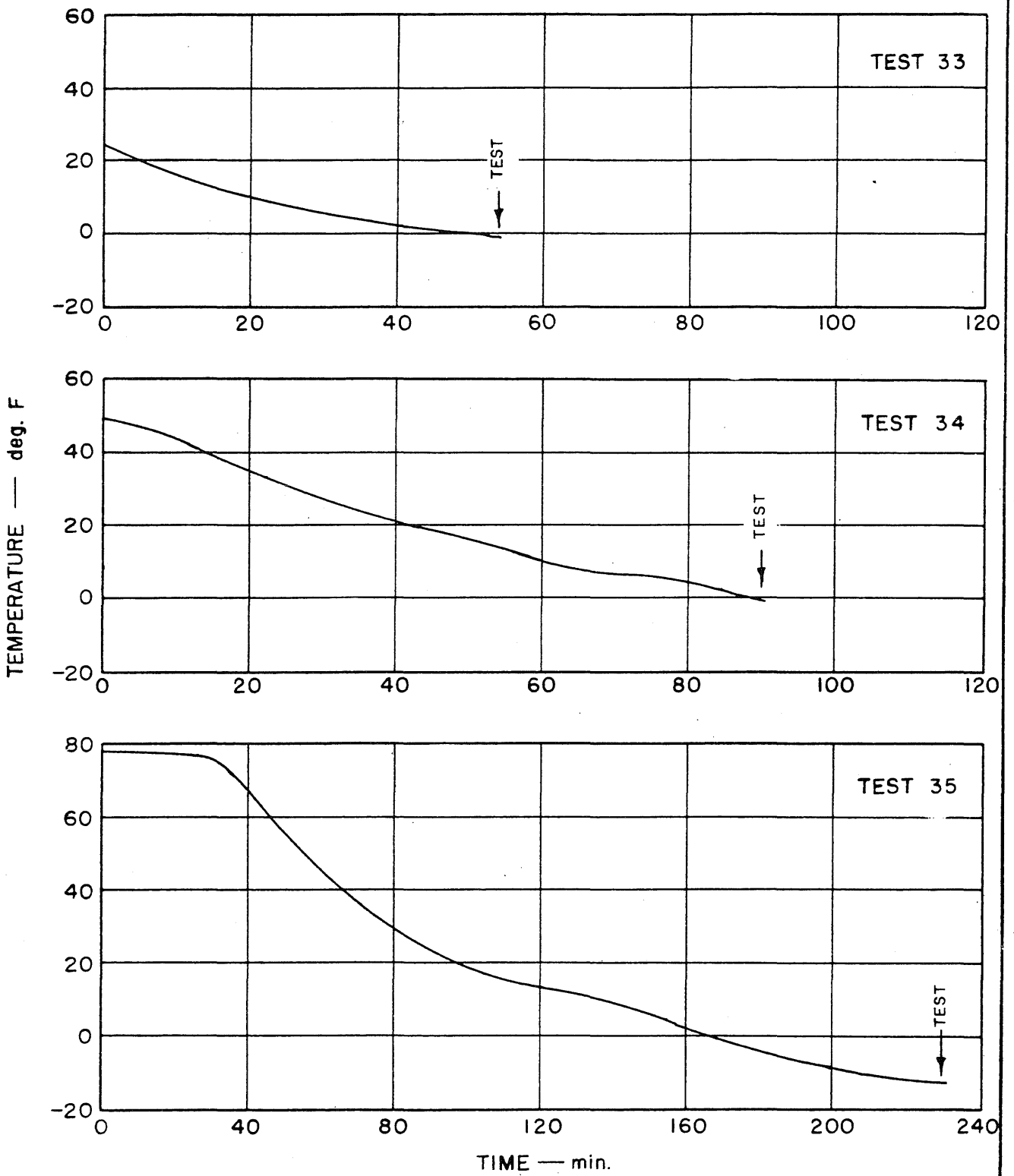
FIG. 12   AVERAGE COOLING CURVES — TESTS 33, 34, AND 35
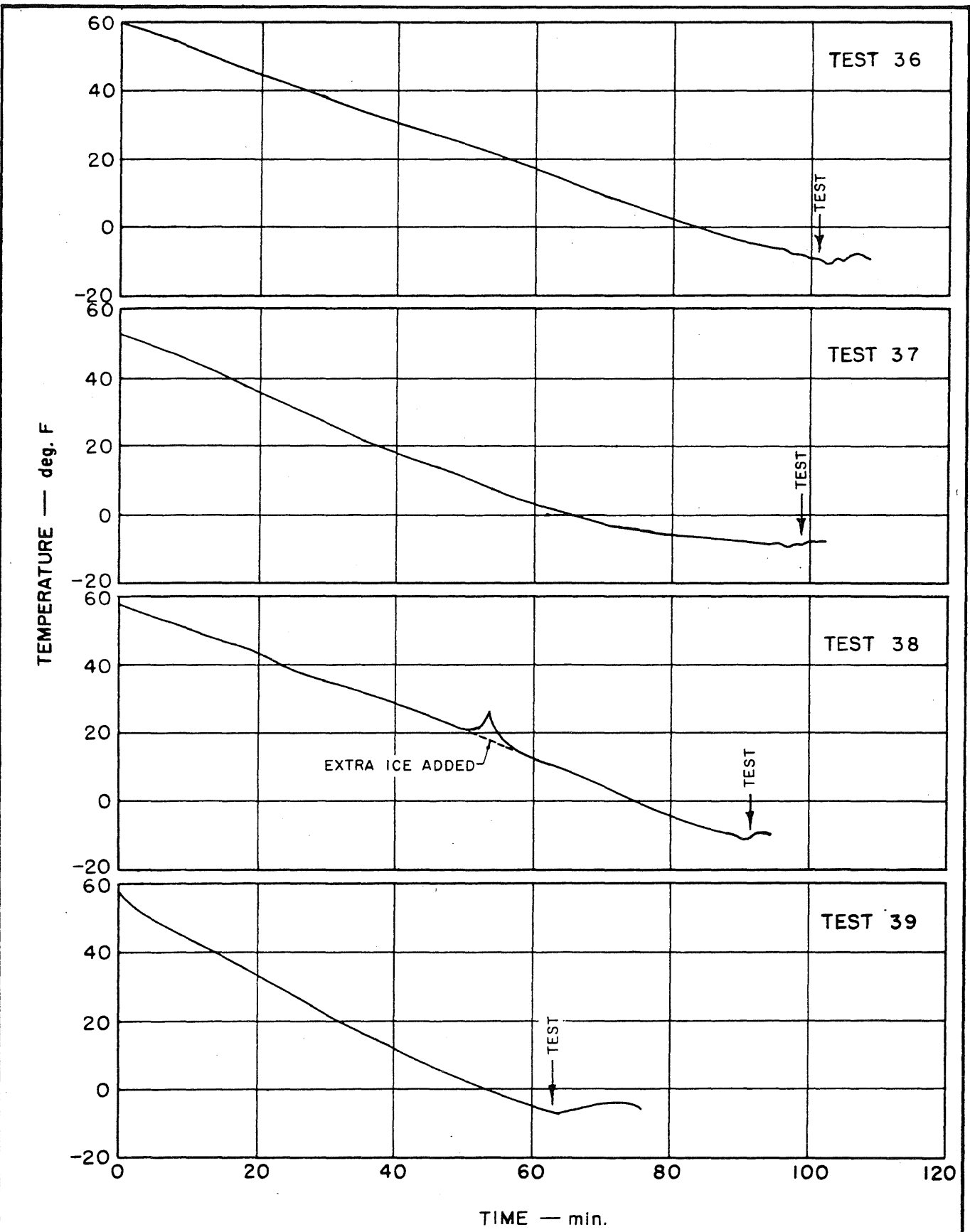
FIG. 13 AVERAGE COOLING CURVES — TESTS 36, 37, 38, AND 39
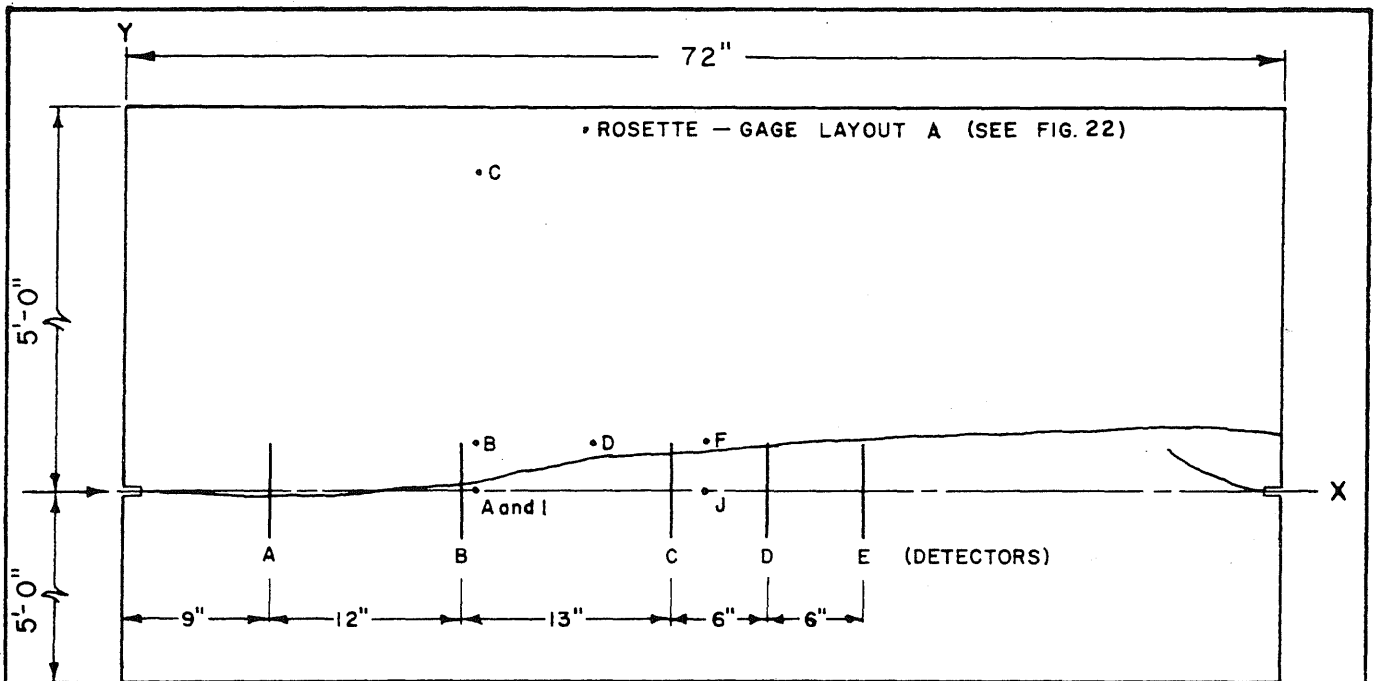
Y ← 72" → X

5'-0"

5'-0"

• ROSETTE — GAGE LAYOUT A (SEE FIG. 22)

•C

•B   •D   •F

A and I   •J

A   B   C   D   E   (DETECTORS)

9"   12"   13"   6"   6"

Rosette No.	Strain Gage No.	Orien-tation	X (in.)	Y (in.)	Test Load Strain (in./in.)	Distance to Fracture (in.)	CRACK PATH X (in.)	Y (in.)
A	1	V	22.0	0	.00067	0.7	1.1	0
	2	H	22.3	0	-.00019	0.8	9	-0.2
	3	D	22.3	0.3	.00024	0.5	15	0
B	4	V	22.0	3.0	.00067	-2.3	18	0.1
	5	H	22.3	3.0	-.00019	-2.2	19	0.2
	6	D	22.3	3.3	.00024	-2.6	22	0.7
C	7	V	22.0	20.0	.00068	-19.0	24	1.2
	8	H	22.3	20.0	-.00018	-19.0	28.5	1.9
	9	D	22.3	20.3	.00026	-19.0	36	2.5
D	10	V	29.0	3.0	.00068	-1.1	45	3.2
	11	H	29.3	3.0	-.00019	-1.0	48	3.4
	12	D	29.3	3.3	.00026	-1.3	54	3.5
F	16	V	36.0	3.0	.00069	-0.5	60	3.7
	17	H	36.3	3.0	-.00018	-0.5	66	3.9
	18	D	36.3	3.3	.00029	-0.8	69	3.9
I	25	V	22.0	0	.00052	0.7	70	3.8
	26	H	22.3	0	-.00017	0.8	72	3.6
	27	D	22.3	0.3	.00016	0.5		
J	28	V	36.0	0	.00053	2.5		
	29	H	36.3	0	-.00018	2.6		
	30	D	36.3	0.3	.00019	2.3		

DYNAMIC STRAIN GAGES

FIG. 14   INSTRUMENTATION LAYOUT AND CRACK PATH — TEST 33

DYNAMIC STRAIN GAGES

Rosette No.	Strain Gage No.	Orientation	X (in.)	Y (in.)	Test Load Strain (in./in.)	Distance to Fracture (in.)
A	1	V	22.0	0	.00068	+3.6
	2	H	22.3	0	-.00018	+3.6
	3	D	22.3	+0.3	.00028	+3.3
B	4	V	29.0	0	.00066	+4.4
	5	H	29.3	0	-.00018	+4.4
	6	D	29.3	+0.3	.00026	+4.1
C	7	V	29.0	+3.0	.00065	+1.4
	8	H	29.3	+3.0	-.00018	+1.4
	9	D	29.3	+3.3	.00019	+1.1
D	10	V	29.0	+6.0	.00068	-1.6
	11	H	29.3	+6.0	-.00018	-1.6
	12	D	29.3	+6.3	.00024	-1.9
E	13	V	29.0	+9.0	.00067	-4.6
	14	H	29.3	+9.0	-.00018	-4.6
	15	D	29.3	+9.3	.00023	-4.9
F	16	V	36.0	0	.00066	+4.8
	17	H	36.3	0	-.00018	+4.8
	18	D	36.3	+0.3	.00021	+4.5
H	22	V	36.0	+6.0	.00066	-1.2
	23	H	36.3	+6.0	-.00018	-1.2
	24	D	36.3	+6.3	.00015	-1.5
I	25	V	36.0	+9.0	.00067	-4.2
	26	H	36.3	+9.0	-.00019	-4.2
	27	D	36.3	+9.3	.00019	-4.5
J	28	V	22.0	0	.00057	+3.6
	29	H	22.3	0	-.00017	+3.6
	30	D	22.3	+0.3	.00021	+3.3
K	31	V	36.0	0	.00057	+4.8
	32	H	36.3	0	-.00017	+4.8
	33	D	36.3	+0.3	.00021	+4.5
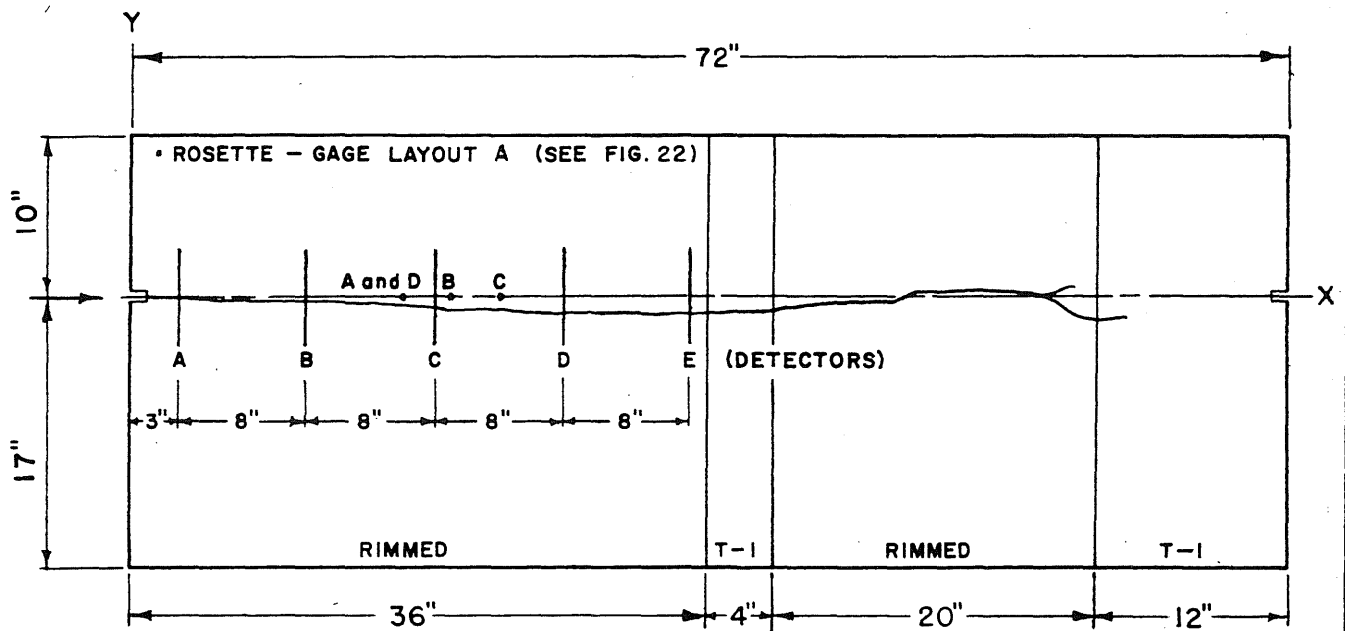
CRACK PATH

X (in.)	Y (in.)
1.1	0
4	.2
6	.4
12	1.5
16.5	2.5
18	2.6
22	3.6
24	3.8
29	4.4
36	4.8
42	5.5
48	5.6
54	5.8
60	6.0
66	6.1
72	6.1

FIG. 15   INSTRUMENTATION LAYOUT AND CRACK PATH — TEST 34

ROSETTE — GAGE LAYOUT A (SEE FIG. 22)

72"

10"

17"

Y

A and D B C

A   B   C   D   E   (DETECTORS)

X

3" 8" 8" 8" 8"

RIMMED   T-1   RIMMED   T-1

36"   4"   20"   12"

DYNAMIC STRAIN GAGES

CRACK PATH

Rosette No.	Strain Gage No.	Orientation	X (in.)	Y (in.)	Test Load Strain (in./in.)	Distance to Fracture (in.)
A	1	V	17.0	0	.00092	-0.5
	2	H	17.3	0	-.00024	-0.5
	3	D	17.3	+0.3	.00035	-0.8
B	4	V	20.0	0	.00093	-0.6
	5	H	20.3	0	-.00022	-0.6
	6	D	20.3	+0.3	.00036	-0.9
C	7	V	23.0	0	.00092	-0.8
	8	H	23.3	0	-.00022	-0.8
	9	D	23.3	+0.3	.00038	-1.1
D	10	V	17.0	0	.00094	-0.5
	11	H	17.3	0	-.00026	-0.5
	12	D	17.3	+0.3	.00029	-0.8

X (in.)	Y (in.)
1.1	0
11	-.2
14.5	-.3
17	-.5
20	-.6
23	-.8
30	-1.1
35	-1.1
40.4	-.9
44	-.3
48.5	0
53	+.3
57	0
60	-1.4
62	Fracture arrested in T-1

FIG. 16   INSTRUMENTATION   LAYOUT   AND   CRACK   PATH — TEST   35
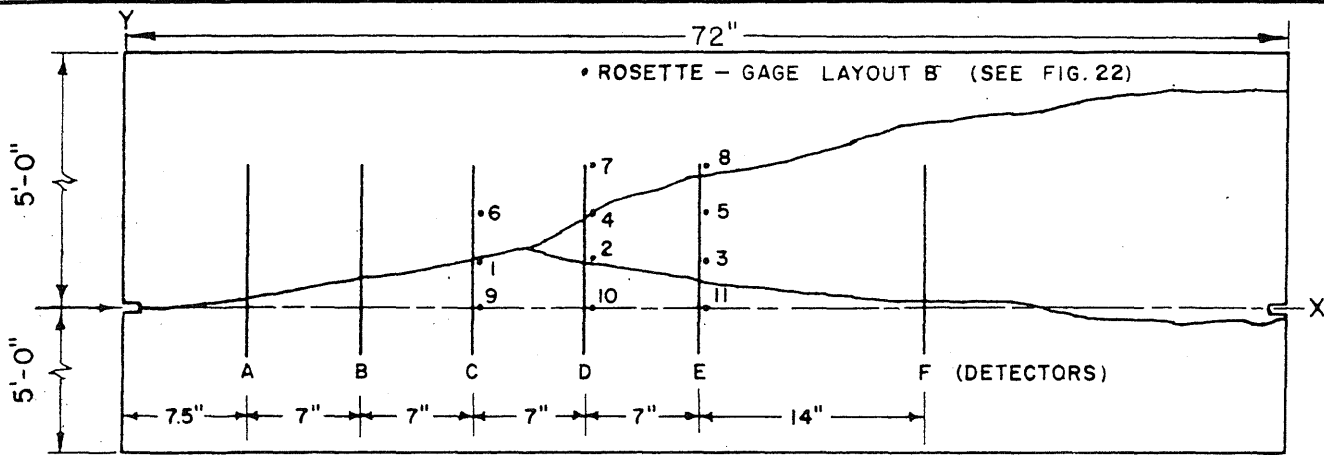
DYNAMIC STRAIN GAGES

Rosette No.	Strain Gage No.	Orientation	X (in.)	Y (in.)	Test Load Strain (in./in.)	Distance to Fracture (in.)
1	1	H	22.0	3.0	-.00016	0.0 (Lower)
	2	D	22.3	3.3	.00022	0.0 "
	3	V	22.0	3.3	.00070	0.15 "
2	6	H	29.0	3.0	-.00017	0.15 "
	7	D	29.3	3.3	.00026	0.50 "
	8	V	29.0	3.3	.00074	0.55 "
3	11	H	36.0	3.0	-.00017	1.35 "
	12	D	36.3	3.3	.00027	1.80 "
	13	V	36.0	3.3	.00070	1.70 "
4	16	H	29.0	6.0	-.00016	0.0 (Upper)
	17	D	29.3	6.3	.00020	0.10 "
	18	V	29.0	6.3	.00071	0.10 "
5	21	H	36.0	6.0	-.00017	2.60 "
	22	D	36.3	6.3	.00026	2.15 "
	23	V	36.0	6.3	.00069	2.20 "
6	4	D	22.3	6.3	.00017	-3.00 (Lower)
	5	V	22.0	6.3	.00070	-3.10 "
	24	H	22.0	6.0	-.00016	-2.80 "
7	26	H	29.0	9.0	-.00015	-3.00 (Upper)
	27	D	29.3	9.3	.00026	-3.10 "
	28	V	29.0	9.3	.00072	-3.30 "
8	29	H	36.0	9.0	-.00017	-0.45 "
	32	D	36.3	9.3	.00027	-0.80 "
	31	V	36.0	9.3	.00071	-0.75 "
9	9	D	22.3	0.3	.00021	3.05 (Lower)
	10	V	22.0	0.3	.00068	2.90 "
	25	H	22.0	0.0	-.00017	3.25 "
10	14	D	29.3	0.3	.00030	2.55 "
	15	V	29.0	0.3	.00069	2.55 "
	30	H	29.0	0.0	-.00017	2.85 "
11	19	D	36.3	0.3	.00027	1.15 "
	20	V	36.0	0.3	.00070	1.15 "
	33	H	36.0	0.0	-.00017	1.65 "

CRACK PATH

X (in.)	Y (in.)	
1.1	0	
5	.2	
10	.9	
15	1.9	
20	2.6	
22	3.2	
25.0*	3.8	

	(U)	(L)
26	4.2	3.4
27	4.6	3.1
29	5.9	2.8
30	6.5	2.7
35	8.1	1.9
38	8.7	1.2
45	10.3	0.7
48	11.3	0.3
52	11.8	0.3
55	12.1	0.3
57	12.3	0
59	12.9	-0.4
65	13.5	-0.9
66.5	13.5	-1.0
69.5	13.5	-0.8
70	13.5	-1.0
72	13.6	-0.7

*Crack Branched
(U)= Upper Crack
(L)= Lower Crack

FIG. 17 INSTRUMENTATION LAYOUT AND CRACK PATH — TEST 36
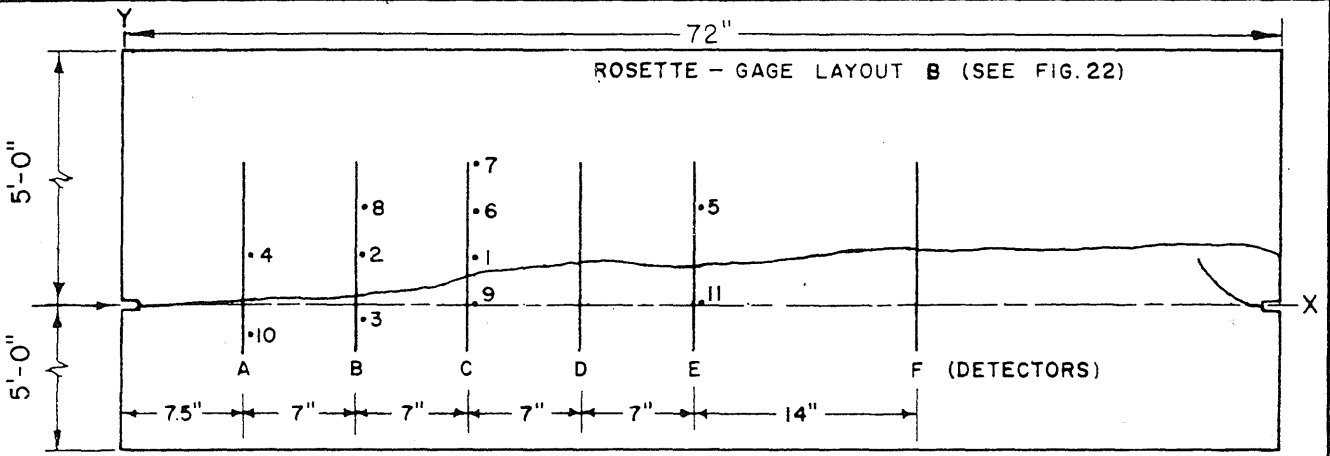
ROSETTE – GAGE LAYOUT B (SEE FIG.22)

DYNAMIC STRAIN GAGES

CRACK PATH

Rosette No.	Strain Gage No.	Orientation	X (in.)	Y (in.)	Test Load Strain (in./in.)	Distance to Fracture (in.)
1	1	H	22	3	-.00018	-1.70
	2	D	22.3	3.3	.00022	-2.10
	3	V	22	3.3	.00063	-2.10
2	6	H	15	3	-.00018	-2.40
	7	D	15.3	3.3	.00022	-2.70
	8	V	15	3.3	.00066	-2.70
3	11	H	15	-3	-.00018	+1.65
	12	D	15.3	-2.7	.00023	+1.35
	13	V	15	-2.7	.00065	+1.35
4	16	H	8	3	-.00019	-2.80
	17	D	8.3	3.3	.00023	-3.10
	18	V	8	3.3	.00067	-3.10
5	21	H	36	6	-.00017	-3.65
	22	D	36.3	6.3	.00024	-4.00
	23	V	36	6.3	.00067	-4.00
6	24	H	22	6	-.00017	-4.70
	4	D	22.3	6.3	.00021	-5.10
	5	V	22	6.3	.00067	-5.10
7	26	H	22	9	-.00017	-7.70
	27	D	22.3	9.3	.00027	-8.10
	28	V	22	9.3	.00066	-8.10
8	29	H	15	6	-.00018	-5.40
	32	D	15.3	6.3	.00026	-5.70
	31	V	15	6.3	.00068	-5.70
9	25	H	22	0	-.00016	+1.35
	9	D	22.3	.3	.00027	+1.00
	10	V	22	.3	.00060	+1.00
10	30	H	8	-3	-.00017	+2.20
	14	D	8.3	-2.7	.00018	+1.90
	15	V	8	-2.7	.00061	+1.90
11	33	H	36	0	-.00017	+2.35
	19	D	36.3	.3	.00023	+2.00
	20	V	36	.3	.00066	+2.00

X (in.)	Y (in.)
1.1	0
3	0
8	.2
15	.6
20	1.1
22	1.6
25	1.8
29	2.2
32.5	2.6
35.5	2.6
36	2.4
39	2.4
49	3.5
55	3.6
64	3.6
69	3.7
70	3.6
72	3.2

FIG. 18   INSTRUMENTATION   LAYOUT   AND   CRACK   PATH   —   TEST   37

ROSETTE — GAGE LAYOUT **B** (SEE FIG. 22)

72"

5'-0"

5'-0"

A   B   C   D   E   F (DETECTORS)

7.5"   7"   7"   7"   7"   14"

DYNAMIC STRAIN GAGES

Rosette No.	Strain Gage No.	Orientation	X (in.)	Y (in.)	Test Load Strain (in./in.)	Distance to Fracture (in.)
1	1	H	50	6	-.00017	-0.70
	2	D	50.3	6.3	.00018	-1.05
	3	V	50	6.3	.00046	-1.05
2	6	H	43	6	-.00018	-1.05
	7	D	43.3	6.3	.00019	-1.30
	8	V	43	6.3	.00056	-1.40
3	11	H	36	3	-.00017	+1.65
	12	D	36.3	3.3	.00018	+1.25
	13	V	36	3.3	.00050	+1.25
4	16	H	43	9	-.00019	-4.05
	17	D	43.3	9.3	.00021	-4.30
	18	V	43	9.3	.00056	-4.40
5	21	H	36	6	-.00017	-1.30
	22	D	36.3	6.3	.00014	-1.73
	23	V	36	6.3	.00060	-1.73
6	24	H	50	9	-.00017	-3.70
	4	D	50.3	9.3	.00015	-4.05
	5	V	50	9.3	.00056	-4.05
7	26	H	43	12	-.00018	-7.05
	27	D	43.3	12.3	.00018	-7.30
	28	V	43	12.3	.00044	-7.40
8	29	H	50	12	-.00018	-6.70
	32	D	50.3	12.3	.00023	-7.05
	31	V	50	12.3	.00057	-7.05
9	25	H	50	3	-.00017	+2.35
	9	D	50.3	3.3	.00021	+2.10
	10	V	50	3.3	.00056	+2.00
10	30	H	43	3	-.00017	+1.95
	14	D	43.3	3.3	.00028	+1.70
	15	V	43	3.3	.00056	+1.65
11	33	H	36	0	-.00018	+4.65
	19	D	36.3	.3	.00009	+4.30
	20	V	36	.3	.00054	+4.30

CRACK PATH

X (in.)	Y (in.)
1.1	0
5.0	.2
6.0	.3
10	.8
22	2.9
24	3.2
27	3.5
30	3.8
35	4.6
40	4.9
45	5.1
50	5.4
54	5.4
56	5.3
60	5.4
65	5.5
70	5.5
72	5.4

FIG. 19 INSTRUMENTATION LAYOUT AND CRACK PATH — TEST 38
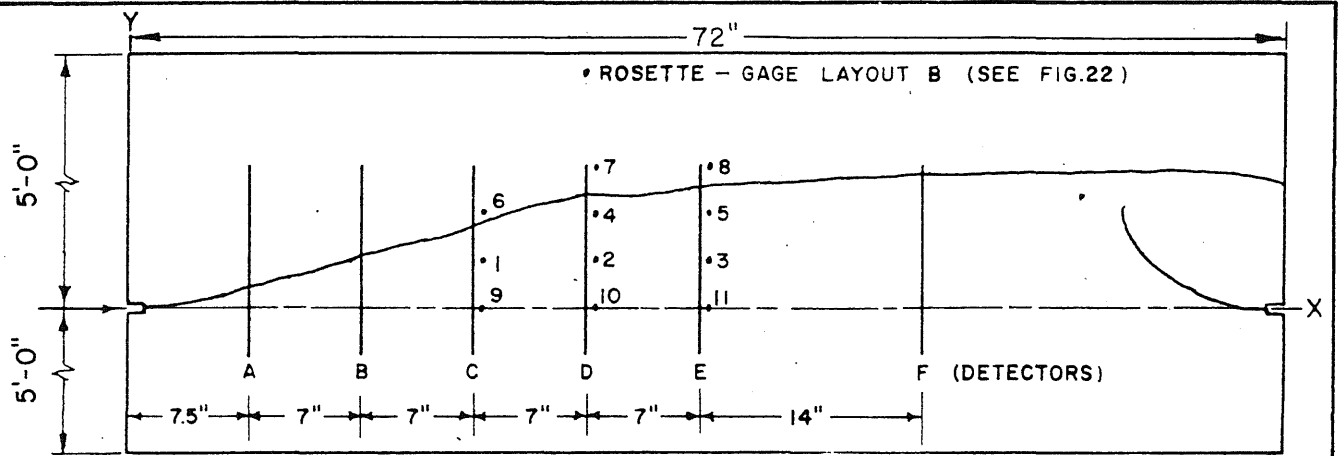
FIG. 20 INSTRUMENTATION LAYOUT AND CRACK PATH — TEST 39

DYNAMIC STRAIN GAGES

Rosette No.	Strain Gage No.	Orientation	X (in.)	Y (in.)	Test Load Strain (in./in.)	Distance to Fracture (in.)
1	1	H	22	3	-.00017	+2.29
	2	D	22.3	3.3	.00021	+2.10
	3	V	22	3.3	.00062	+1.96
2	6	H	29	3	-.00017	+4.14
	7	D	29.3	3.3	.00019	+3.90
	8	V	29	3.3	.00061	+3.85
3	11	H	36	3	-.00017	+4.50
	12	D	36.3	3.3	.00019	+4.22
	13	V	36	3.3	.00058	+4.12
4	16	H	29	6	-.00016	+1.09
	17	D	29.3	6.3	.00022	+0.88
	18	V	29	6.3	.00060	+0.85
5	21	H	36	6	-.00017	+1.55
	22	D	36.3	6.3	.00023	+1.14
	23	V	36	6.3	.00062	+1.12
6	24	H	22	6	-.00017	-0.73
	4	D	22.3	6.3	.00025	-0.90
	5	V	22	6.3	.00056	-1.08
7	26	H	29	9	-.00018	-1.76
	27	D	29.3	9.3	.00020	-2.07
	28	V	29	9.3	.00061	-2.12
8	29	H	36	9	-.00018	-1.47
	32	D	36.3	9.3	.00023	-1.80
	31	V	36	9.3	.00062	-1.85
9	25	H	22	0	-.00017	+5.27
	9	D	22.3	0.3	.00022	+5.10
	10	V	22	0.3	.00059	+4.98
10	30	H	29	0	-.00019	+7.17
	14	D	29.3	0.3	.00019	+6.85
	15	V	29	0.3	.00059	+6.89
11	33	H	36	0	-.00017	+7.50
	19	D	36.3	0.3	.00026	+7.20
	20	V	36	0.3	.00060	+7.14

CRACK PATH

X (in.)	Y (in.)
1.1	0
6	0.7
10	1.8
15	3.3
20	4.6
21	4.8
25	6.3
28	7.1
32	7.0
35	7.4
40	7.9
45	8.2
50	8.4
55	8.5
60	8.5
65	8.6
69	8.4
72	7.9

FIG. 21   TYPICAL STRAIN TRACES AND COMPUTED PRINCIPAL STRAINS
FOR ROSETTES LOCATED AT VARIOUS DISTANCES FROM
THE FRACTURE
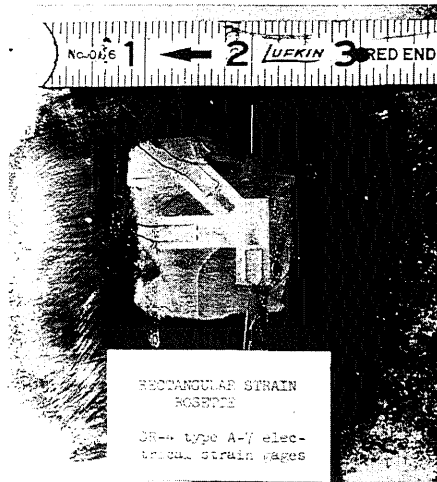
RECTANGULAR STRAIN
ROSETTE

SR-4 type A-7 elec-
trical strain gages

< 0.7 in.

◄── DIRECTION OF FRACTURE

GAGE   LAYOUT   A

TYPICAL LAYOUT FOR A-7
STRAIN GAGE ROSETTE USED
IN TESTS 36, 37, 38, and 39

< 0.7 in.
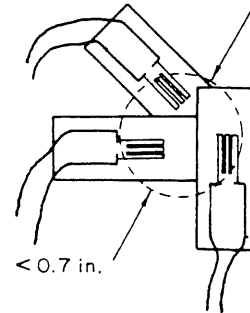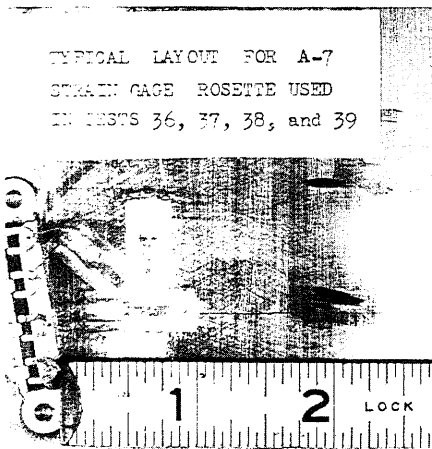
◄── DIRECTION OF FRACTURE
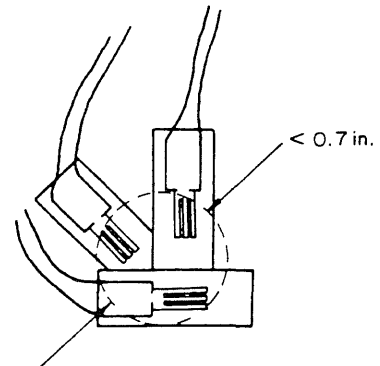
GAGE   LAYOUT   B

FIG. 22   COMPONENT GAGE LAYOUTS   A   AND   B
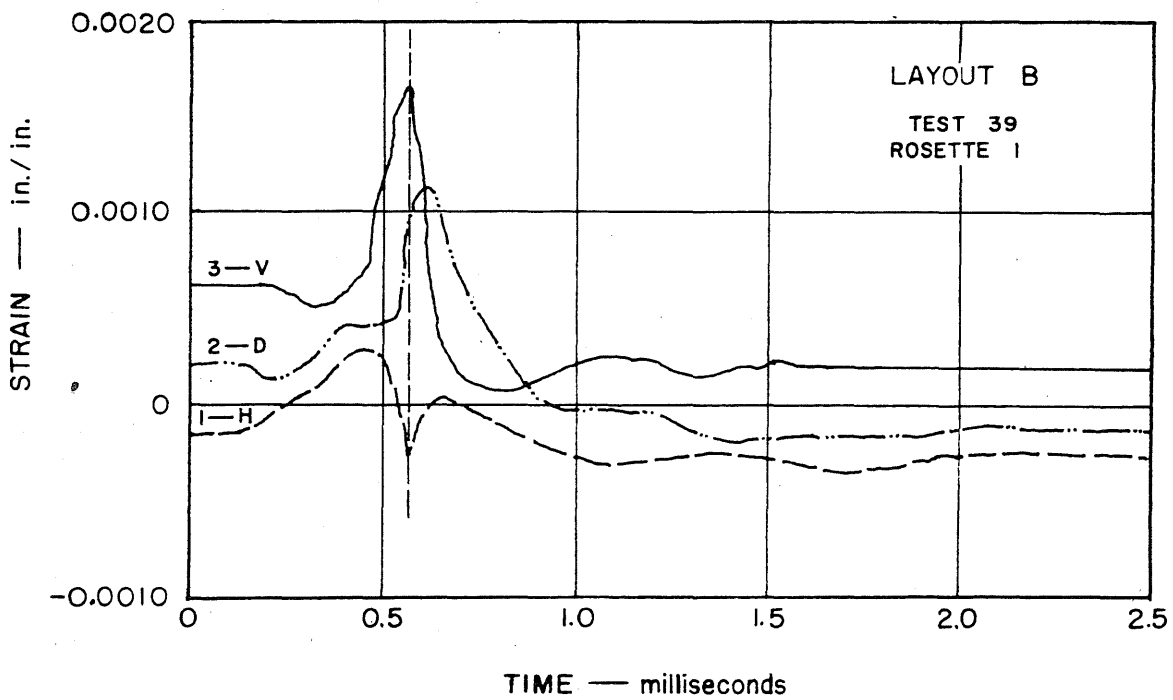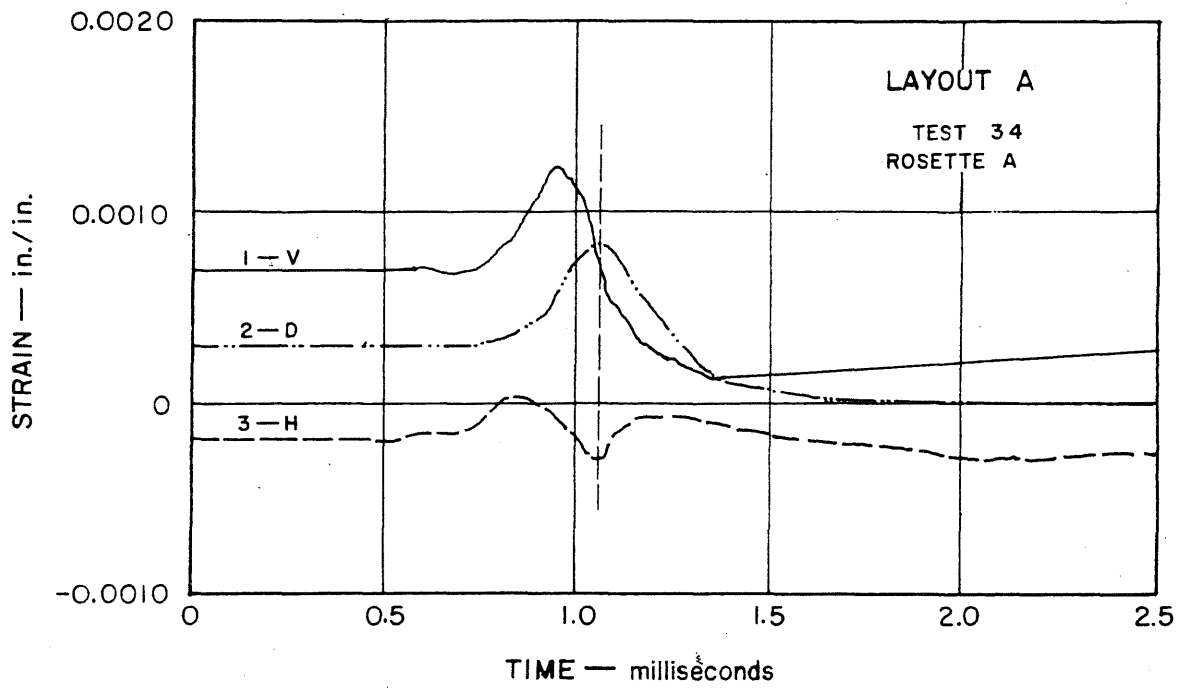
FIG. 23 TYPICAL STRAIN TRACES FROM COMPONENT
GAGE LAYOUTS A AND B
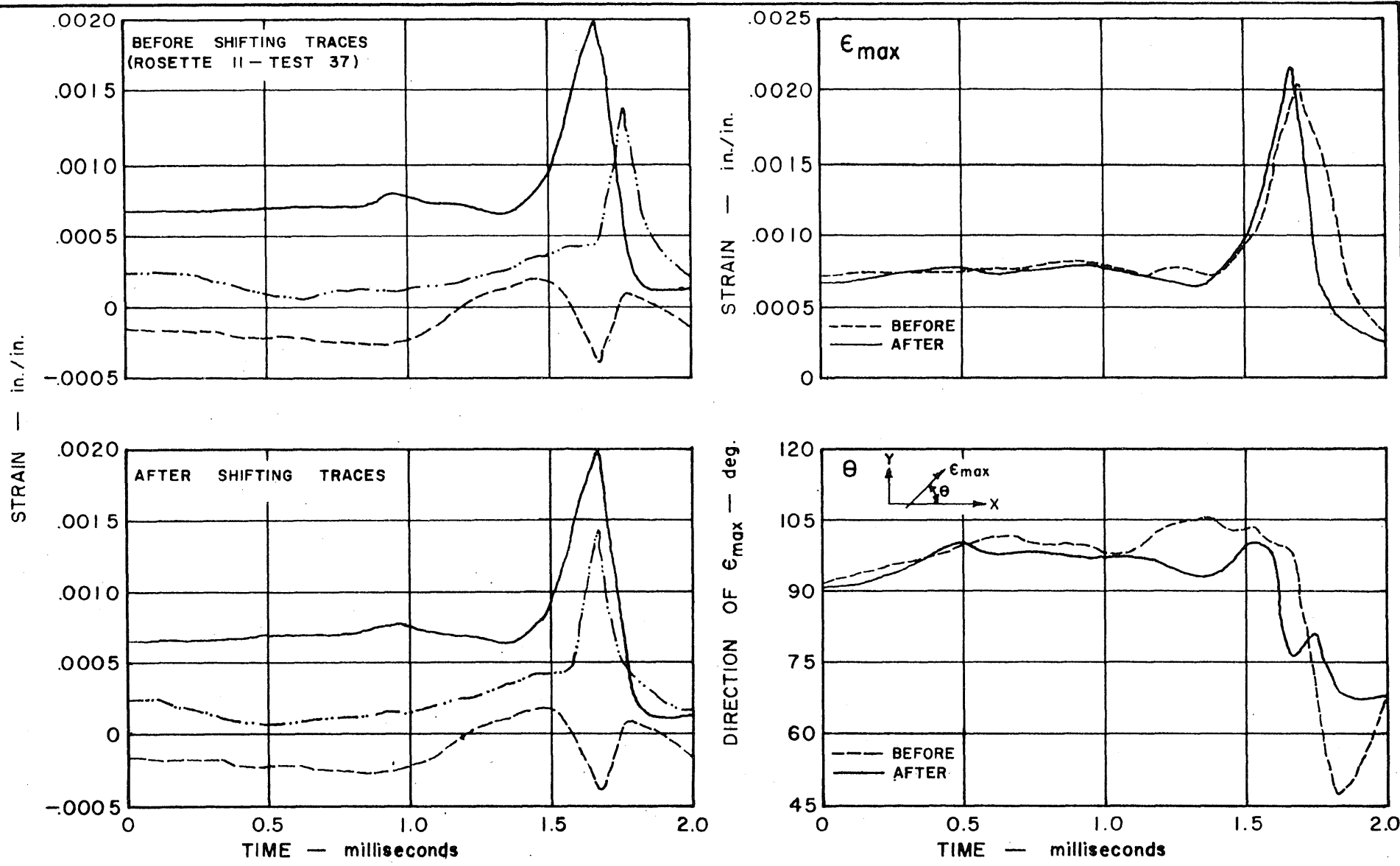
FIG. 24 EFFECT OF SHIFTING COMPONENT GAGE TRACES ON PRINCIPAL STRAINS
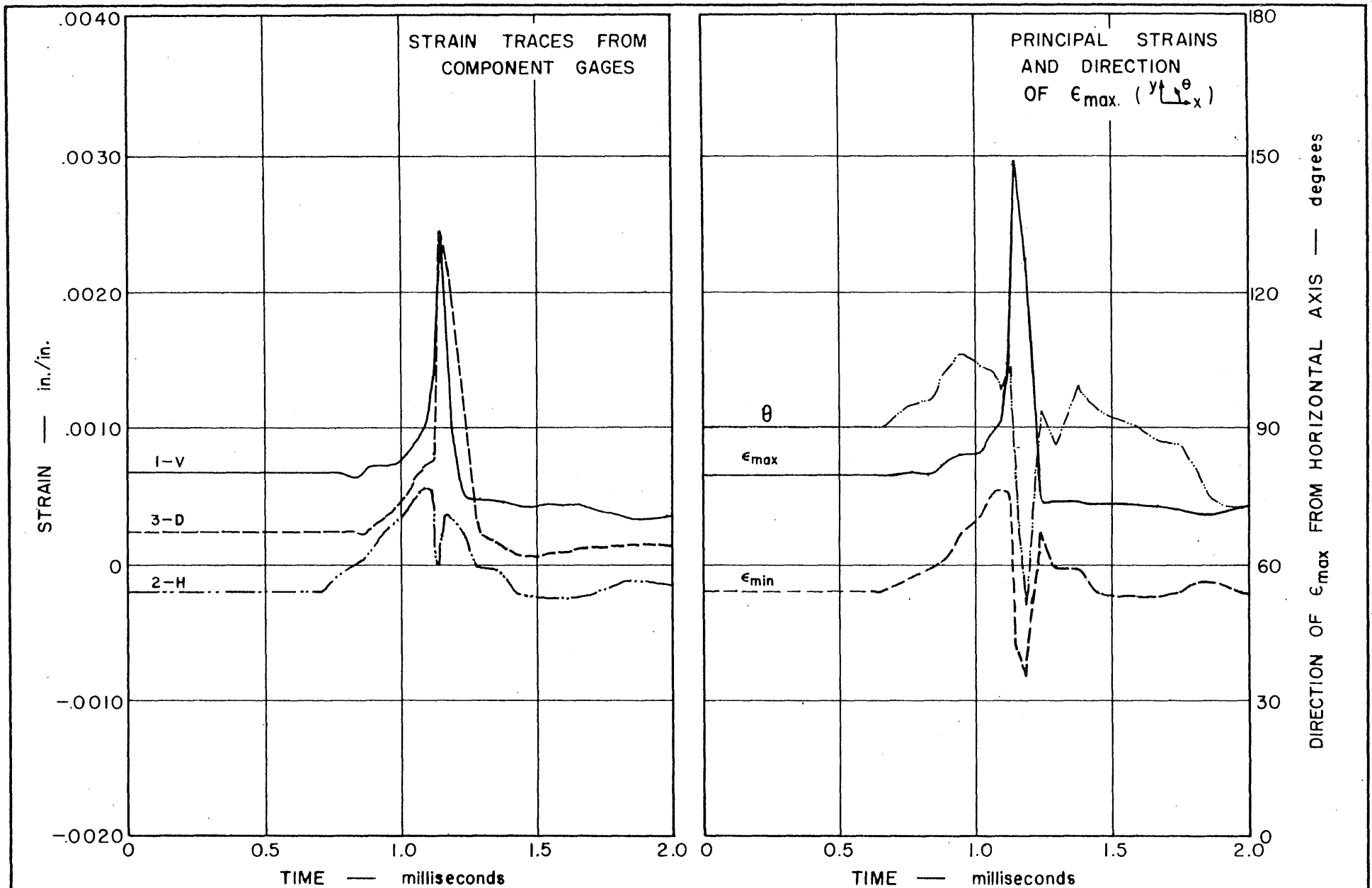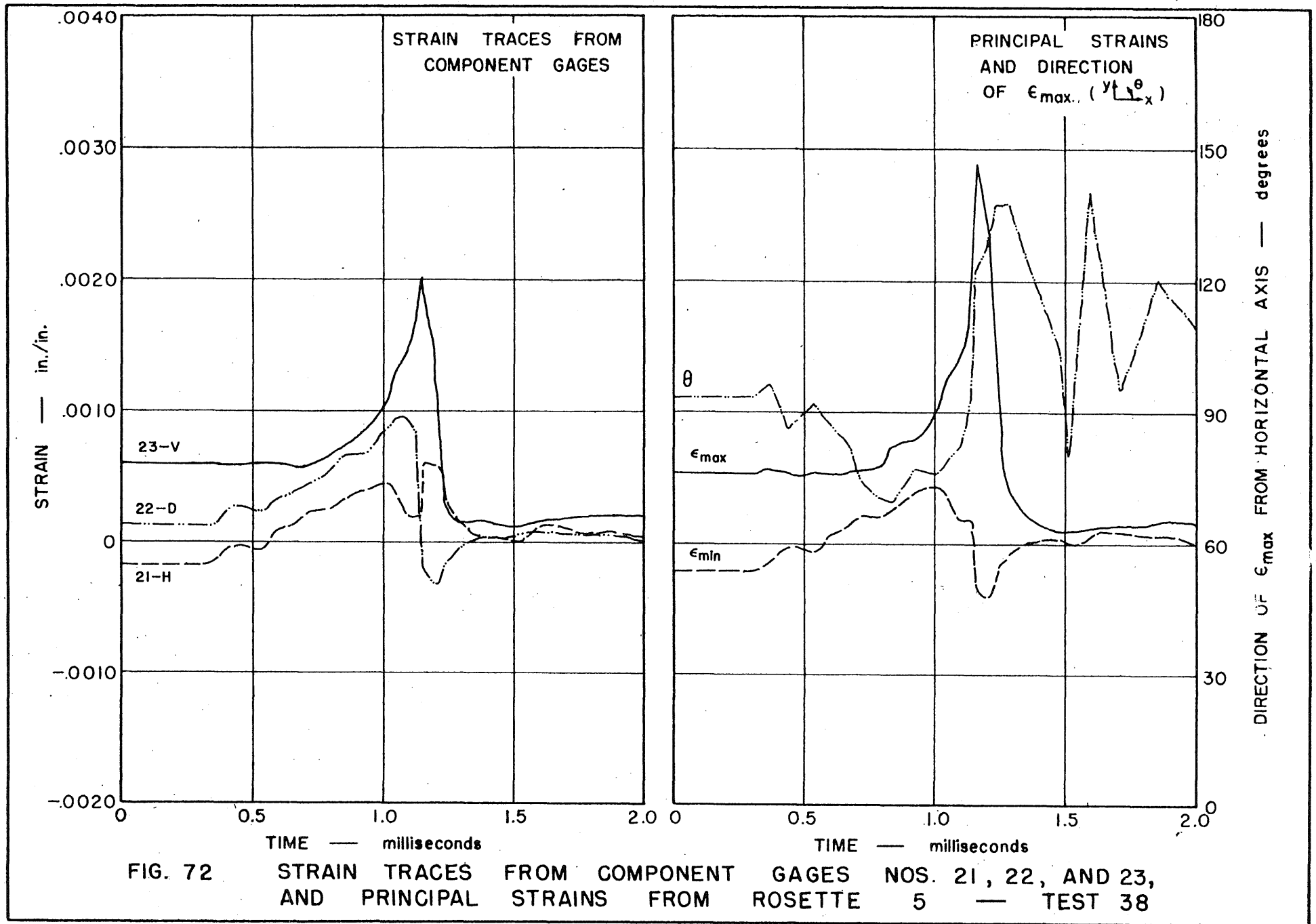
FIG. 25   STRAIN   TRACES   FROM   COMPONENT   GAGES   NOS.   1, 2, AND 3,
AND   PRINCIPAL   STRAINS   FROM   ROSETTE   A   —   TEST 33
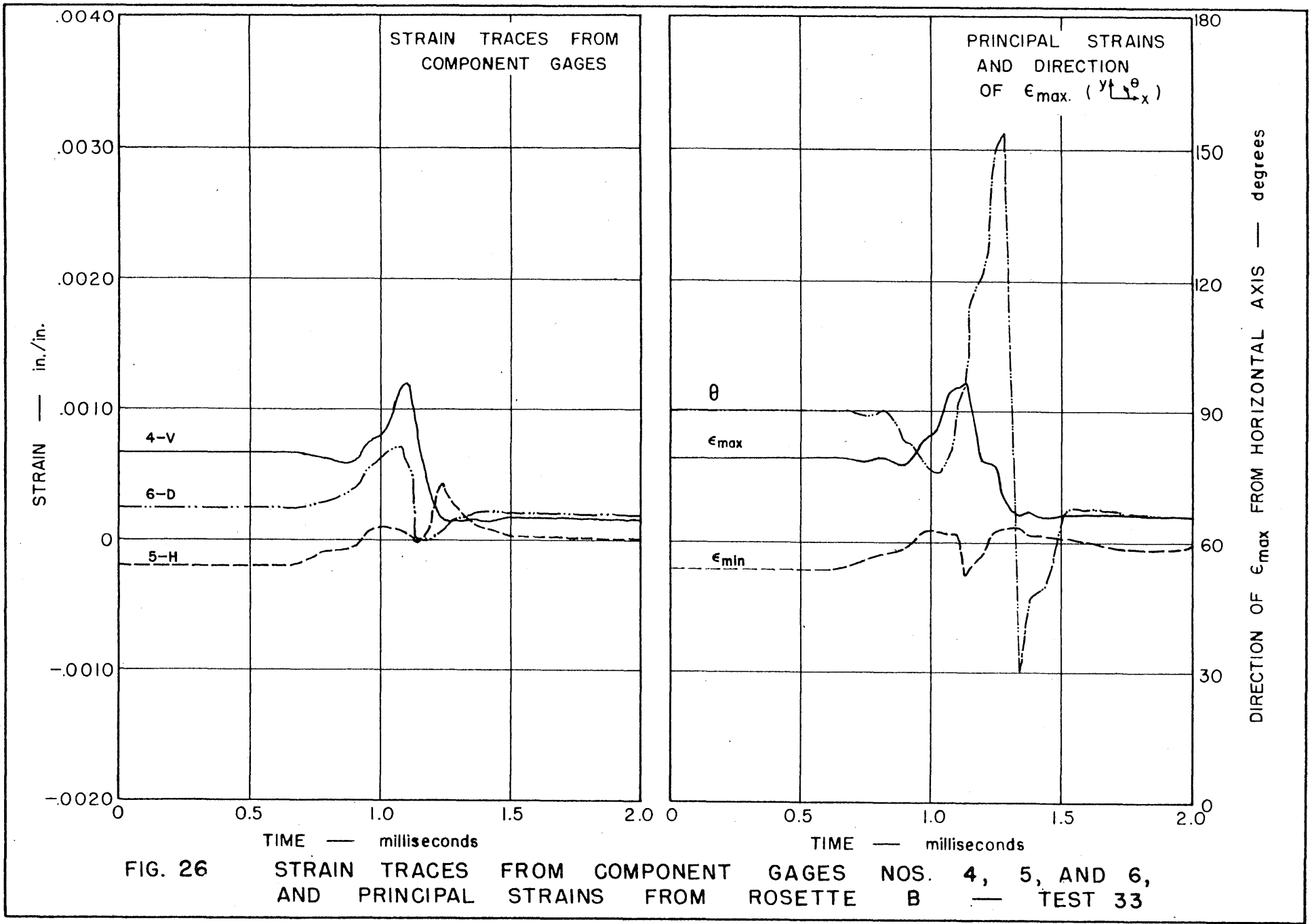
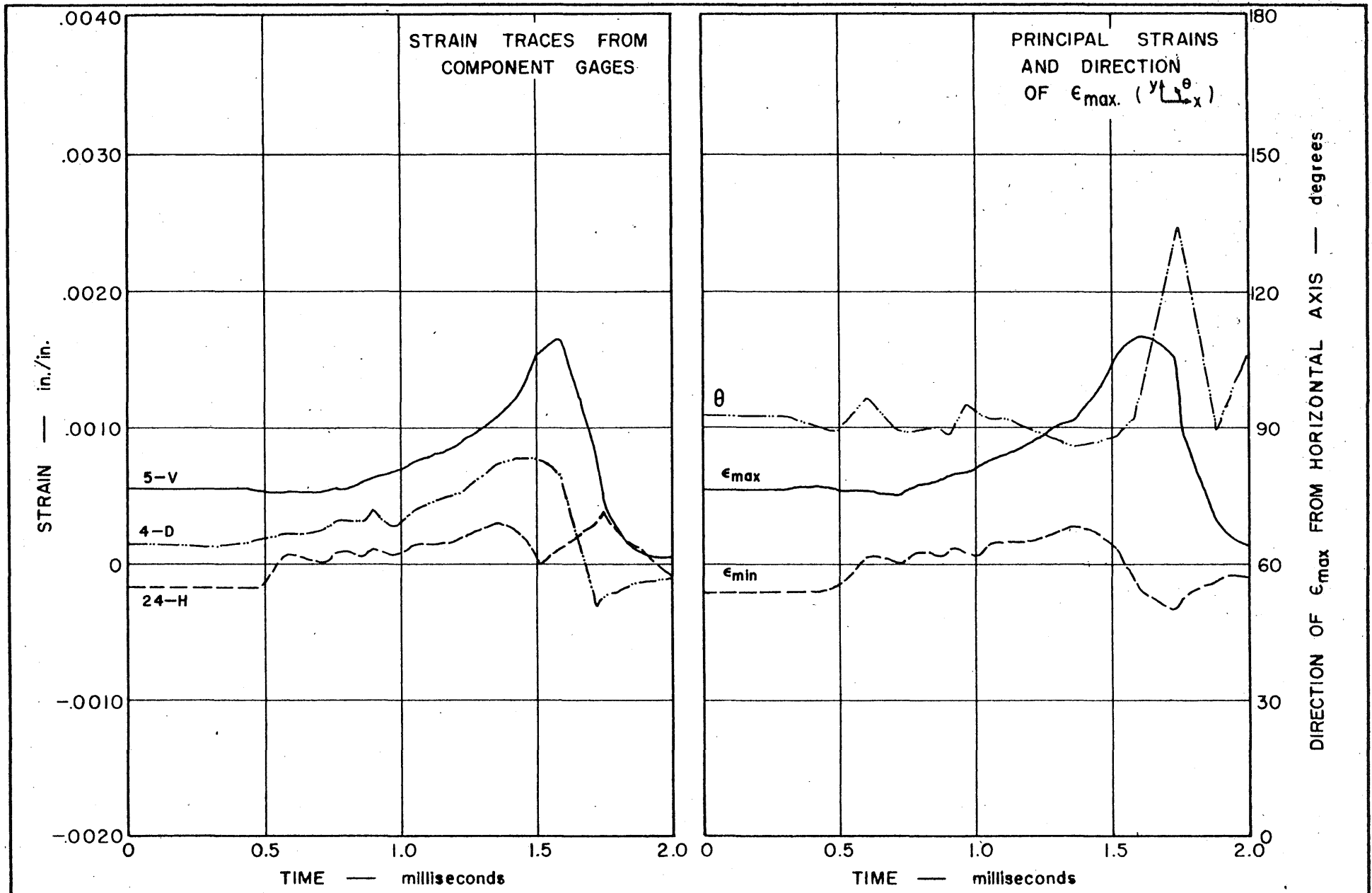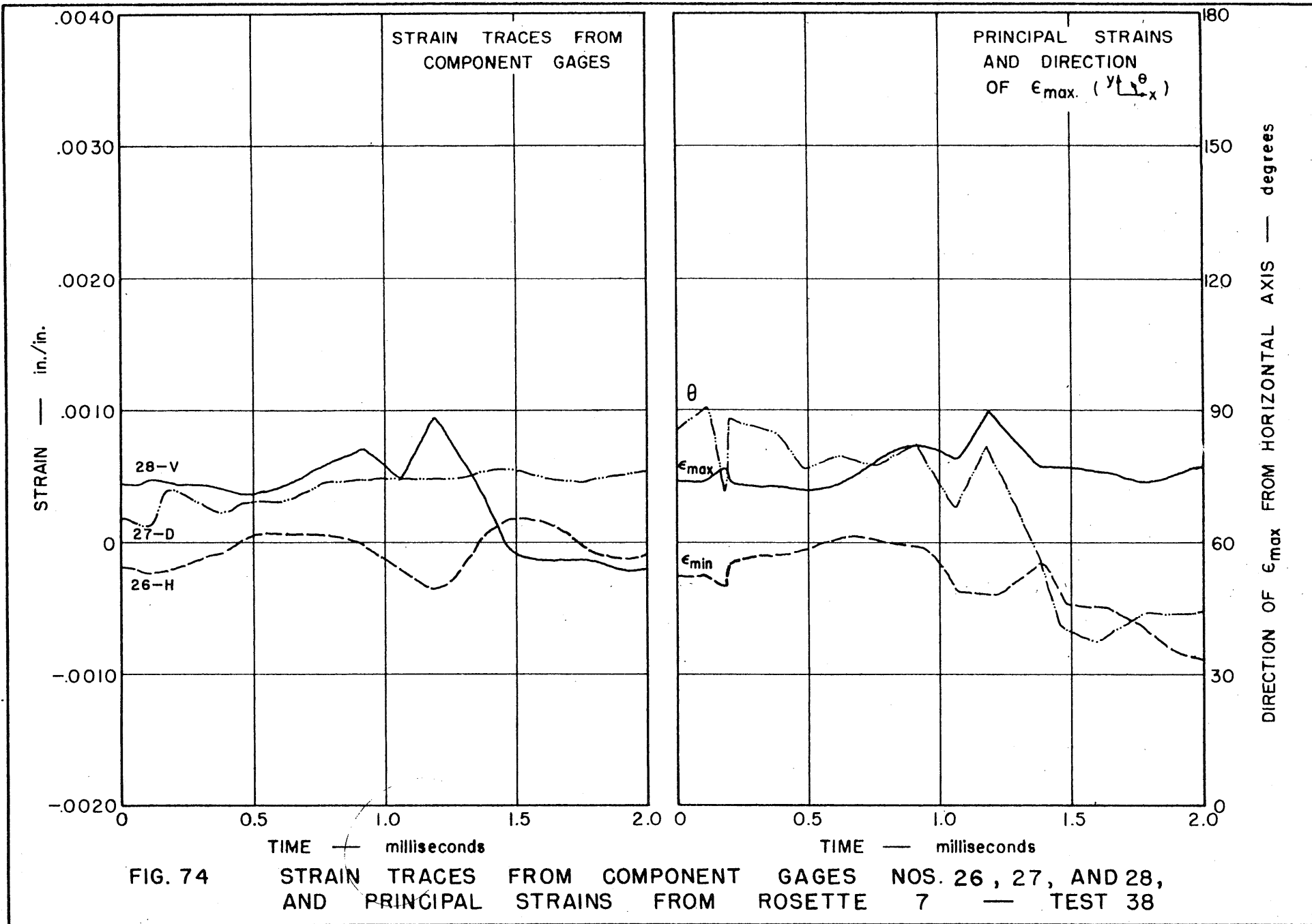FIG. 26   STRAIN   TRACES   FROM   COMPONENT   GAGES   NOS.   4,   5,   AND   6,
AND   PRINCIPAL   STRAINS   FROM   ROSETTE   B   —   TEST   33
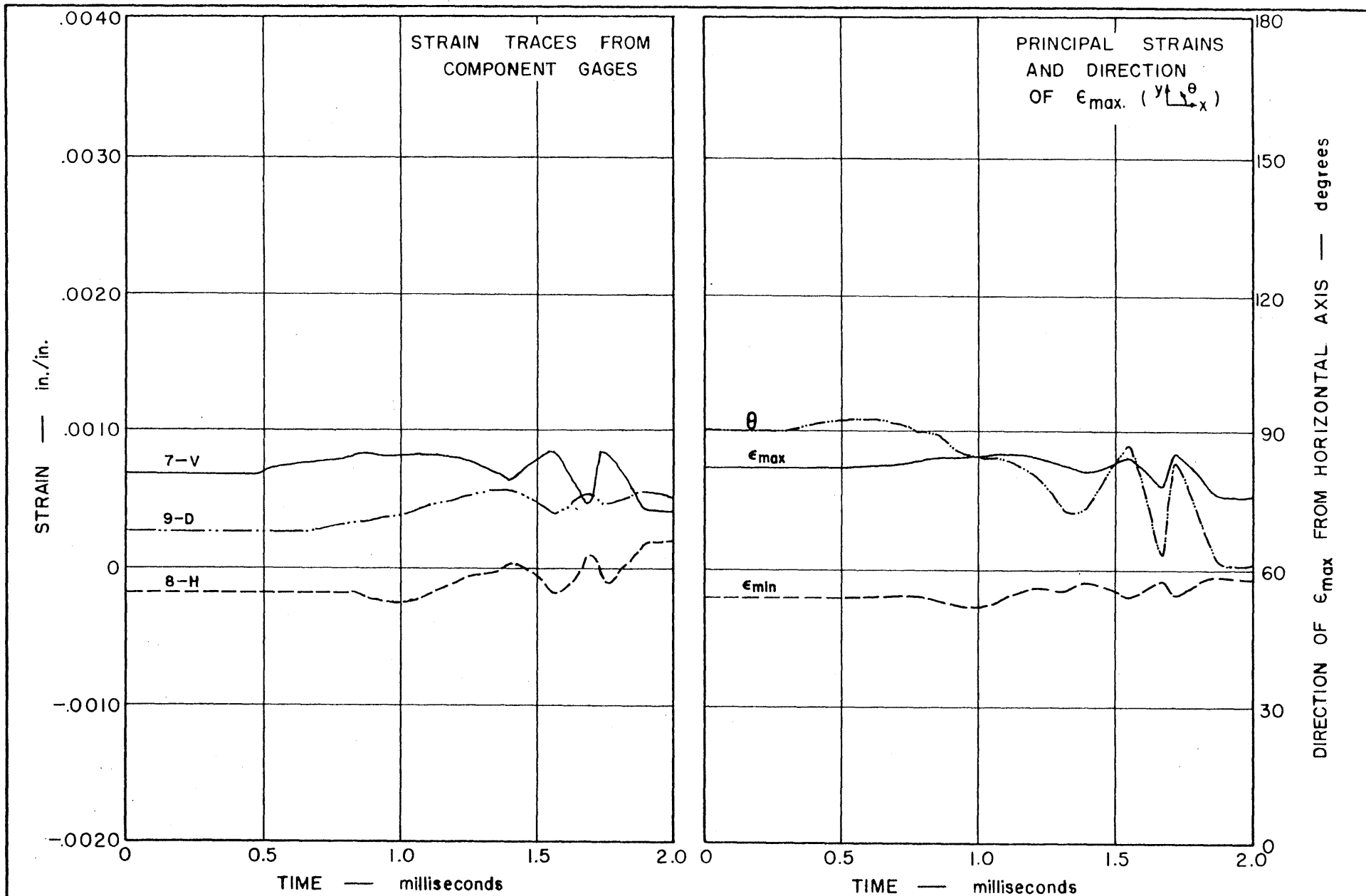
FIG. 27   STRAIN TRACES FROM COMPONENT GAGES NOS. 7, 8, AND 9,
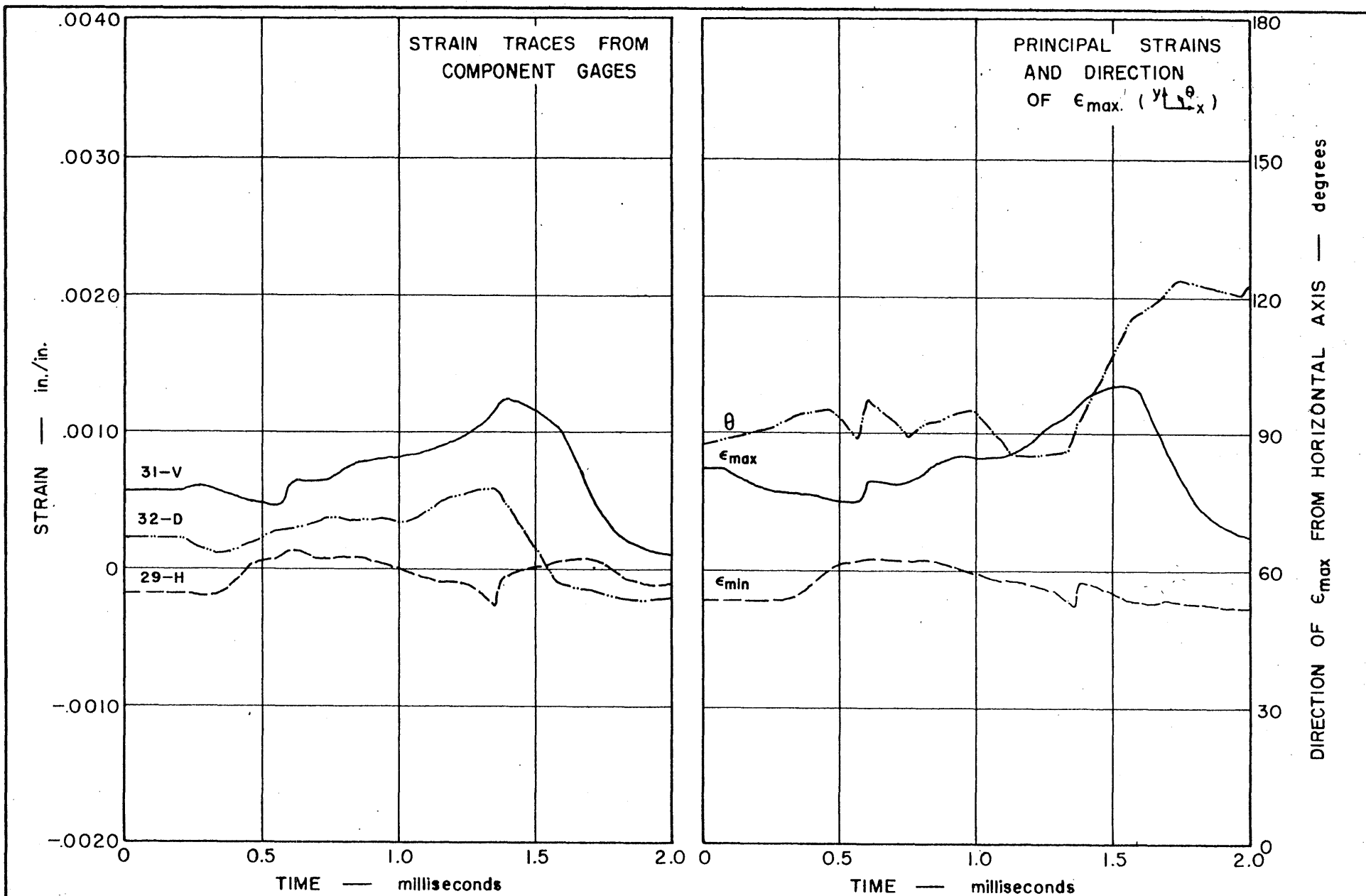AND   PRINCIPAL   STRAINS   FROM   ROSETTE   C   —   TEST 33
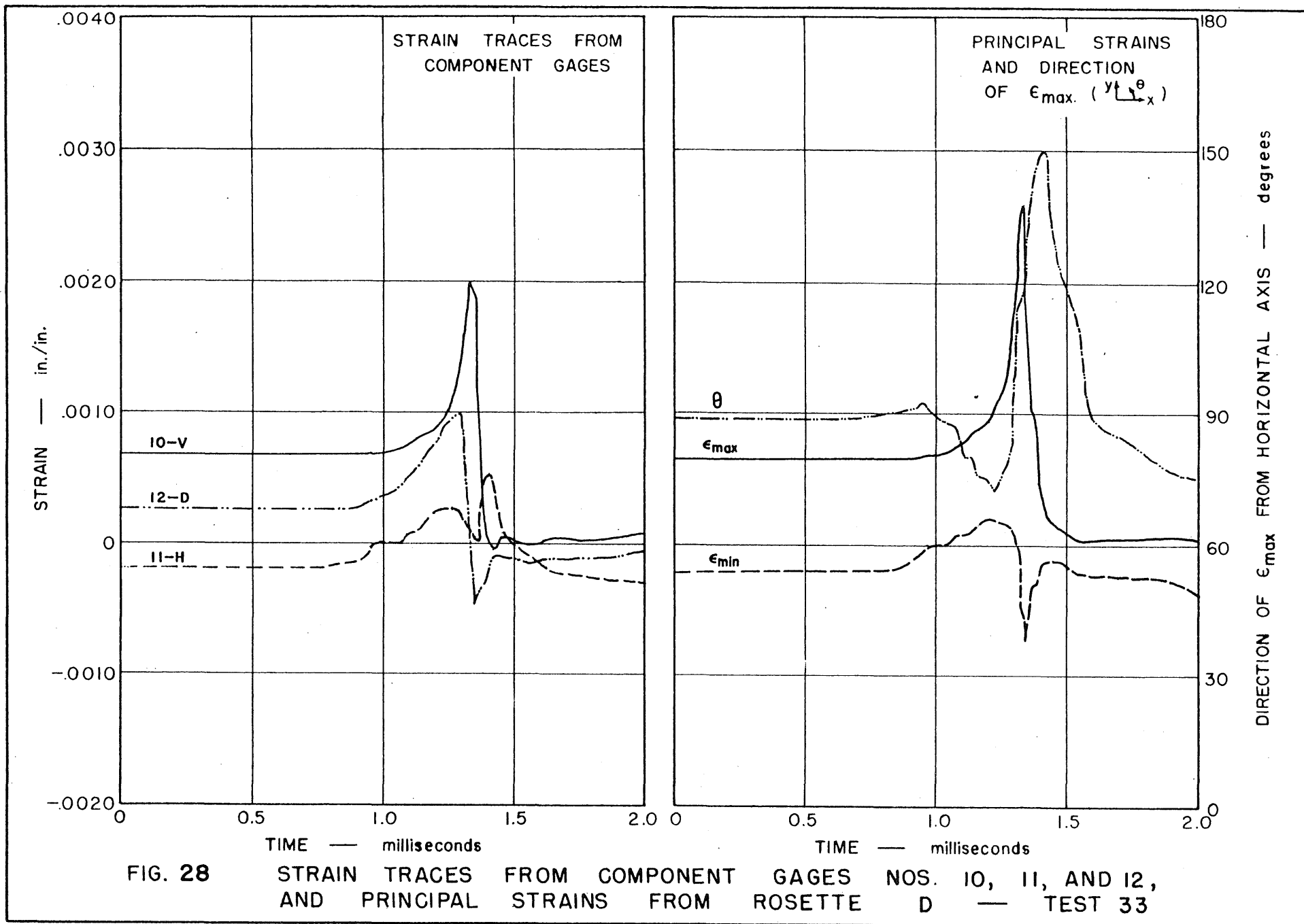
FIG. 28   STRAIN   TRACES   FROM   COMPONENT   GAGES   NOS.   10,   11,   AND   12,
AND   PRINCIPAL   STRAINS   FROM   ROSETTE   D   —   TEST 33
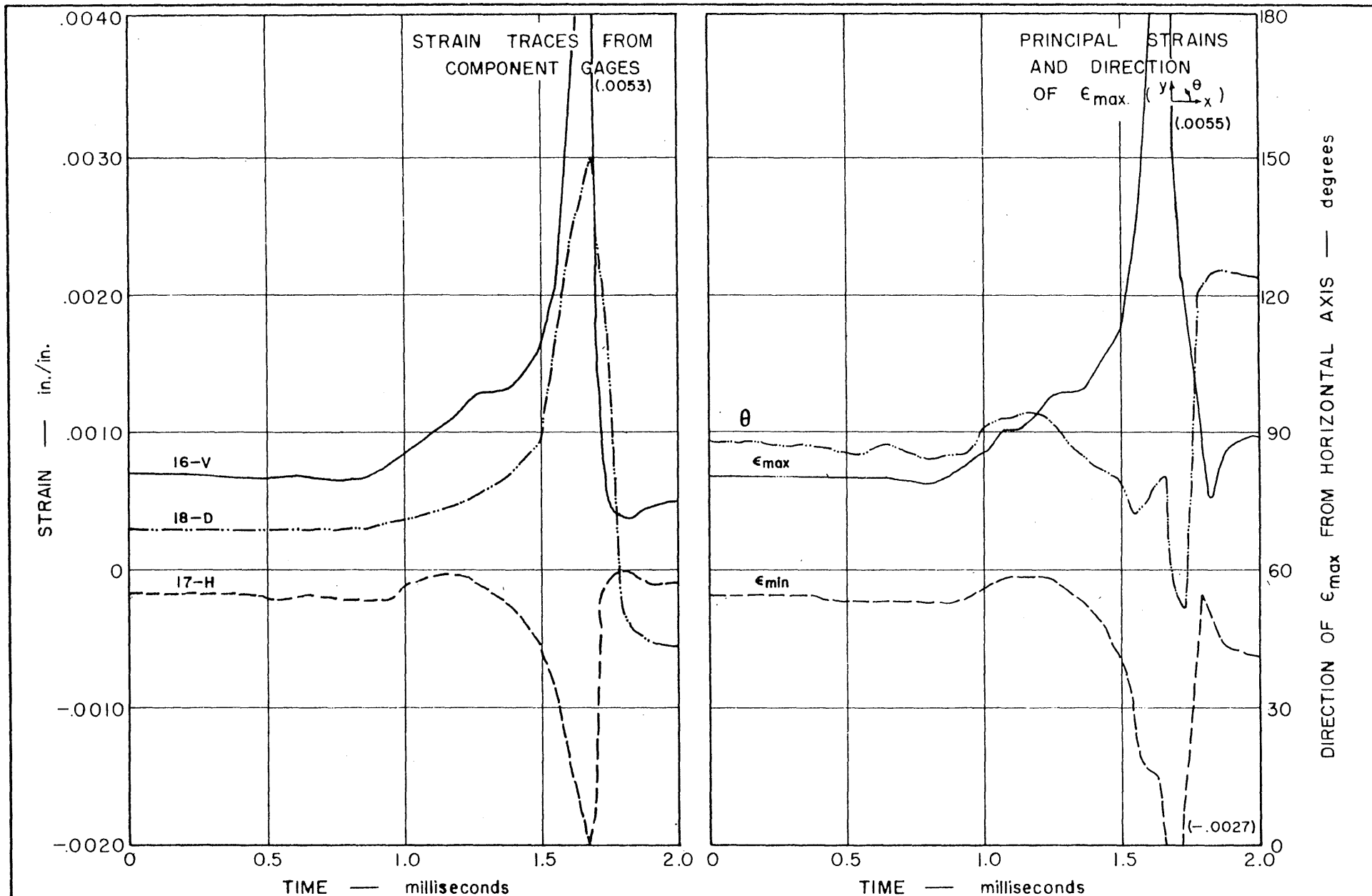
FIG. 29   STRAIN TRACES FROM COMPONENT GAGES NOS. 16, 17, AND 18,
AND PRINCIPAL STRAINS FROM ROSETTE F — TEST 33
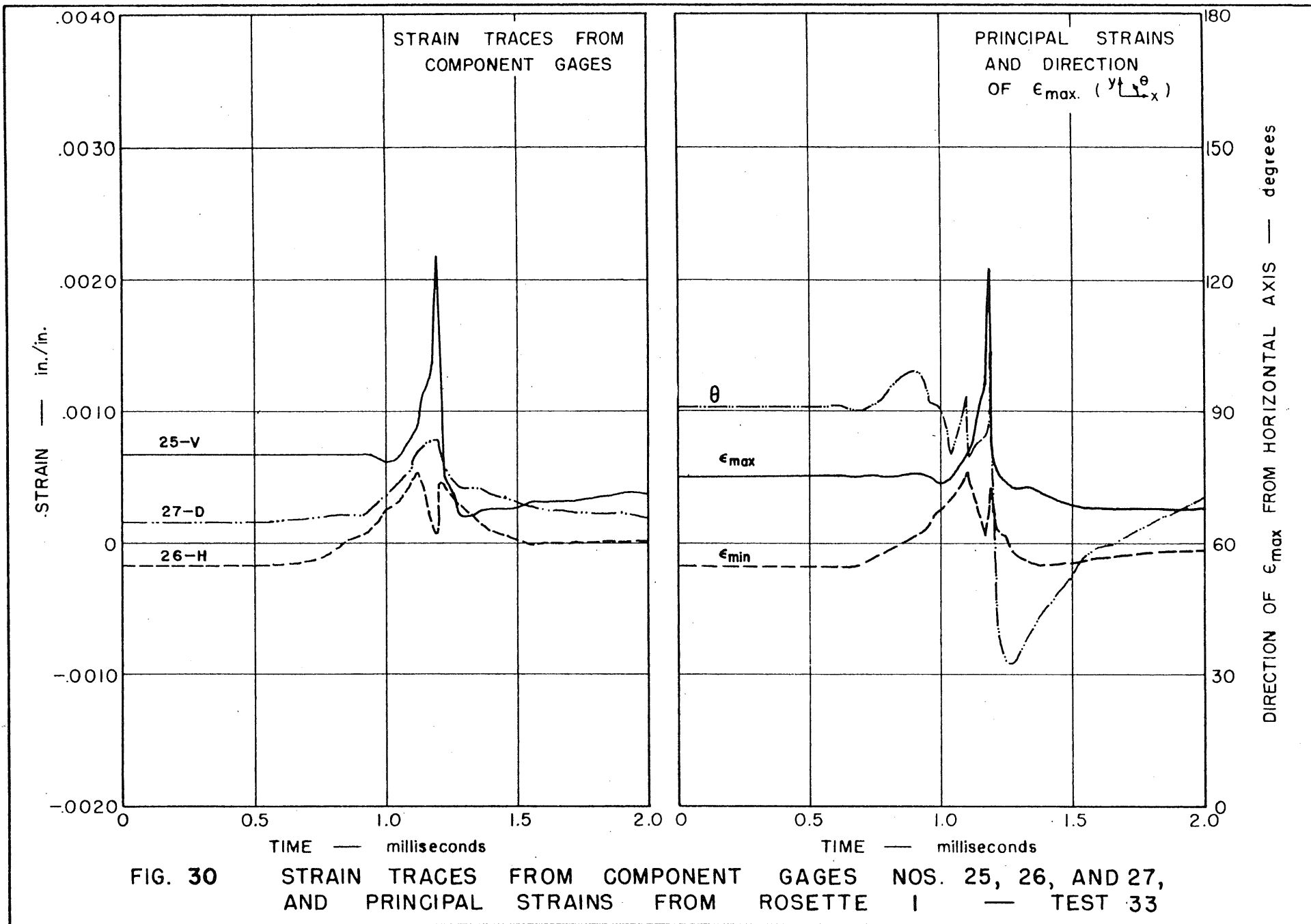
FIG. 30   STRAIN   TRACES   FROM   COMPONENT   GAGES   NOS. 25, 26, AND 27,
AND   PRINCIPAL   STRAINS   FROM   ROSETTE   I   —   TEST 33
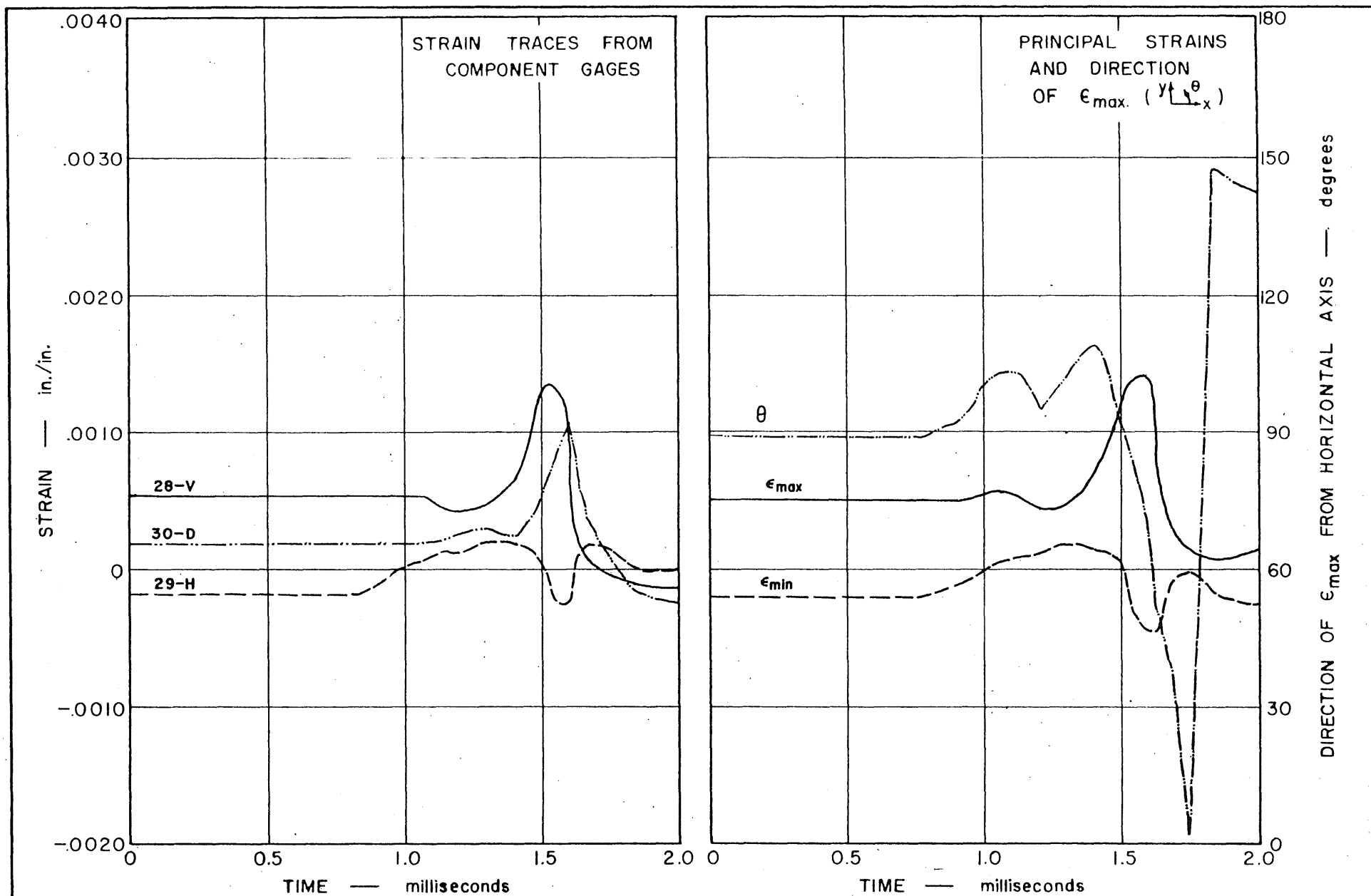
FIG. 31   STRAIN   TRACES   FROM   COMPONENT   GAGES   NOS. 28, 29, AND 30,
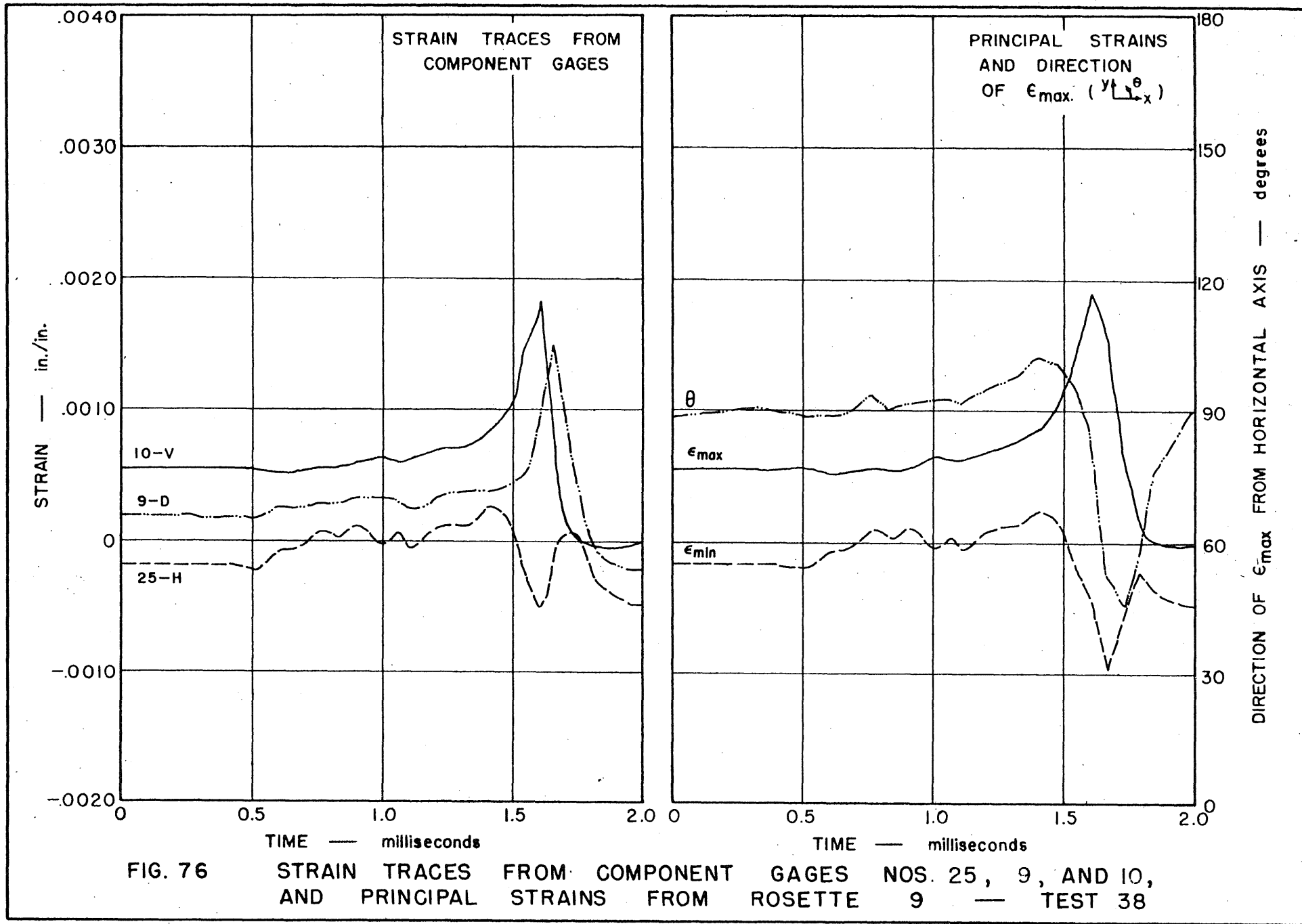   AND   PRINCIPAL   STRAINS   FROM   ROSETTE   J   —   TEST   33
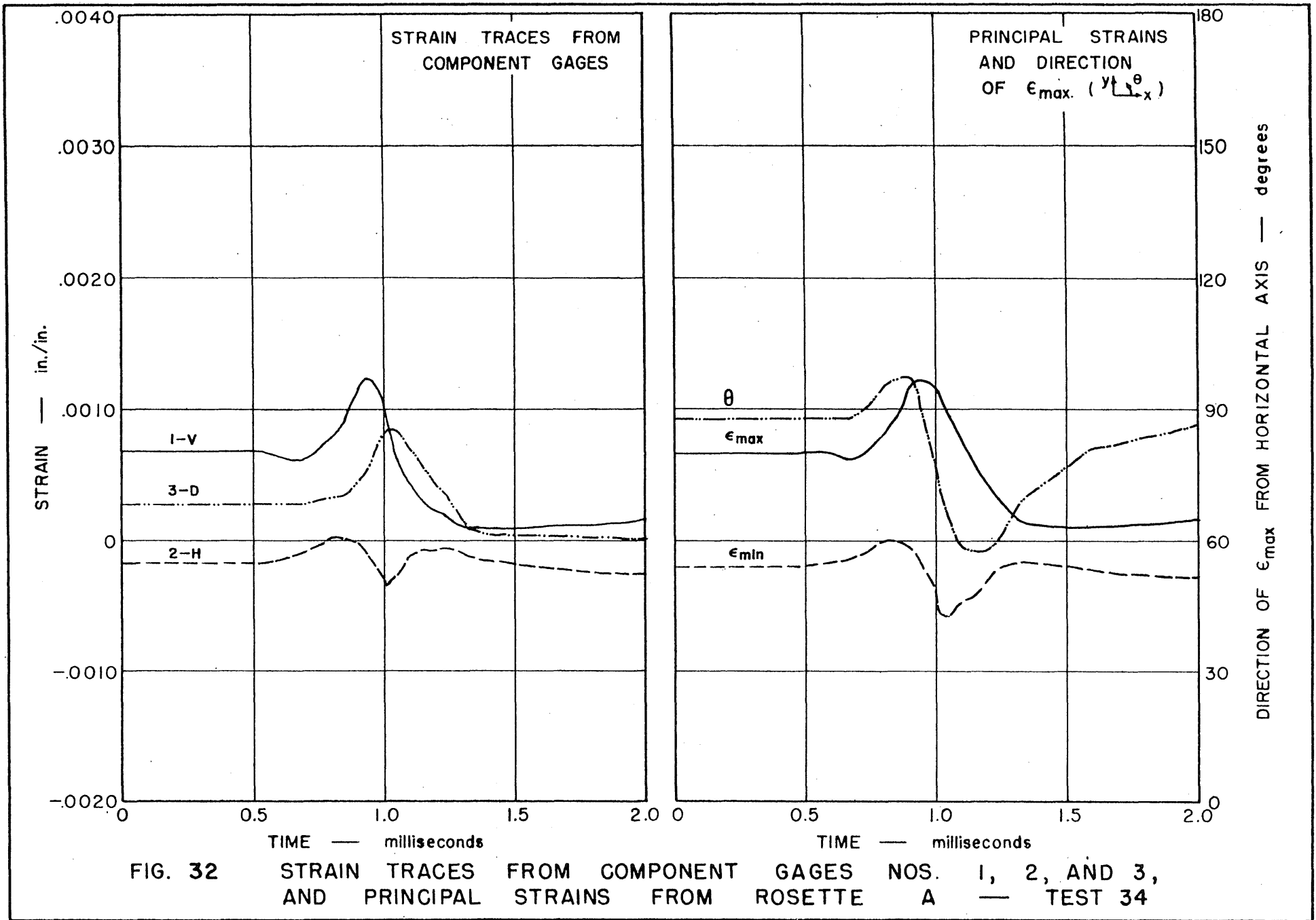
FIG. 32   STRAIN   TRACES   FROM   COMPONENT   GAGES   NOS.   1,   2, AND 3,
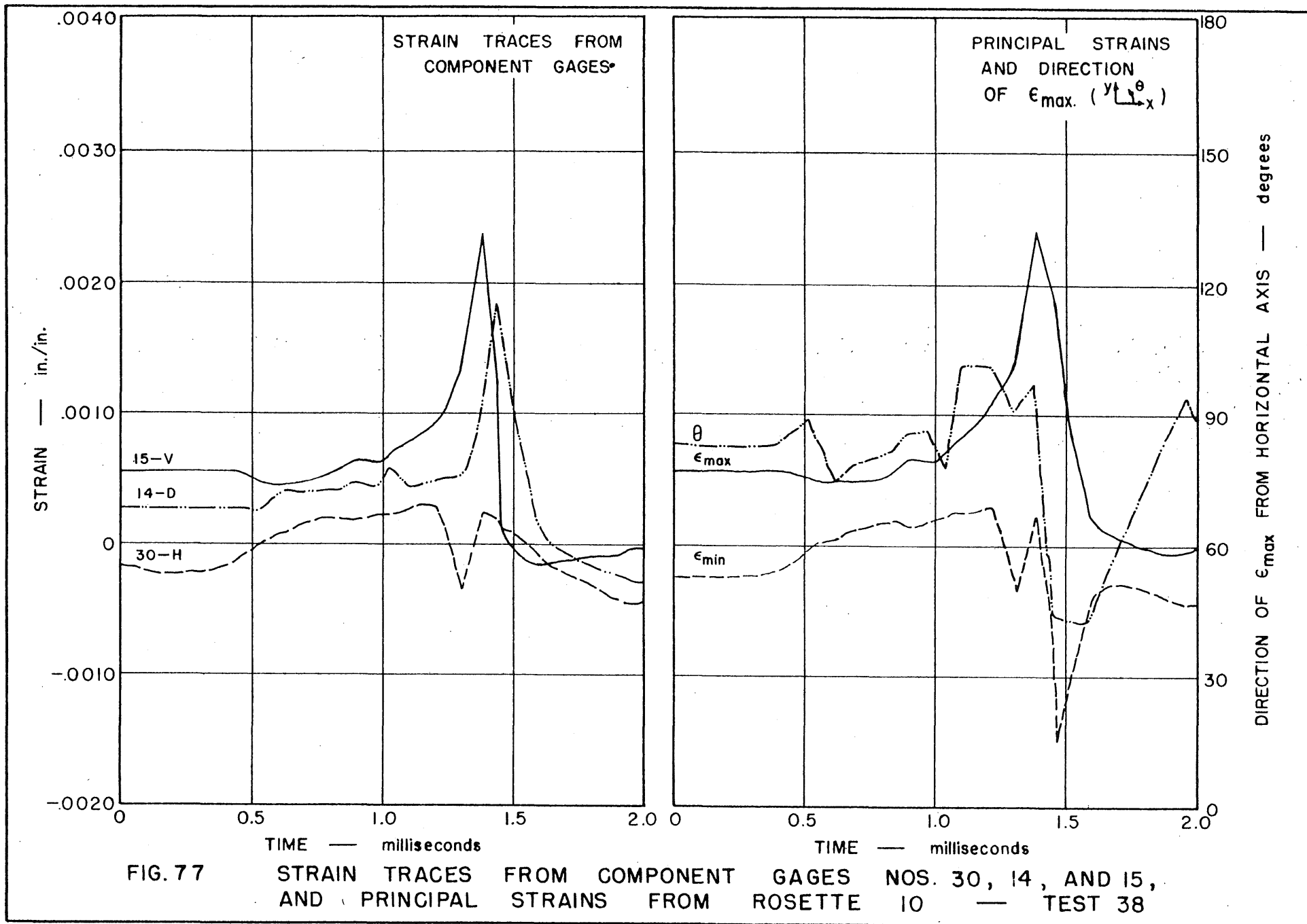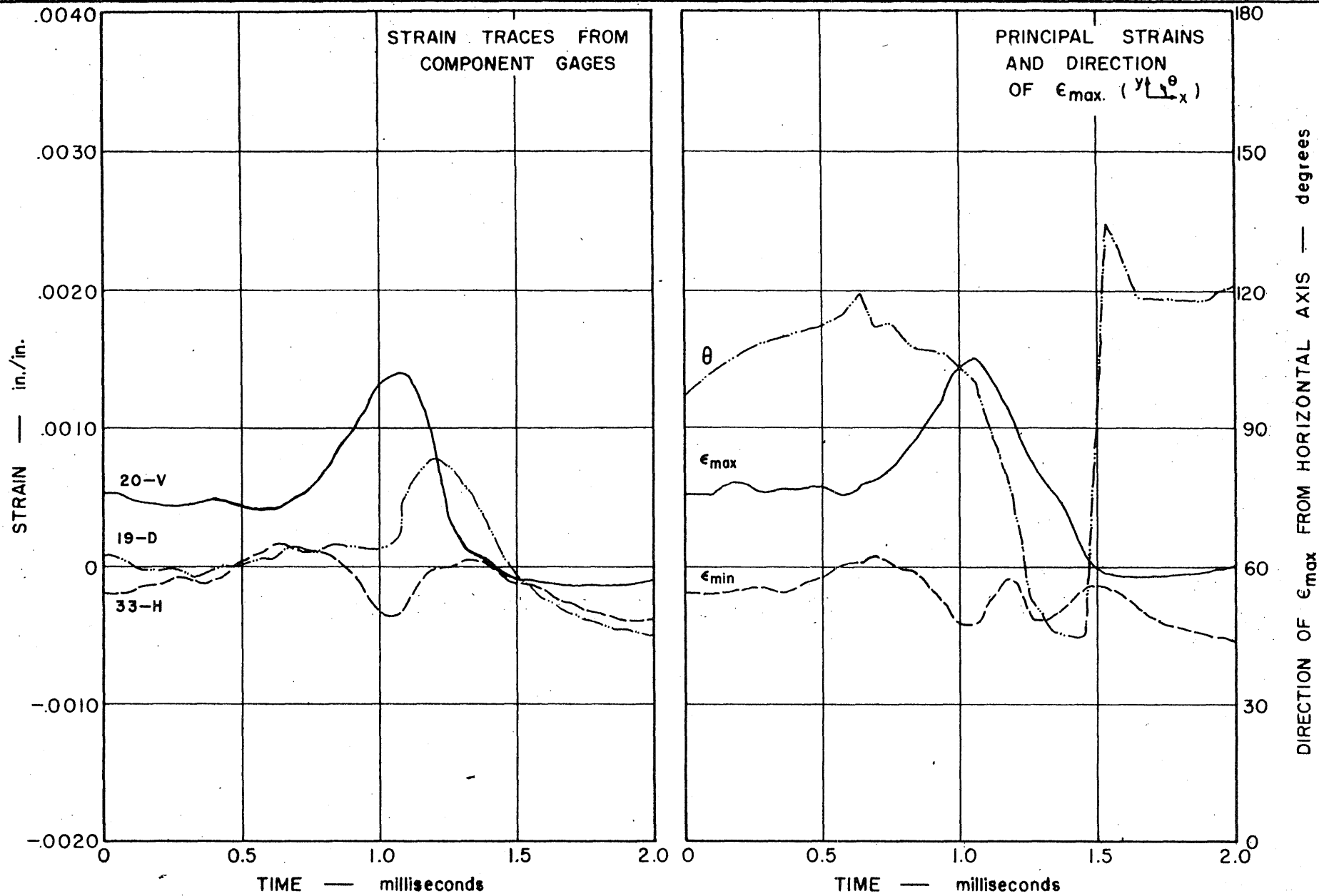AND   PRINCIPAL   STRAINS   FROM   ROSETTE   A   —   TEST 34
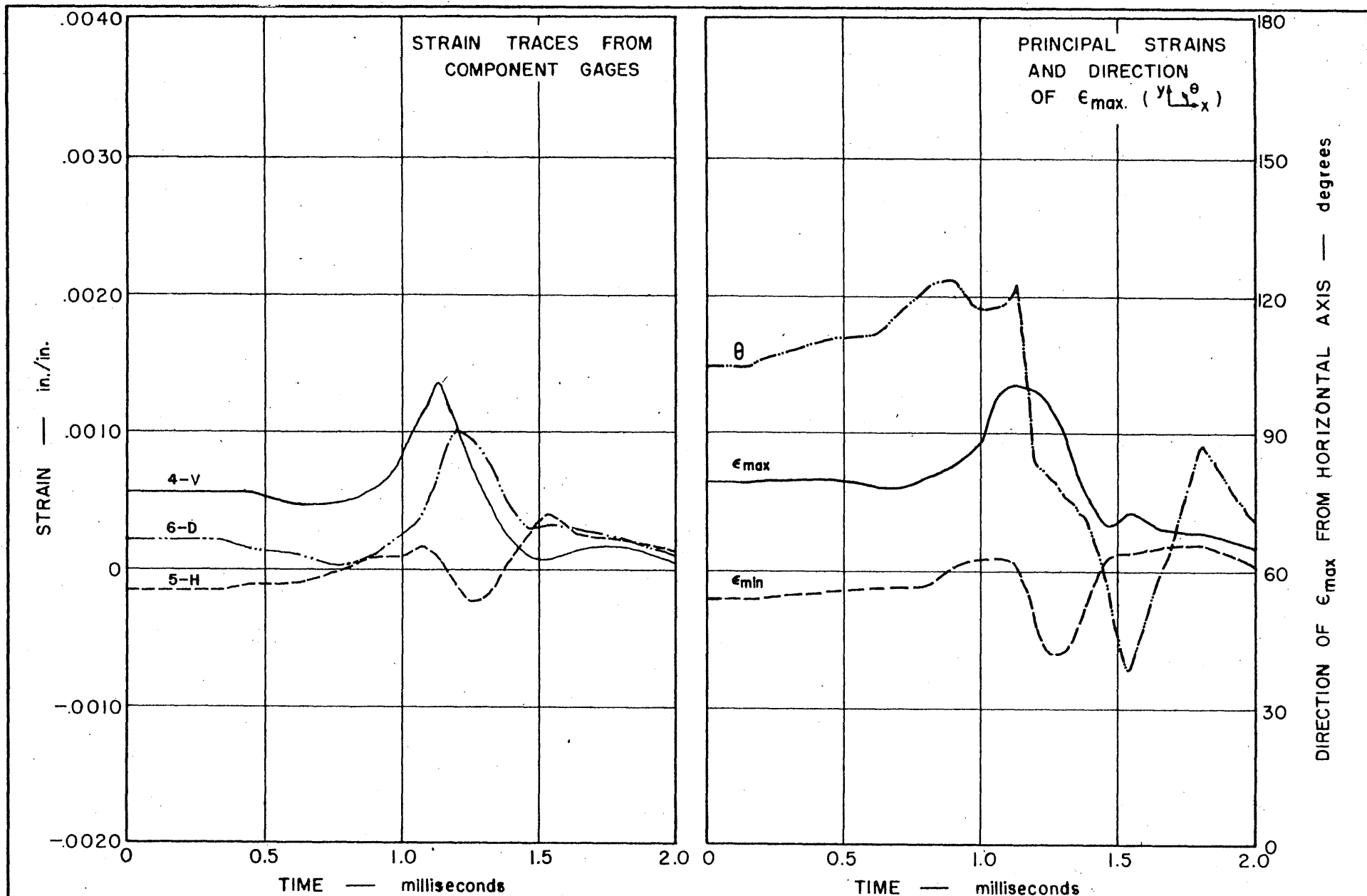
FIG. 33   STRAIN   TRACES   FROM   COMPONENT   GAGES   NOS.   4,   5,   AND   6,
AND   PRINCIPAL   STRAINS   FROM   ROSETTE   B   —   TEST   34
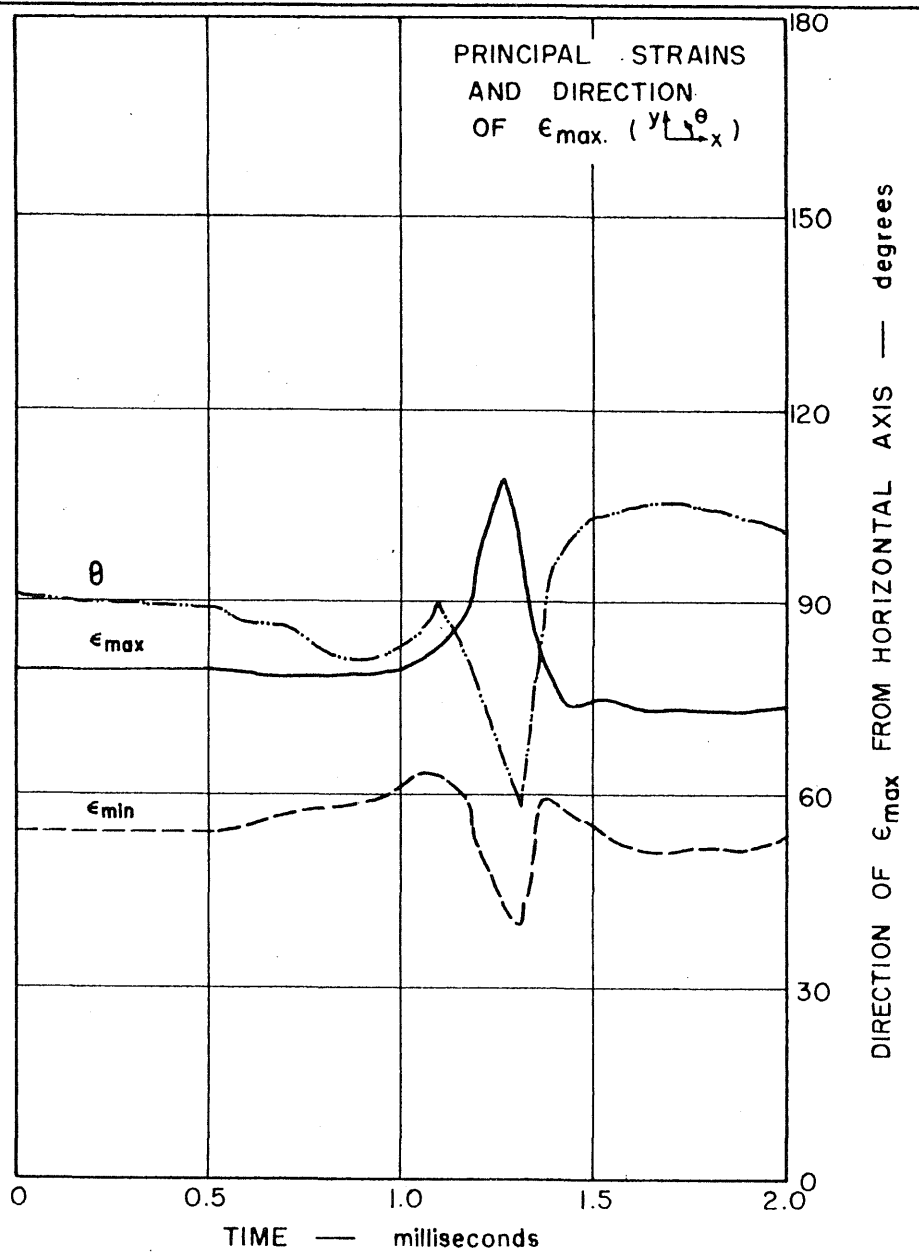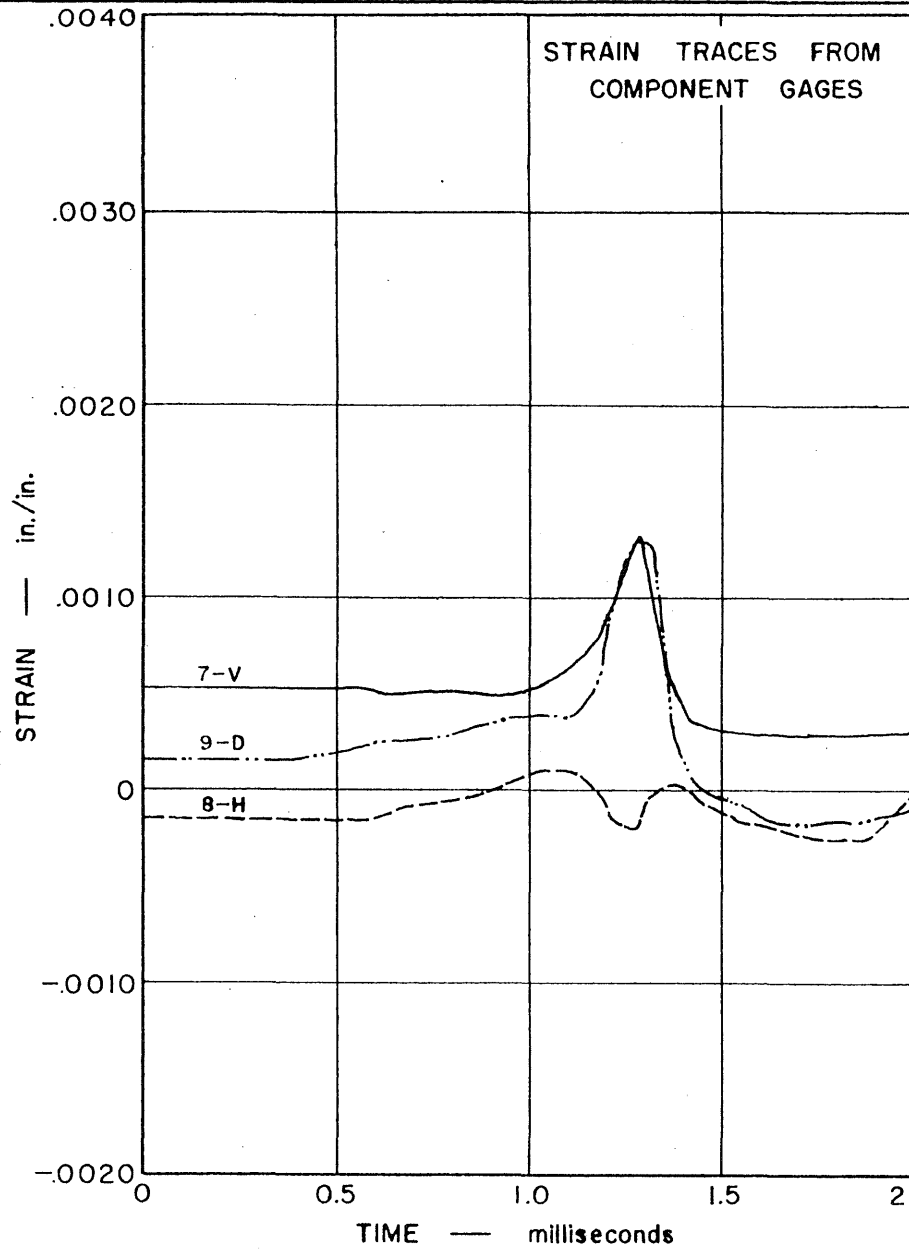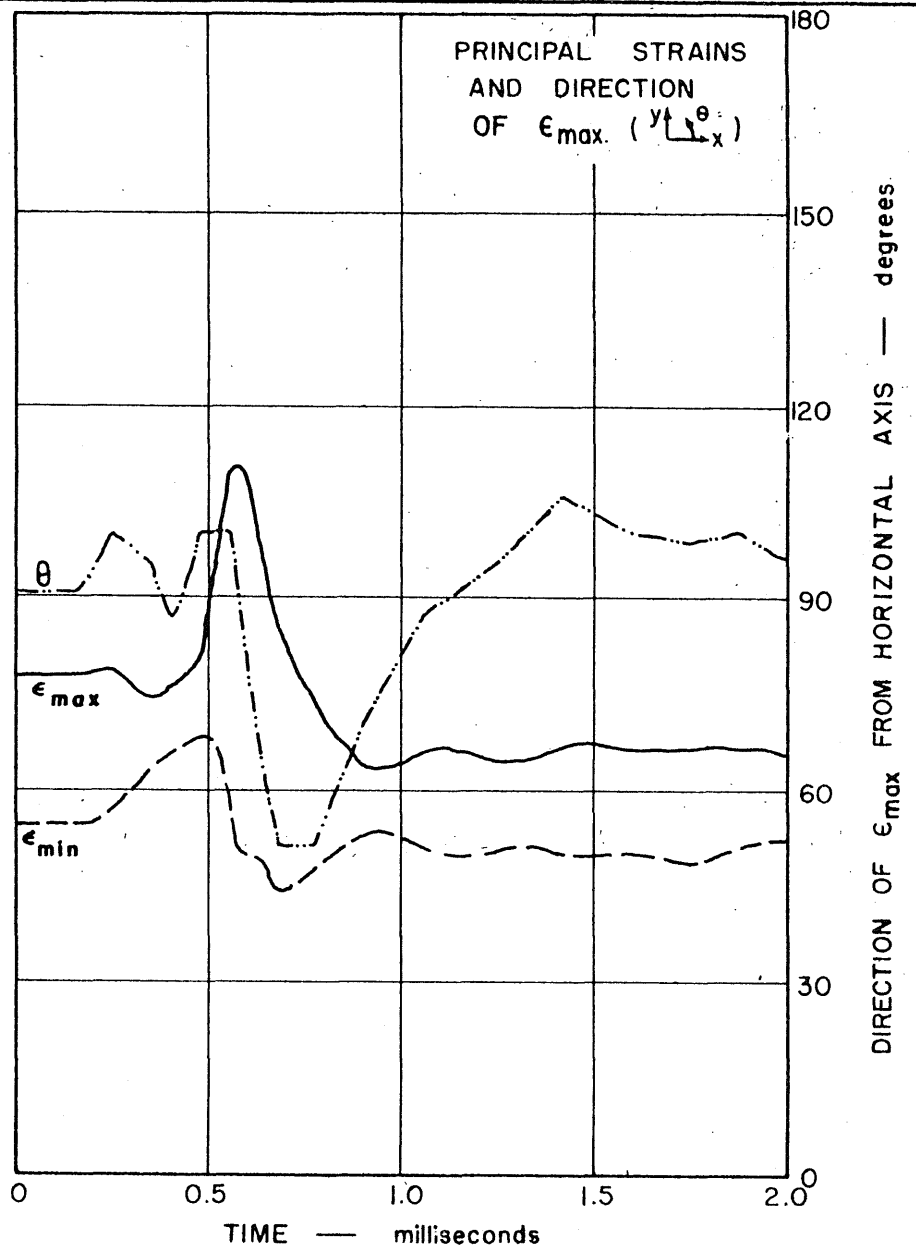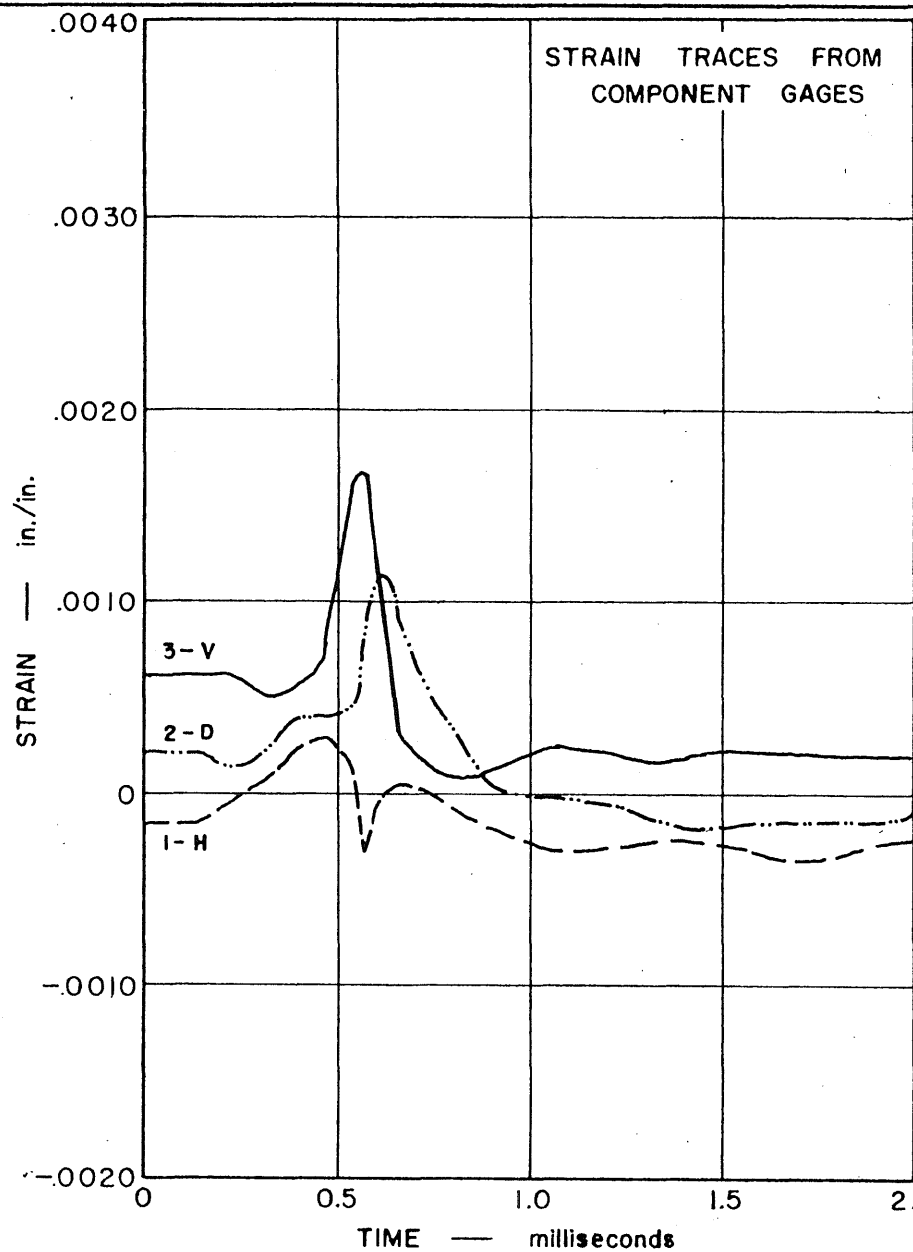
FIG. 34   STRAIN   TRACES   FROM   COMPONENT   GAGES   NOS.   7,   8, AND   9,
AND   PRINCIPAL   STRAINS   FROM   ROSETTE   C   —   TEST   34
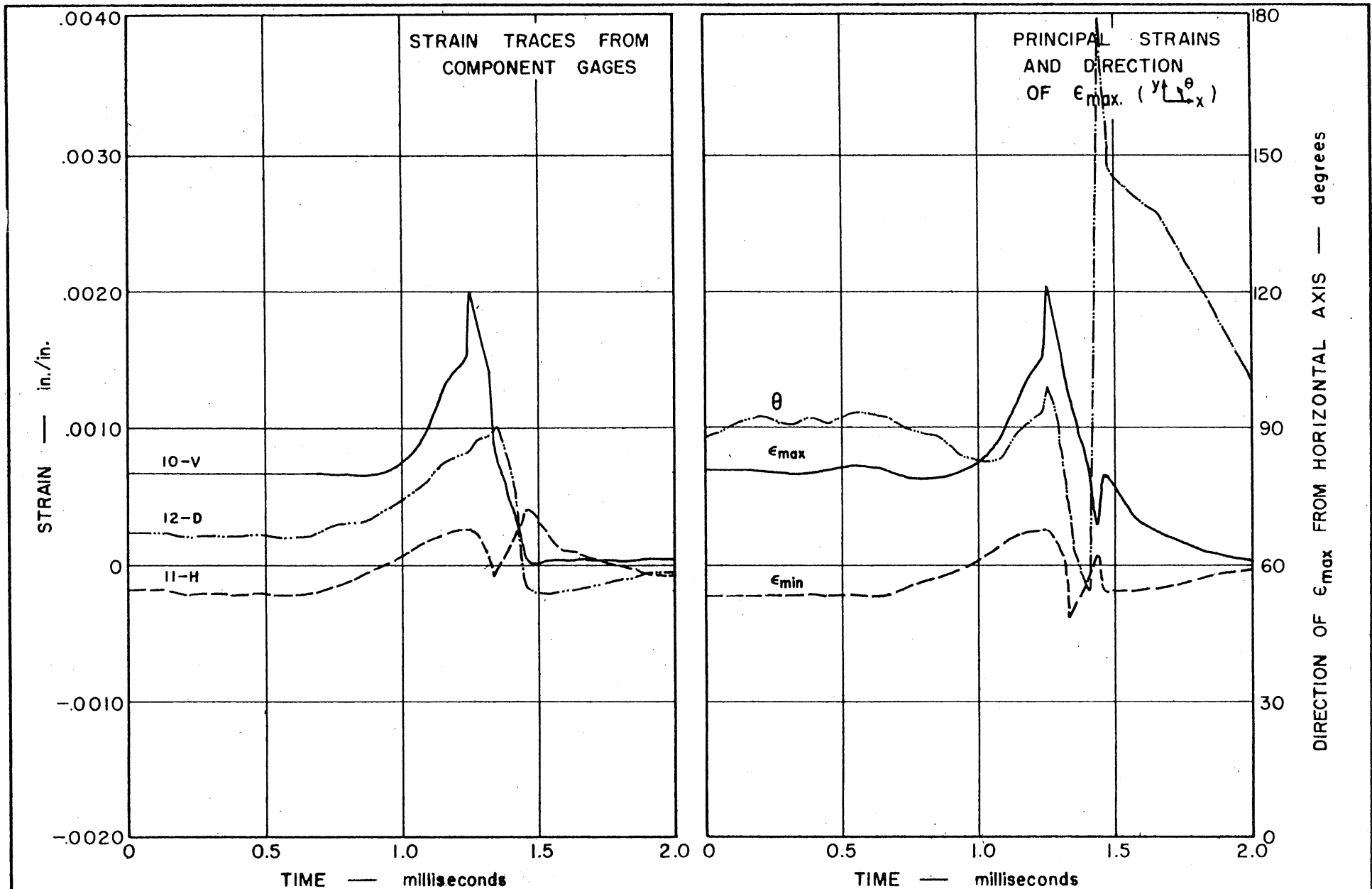
FIG. 35 STRAIN TRACES FROM COMPONENT GAGES NOS. 10, 11, AND 12, AND PRINCIPAL STRAINS FROM ROSETTE D — TEST 34

FIG. 36　　STRAIN　TRACES　FROM　COMPONENT　GAGES　NOS.　13,　14,　AND　15,　AND　PRINCIPAL　STRAINS　FROM　ROSETTE　E　—　TEST　34
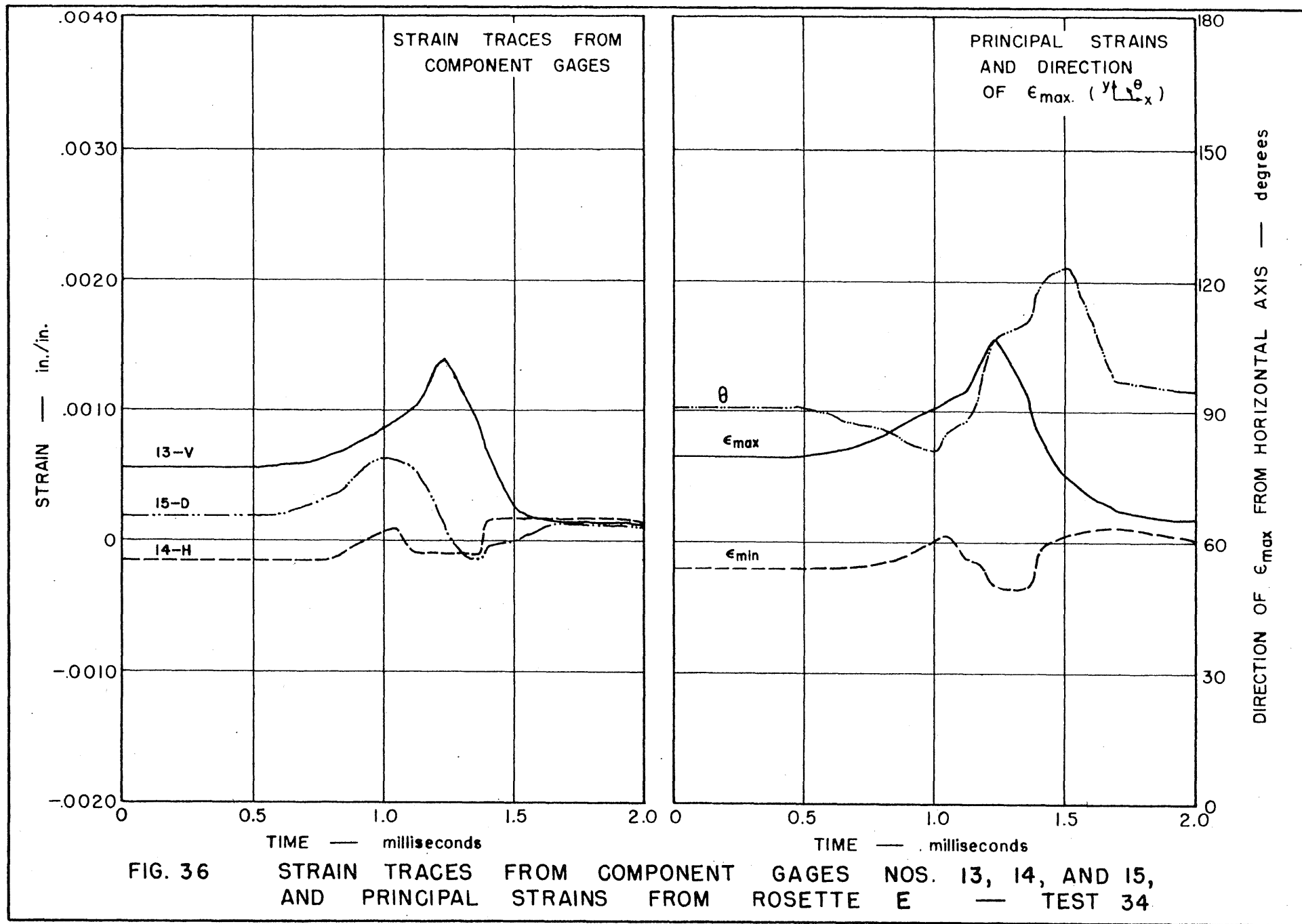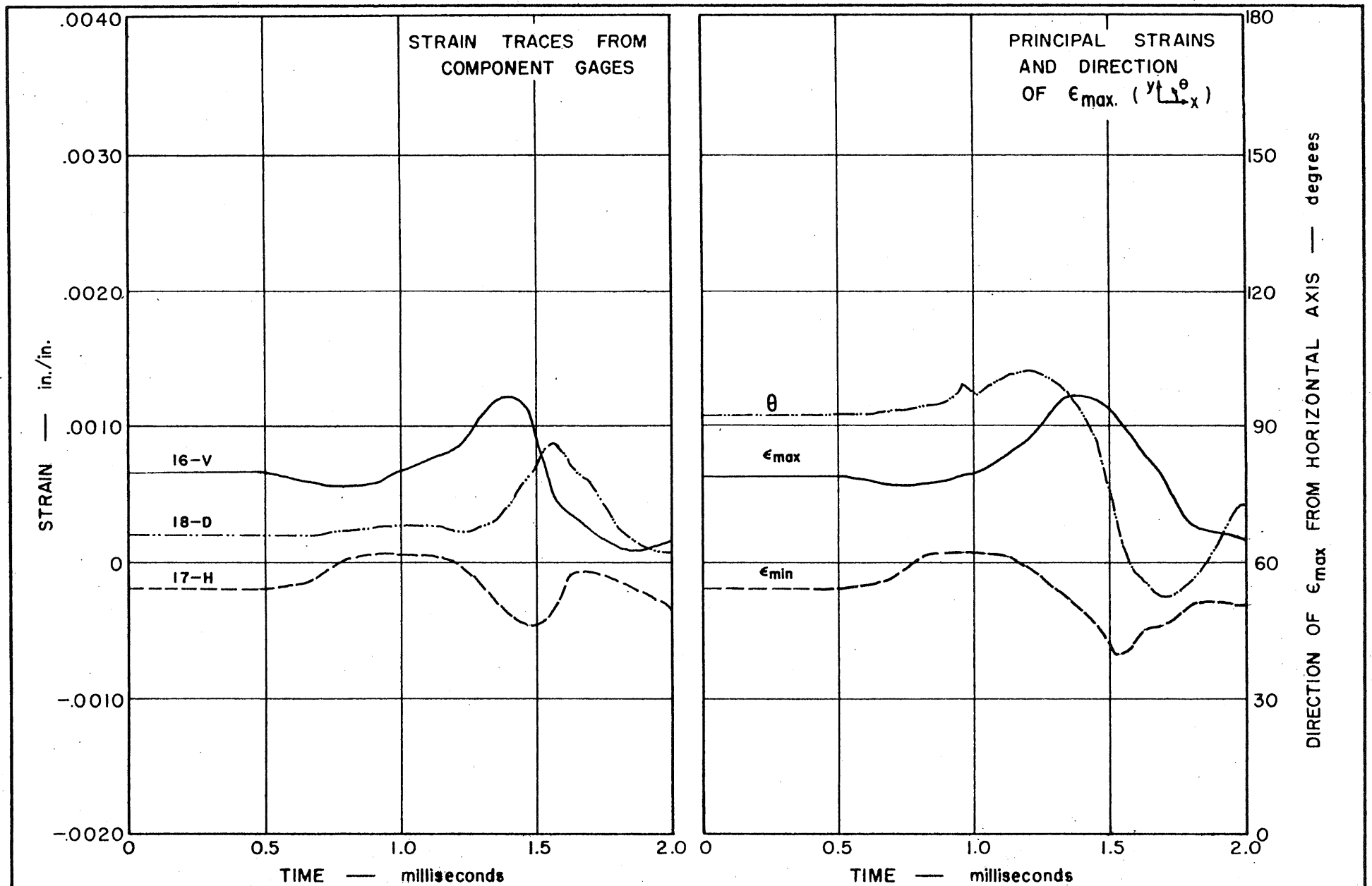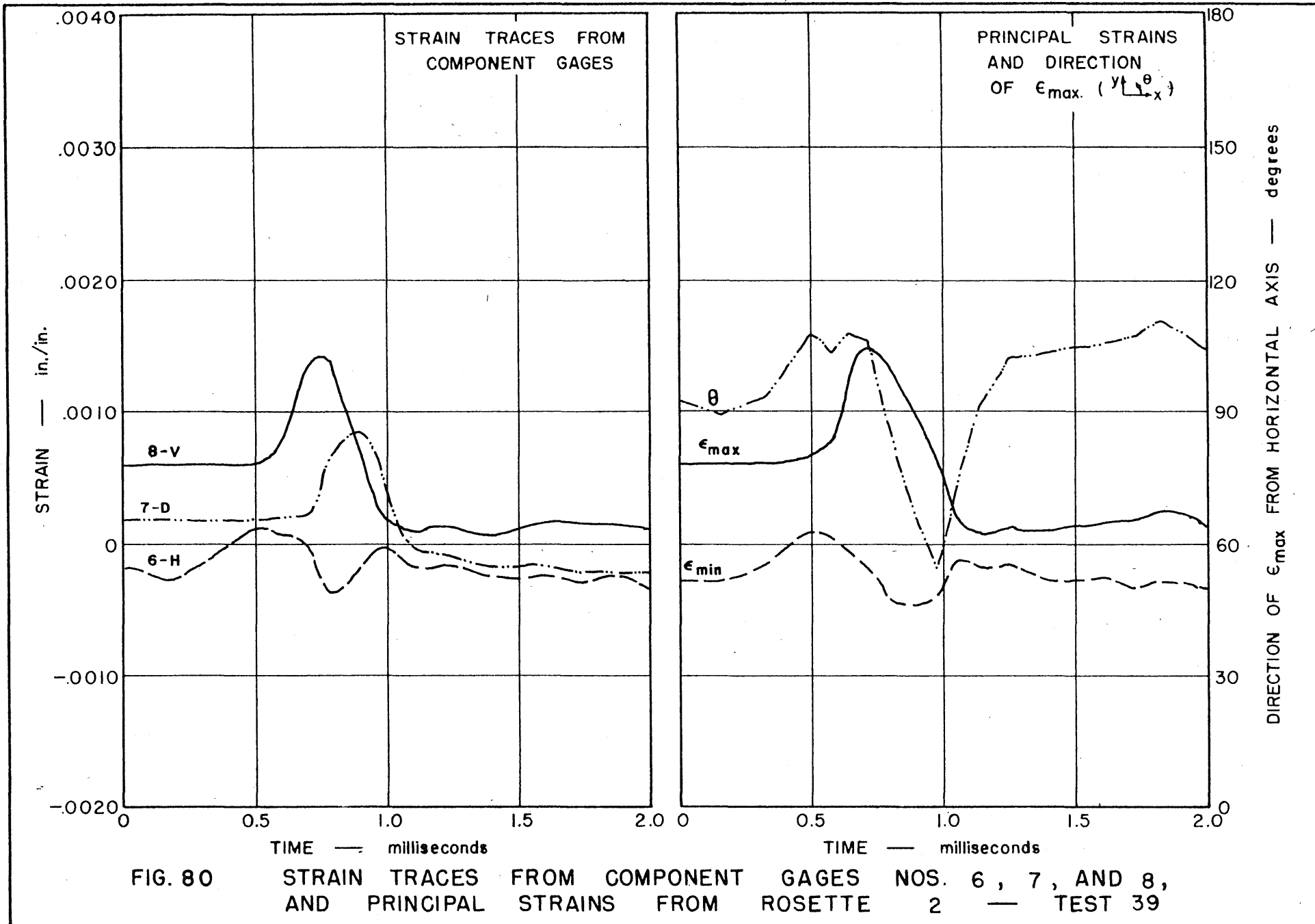
FIG. 37   STRAIN TRACES FROM COMPONENT GAGES NOS. 16, 17, AND 18, AND PRINCIPAL STRAINS FROM ROSETTE F — TEST 34

FIG. 38   STRAIN   TRACES   FROM   COMPONENT   GAGES   NOS. 22, 23, AND 24,
AND   PRINCIPAL   STRAINS   FROM   ROSETTE   H   —   TEST 34
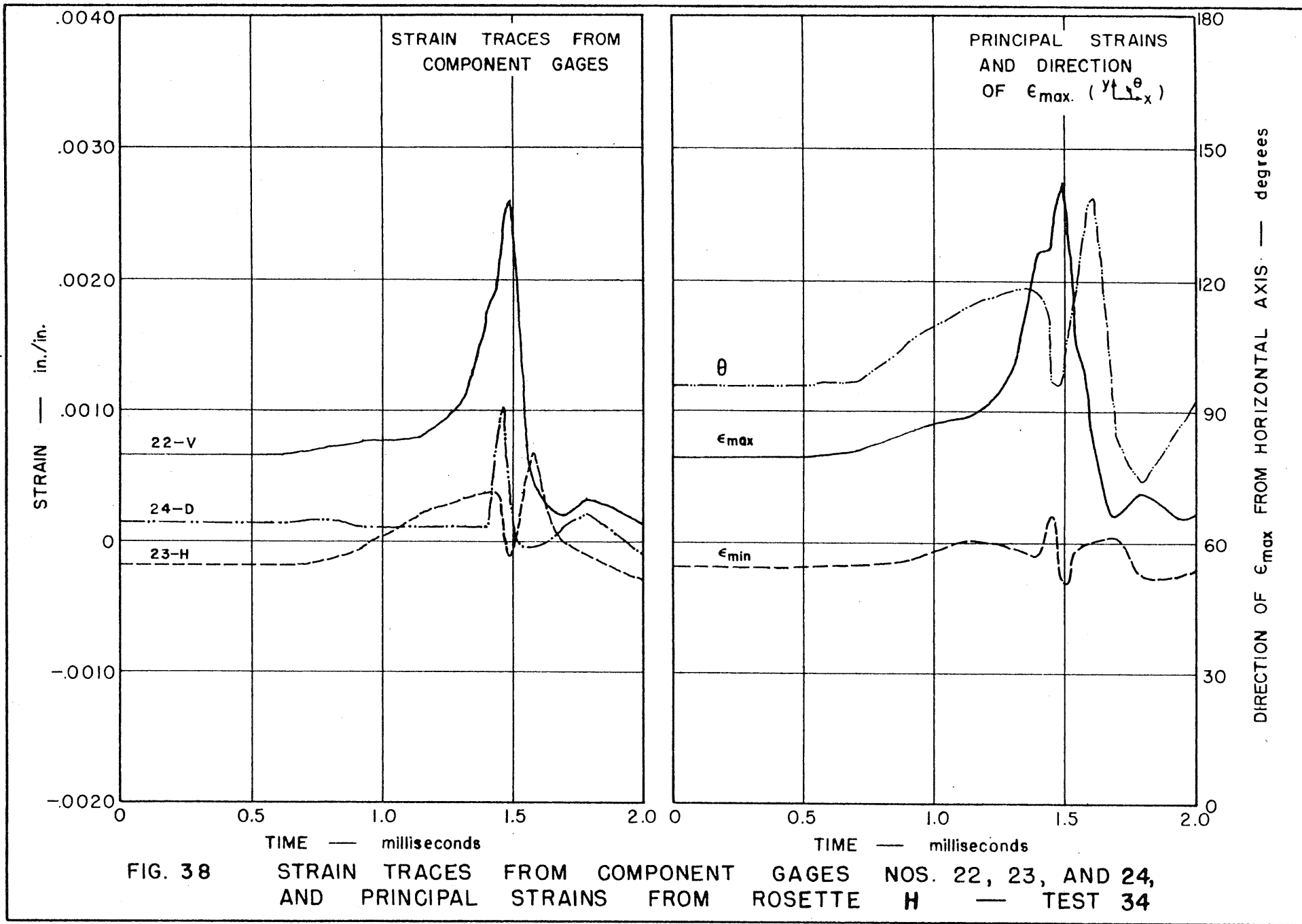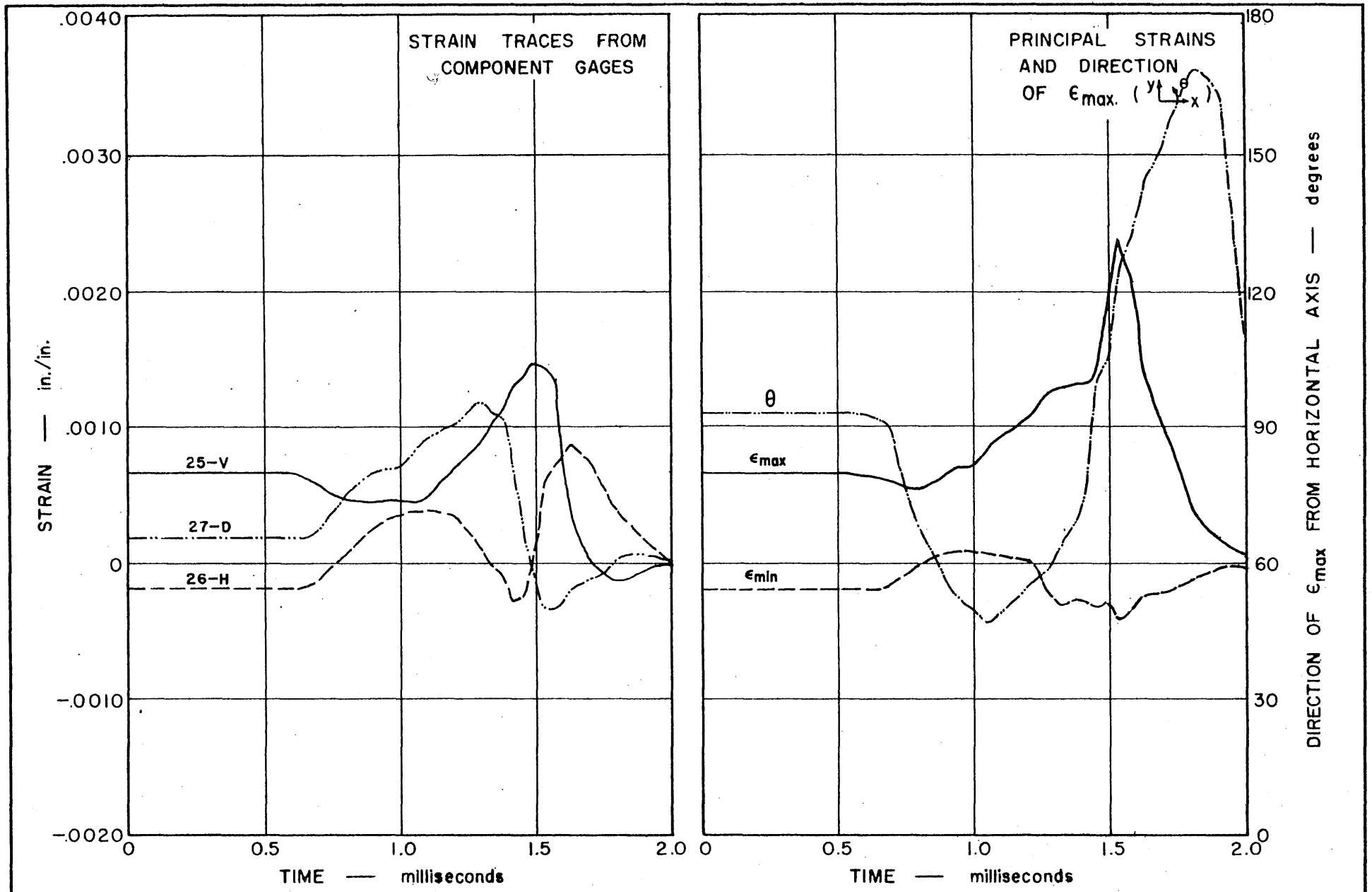
FIG. 39 — STRAIN TRACES FROM COMPONENT GAGES NOS. 25, 26, AND 27, AND PRINCIPAL STRAINS FROM ROSETTE 1 — TEST 34
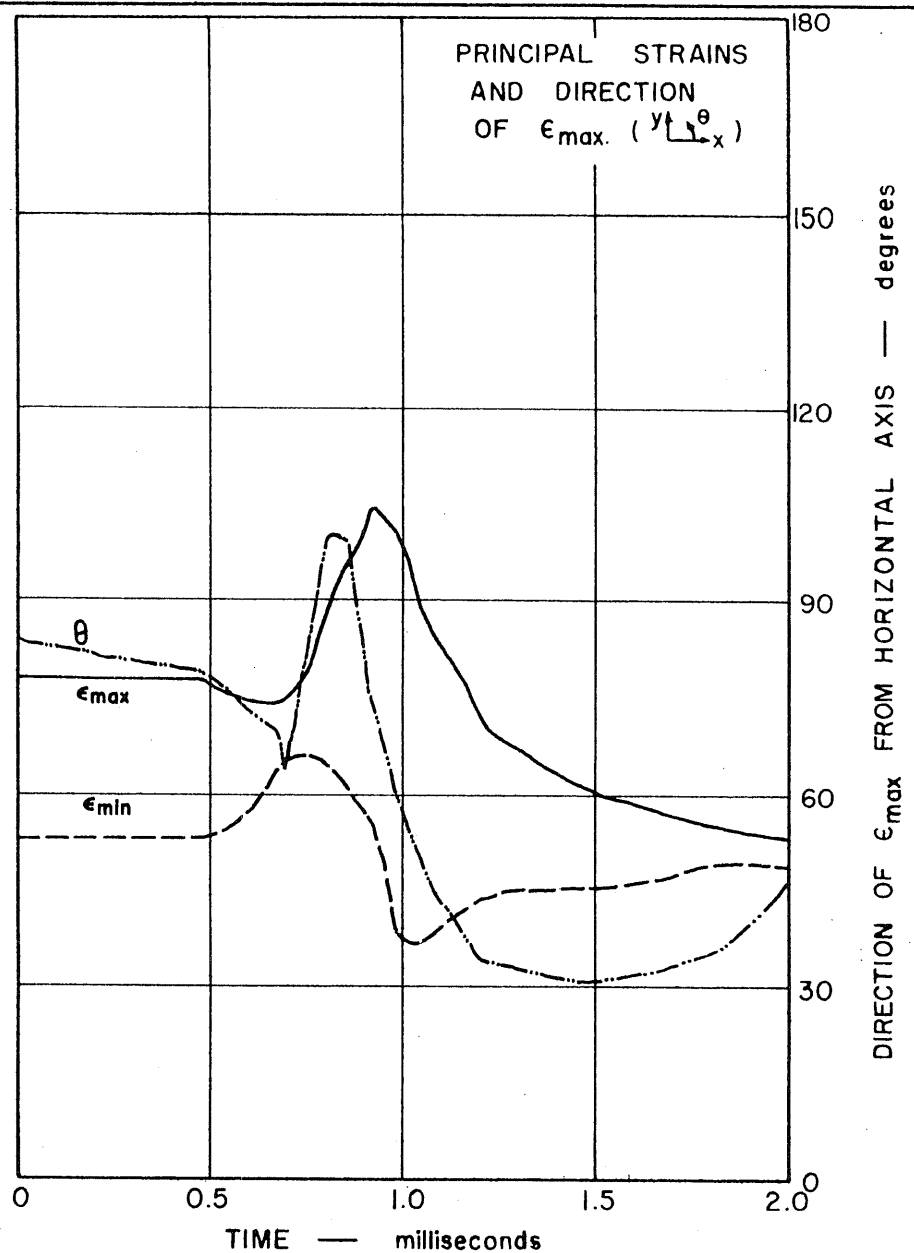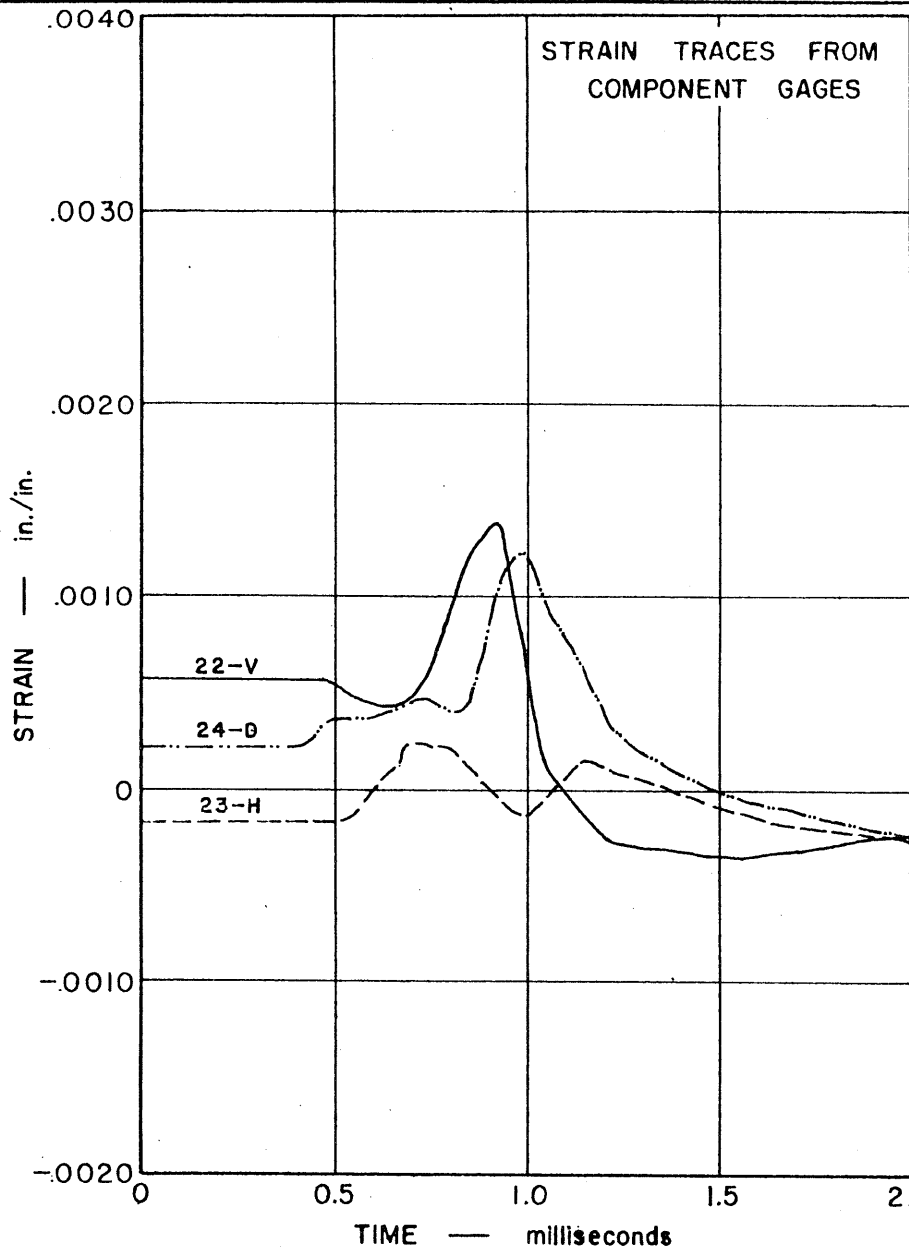
FIG. 40   STRAIN   TRACES   FROM   COMPONENT   GAGES   NOS.   22, 23,   AND 24,
         AND   PRINCIPAL   STRAINS   FROM   ROSETTE   J   —   TEST 34
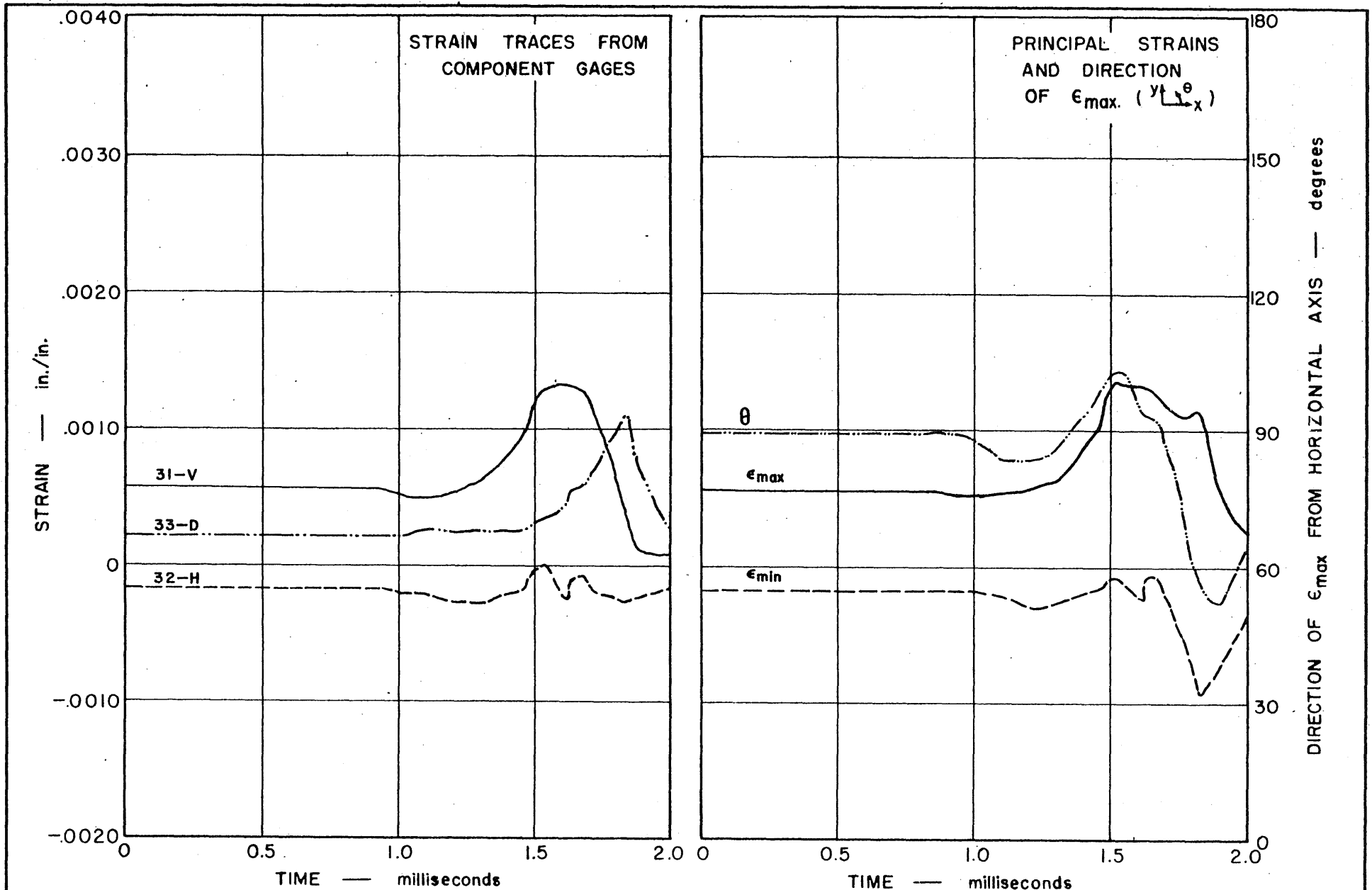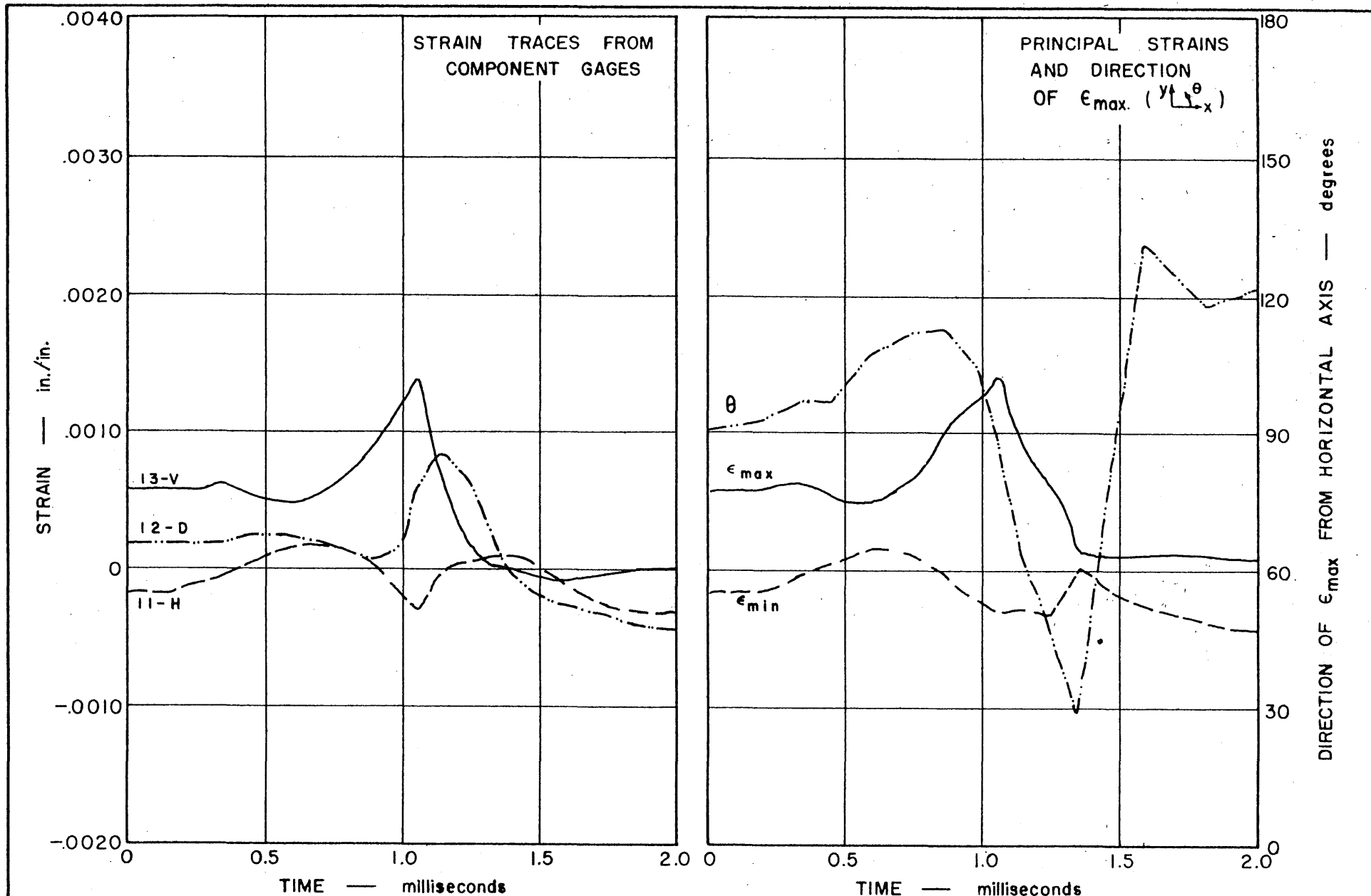
FIG. 41   STRAIN   TRACES   FROM   COMPONENT   GAGES   NOS. 31, 32, AND 33, AND   PRINCIPAL STRAINS   FROM   ROSETTE   K — TEST 34
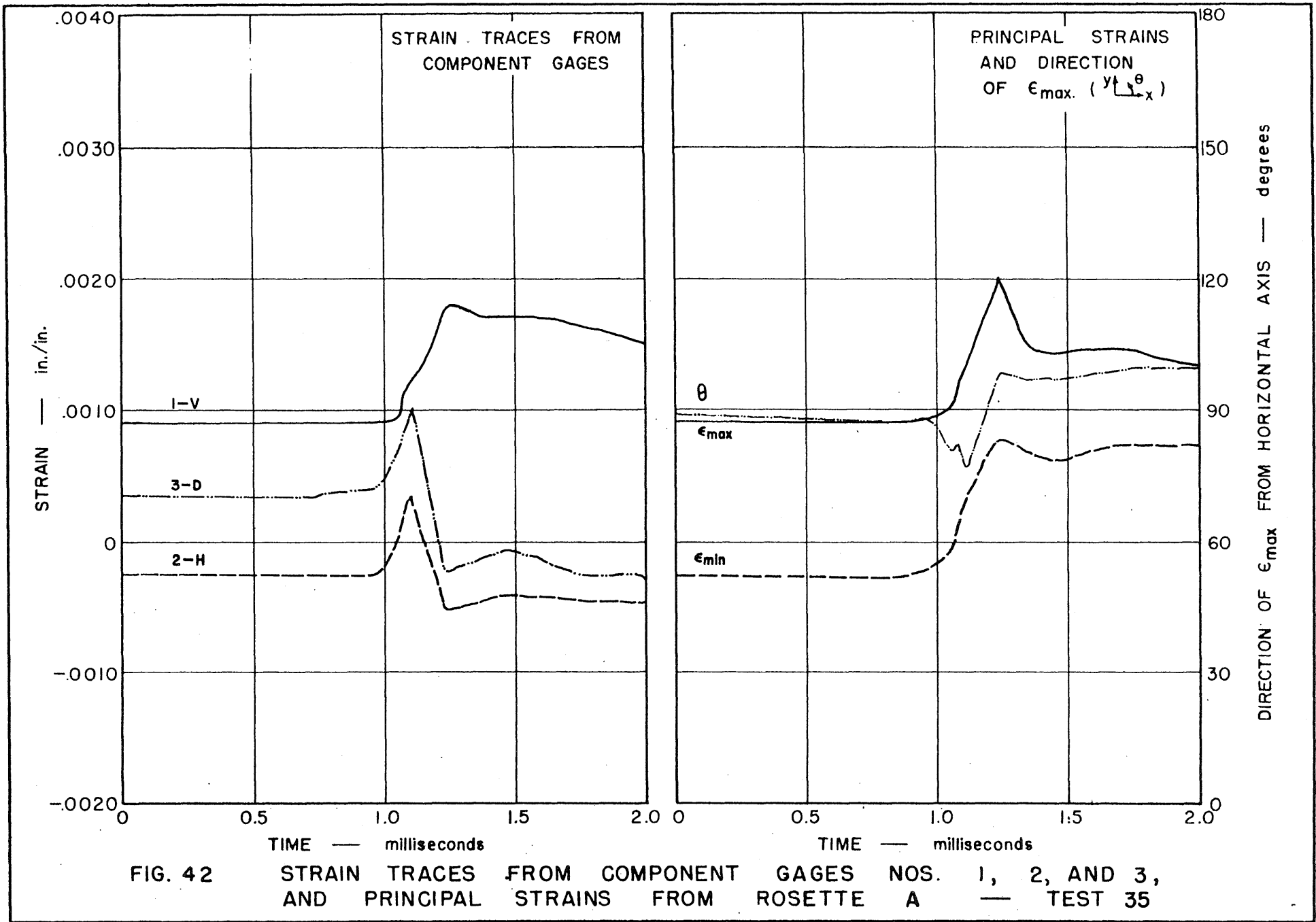
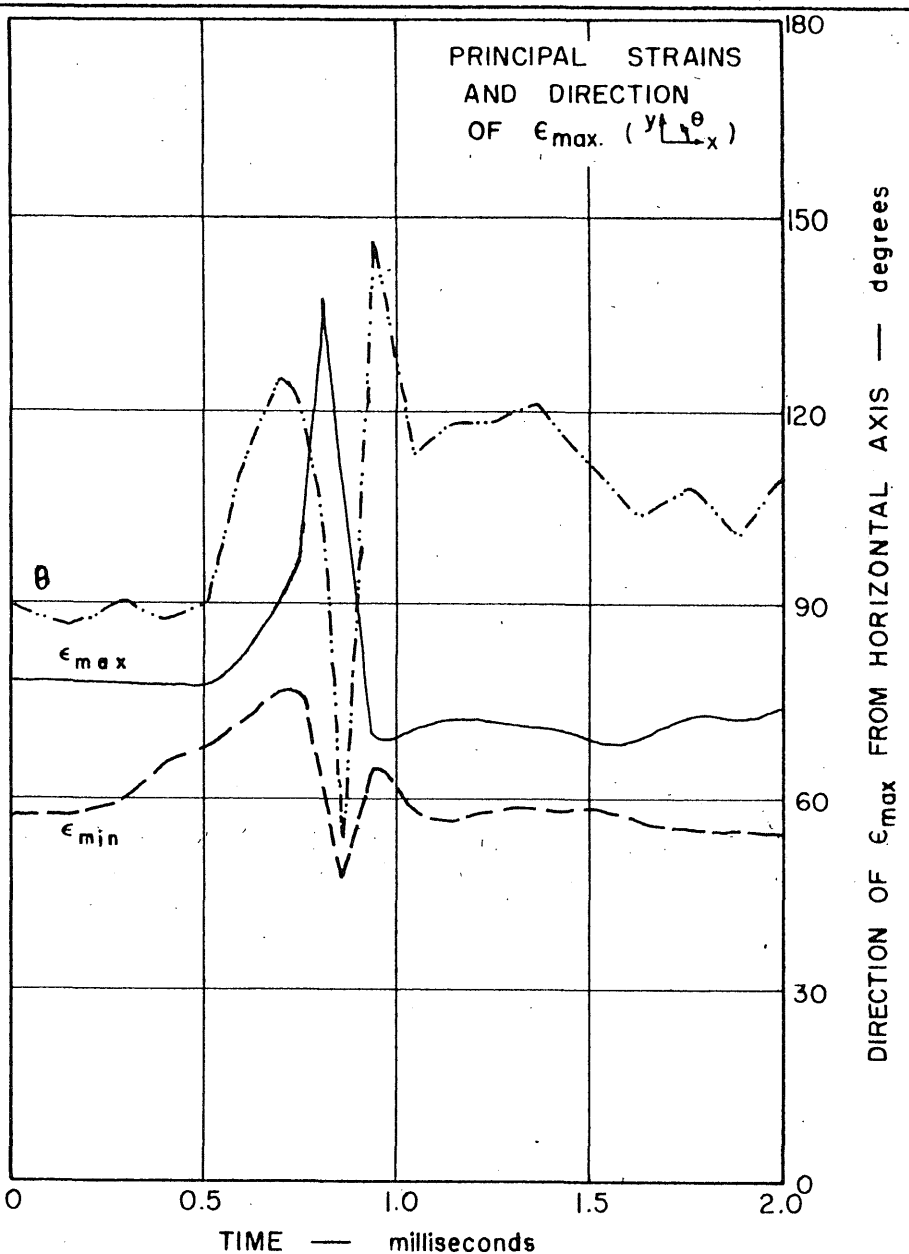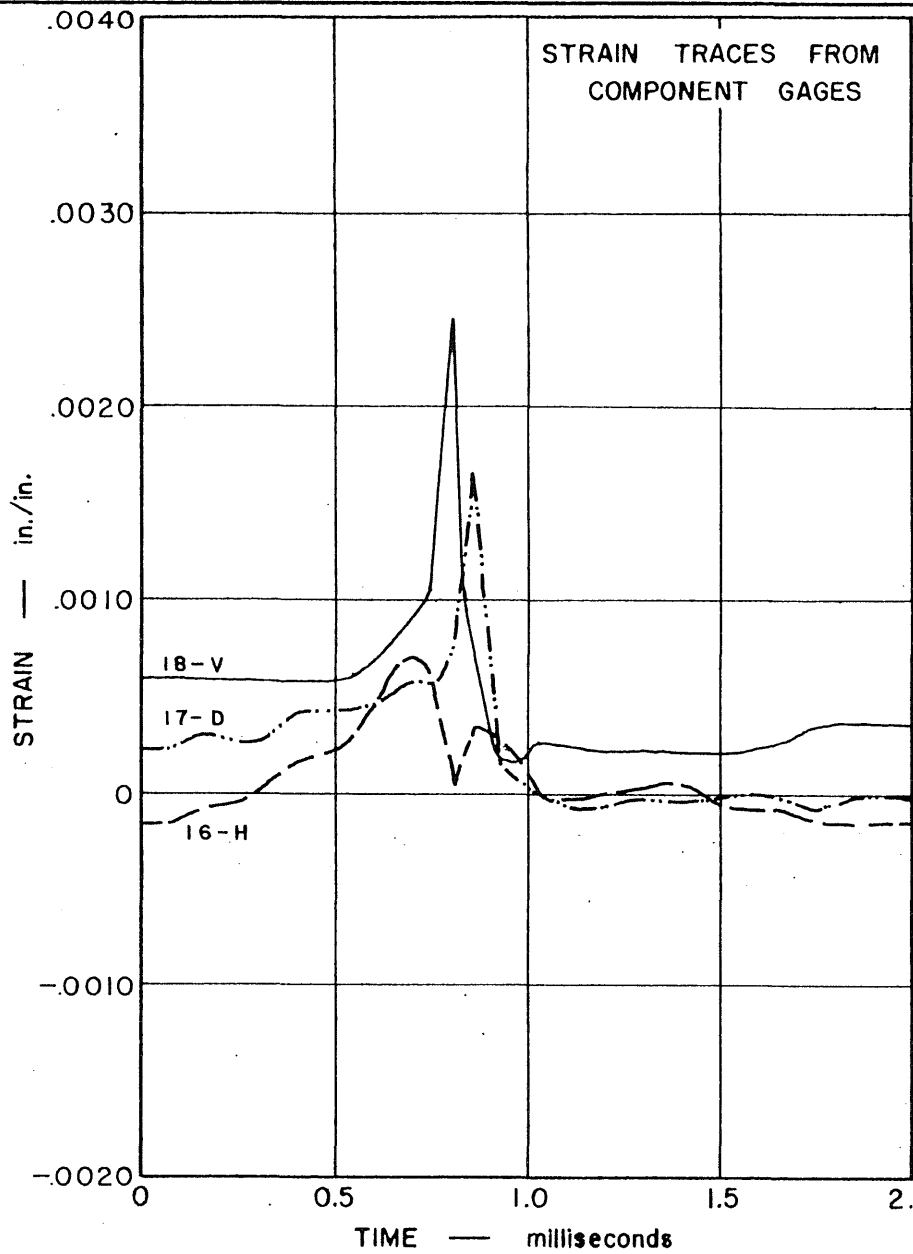FIG. 42   STRAIN TRACES FROM COMPONENT GAGES NOS. 1, 2, AND 3, AND PRINCIPAL STRAINS FROM ROSETTE A — TEST 35
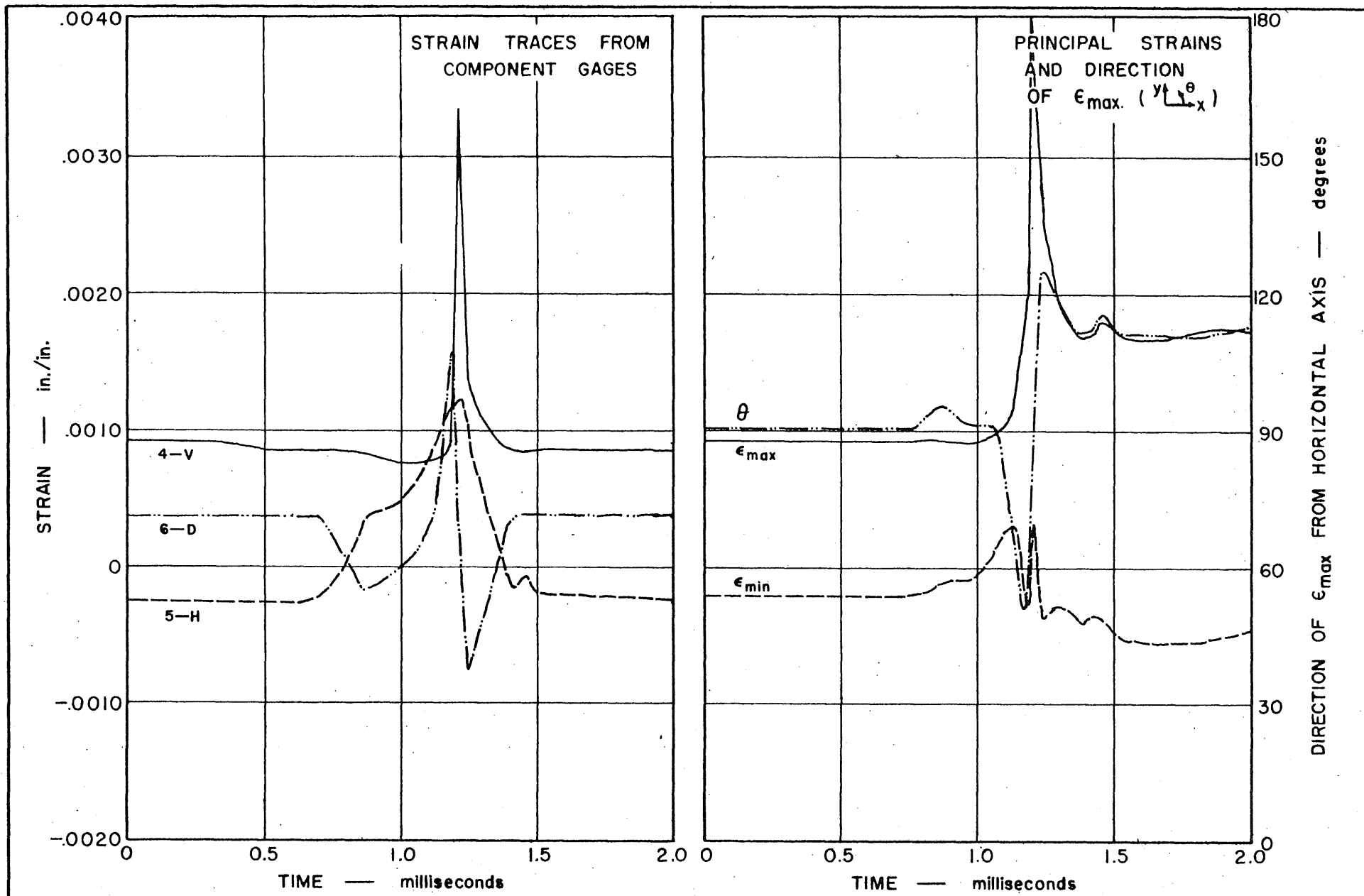
FIG. 43   STRAIN   TRACES   FROM   COMPONENT   GAGES   NOS.   4,   5,   AND   6, AND   PRINCIPAL   STRAINS   FROM   ROSETTE   B   —   TEST   35
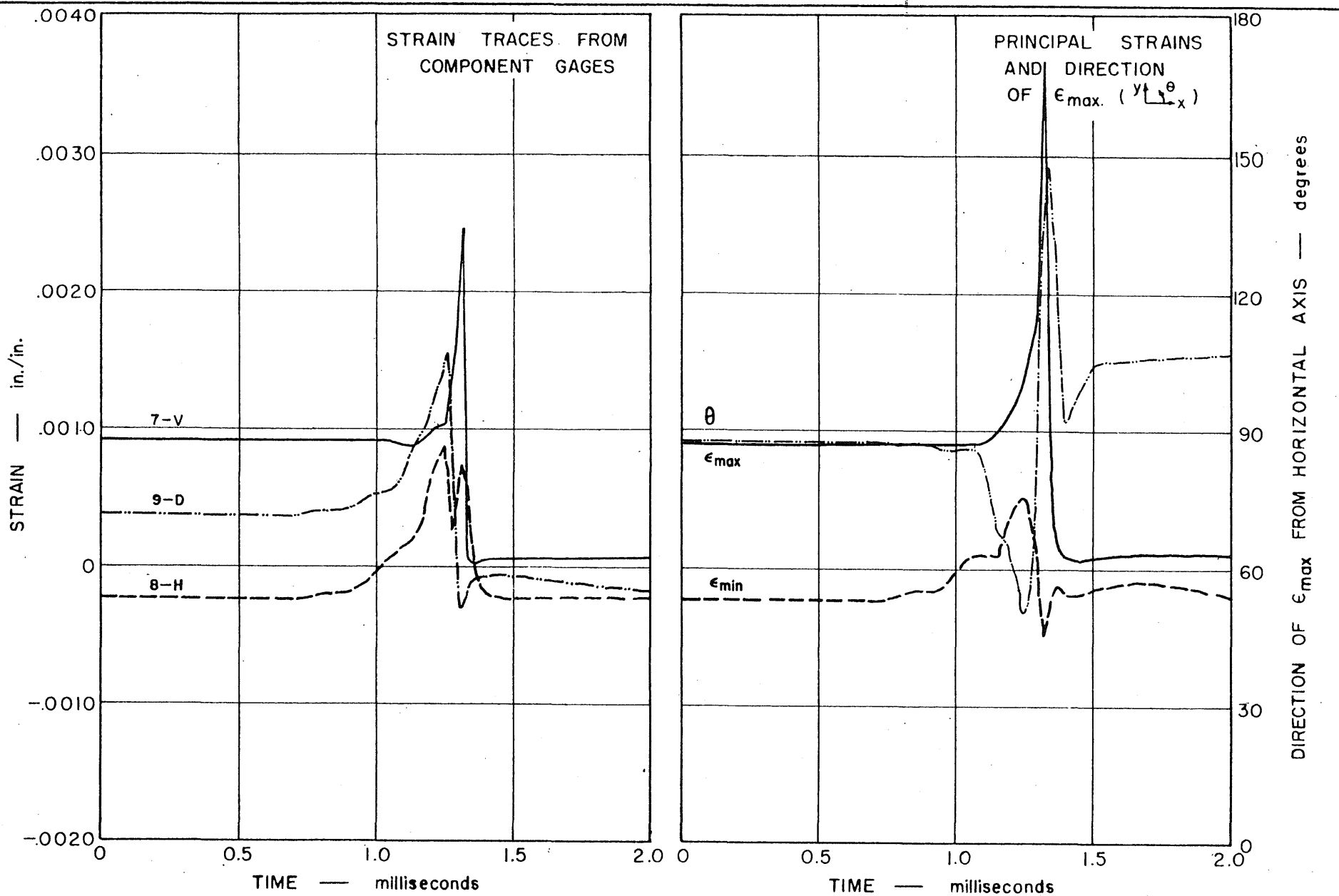
FIG. 44   STRAIN TRACES FROM COMPONENT GAGES NOS. 7, 8, AND 9, AND PRINCIPAL STRAINS FROM ROSETTE C — TEST 35
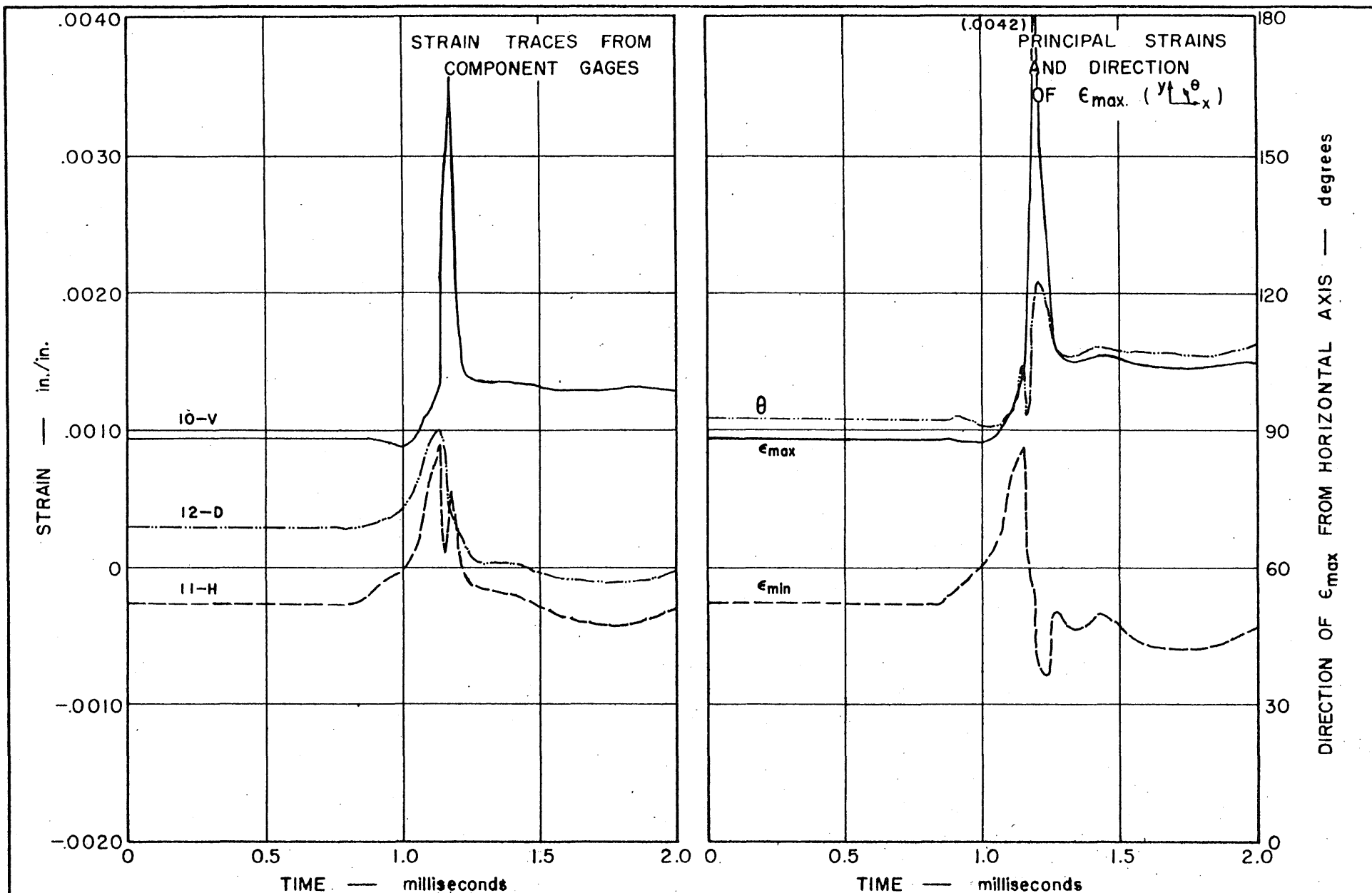
FIG. 45   STRAIN TRACES FROM COMPONENT GAGES NOS. 10, 11, AND 12, AND PRINCIPAL STRAINS FROM ROSETTE D — TEST 35
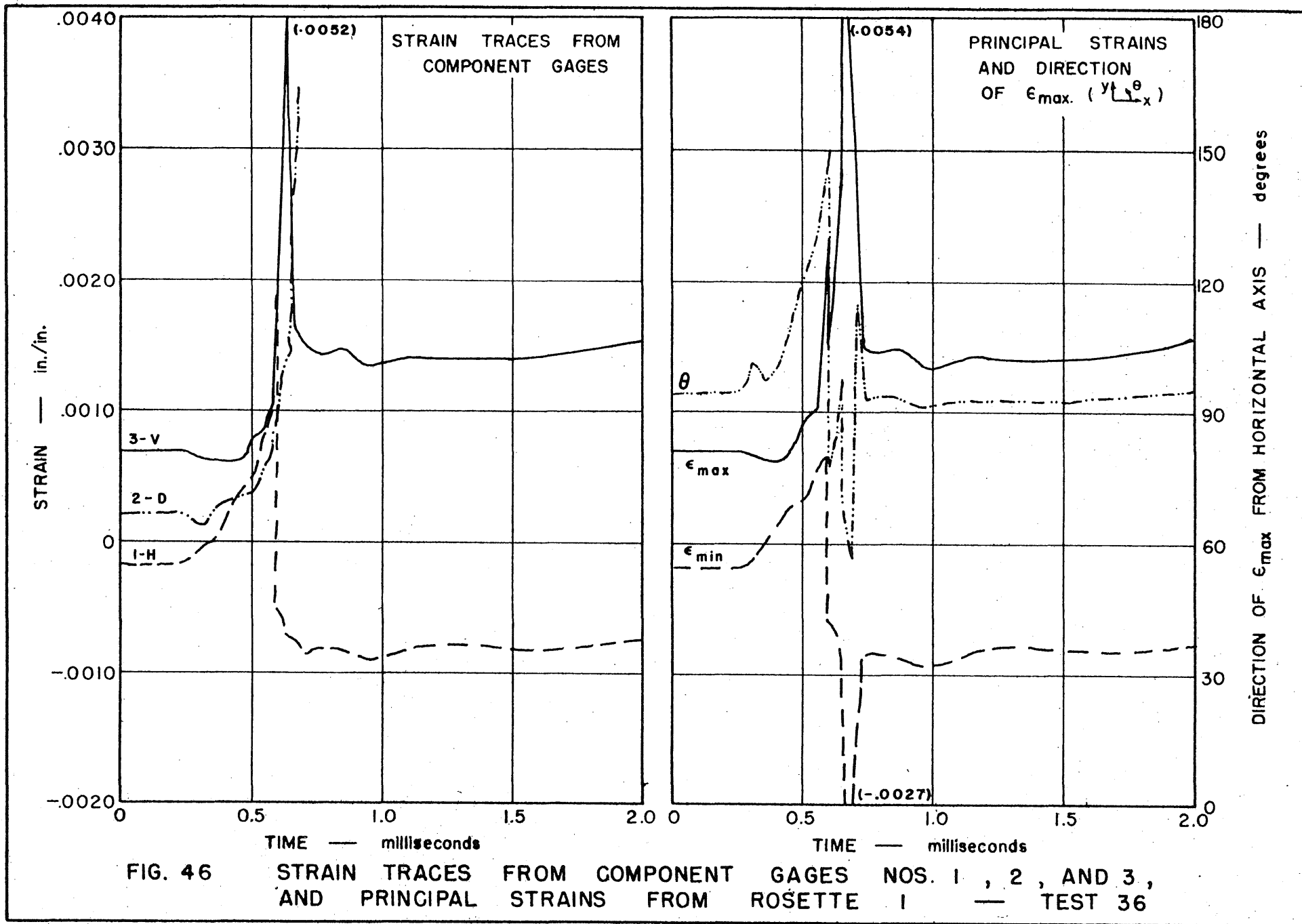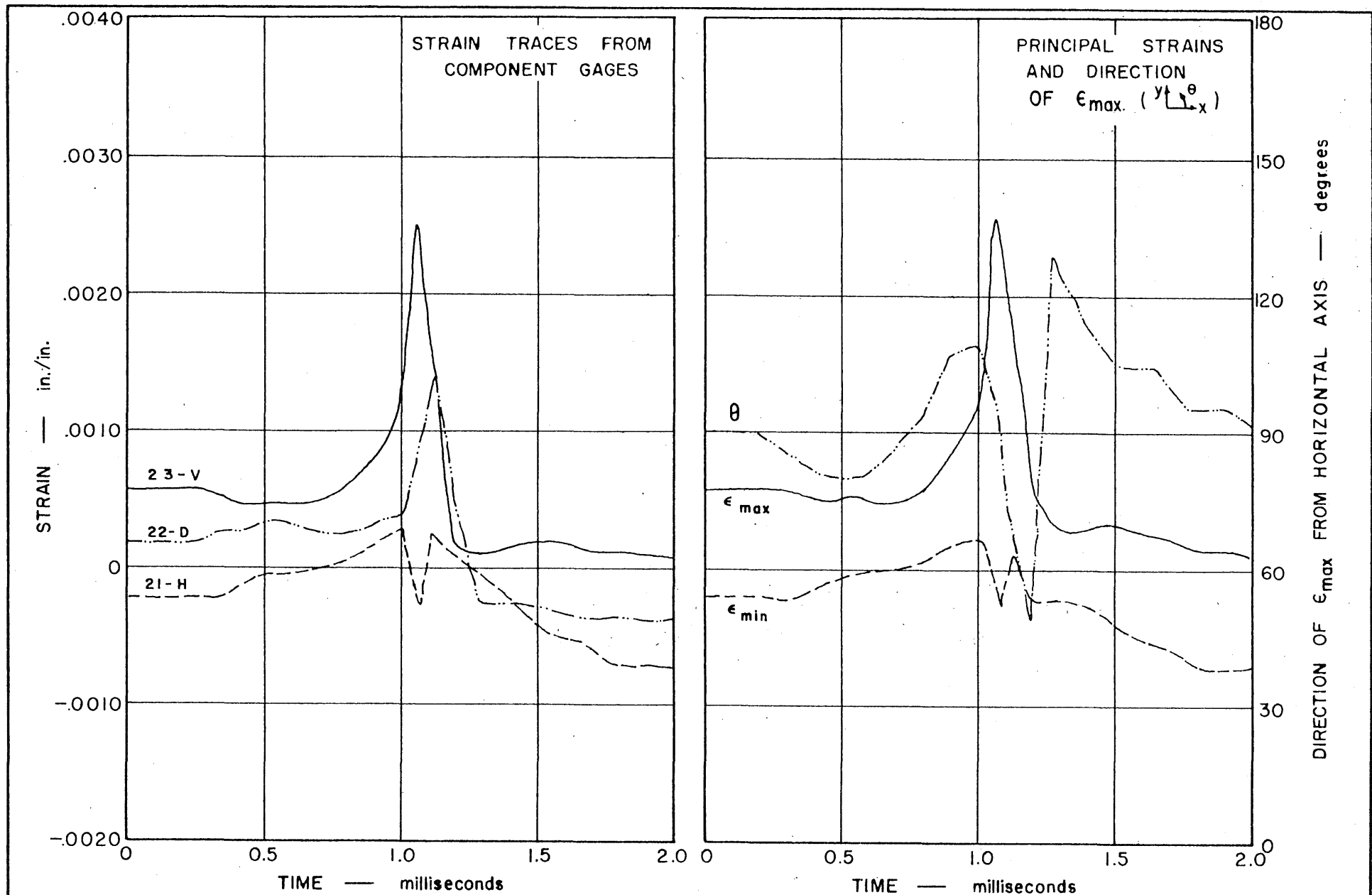
FIG. 46   STRAIN TRACES FROM COMPONENT GAGES NOS. 1 , 2 , AND 3 ,
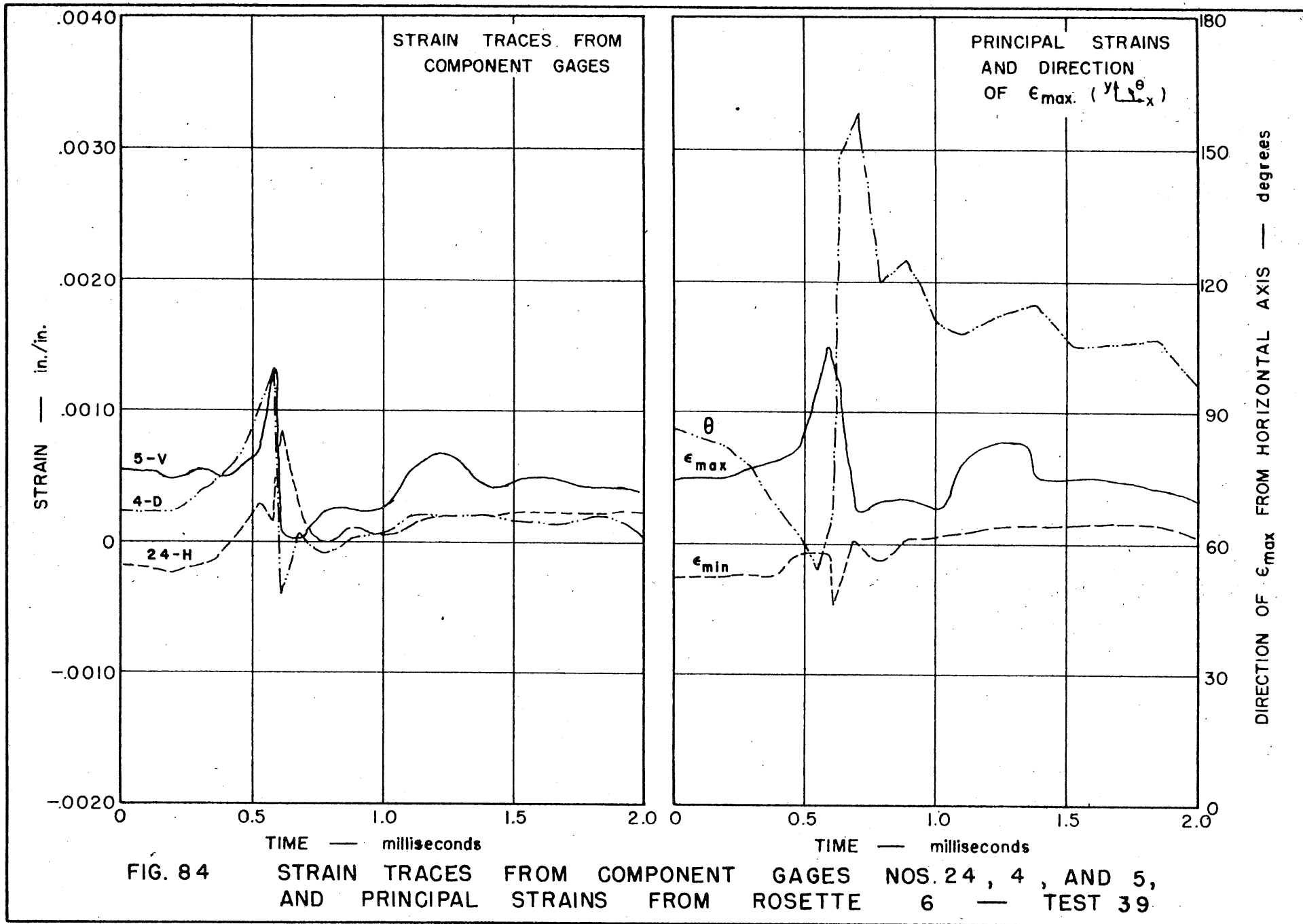AND PRINCIPAL STRAINS FROM ROSETTE 1 — TEST 36
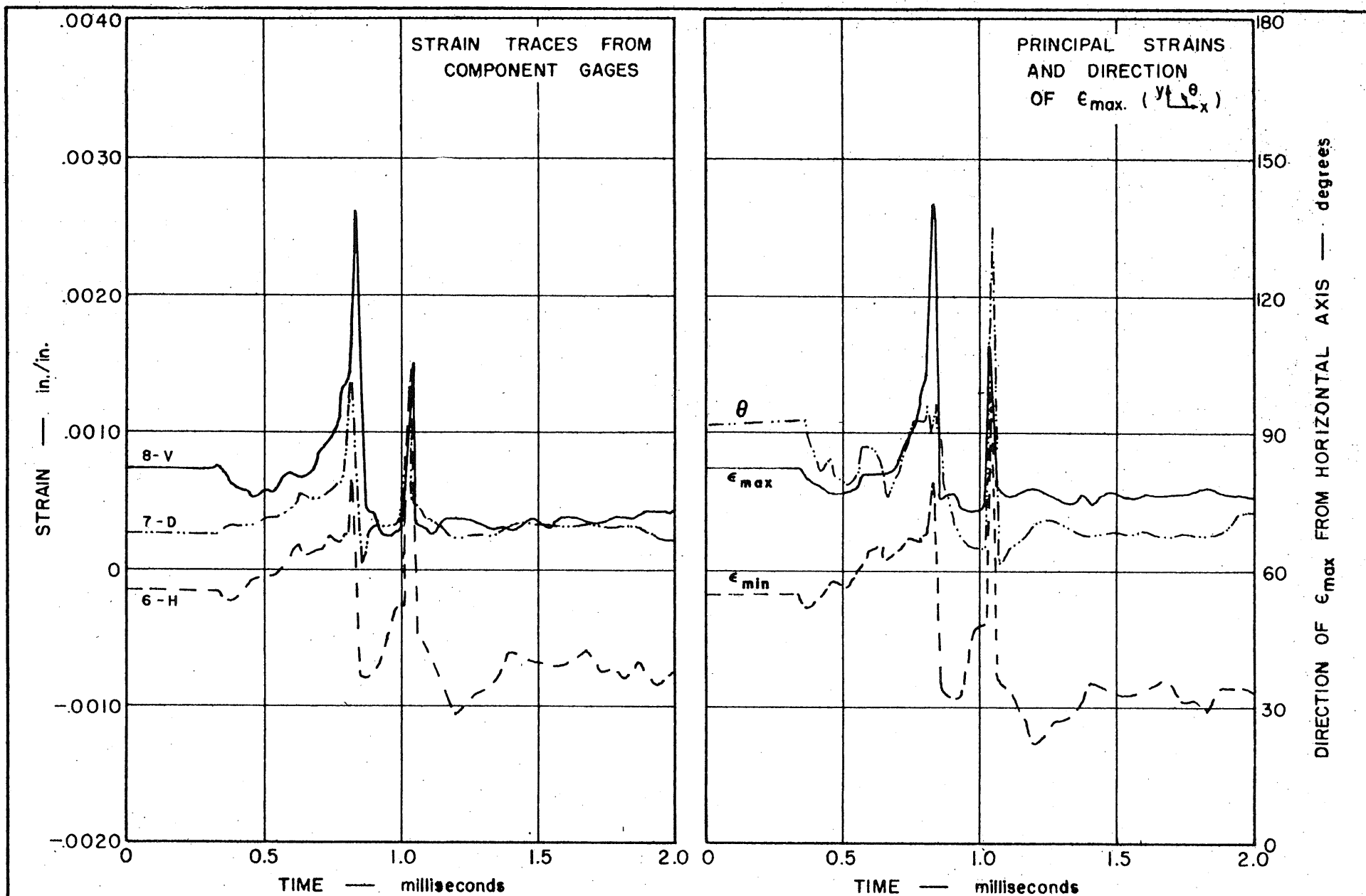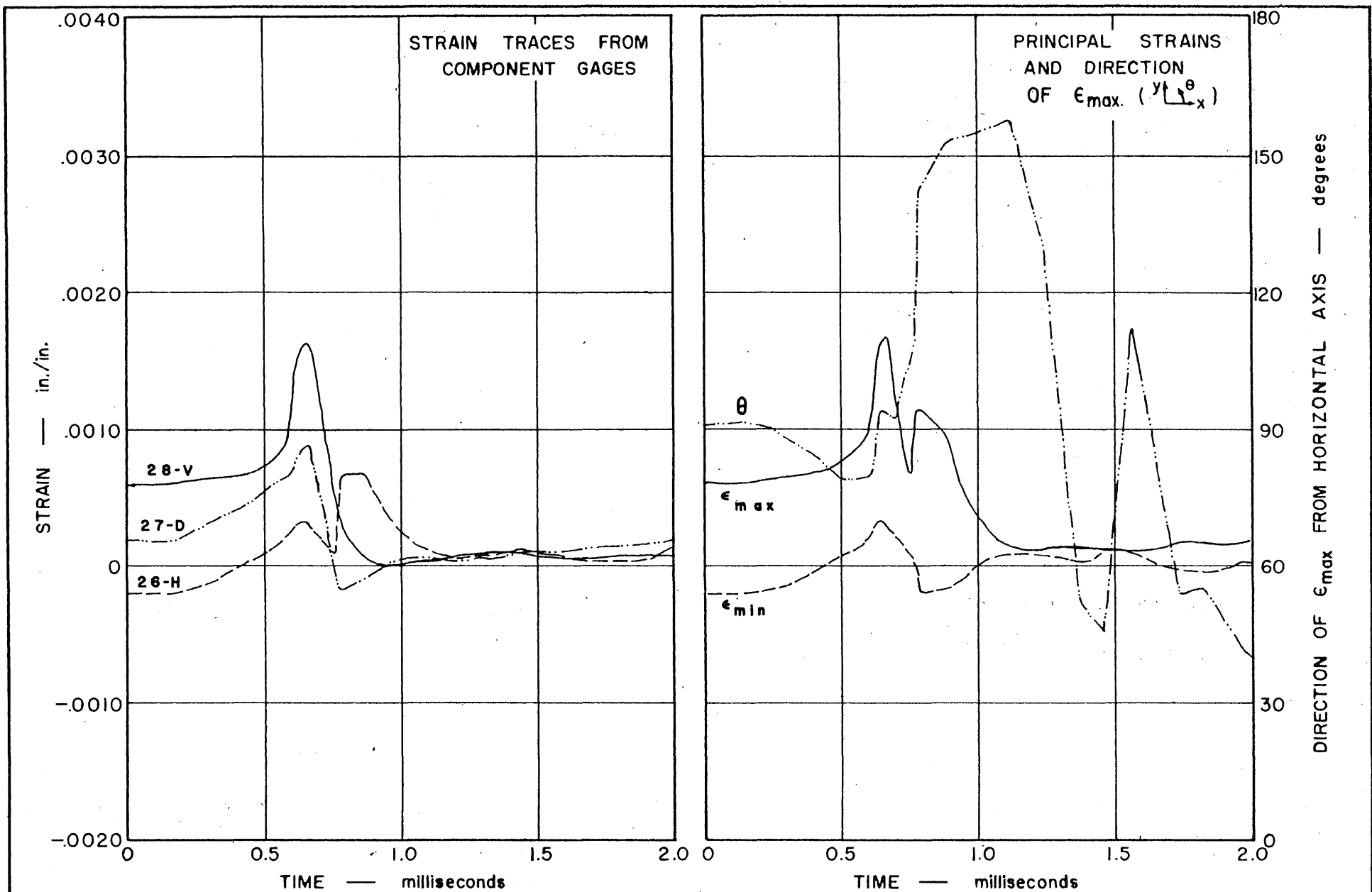
FIG. 47   STRAIN   TRACES   FROM   COMPONENT   GAGES   NOS.   6 , 7 , AND 8 ,
AND   PRINCIPAL   STRAINS   FROM   ROSETTE   2   —   TEST 36
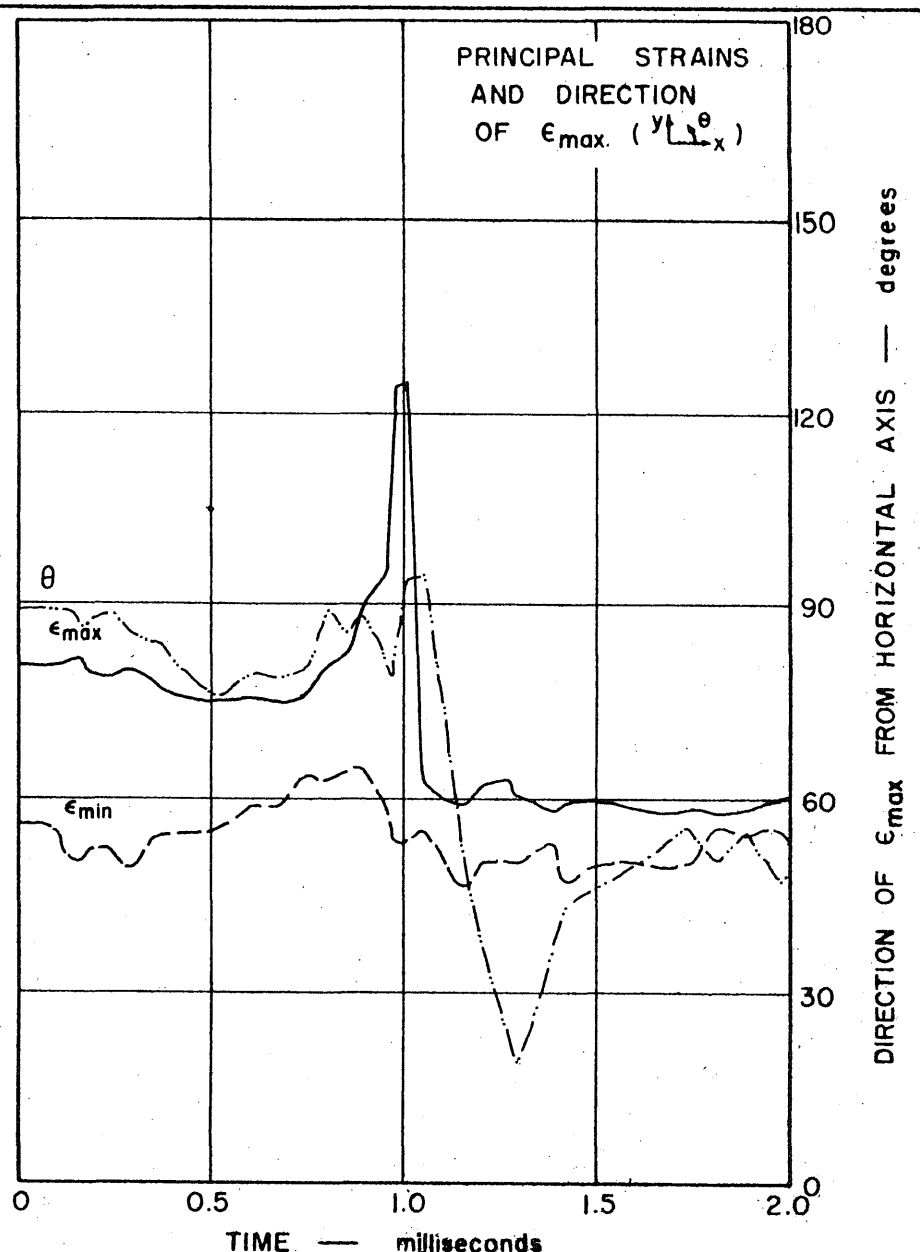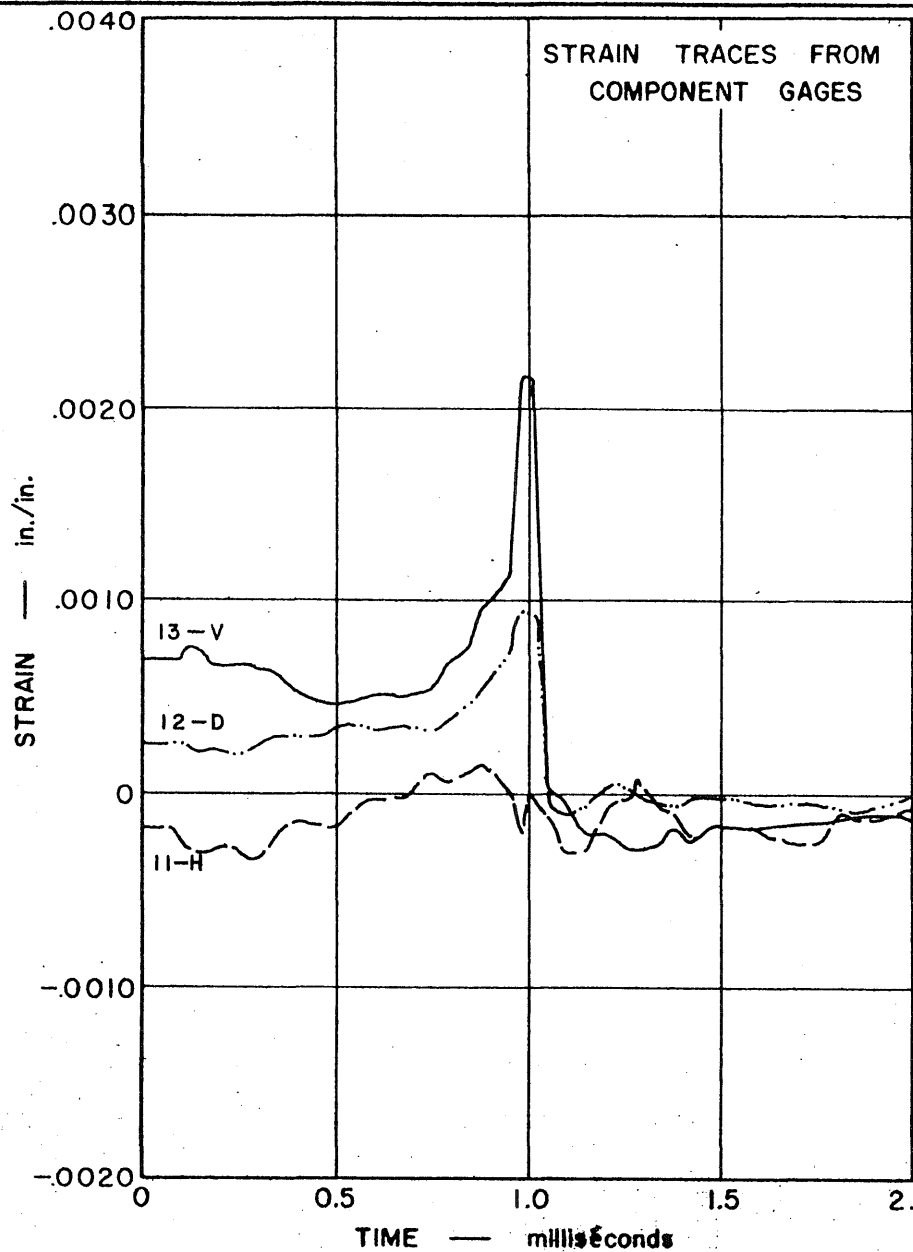
FIG. 48   STRAIN   TRACES   FROM   COMPONENT   GAGES   NOS.   11, 12, AND 13,
AND   PRINCIPAL   STRAINS   FROM   ROSETTE   3   —   TEST 36
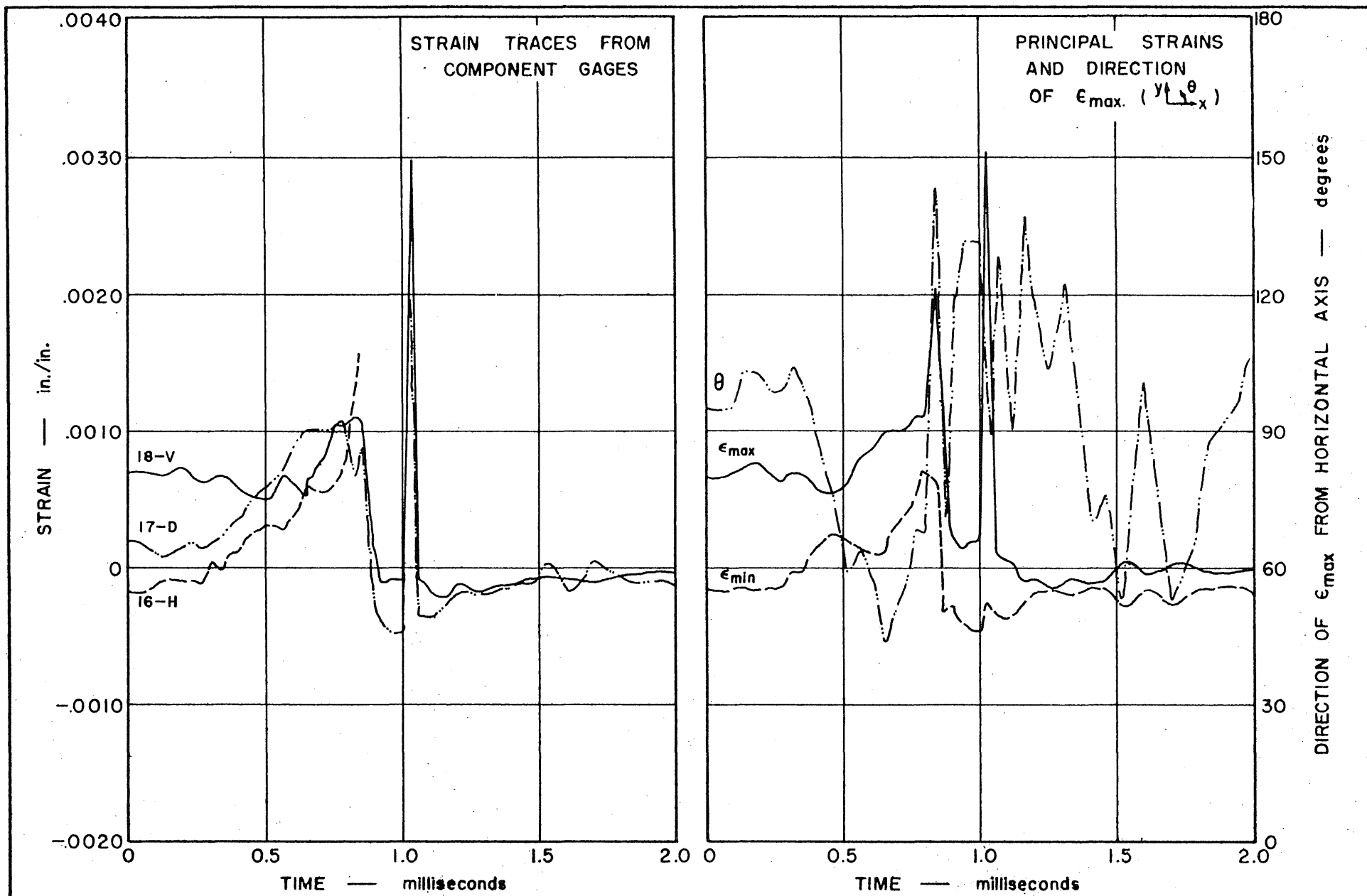
FIG. 49   STRAIN   TRACES   FROM   COMPONENT   GAGES   NOS. 16 , 17, AND 18,
AND   PRINCIPAL   STRAINS   FROM   ROSETTE   4   —   TEST 36
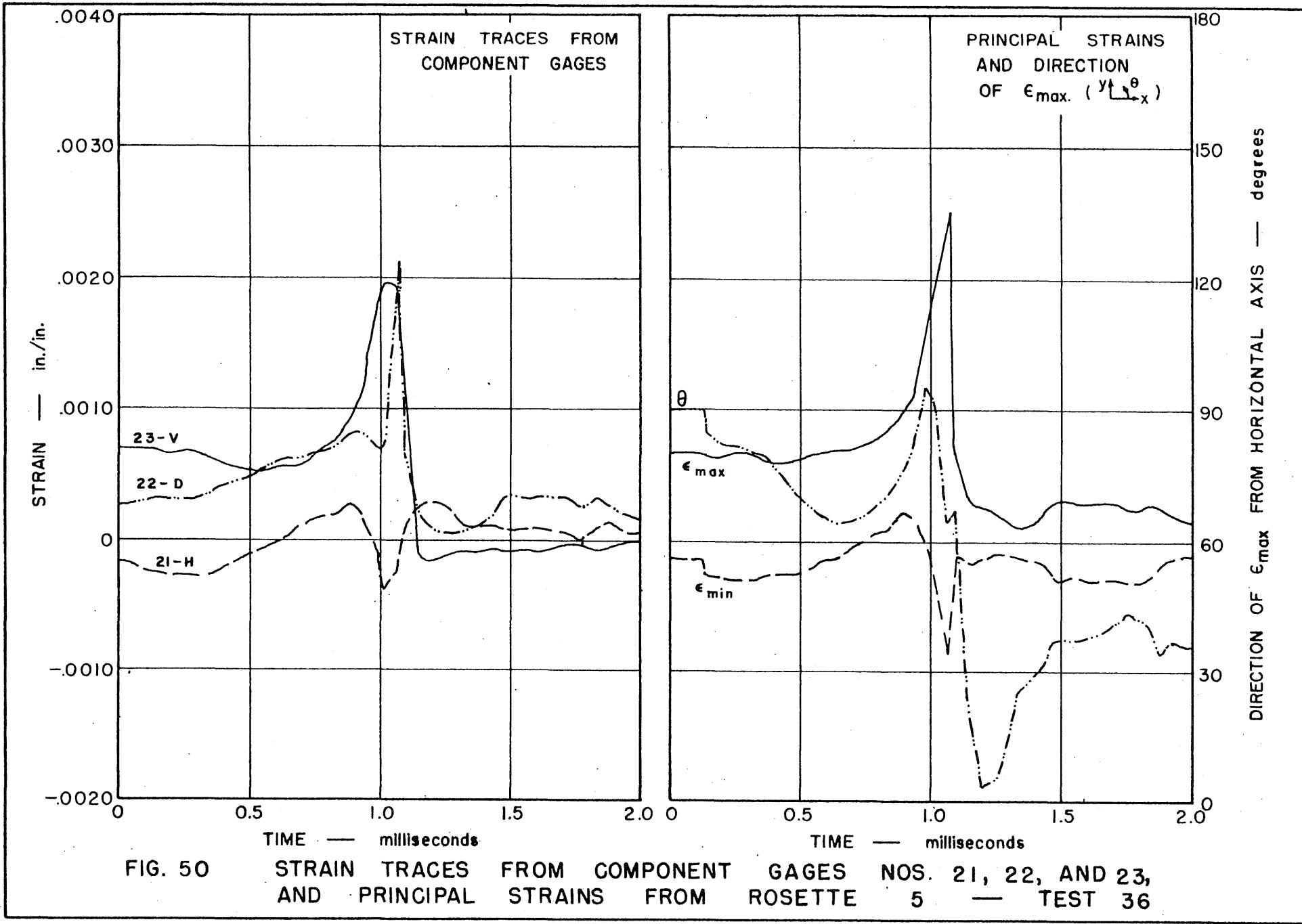
FIG. 50   STRAIN   TRACES   FROM   COMPONENT   GAGES   NOS.   21, 22, AND 23,
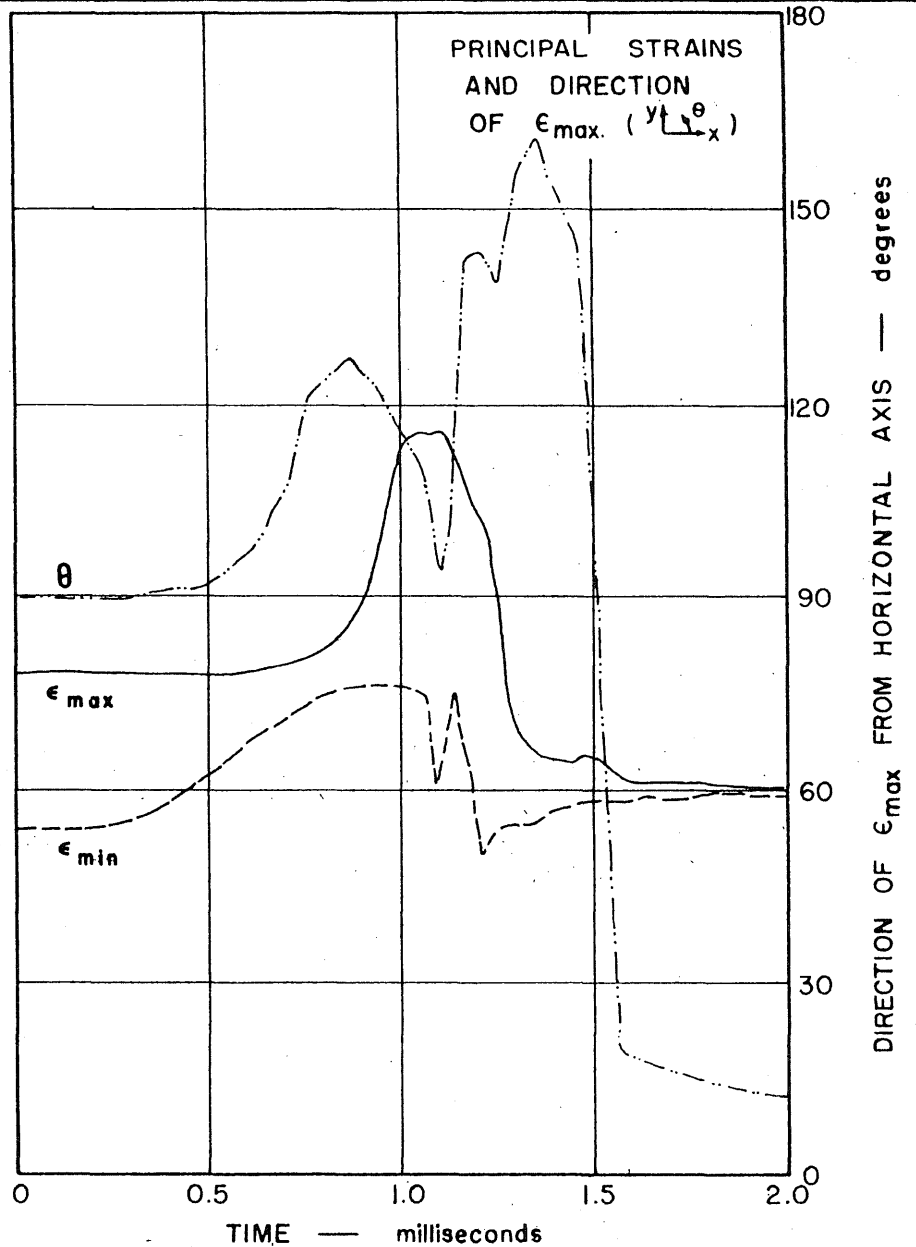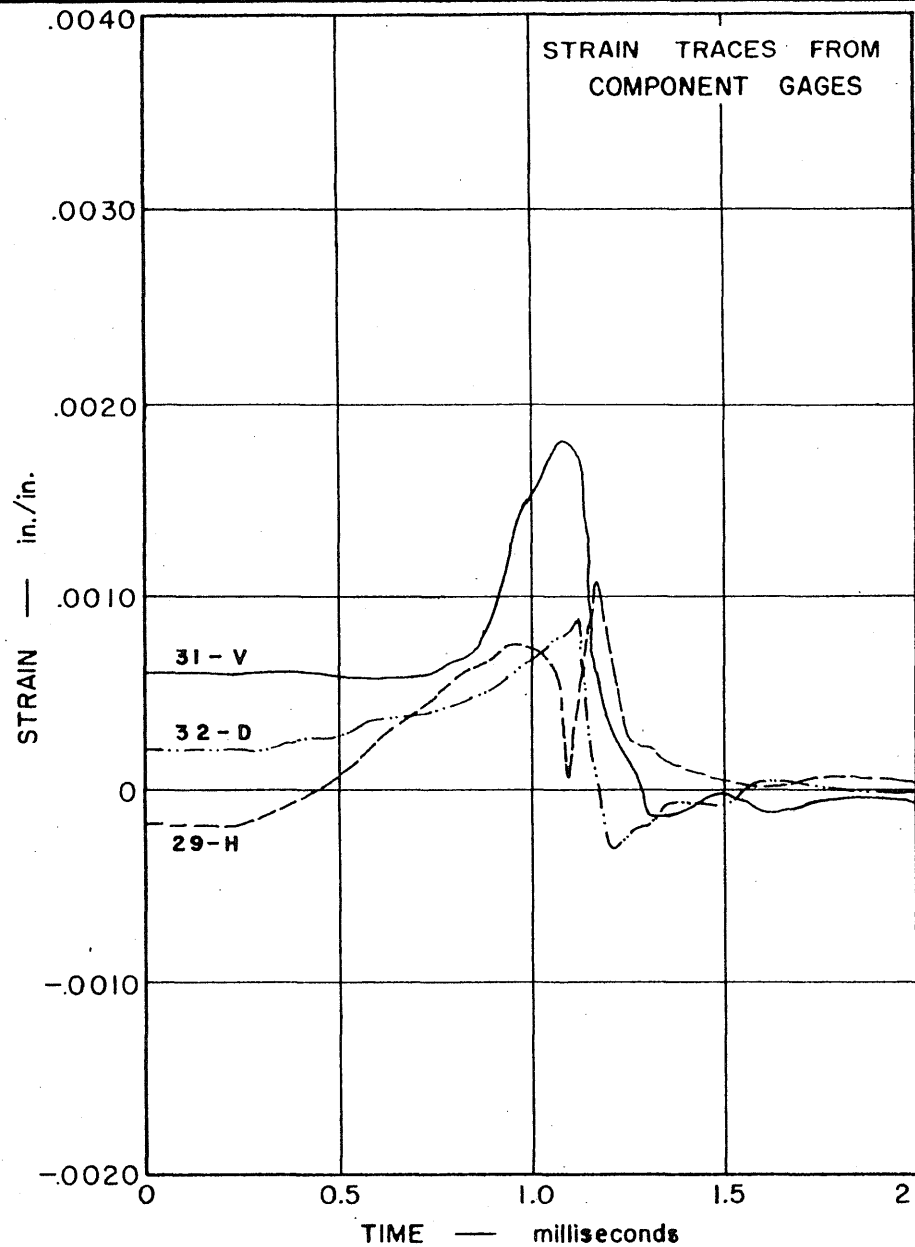AND   PRINCIPAL   STRAINS   FROM   ROSETTE   5   —   TEST 36
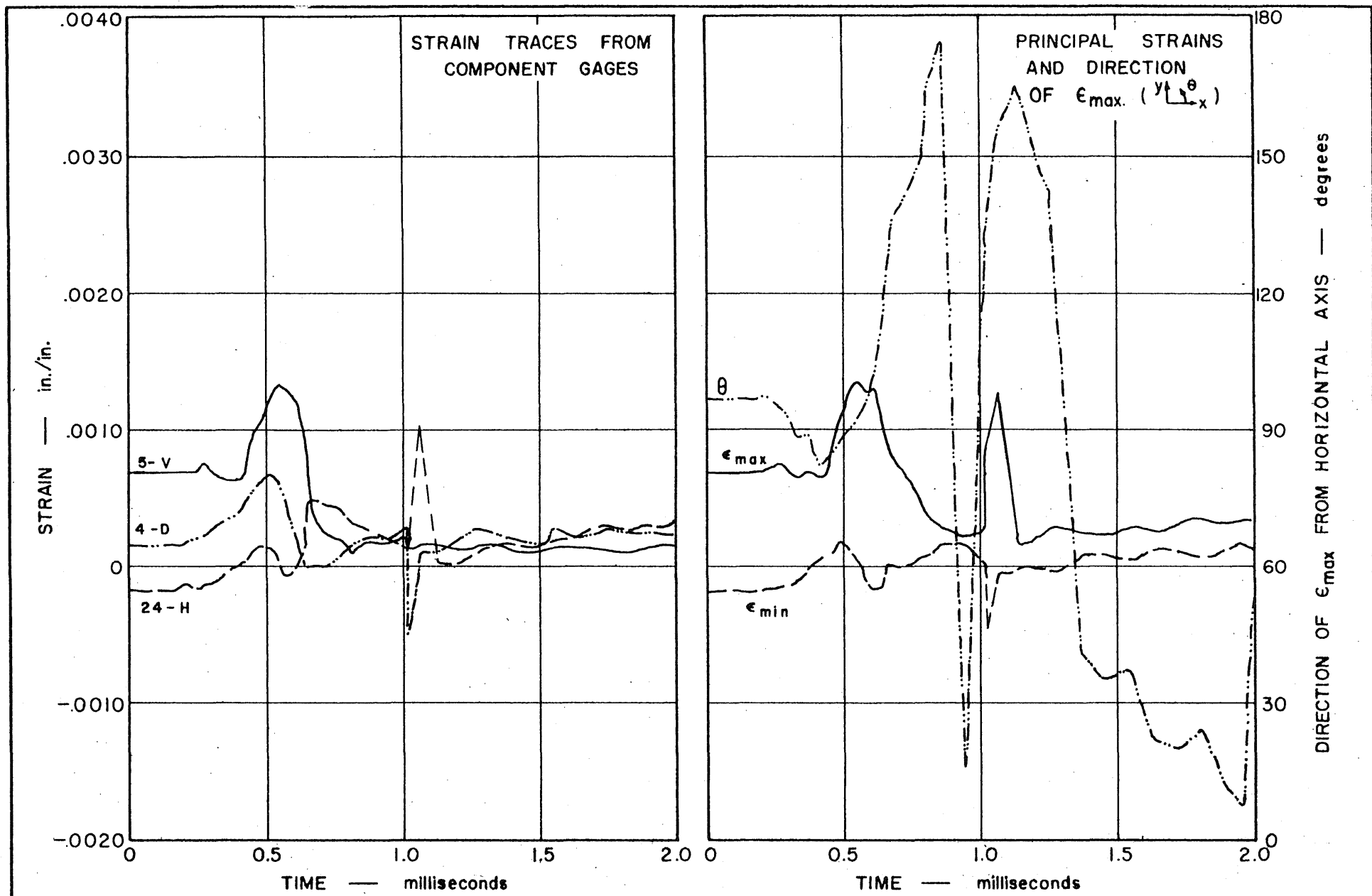
FIG. 51   STRAIN   TRACES   FROM   COMPONENT   GAGES   NOS. 24, 4 , AND 5,
AND   PRINCIPAL   STRAINS   FROM   ROSETTE   6   —   TEST 36
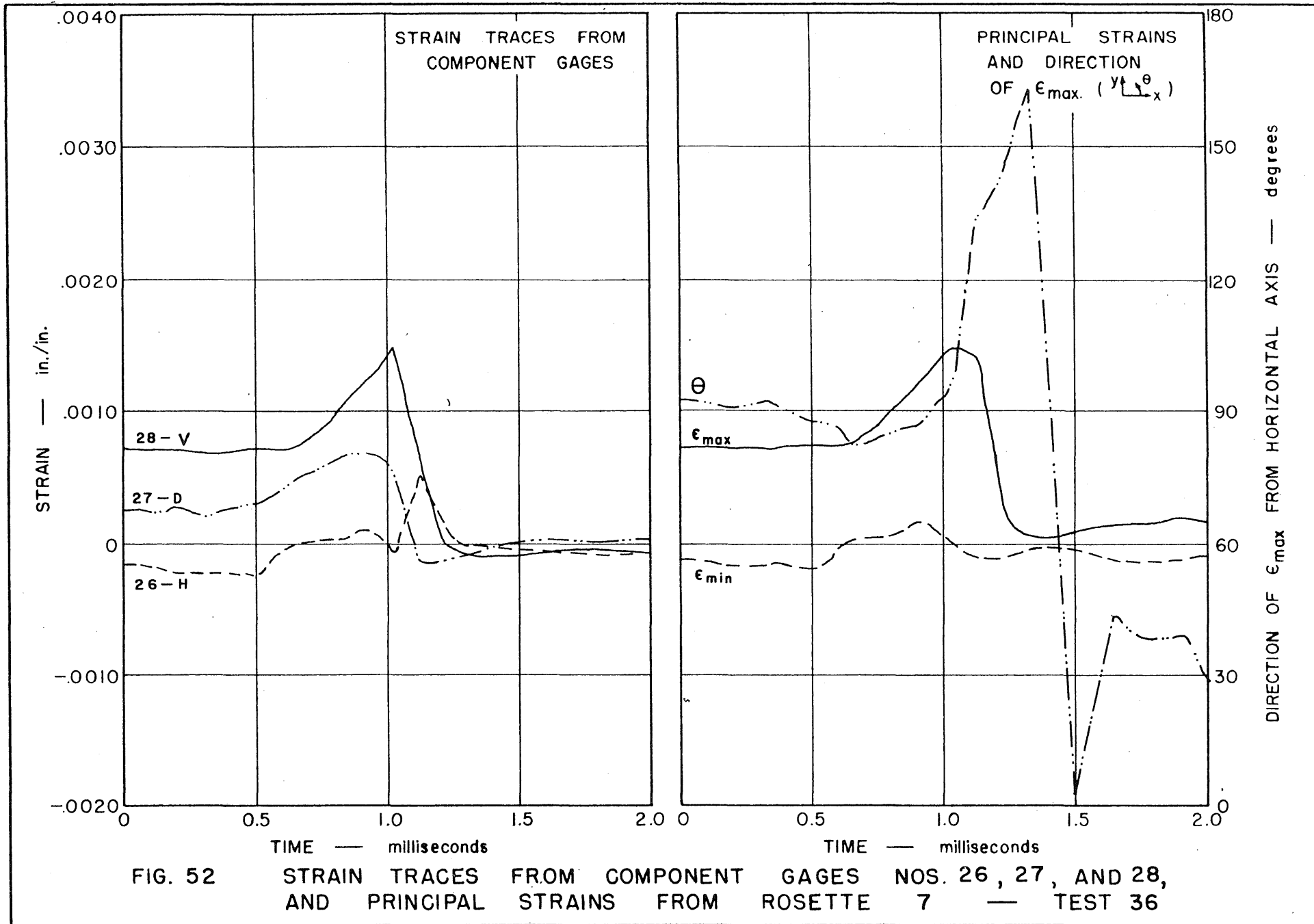
FIG. 52   STRAIN TRACES FROM COMPONENT GAGES NOS. 26, 27, AND 28, AND PRINCIPAL STRAINS FROM ROSETTE 7 — TEST 36
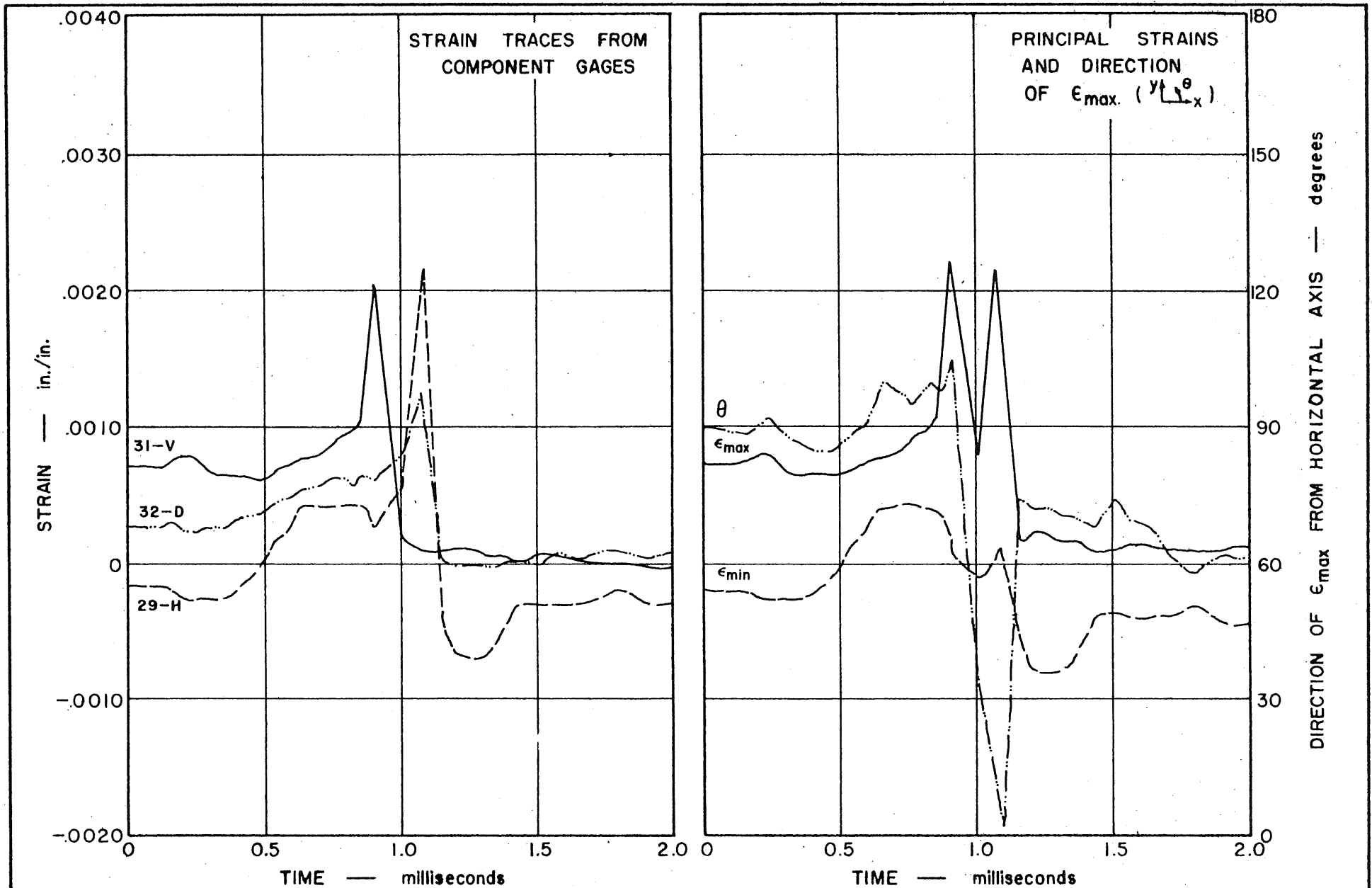
FIG. 53   STRAIN   TRACES   FROM   COMPONENT   GAGES   NOS. 29, 32, AND 31,
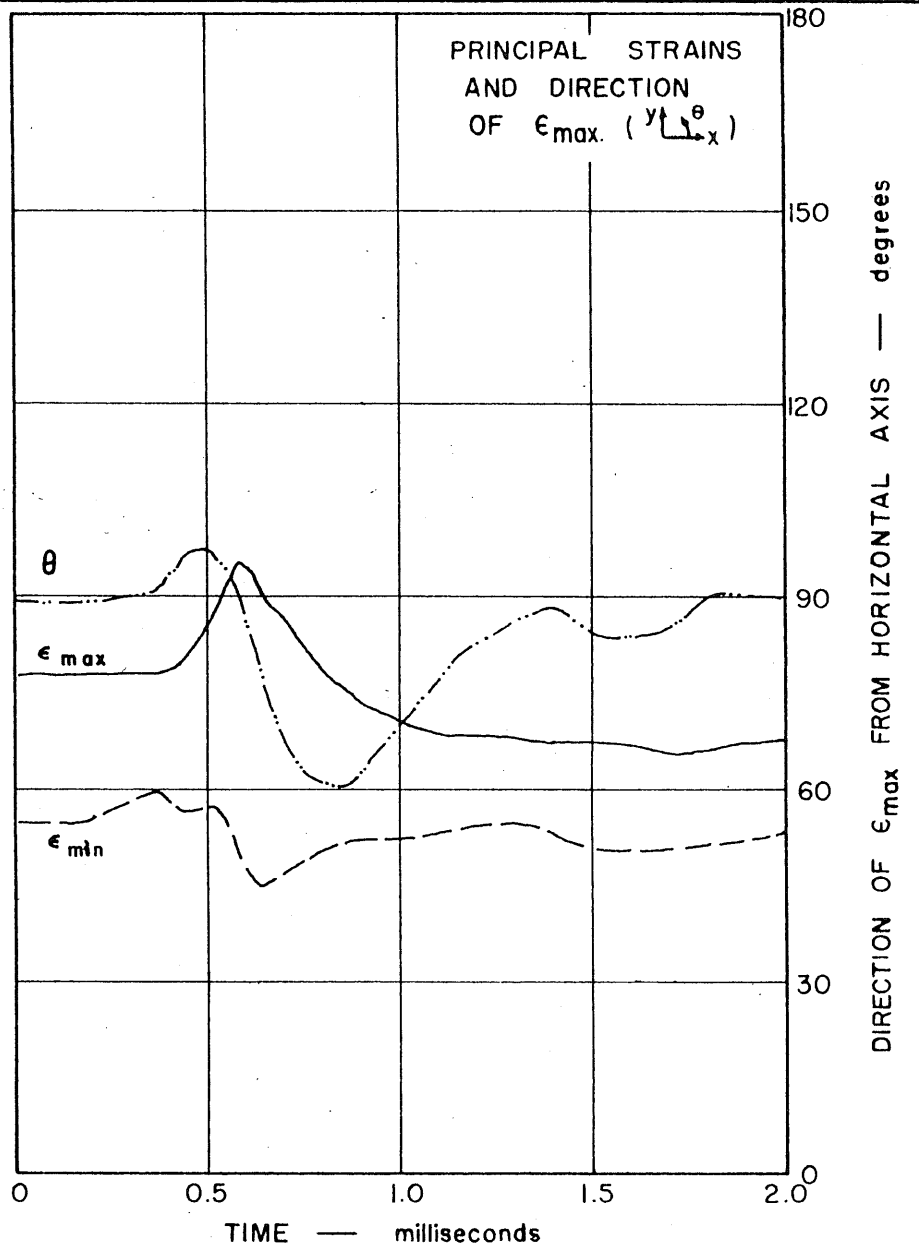AND   PRINCIPAL   STRAINS   FROM   ROSETTE   8   —   TEST 36
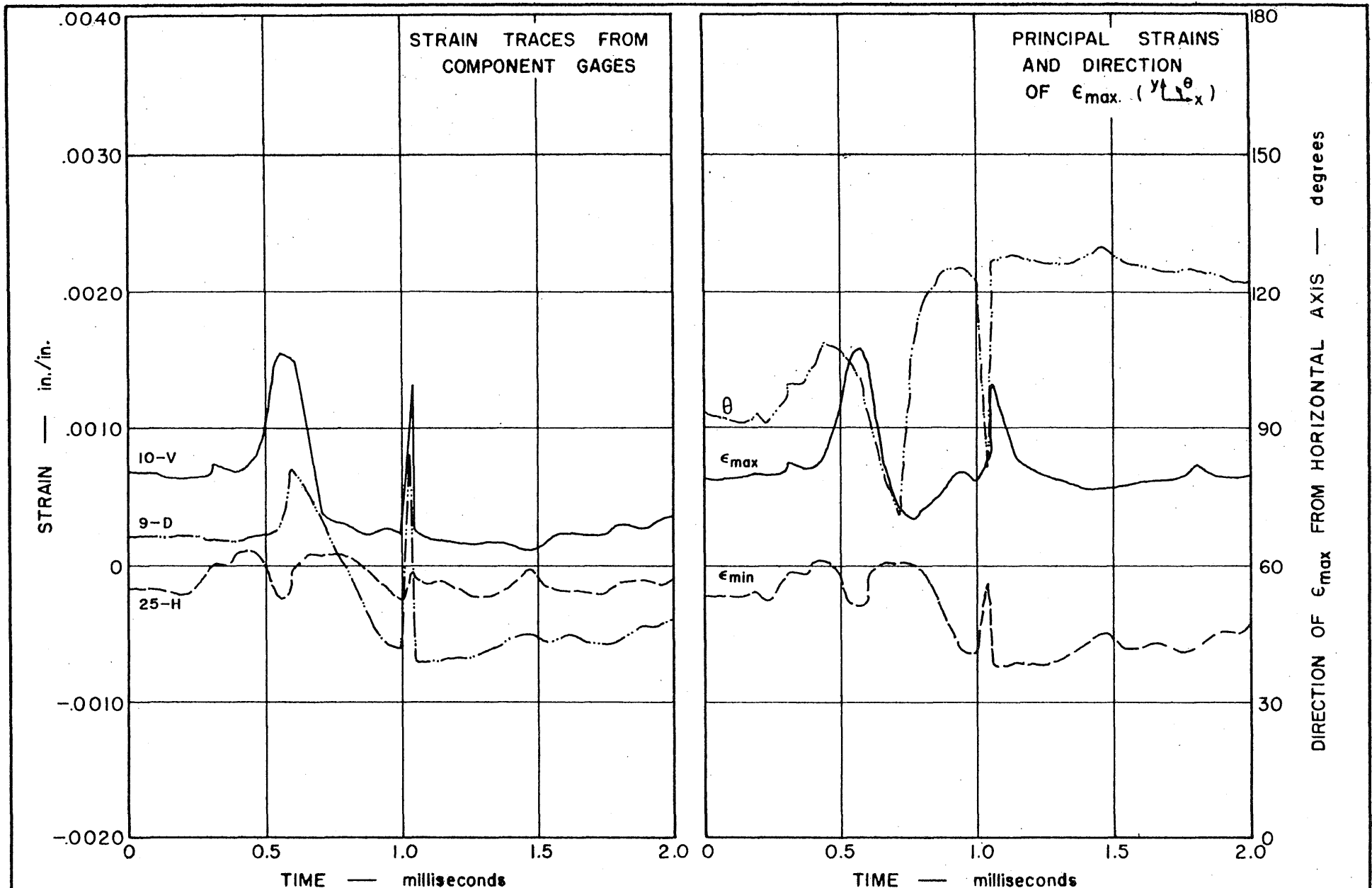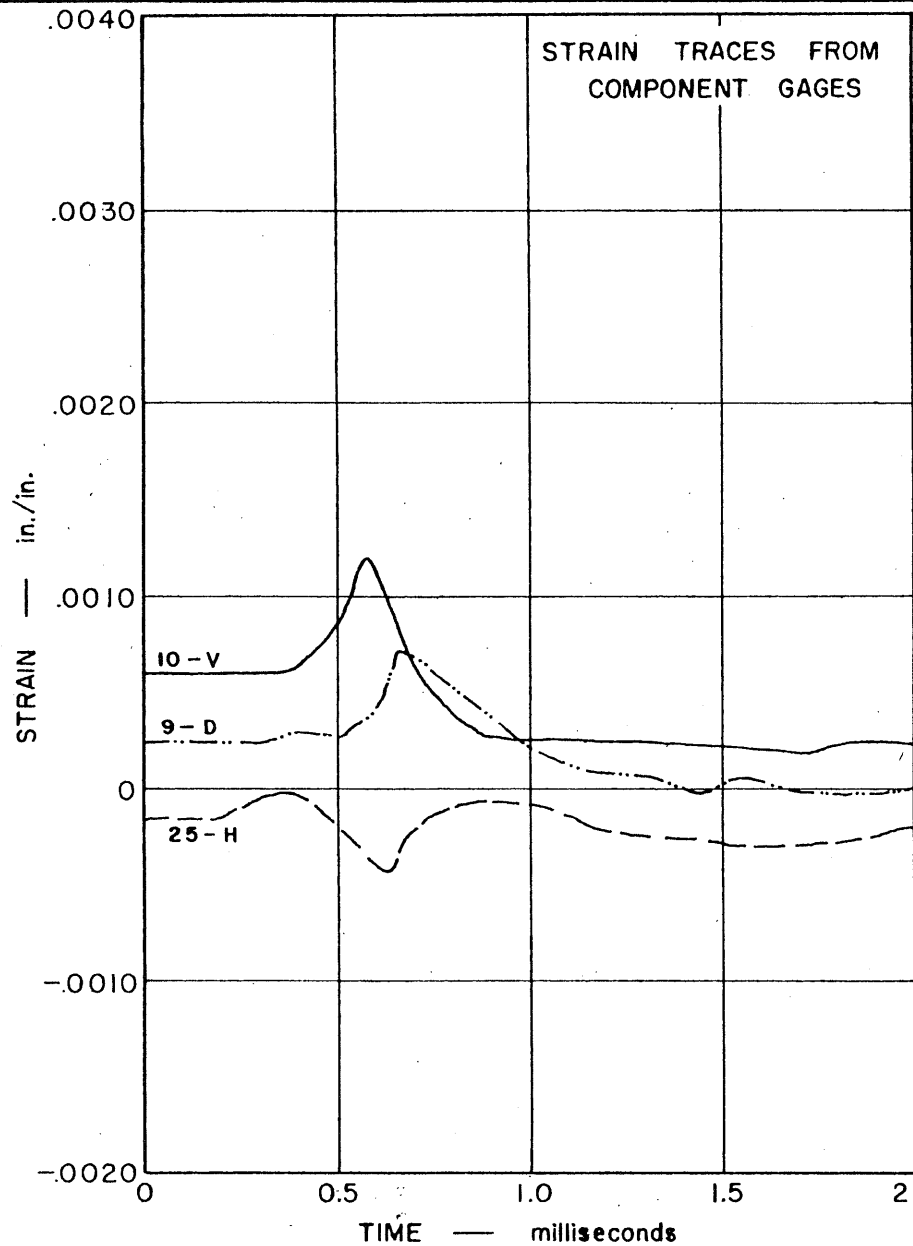
FIG. 54   STRAIN   TRACES   FROM   COMPONENT   GAGES   NOS. 25, 9, AND 10,
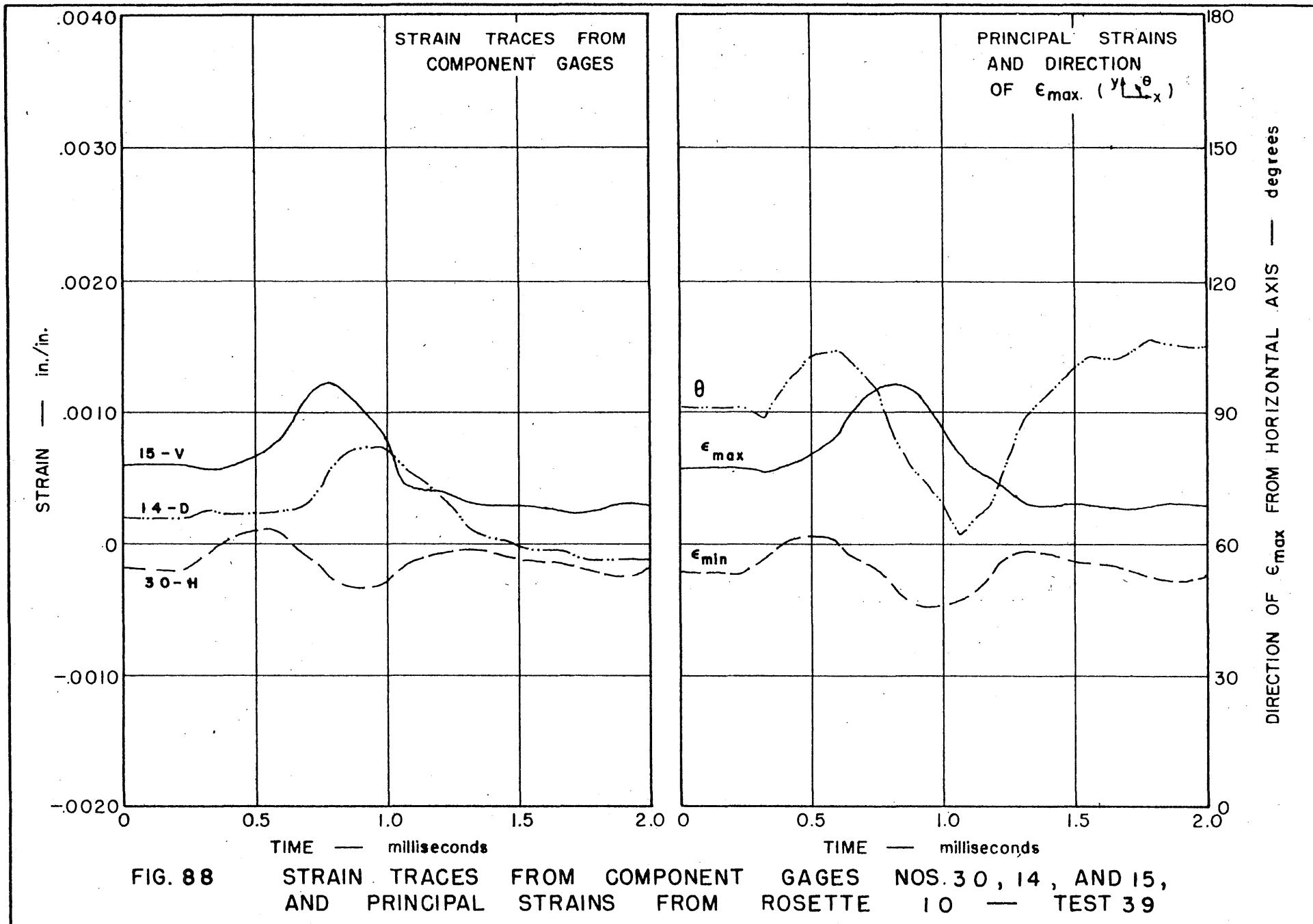   AND   PRINCIPAL   STRAINS   FROM   ROSETTE   9   —   TEST 36
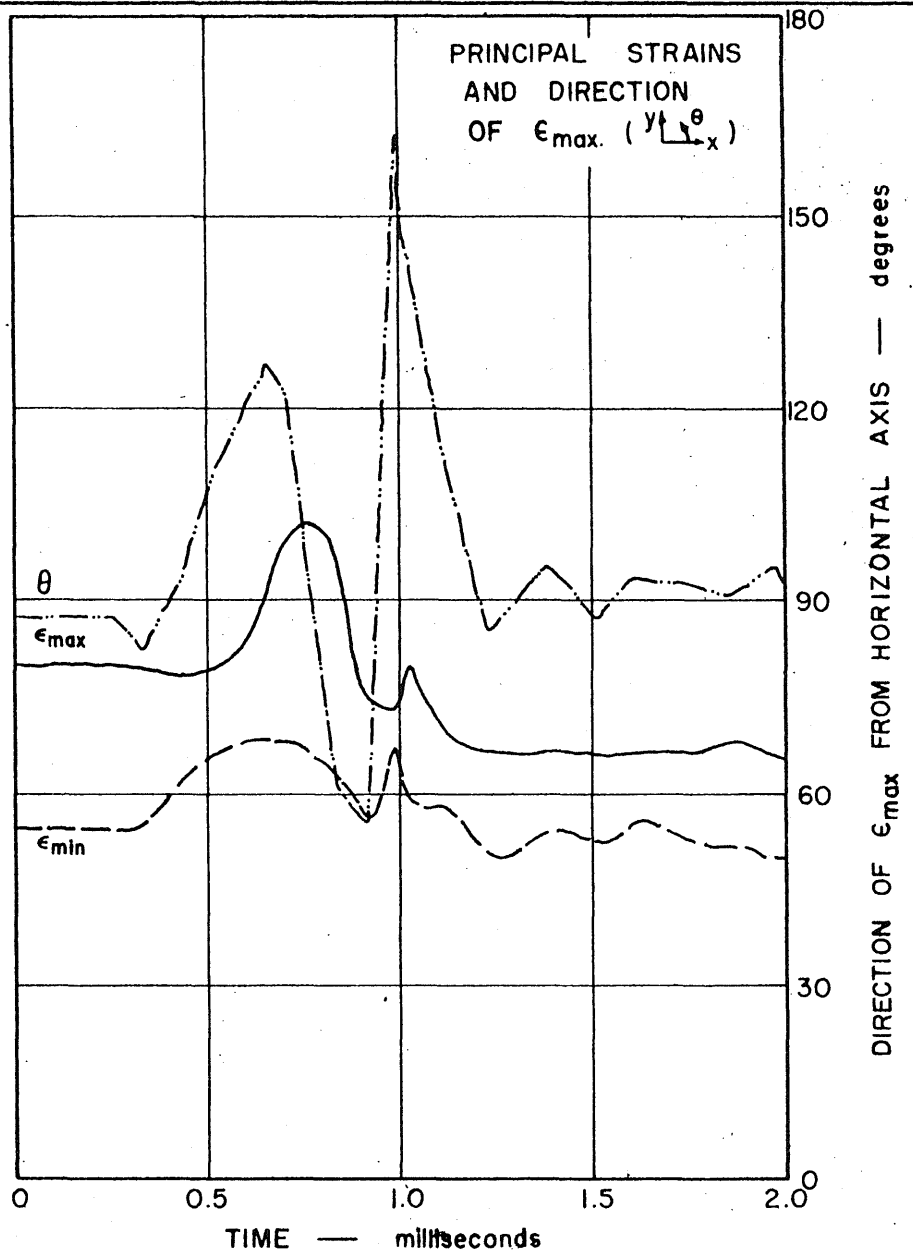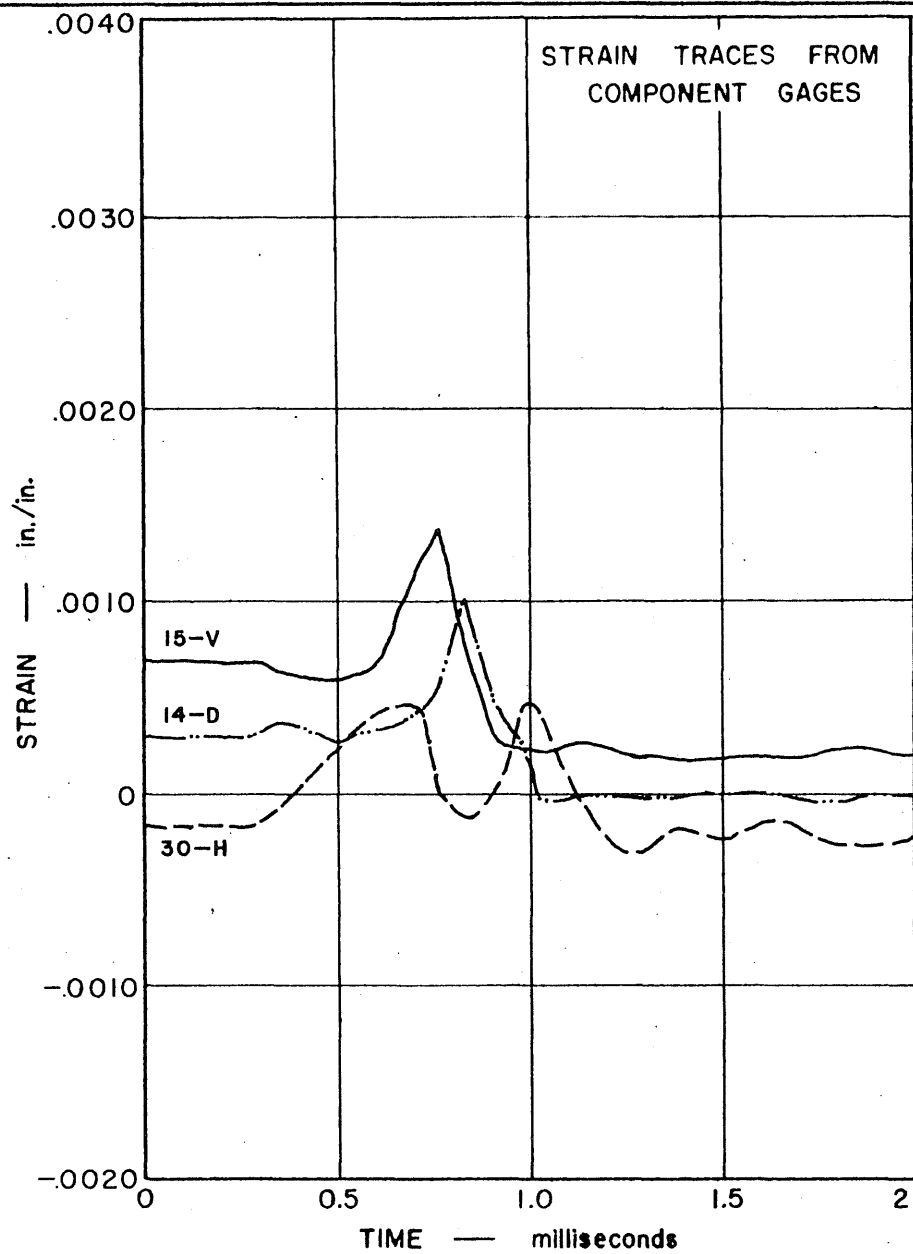
FIG. 55 STRAIN TRACES FROM COMPONENT GAGES NOS. 30, 14, AND 15,
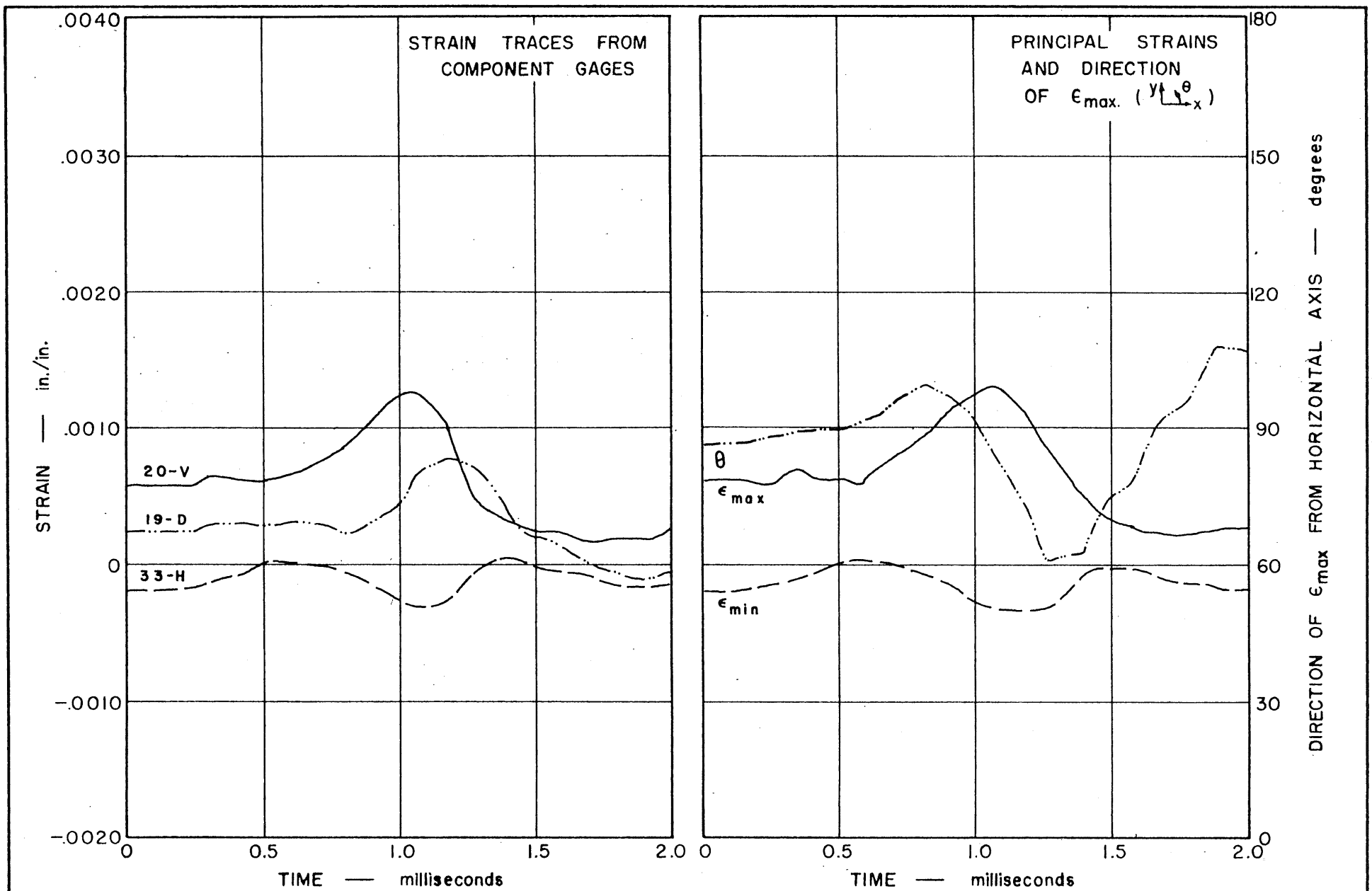AND PRINCIPAL STRAINS FROM ROSETTE 10 — TEST 36
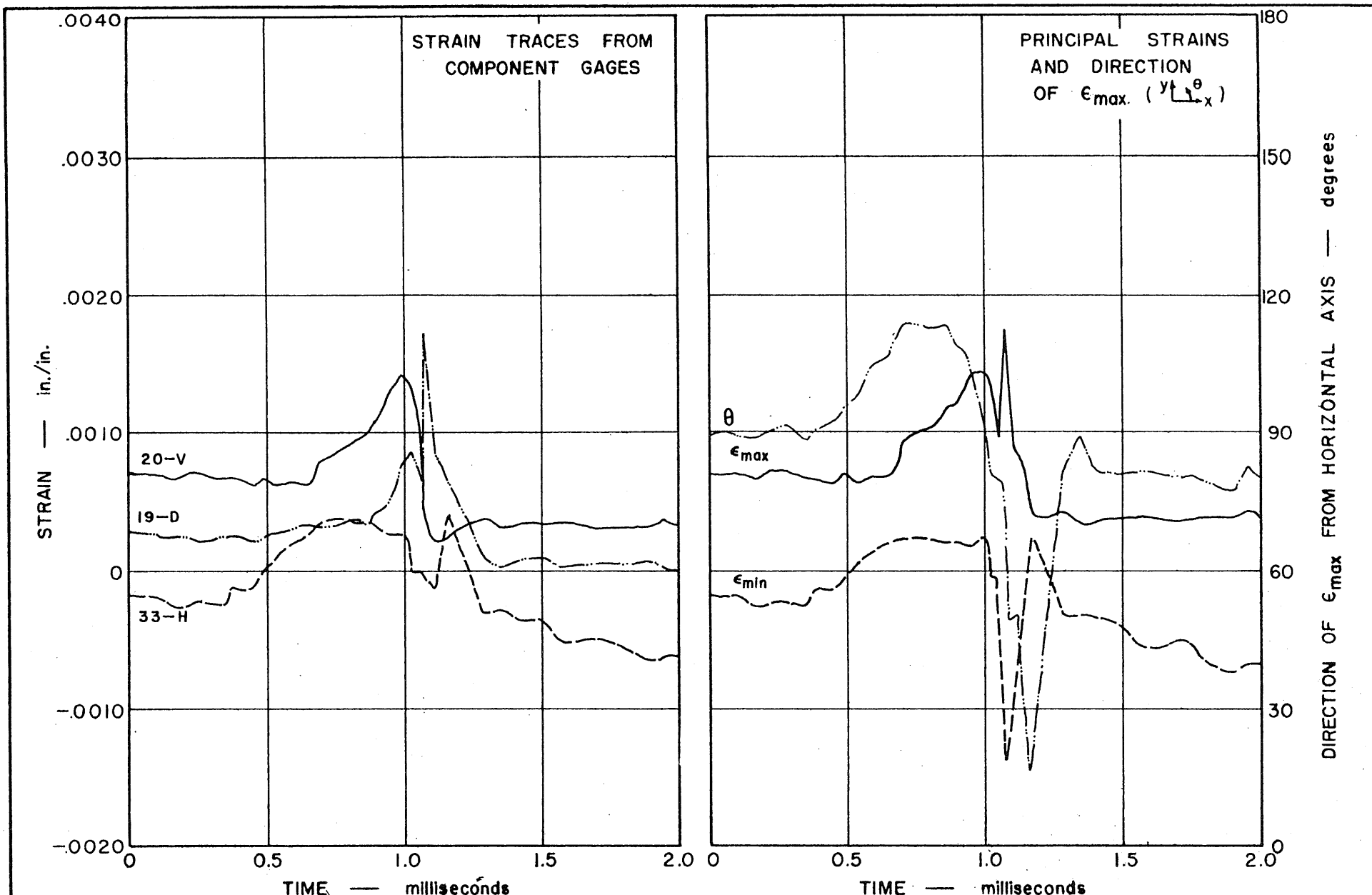
FIG. 56   STRAIN   TRACES   FROM   COMPONENT   GAGES   NOS. 33 , 19 , AND 20,
AND   PRINCIPAL   STRAINS   FROM   ROSETTE   II   —   TEST 36
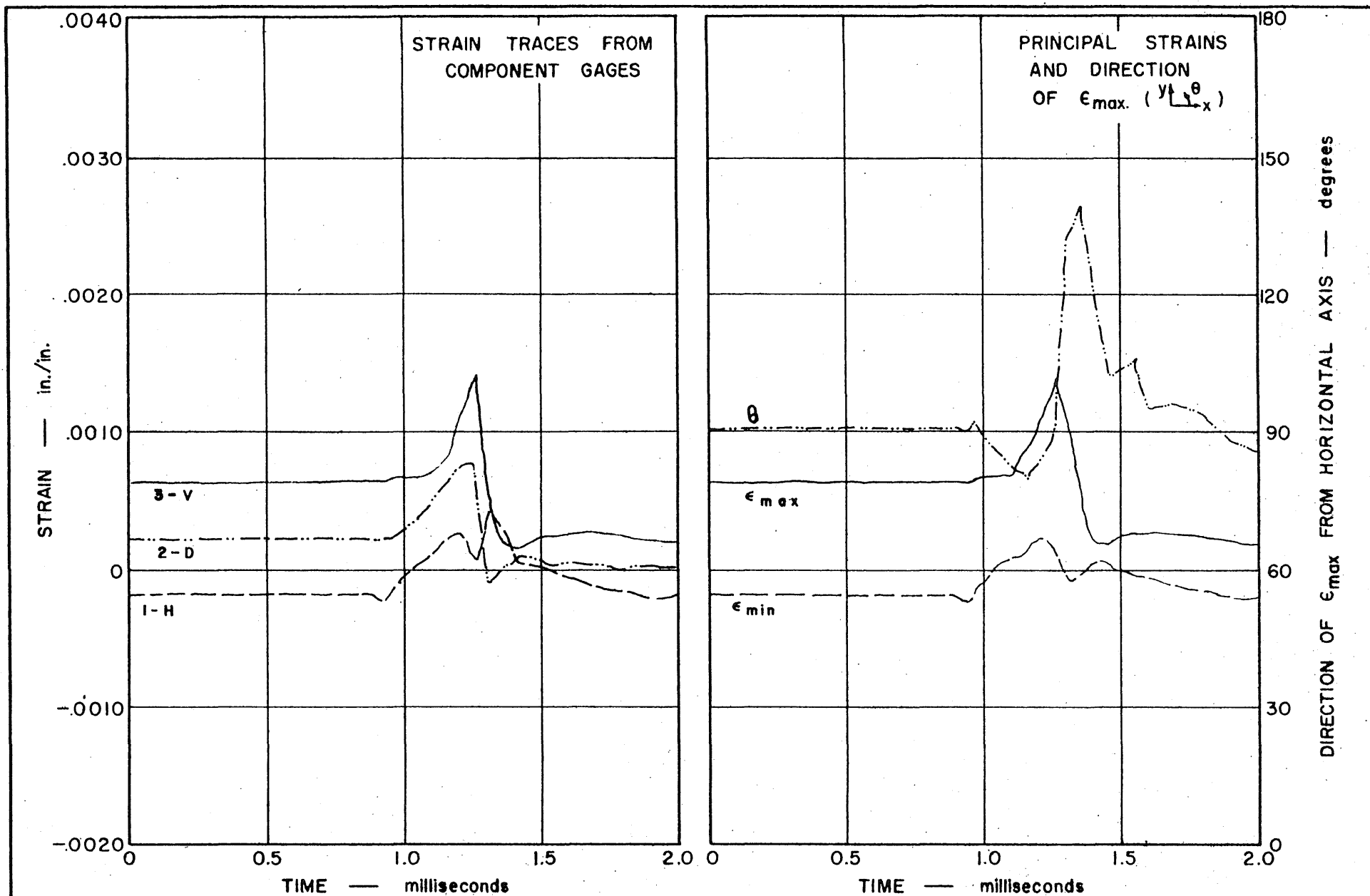
FIG. 57   STRAIN TRACES FROM COMPONENT GAGES NOS. 1, 2, AND 3, AND PRINCIPAL STRAINS FROM ROSETTE 1 — TEST 37
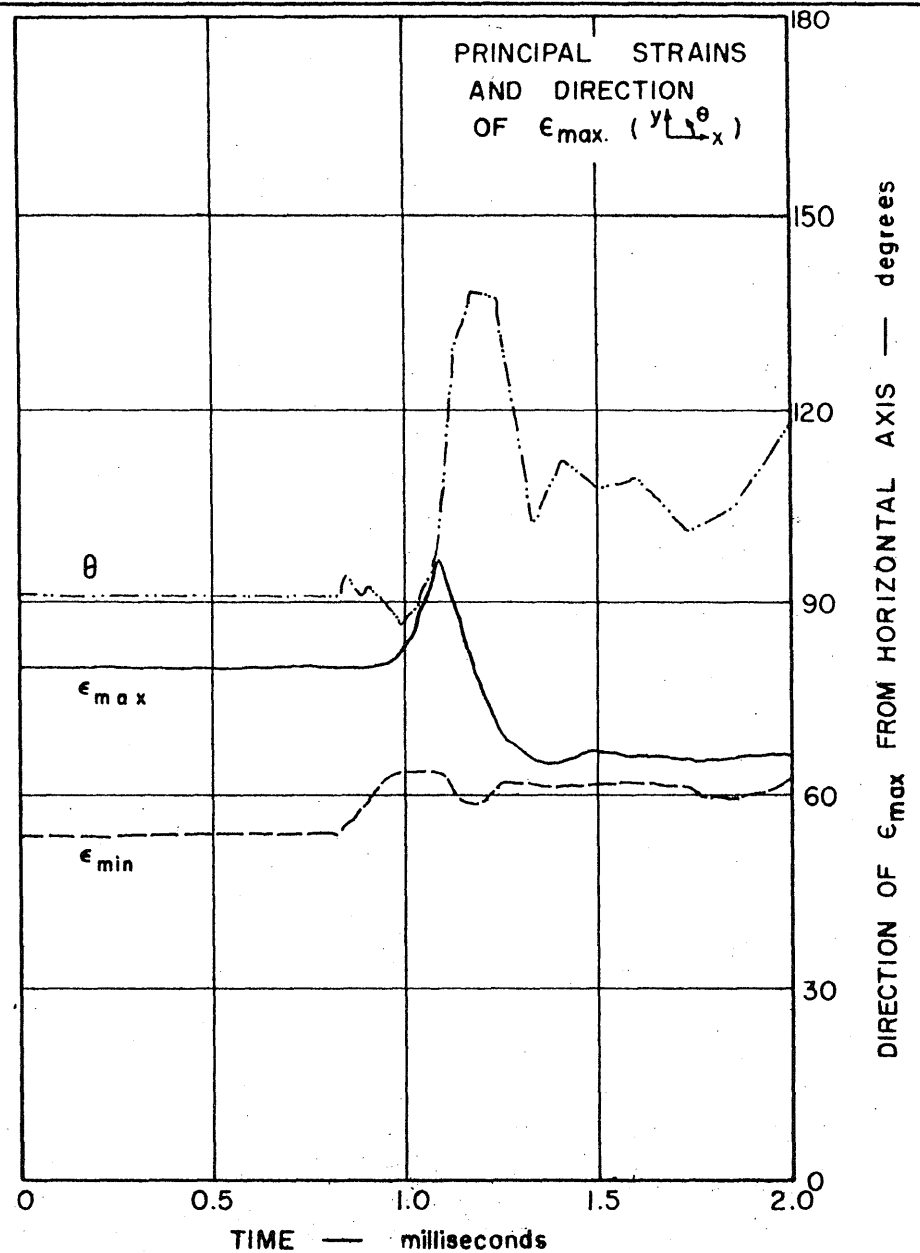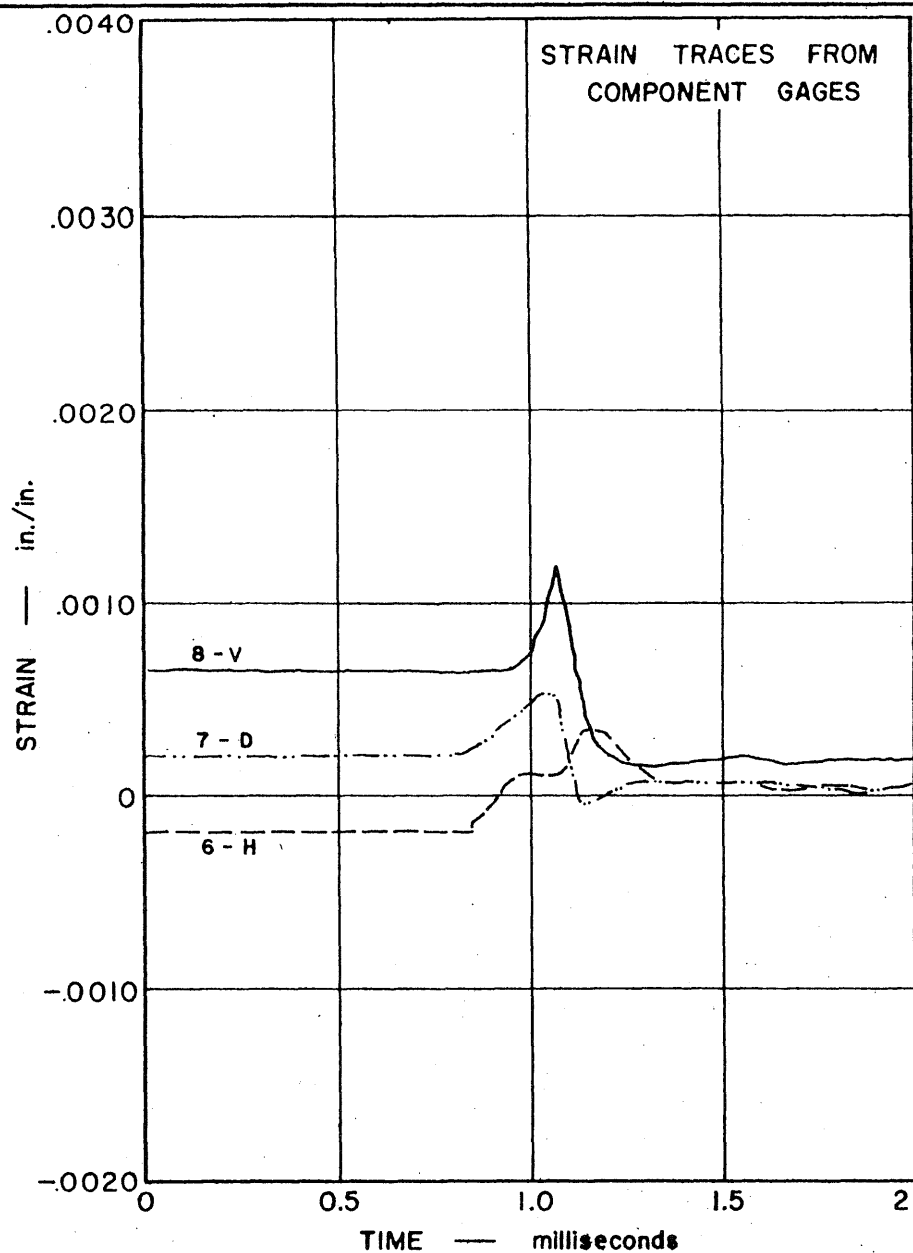
FIG. 58 STRAIN TRACES FROM COMPONENT GAGES NOS. 6 , 7 , AND 8 , AND PRINCIPAL STRAINS FROM ROSETTE 2 — TEST 37
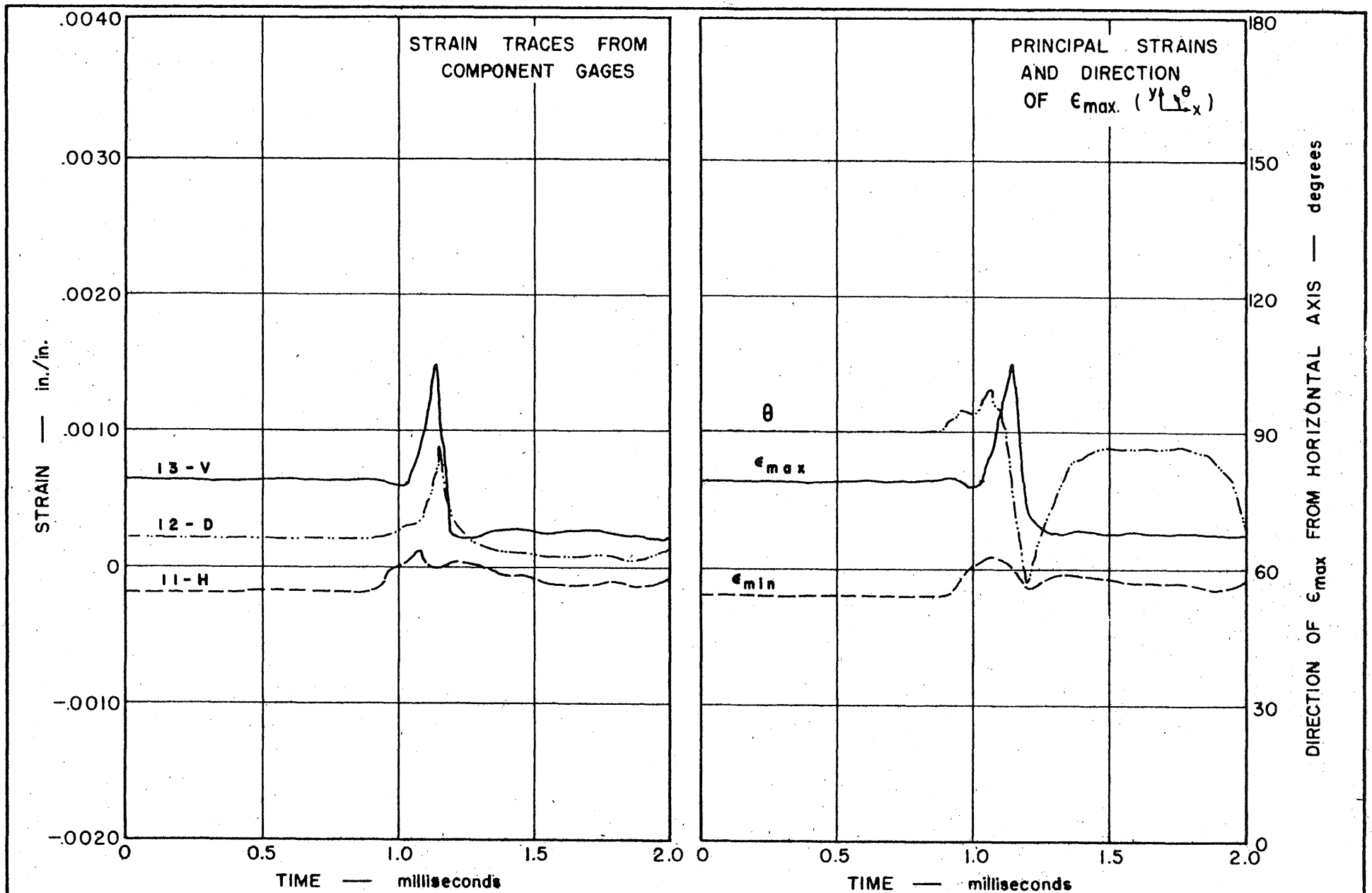
FIG. 59   STRAIN   TRACES   FROM   COMPONENT   GAGES   NOS.   11, 12, AND 13,
AND   PRINCIPAL   STRAINS   FROM   ROSETTE   3   —   TEST 37
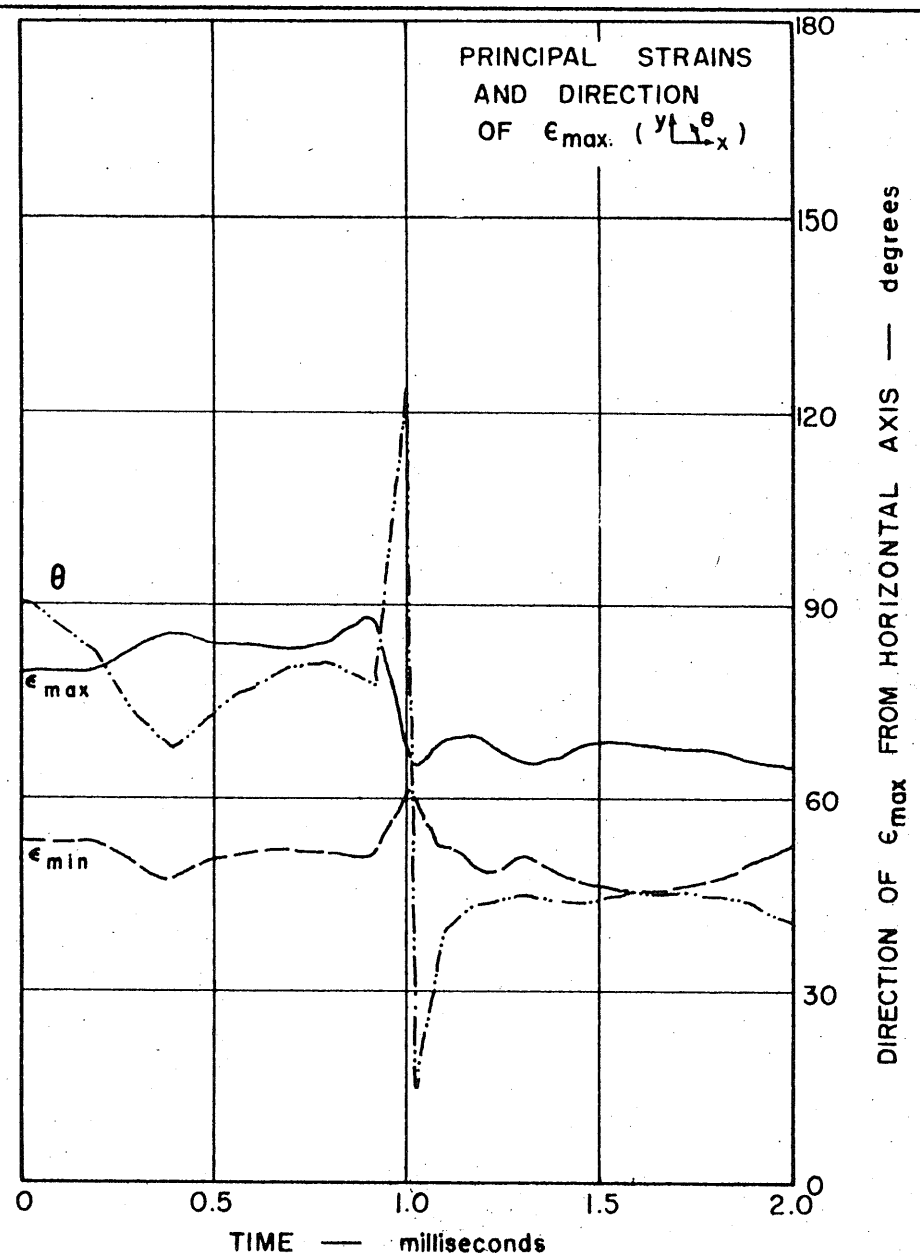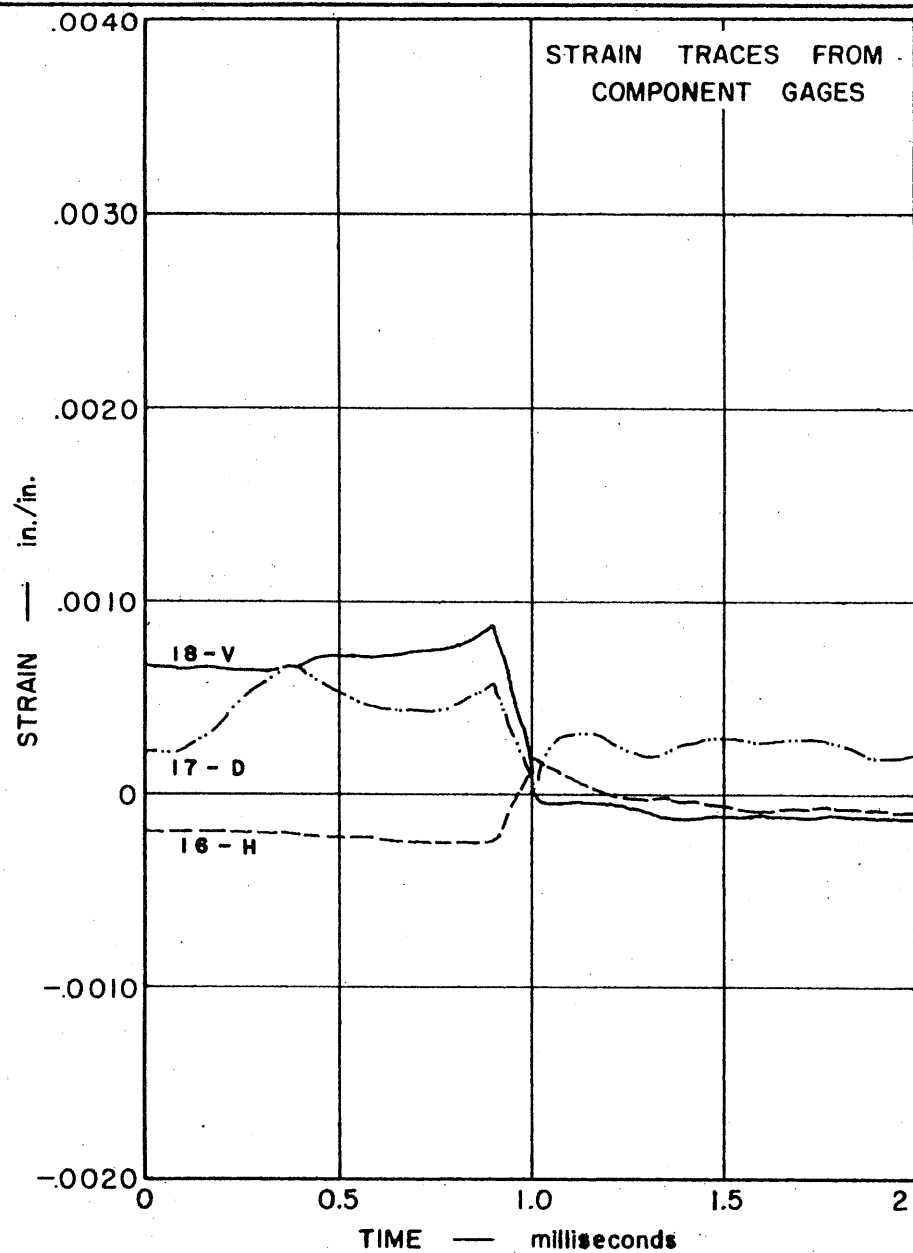
FIG. 60   STRAIN   TRACES   FROM   COMPONENT   GAGES   NOS. 16, 17, AND 18,
AND   PRINCIPAL   STRAINS   FROM   ROSETTE   4 — TEST 37
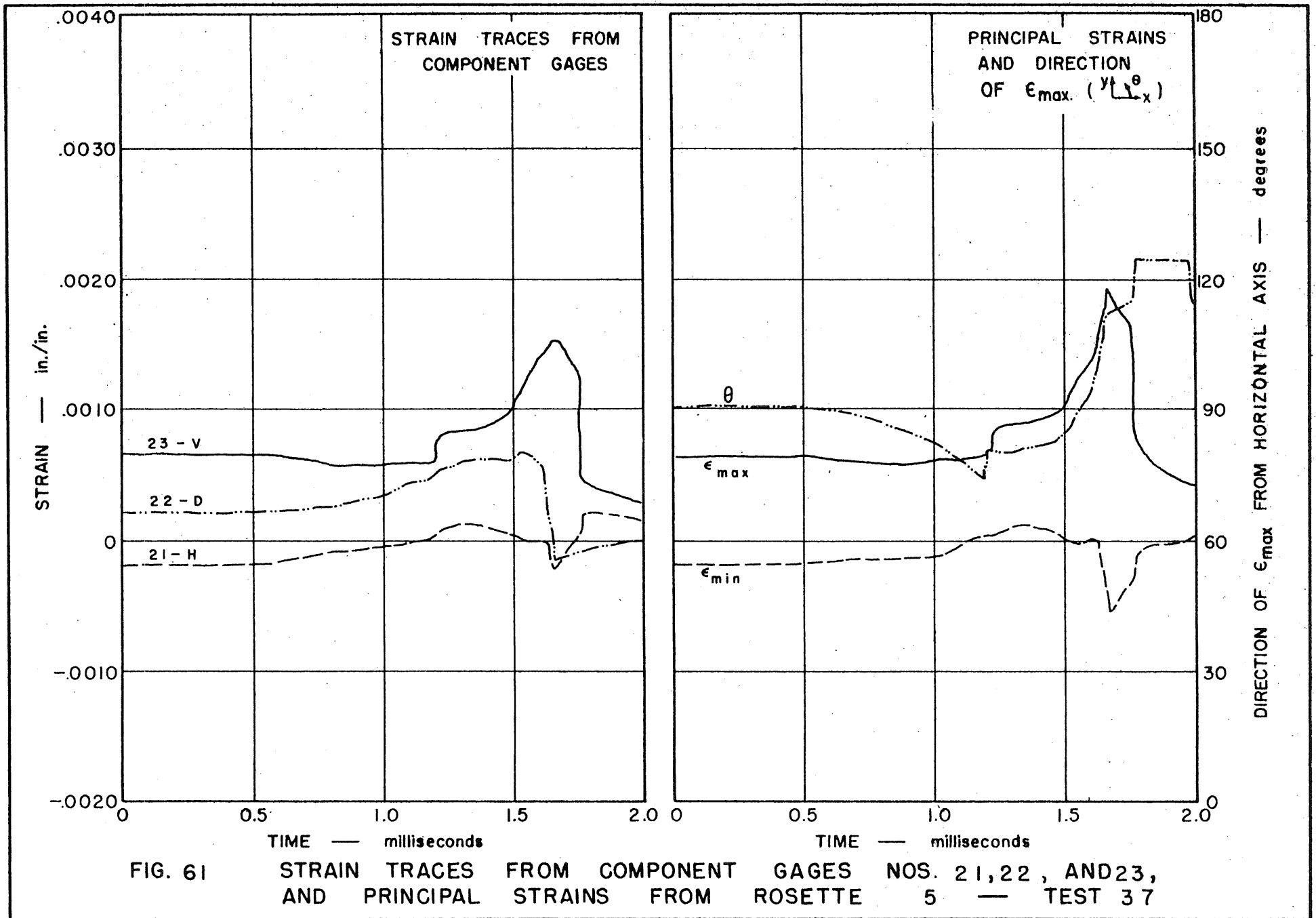
FIG. 61   STRAIN   TRACES   FROM   COMPONENT   GAGES   NOS. 21, 22, AND 23,
AND   PRINCIPAL   STRAINS   FROM   ROSETTE   5   —   TEST 37
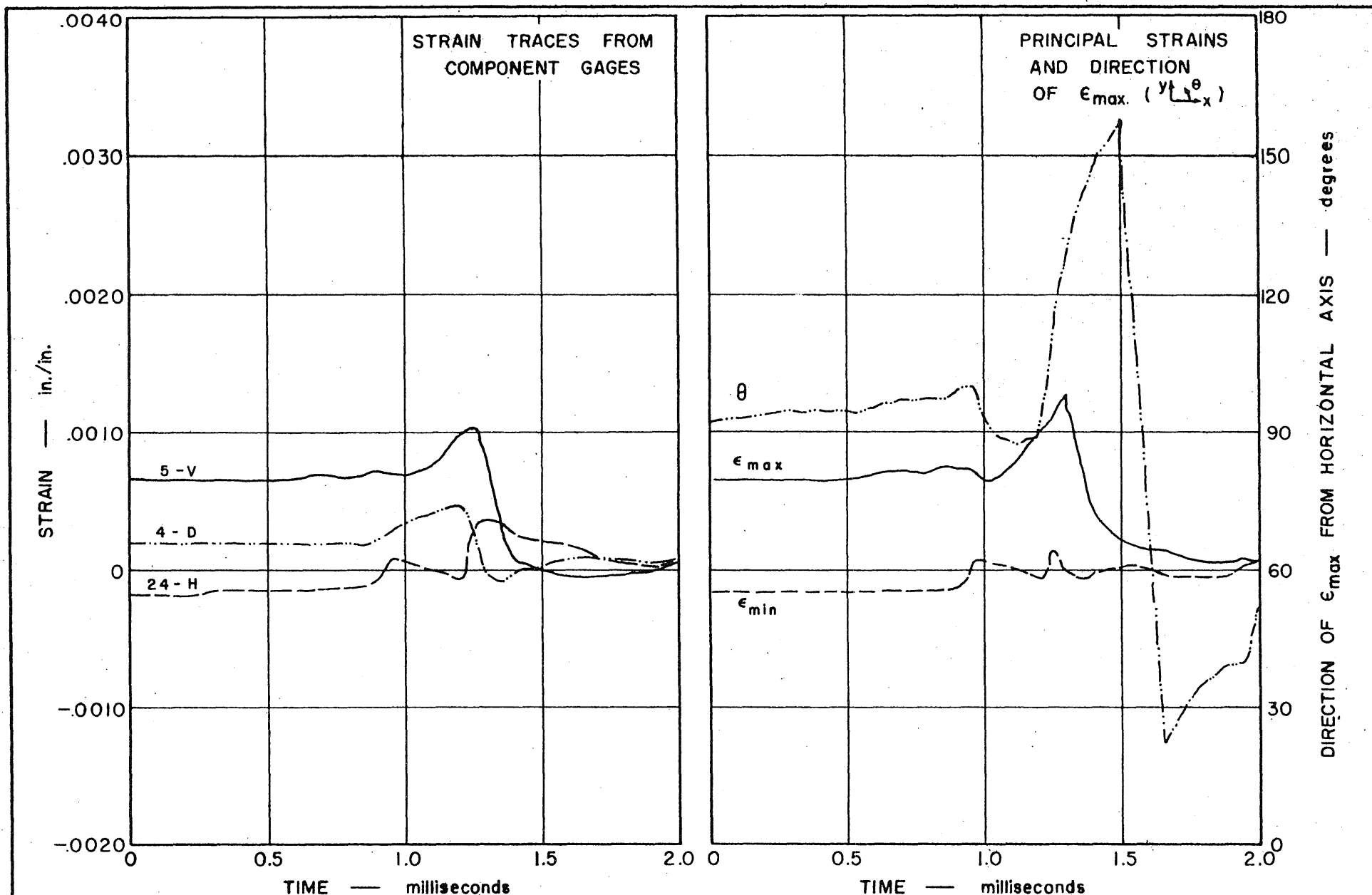
FIG. 62   STRAIN   TRACES   FROM   COMPONENT   GAGES   NOS. 24 , 4 , AND 5 ,
AND   PRINCIPAL   STRAINS   FROM   ROSETTE   6 — TEST 37
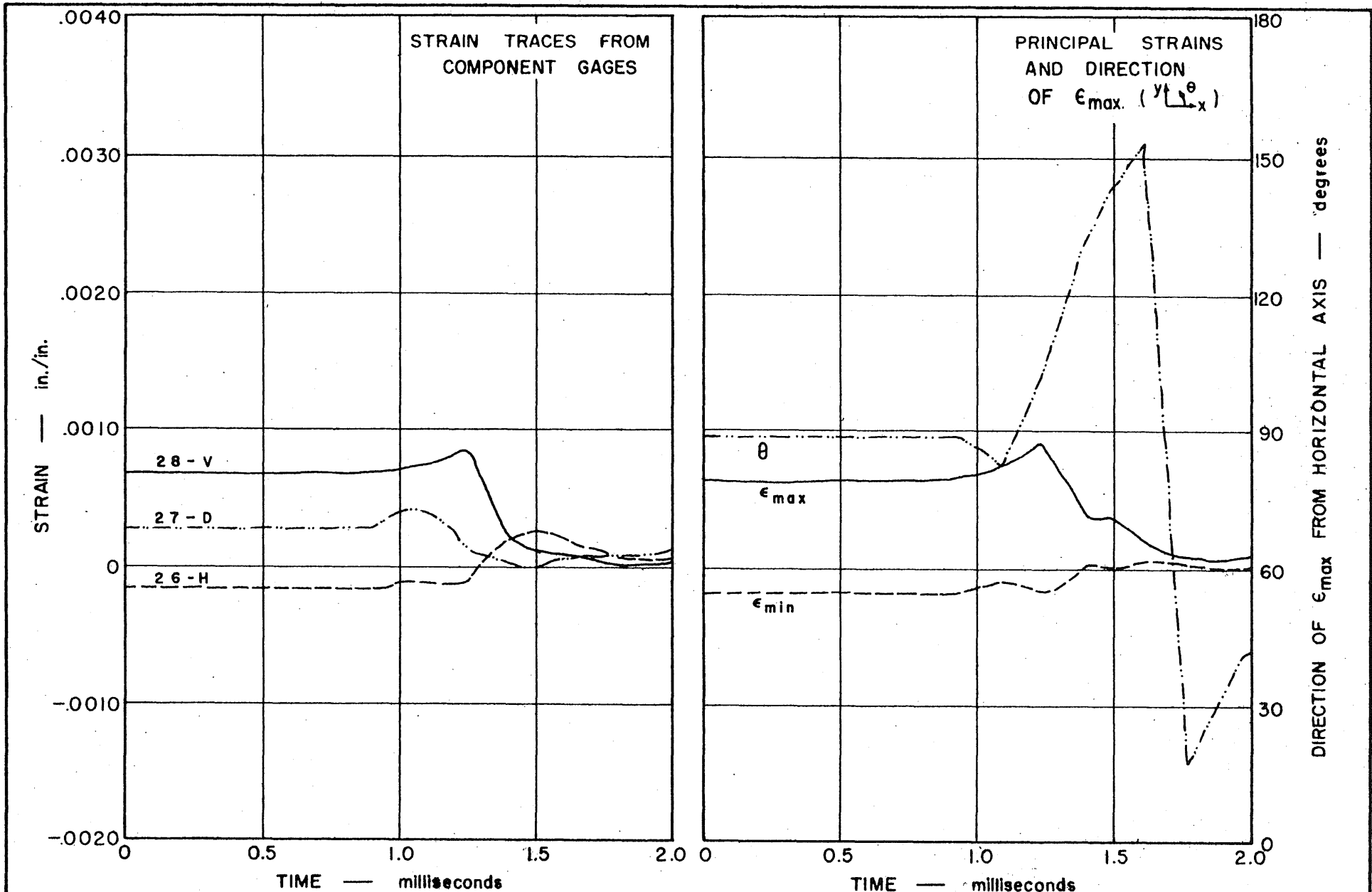
FIG. 63   STRAIN   TRACES   FROM   COMPONENT   GAGES   NOS. 26, 27, AND 28, AND   PRINCIPAL   STRAINS   FROM   ROSETTE   7   —   TEST 37
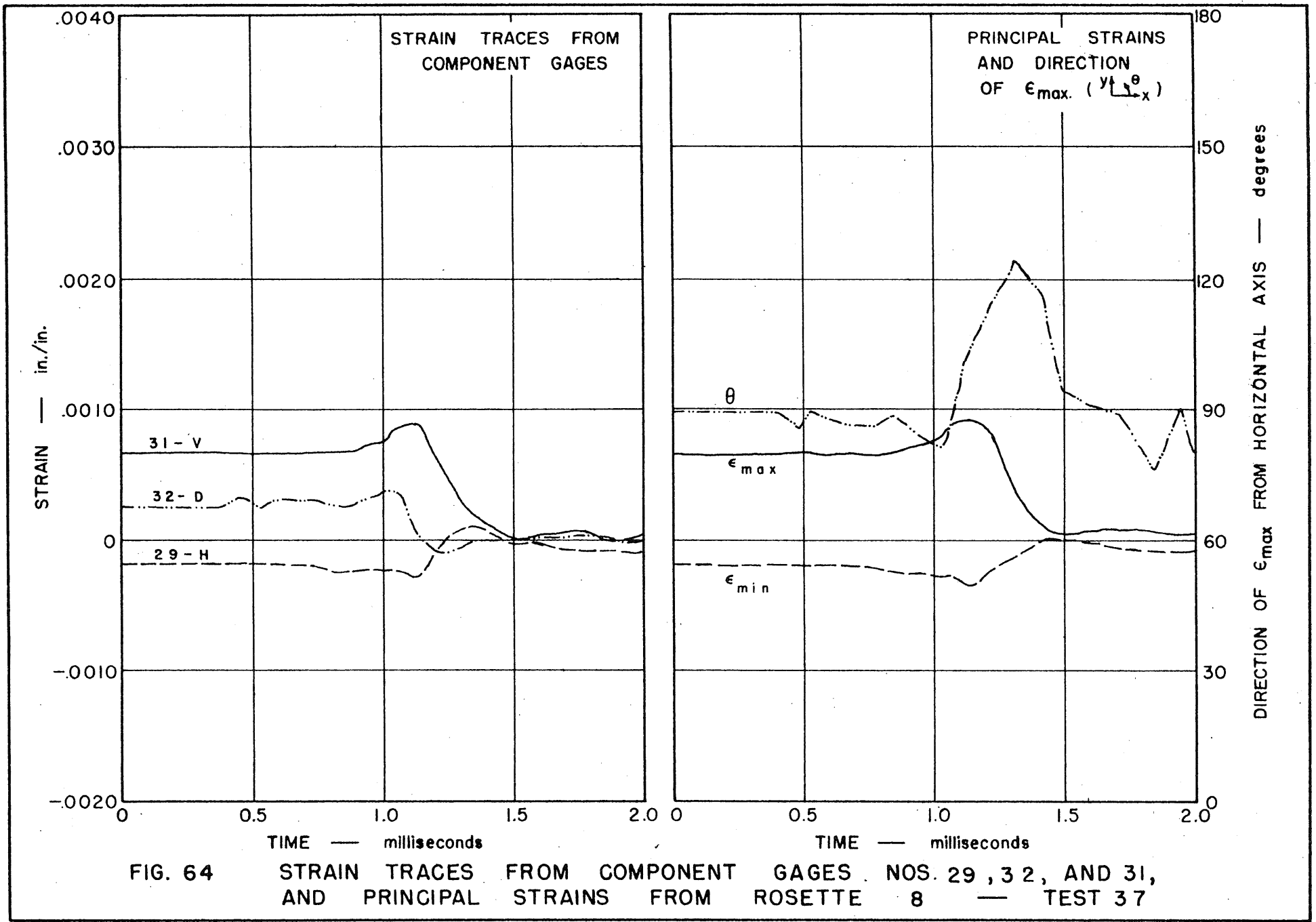
FIG. 64   STRAIN TRACES FROM COMPONENT GAGES NOS. 29, 32, AND 31,
AND PRINCIPAL STRAINS FROM ROSETTE 8 — TEST 37
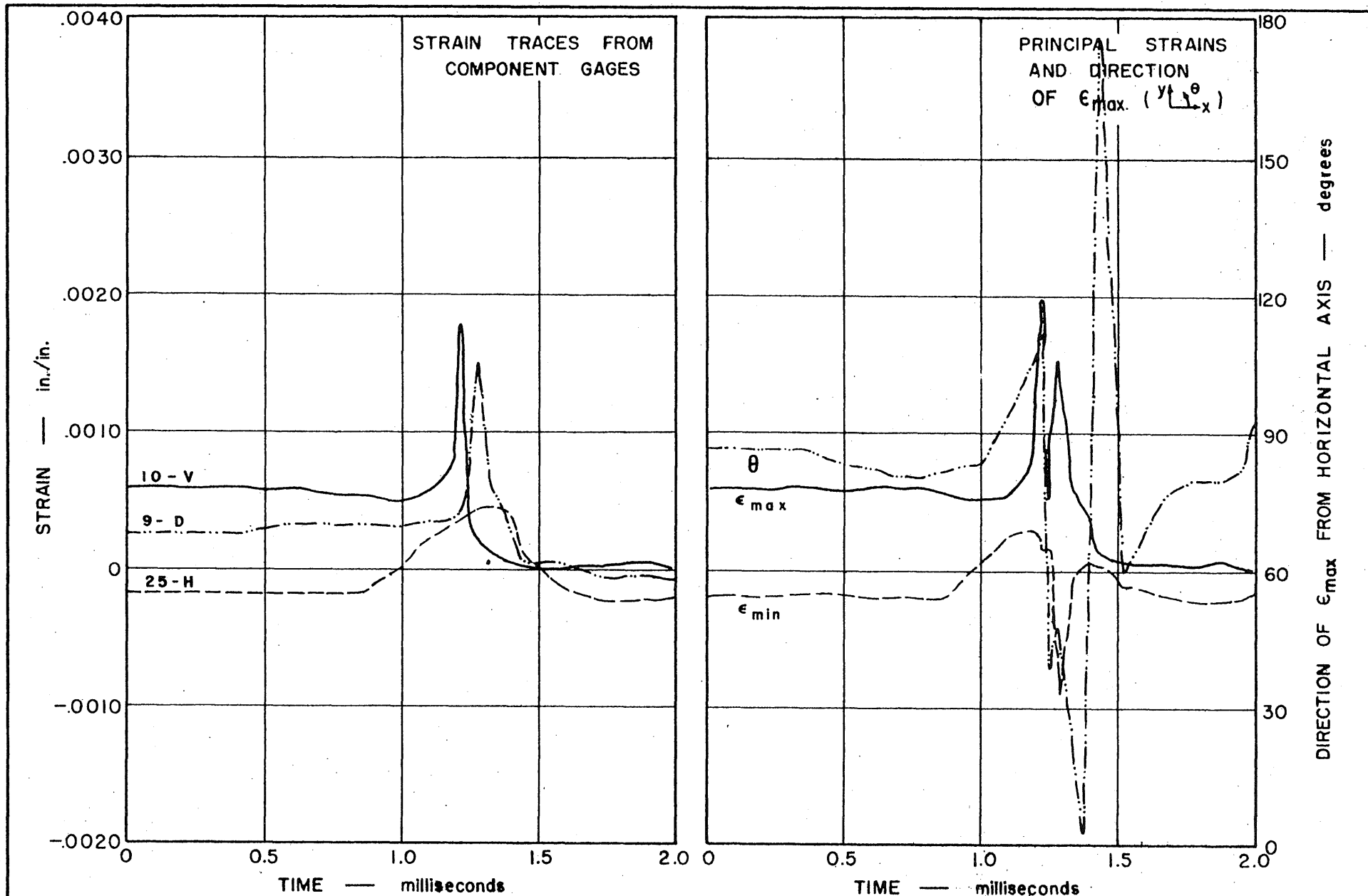
FIG. 65 STRAIN TRACES FROM COMPONENT GAGES NOS. 25, 9, AND 10, AND PRINCIPAL STRAINS FROM ROSETTE 9 — TEST 37
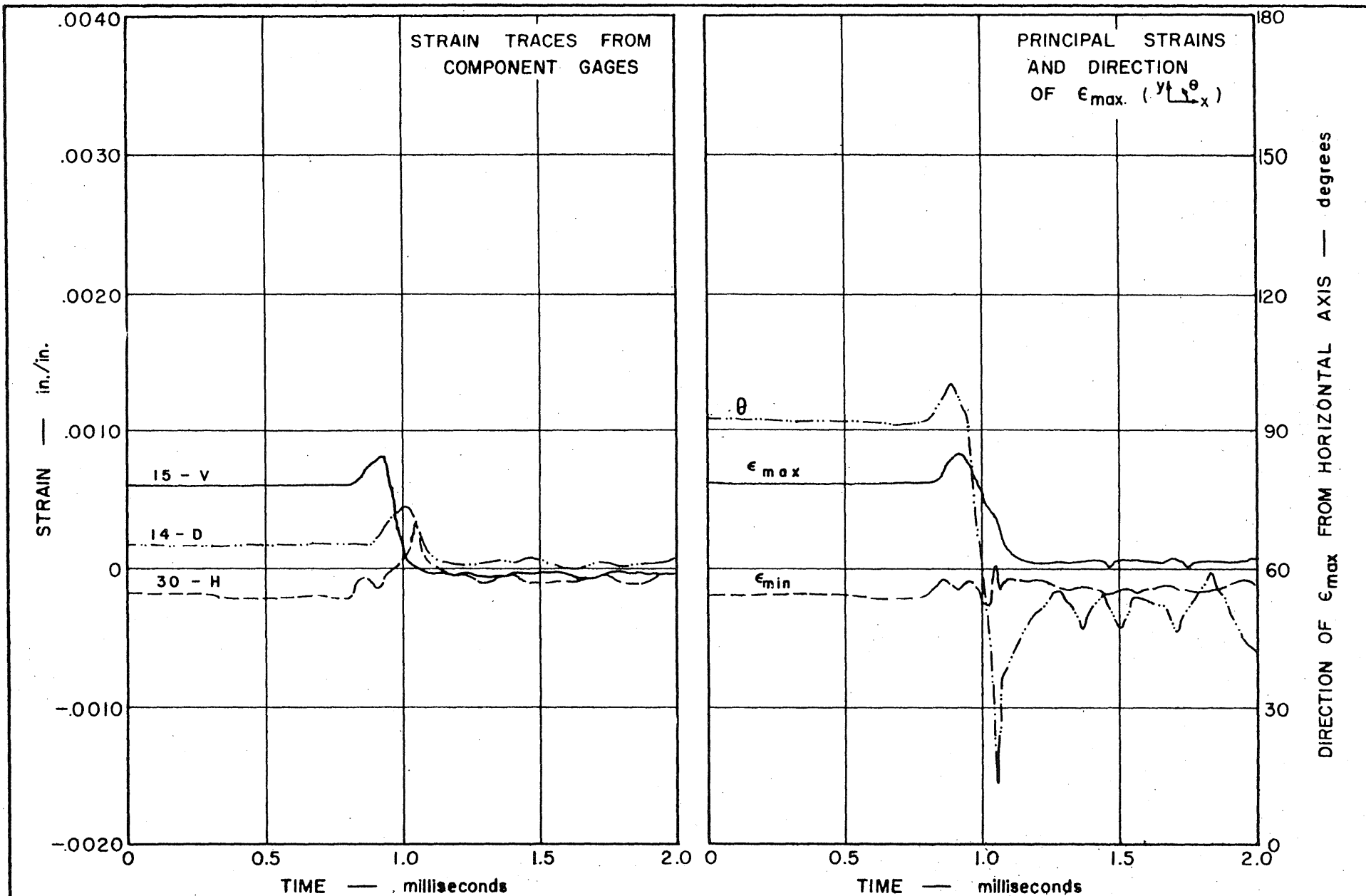
FIG. 66   STRAIN   TRACES   FROM   COMPONENT   GAGES   NOS. 30, 14, AND 15,
AND   PRINCIPAL   STRAINS   FROM   ROSETTE   10 — TEST 37
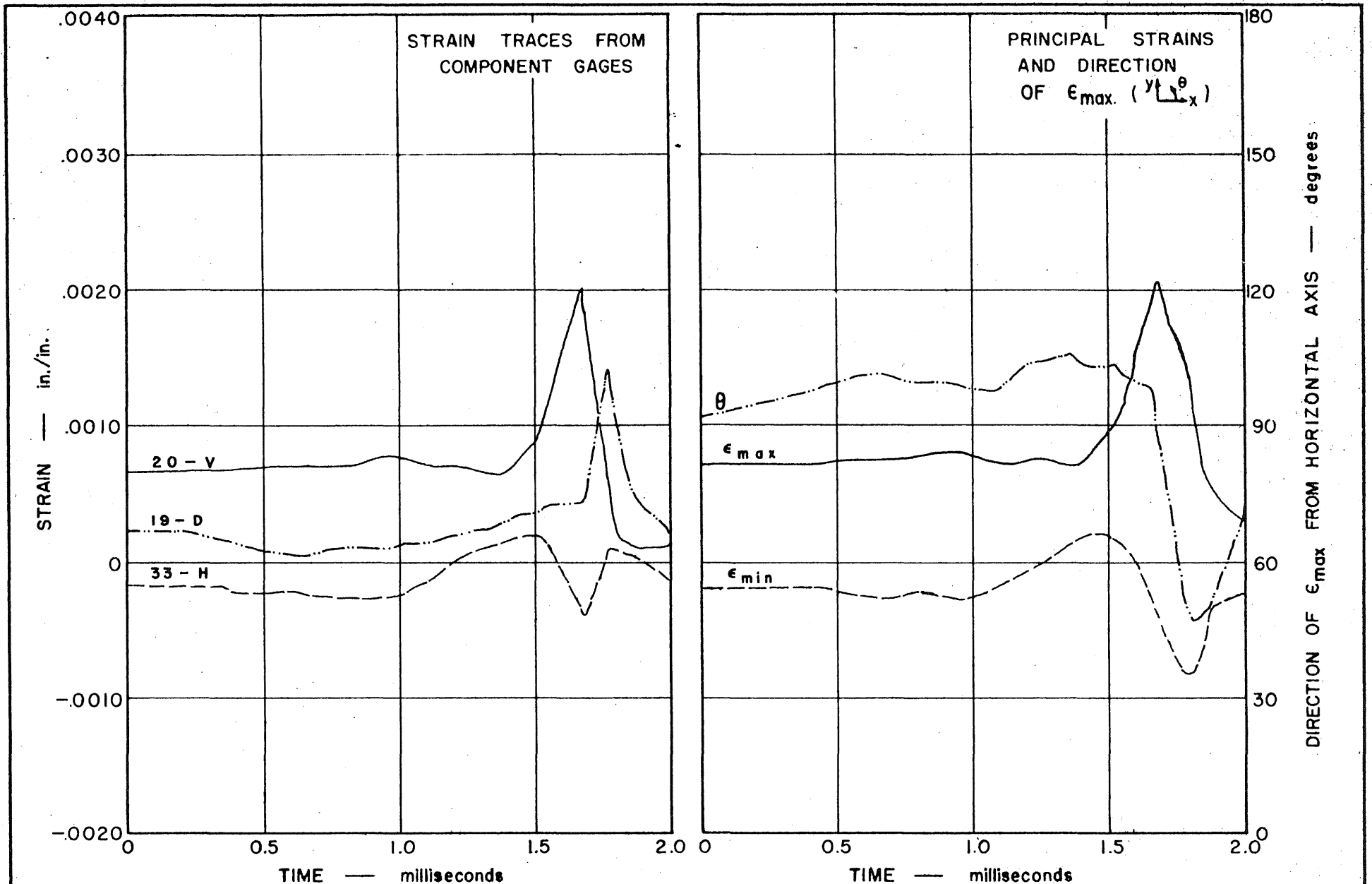
FIG. 67 STRAIN TRACES FROM COMPONENT GAGES NOS. 33, 19, AND 20, AND PRINCIPAL STRAINS FROM ROSETTE 11 — TEST 37
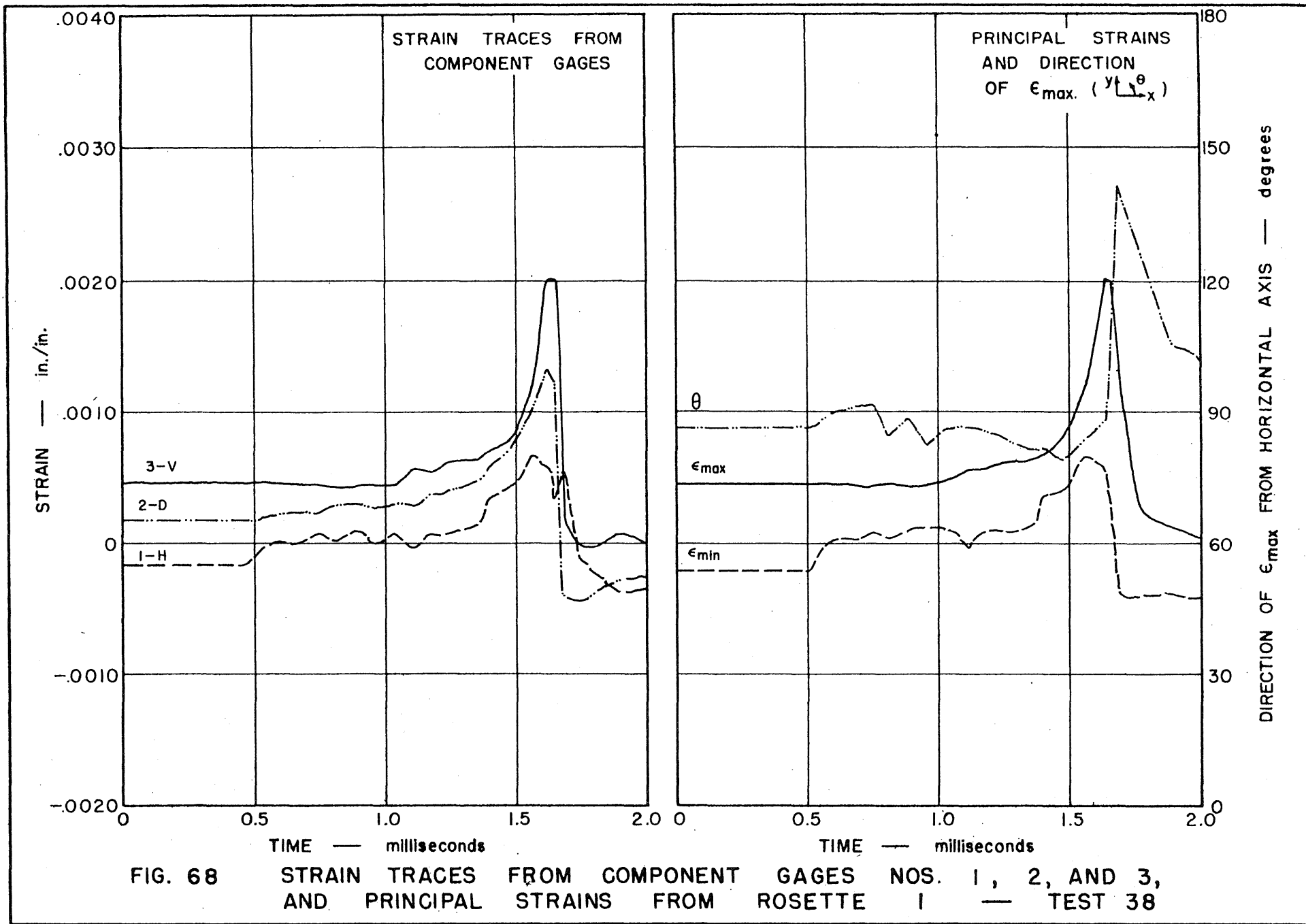
FIG. 68   STRAIN   TRACES   FROM   COMPONENT   GAGES   NOS.   1,   2,   AND   3,
AND   PRINCIPAL   STRAINS   FROM   ROSETTE   1   —   TEST 38
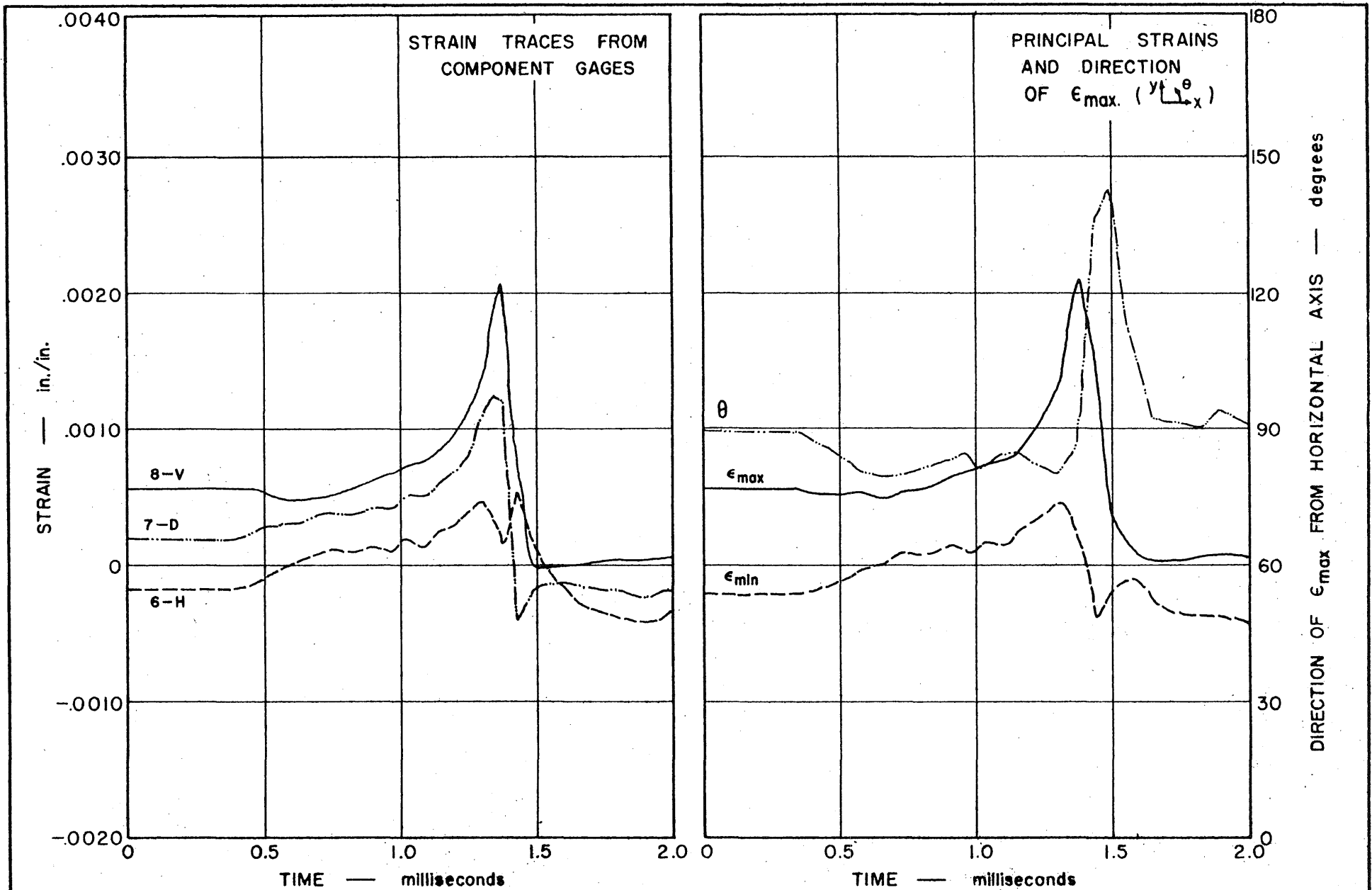
FIG. 69   STRAIN TRACES FROM COMPONENT GAGES NOS. 6, 7, AND 8, AND PRINCIPAL STRAINS FROM ROSETTE 2 — TEST 38

FIG. 70   STRAIN TRACES FROM COMPONENT GAGES NOS. 11, 12, AND 13,
           AND PRINCIPAL STRAINS FROM ROSETTE 3 — TEST 38
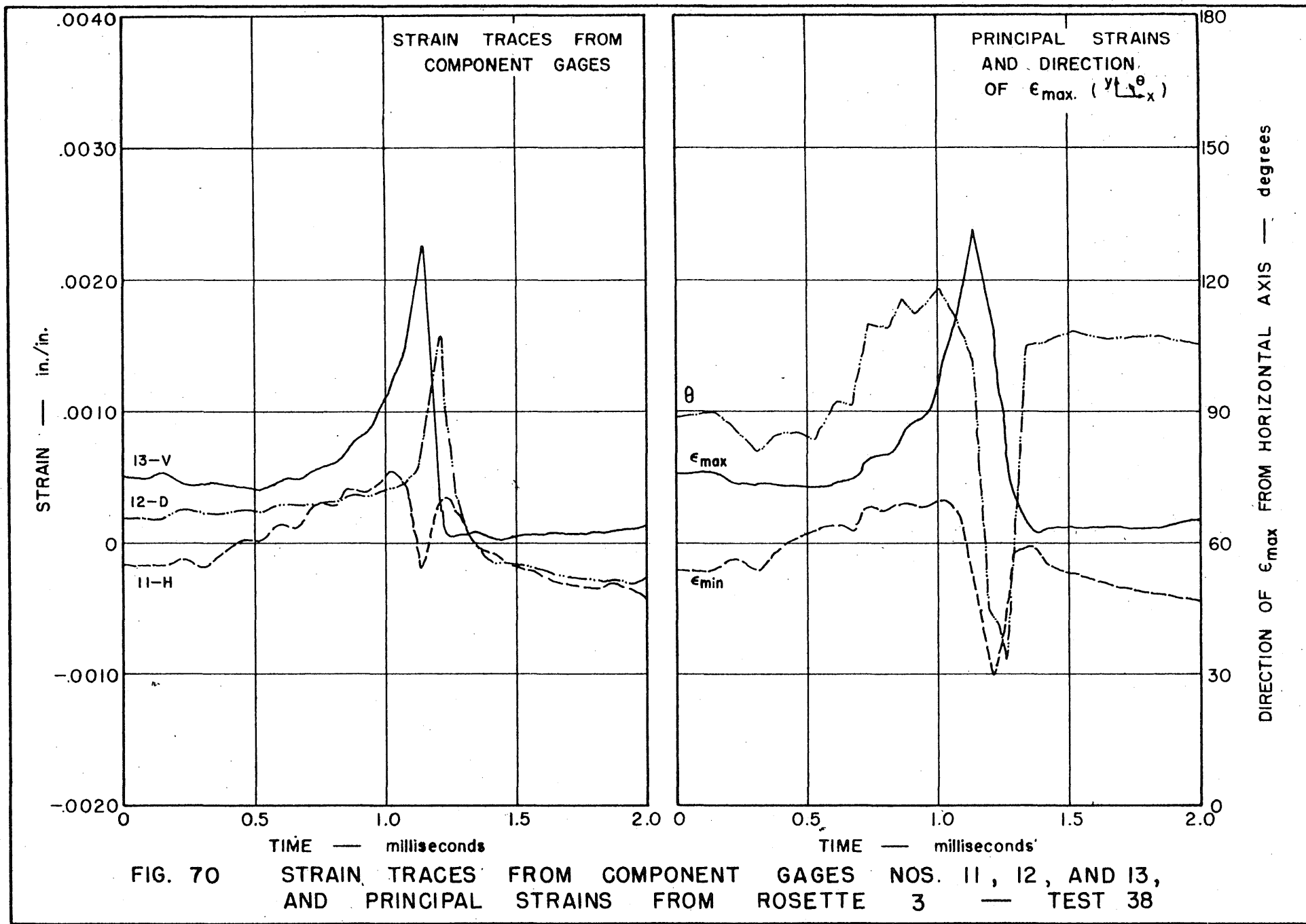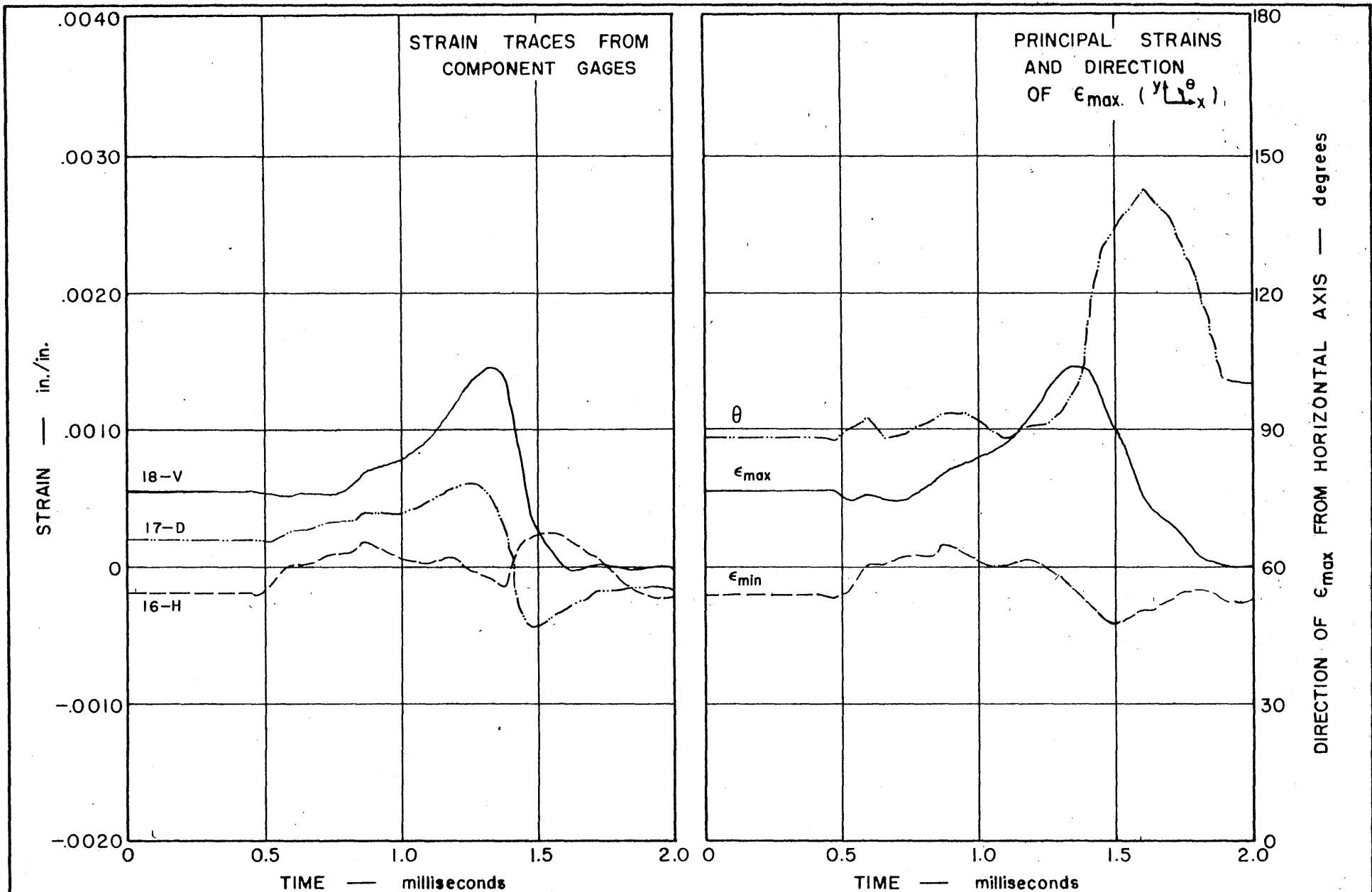
FIG. 71   STRAIN TRACES FROM COMPONENT GAGES NOS. 16, 17, AND 18, AND PRINCIPAL STRAINS FROM ROSETTE 4 — TEST 38

FIG. 72   STRAIN   TRACES   FROM   COMPONENT   GAGES   NOS. 21 , 22, AND 23,
           AND   PRINCIPAL   STRAINS   FROM   ROSETTE   5   —   TEST 38

FIG. 73   STRAIN   TRACES   FROM   COMPONENT   GAGES   NOS. 24, 4, AND 5,
         AND   PRINCIPAL   STRAINS   FROM   ROSETTE   6   —   TEST 38

FIG. 74   STRAIN   TRACES   FROM   COMPONENT   GAGES   NOS. 26, 27, AND 28,
AND   PRINCIPAL   STRAINS   FROM   ROSETTE   7   —   TEST 38

FIG. 75   STRAIN   TRACES   FROM   COMPONENT   GAGES   NOS. 29, 32, AND 31,
AND   PRINCIPAL   STRAINS   FROM   ROSETTE   8   —   TEST   38

FIG. 76   STRAIN   TRACES   FROM· COMPONENT   GAGES   NOS. 25,   9, AND 10,
AND   PRINCIPAL   STRAINS   FROM   ROSETTE   9   —   TEST 38

FIG. 77   STRAIN TRACES FROM COMPONENT GAGES NOS. 30, 14, AND 15, AND PRINCIPAL STRAINS FROM ROSETTE 10 — TEST 38

FIG. 78 STRAIN TRACES FROM COMPONENT GAGES NOS. 33, 19, AND 20, AND PRINCIPAL STRAINS FROM ROSETTE 11 — TEST 38

FIG. 79   STRAIN   TRACES   FROM   COMPONENT   GAGES   NOS. 1 , 2, AND 3,
AND   PRINCIPAL   STRAINS   FROM   ROSETTE   1 —   TEST 39

FIG. 80   STRAIN   TRACES   FROM   COMPONENT   GAGES   NOS. 6 , 7 , AND 8 ,
AND   PRINCIPAL   STRAINS   FROM   ROSETTE   2   —   TEST 39

FIG. 81   STRAIN TRACES FROM COMPONENT GAGES NOS. 11, 12, AND 13, AND PRINCIPAL STRAINS FROM ROSETTE 3 — TEST 39

FIG. 82   STRAIN   TRACES   FROM   COMPONENT   GAGES   NOS. 16, 17, AND 18,
AND   PRINCIPAL   STRAINS   FROM   ROSETTE   4   —   TEST 39

FIG. 83   STRAIN   TRACES   FROM   COMPONENT   GAGES   NOS. 21, 22, AND 23,
AND   PRINCIPAL   STRAINS   FROM   ROSETTE   5   —   TEST 39

FIG. 84   STRAIN   TRACES   FROM   COMPONENT   GAGES   NOS. 24 , 4 , AND 5,
AND   PRINCIPAL   STRAINS   FROM   ROSETTE   6 — TEST 39

FIG. 85   STRAIN   TRACES   FROM   COMPONENT   GAGES   NOS. 26, 27, AND 28,
AND   PRINCIPAL   STRAINS   FROM   ROSETTE   7   —   TEST 39

FIG. 86   STRAIN   TRACES   FROM   COMPONENT   GAGES   NOS. 2 9 , 3 2 , AND 31,
AND   PRINCIPAL   STRAINS   FROM   ROSETTE   8   —   TEST 3 9

FIG. 87   STRAIN   TRACES   FROM   COMPONENT   GAGES   NOS. 25, 9 , AND IO ,
AND   PRINCIPAL   STRAINS   FROM   ROSETTE   9   —   TEST 39

FIG. 88   STRAIN   TRACES   FROM   COMPONENT   GAGES   NOS. 30, 14, AND 15,
AND   PRINCIPAL   STRAINS   FROM   ROSETTE   10 — TEST 39

FIG. 89   STRAIN TRACES FROM COMPONENT GAGES NOS. 3 3, 19, AND 20, AND PRINCIPAL STRAINS FROM ROSETTE 11 — TEST 39
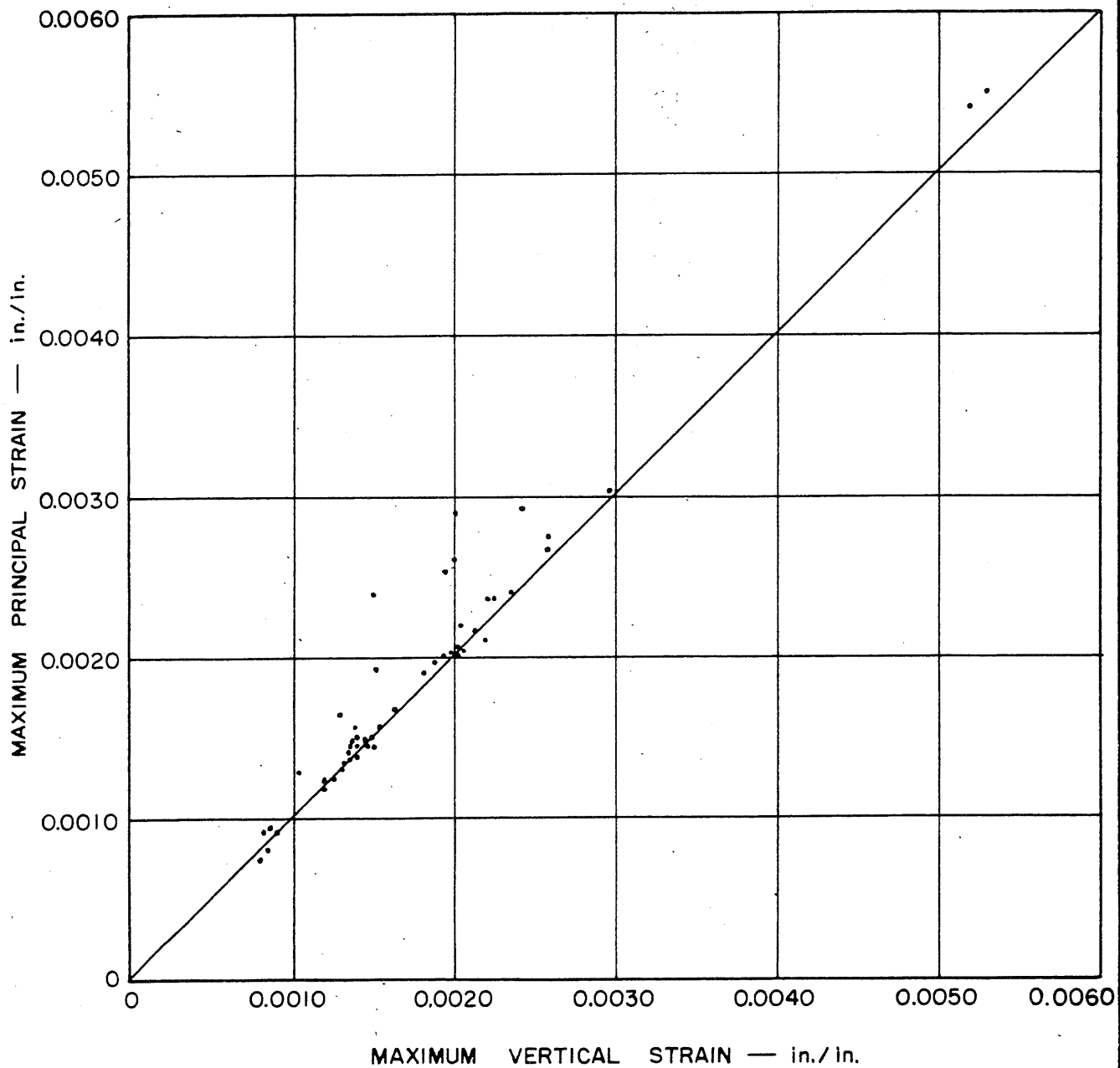
FIG. 90   COMPARISON OF MAXIMUM PRINCIPAL AND
VERTICAL STRAIN MAGNITUDES
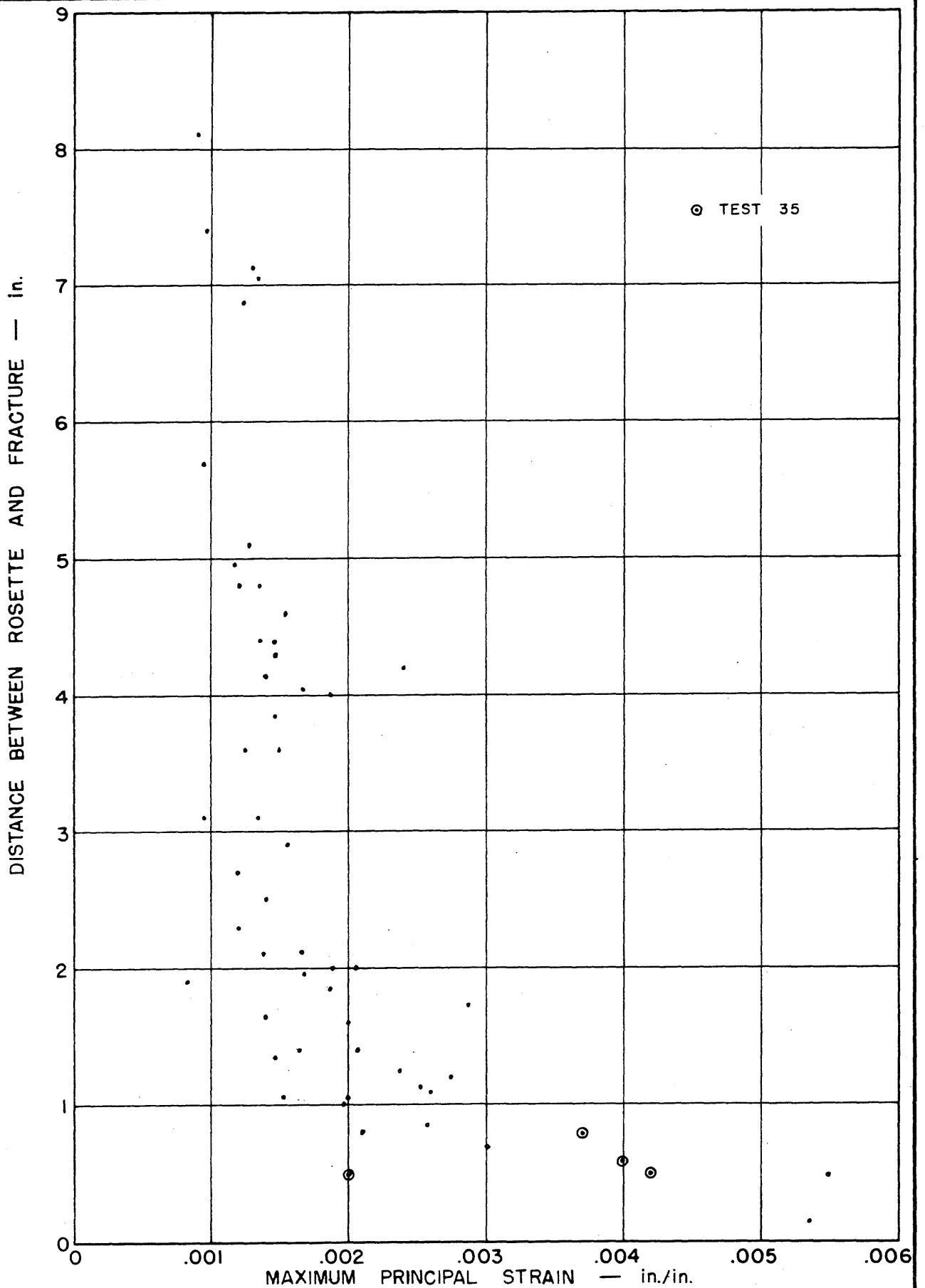
FIG. 91   MAXIMUM   PRINCIPAL   STRAIN   VERSUS
DISTANCE   BETWEEN   ROSETTE   AND   FRACTURE
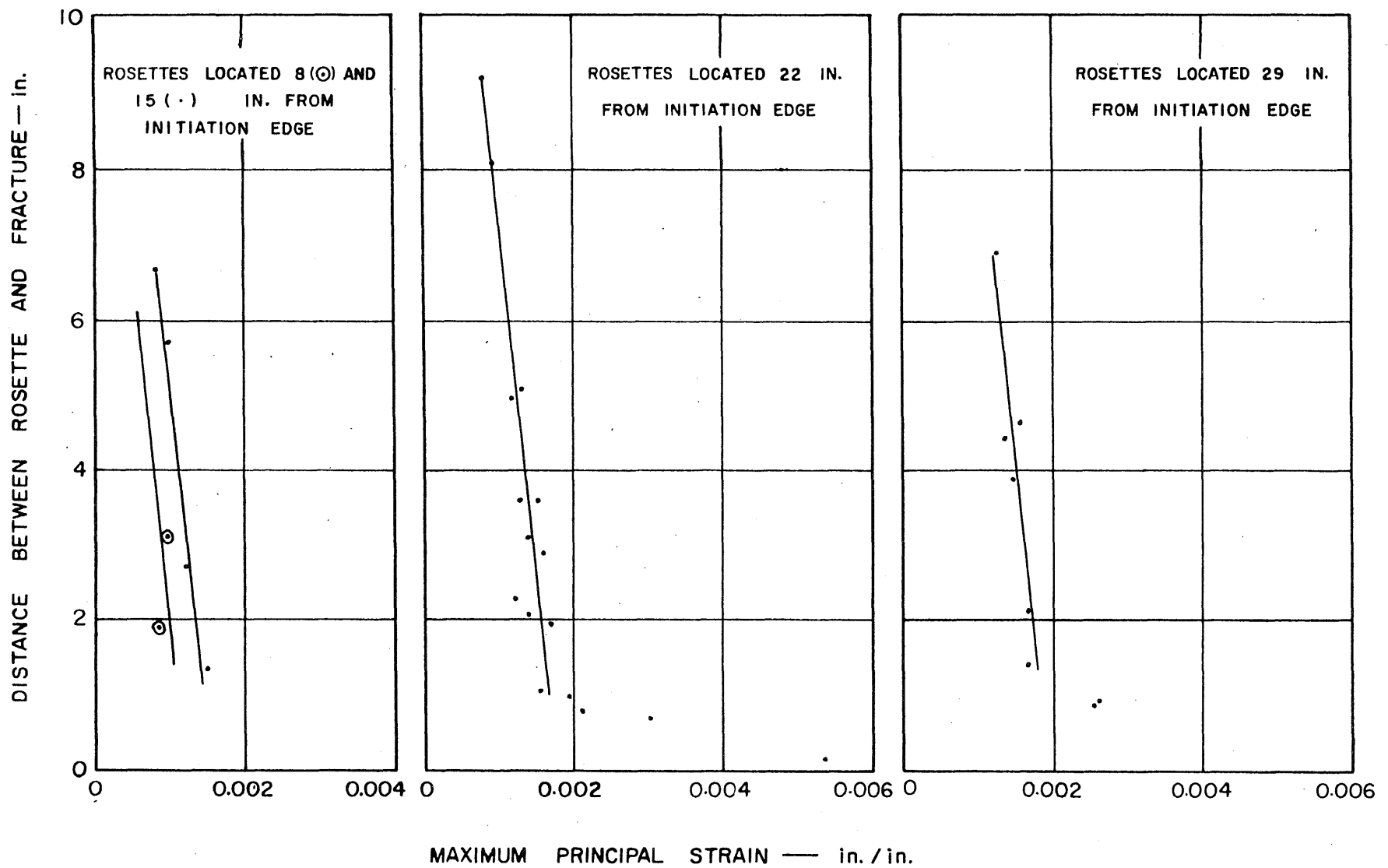
FIG. 92   MAXIMUM PRINCIPAL STRAIN VERSUS DISTANCE BETWEEN ROSETTE AND FRACTURE
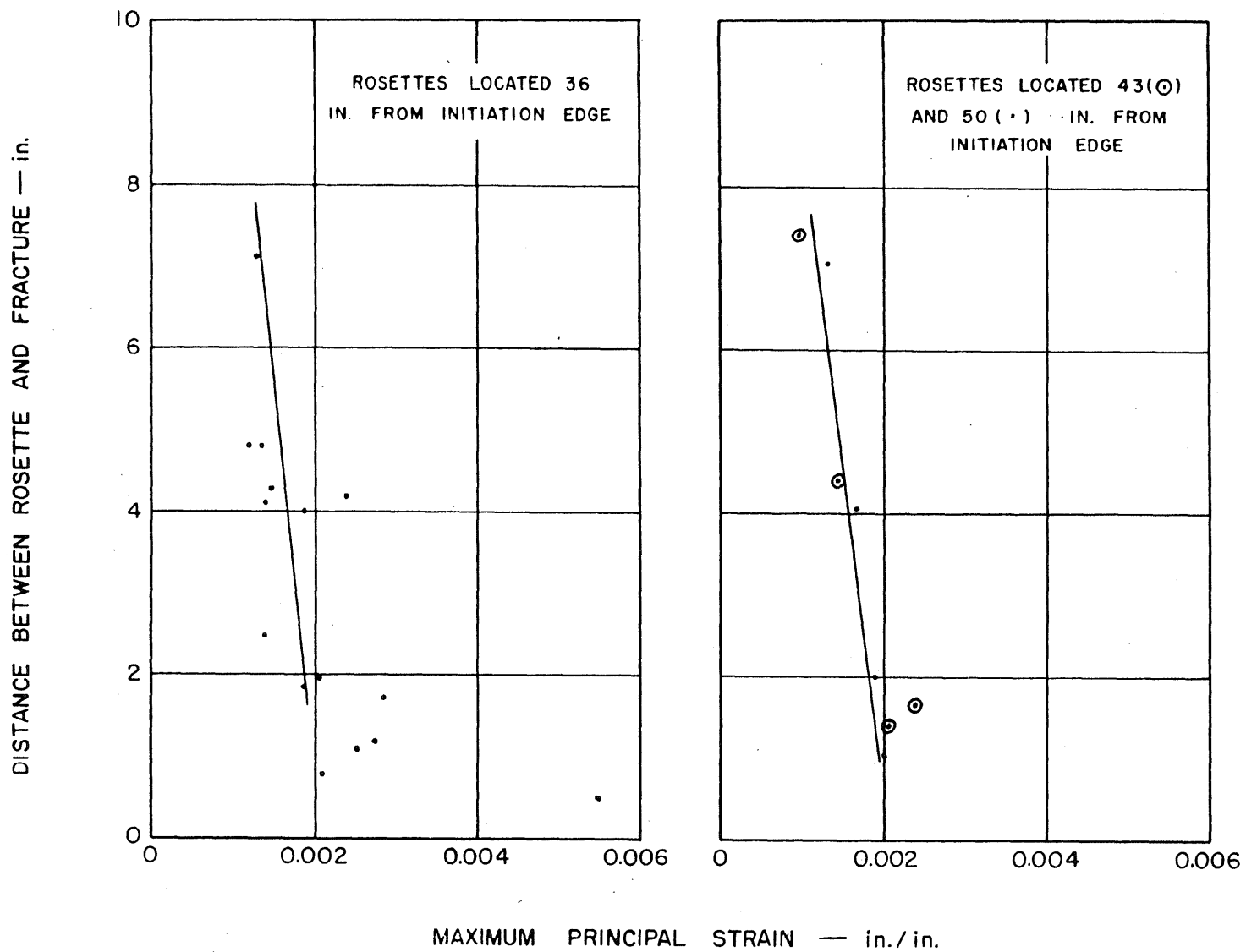
FIG. 93   MAXIMUM PRINCIPAL   STRAIN VERSUS DISTANCE BETWEEN ·ROSETTE AND FRACTURE
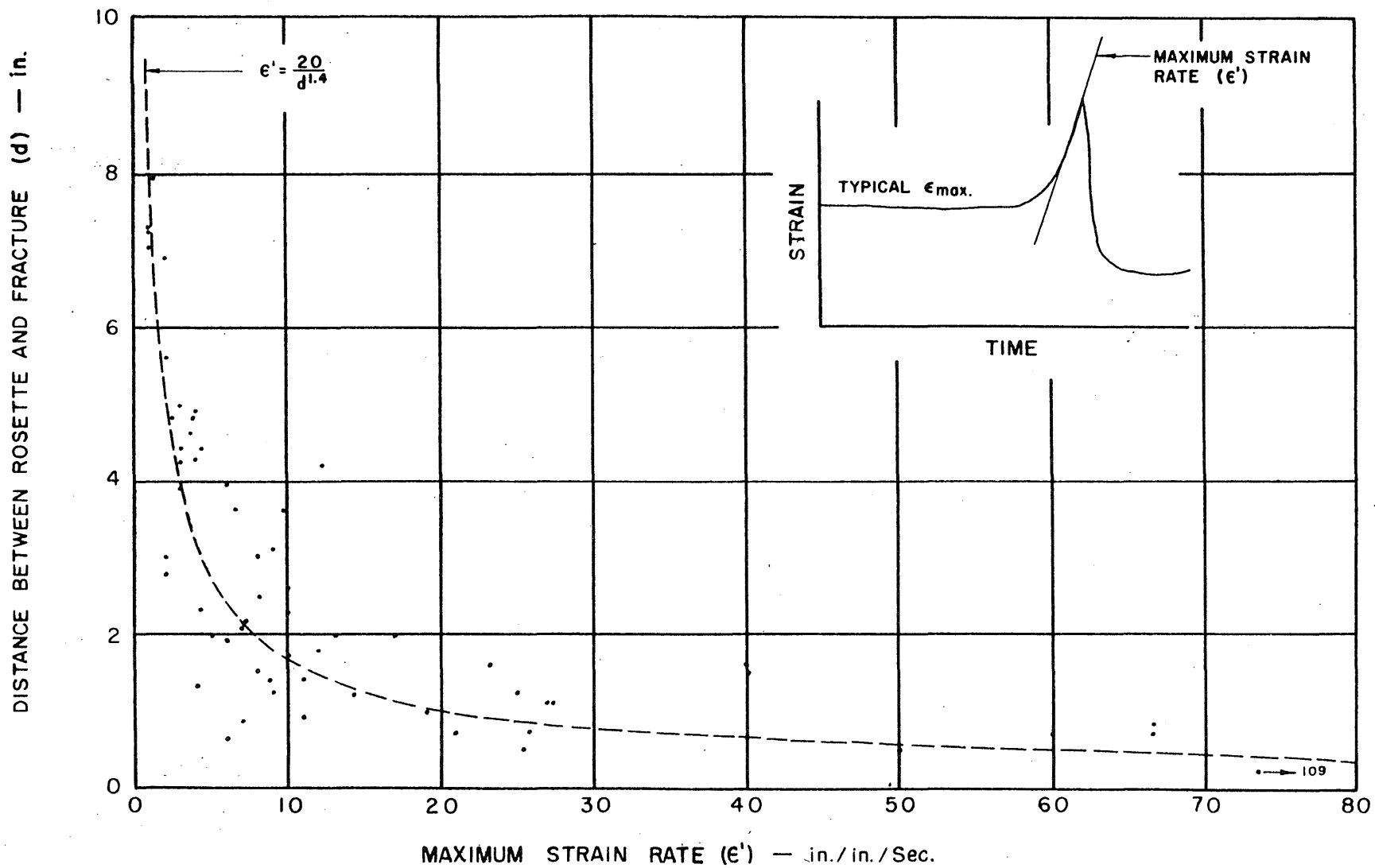
FIG. 94   MAXIMUM STRAIN RATE VERSUS DISTANCE BETWEEN ROSETTE AND FRACTURE
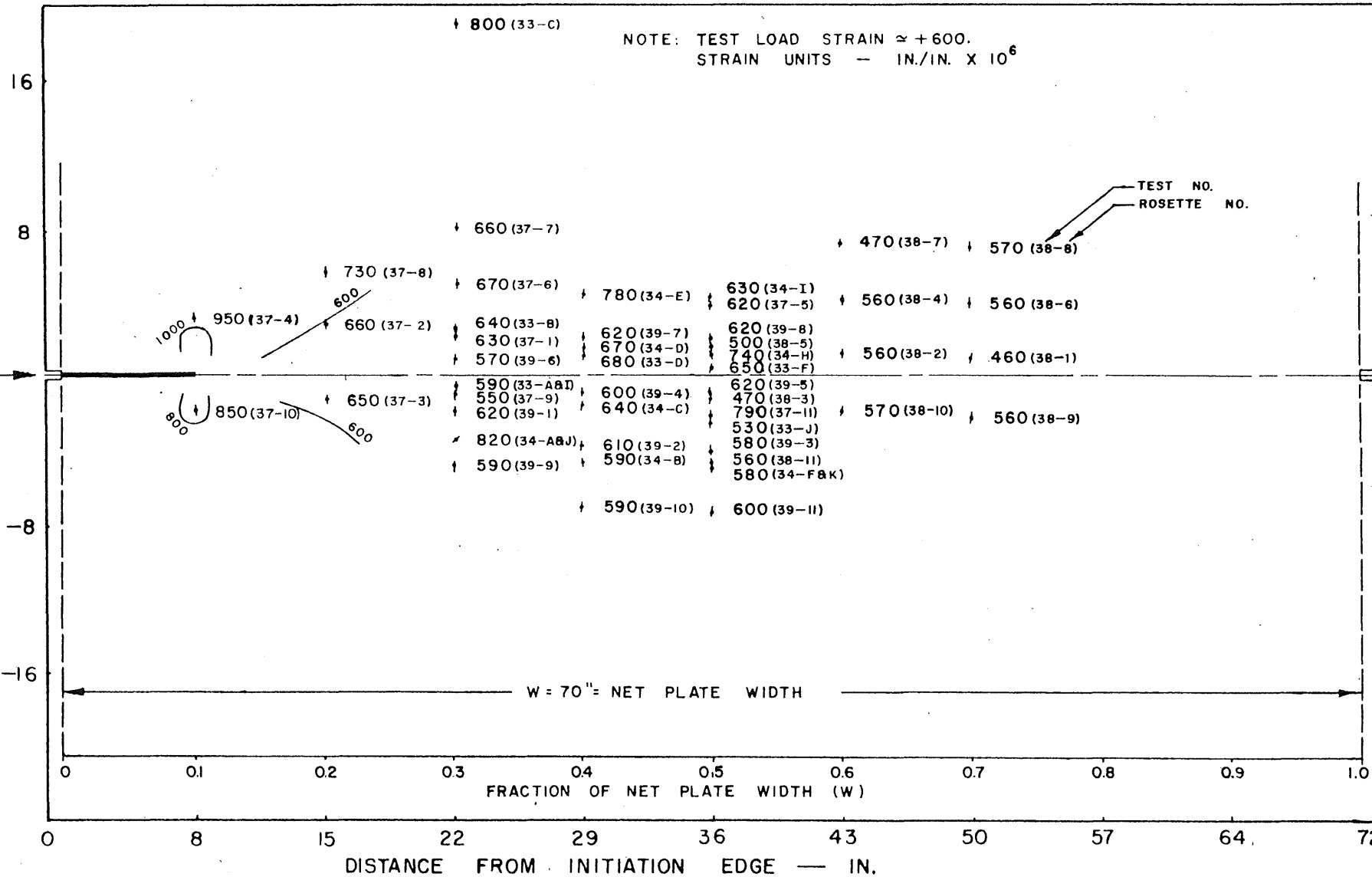
FIG. 95 MAXIMUM PRINCIPAL STRAIN CONTOURS FOR 8 — IN. CRACK
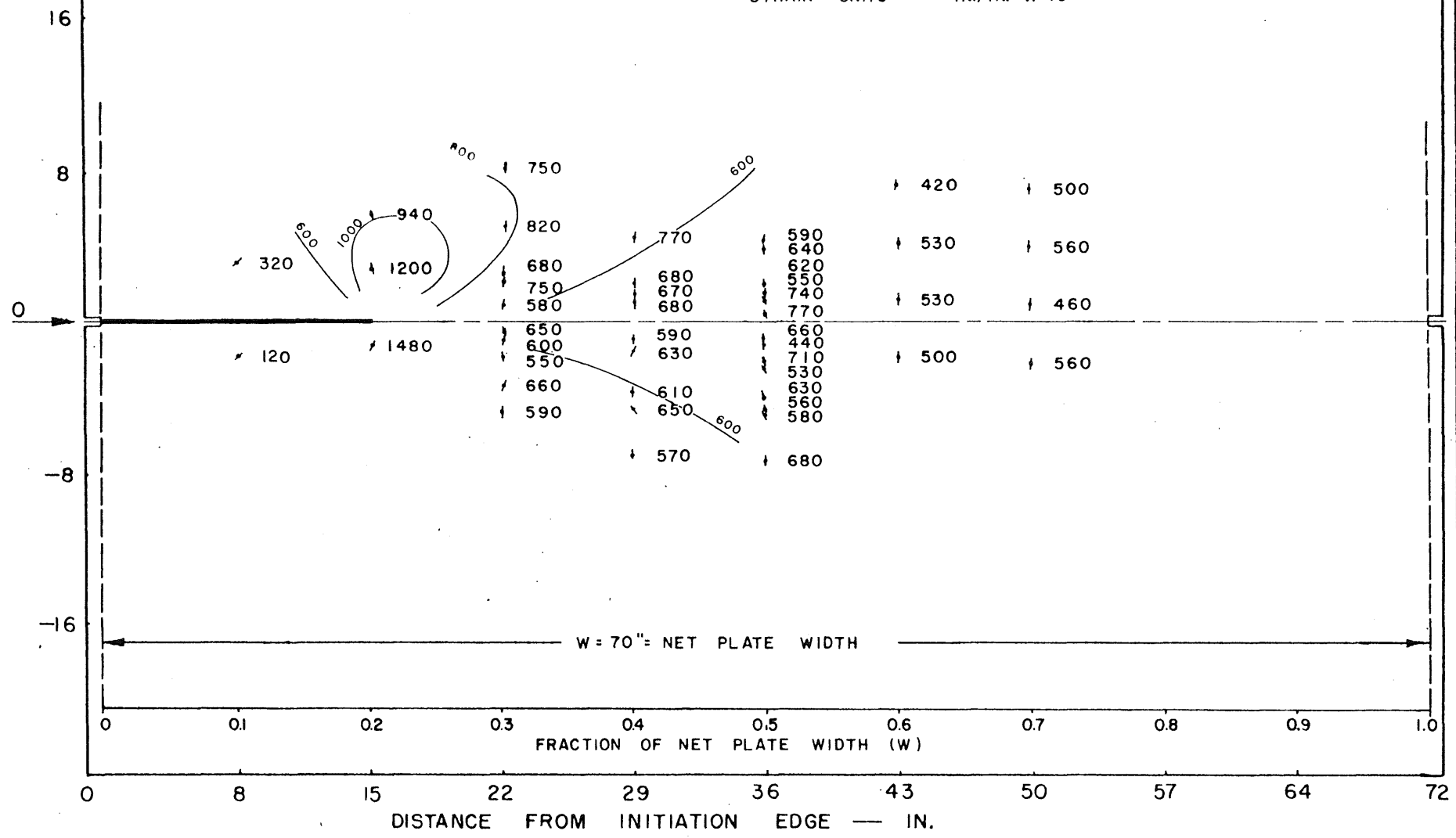
FIG. 96 MAXIMUM PRINCIPAL STRAIN CONTOURS FOR 15 — IN. CRACK
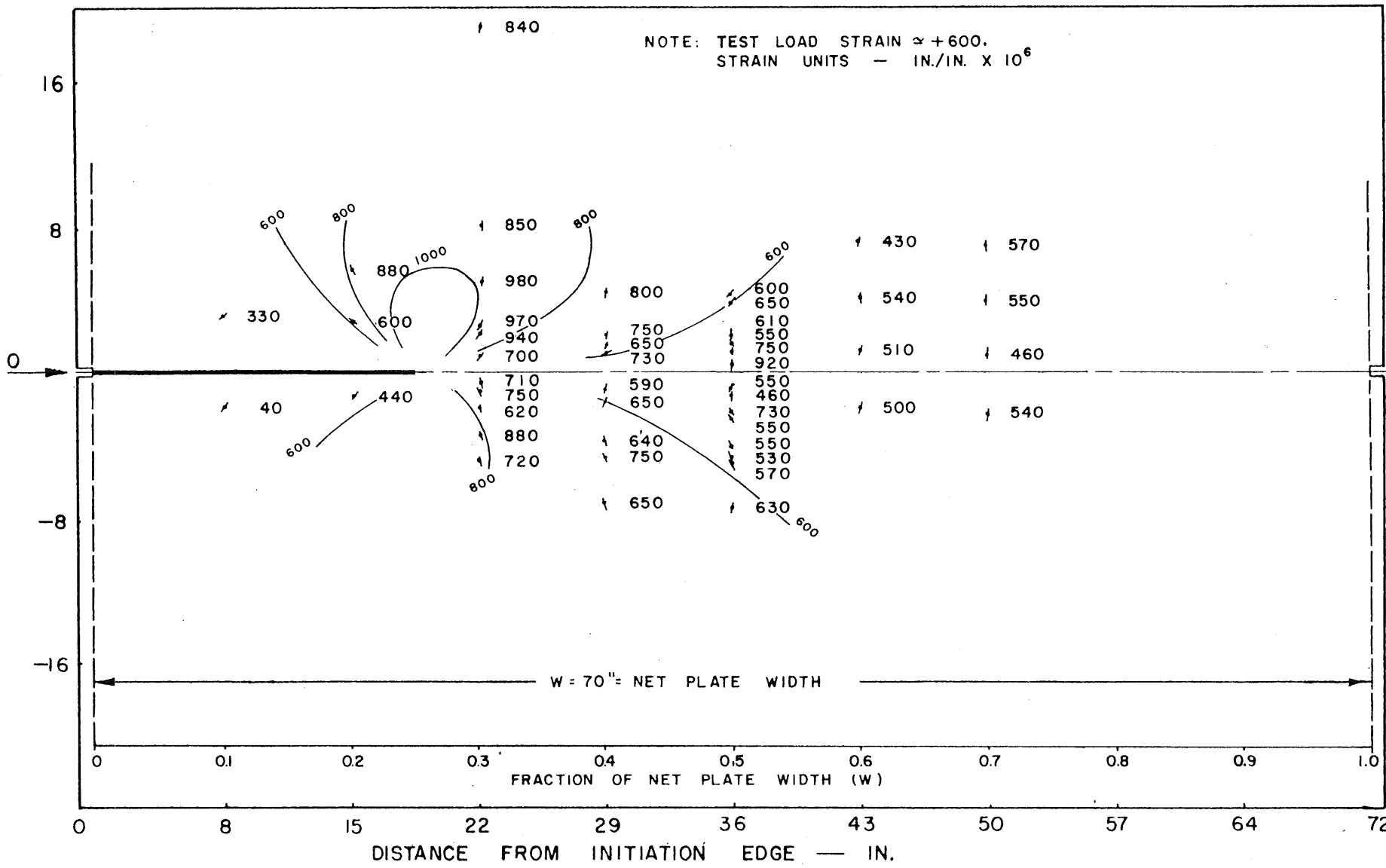
FIG. 97   MAXIMUM PRINCIPAL STRAIN CONTOURS FOR 18.5 — IN. CRACK

FIG. 98 MAXIMUM PRINCIPAL STRAIN CONTOURS FOR 22 — IN. CRACK
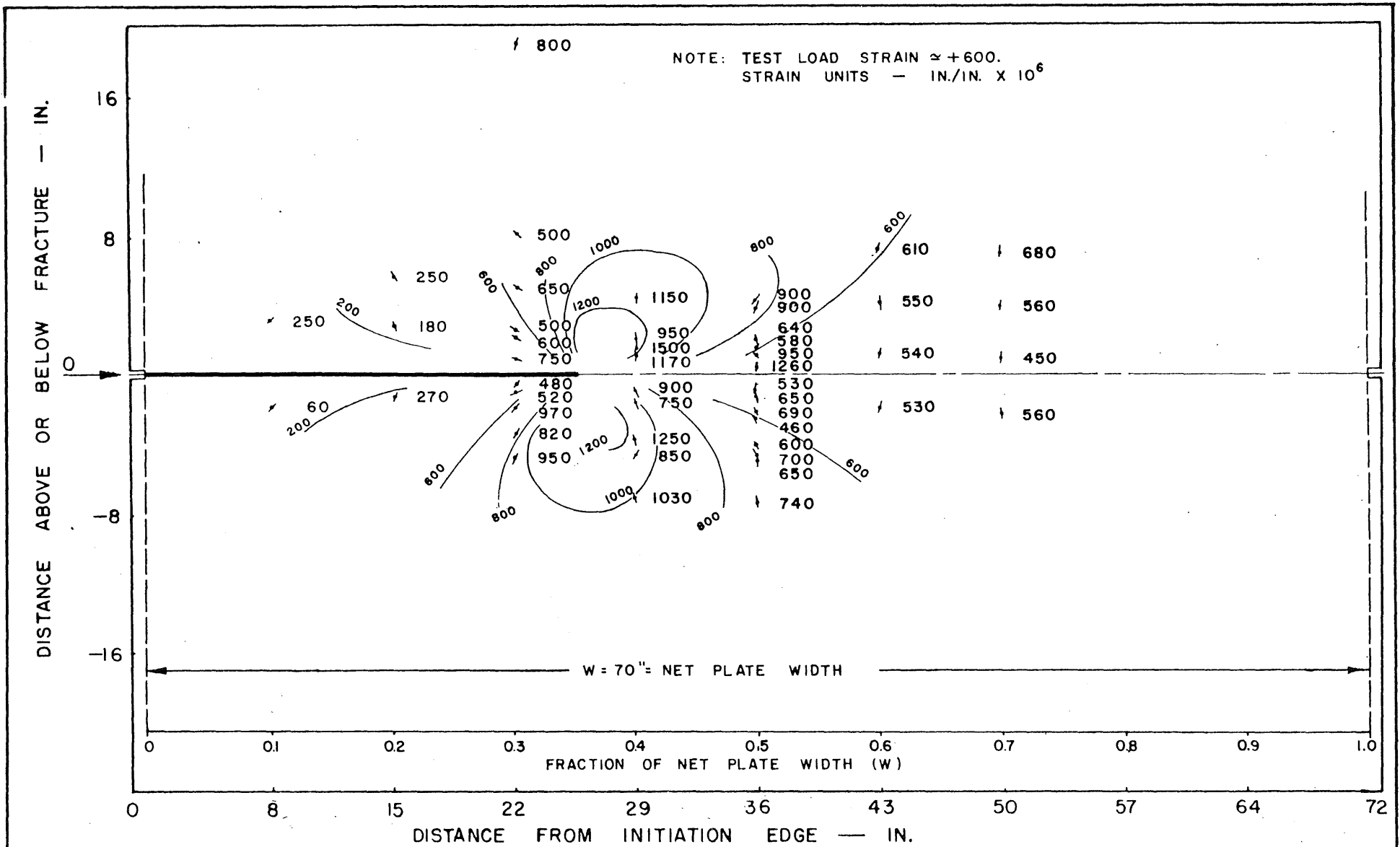
FIG. 99 MAXIMUM PRINCIPAL STRAIN CONTOURS FOR 25.5 — IN. CRACK
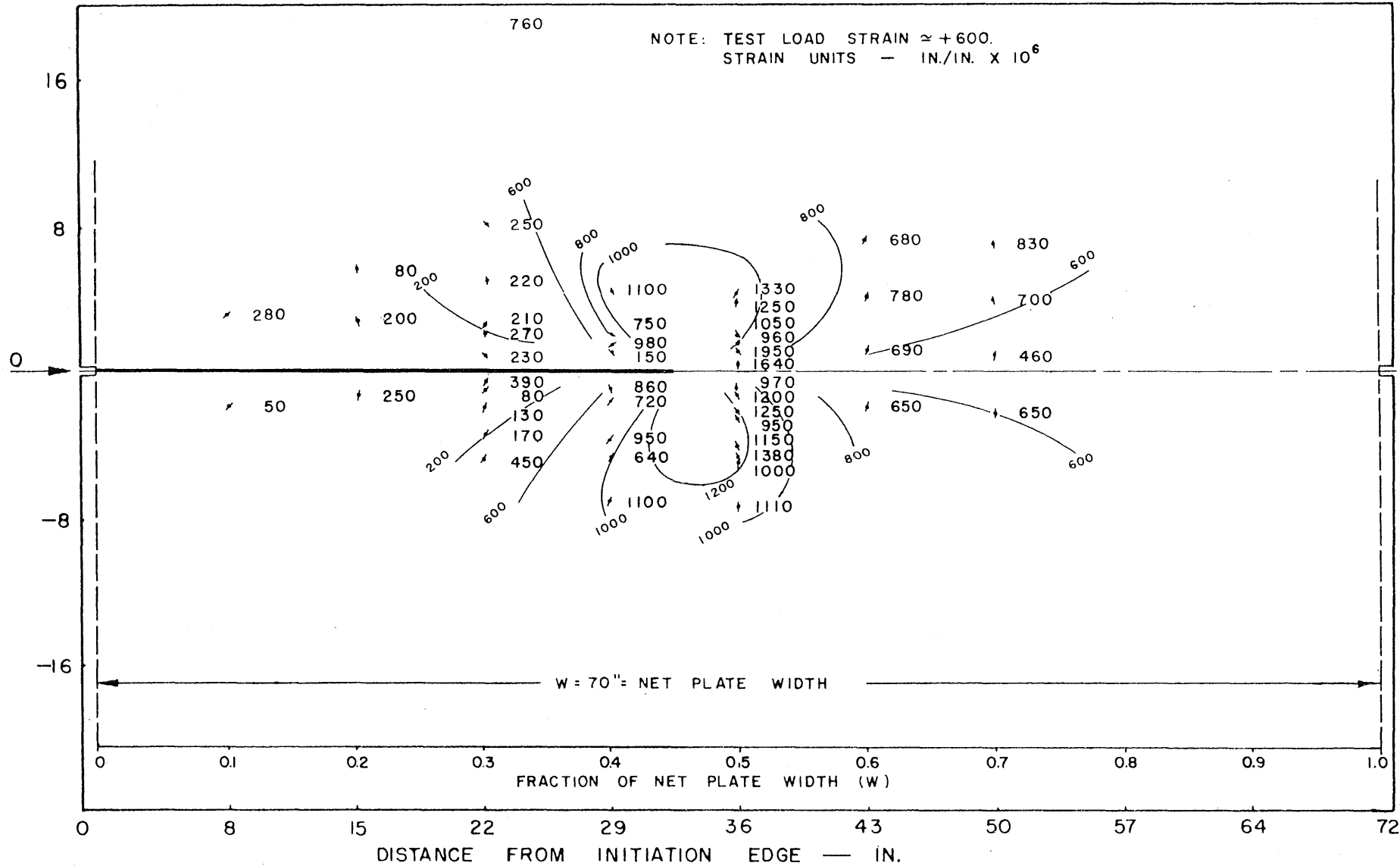
FIG. 100   MAXIMUM PRINCIPAL STRAIN CONTOURS FOR 29 —   IN. CRACK

FIG. 101   MAXIMUM   PRINCIPAL   STRAIN   CONTOURS   FOR   32.5 — IN.   CRACK
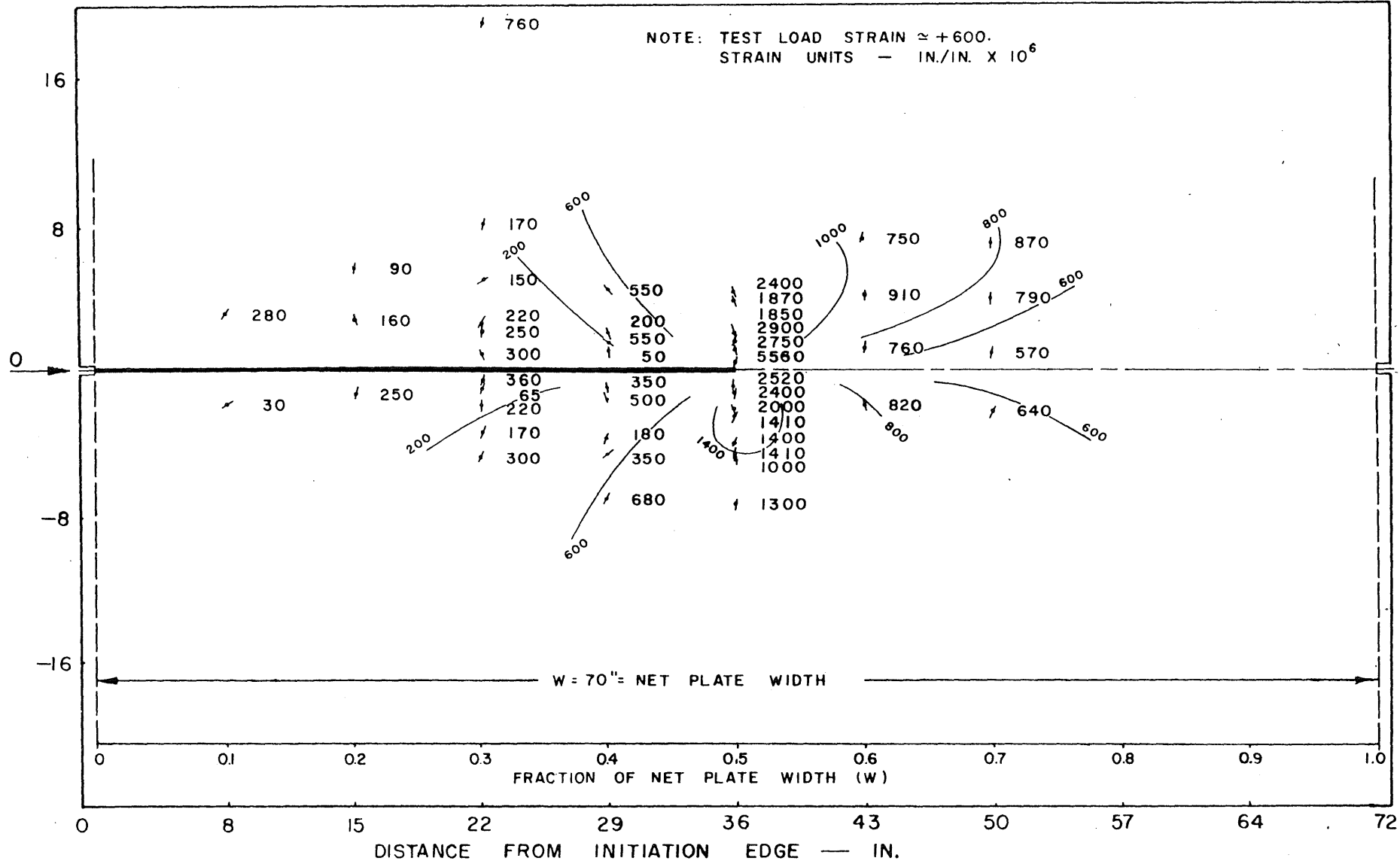
FIG. 102   MAXIMUM PRINCIPAL STRAIN CONTOURS FOR 36 — IN. CRACK
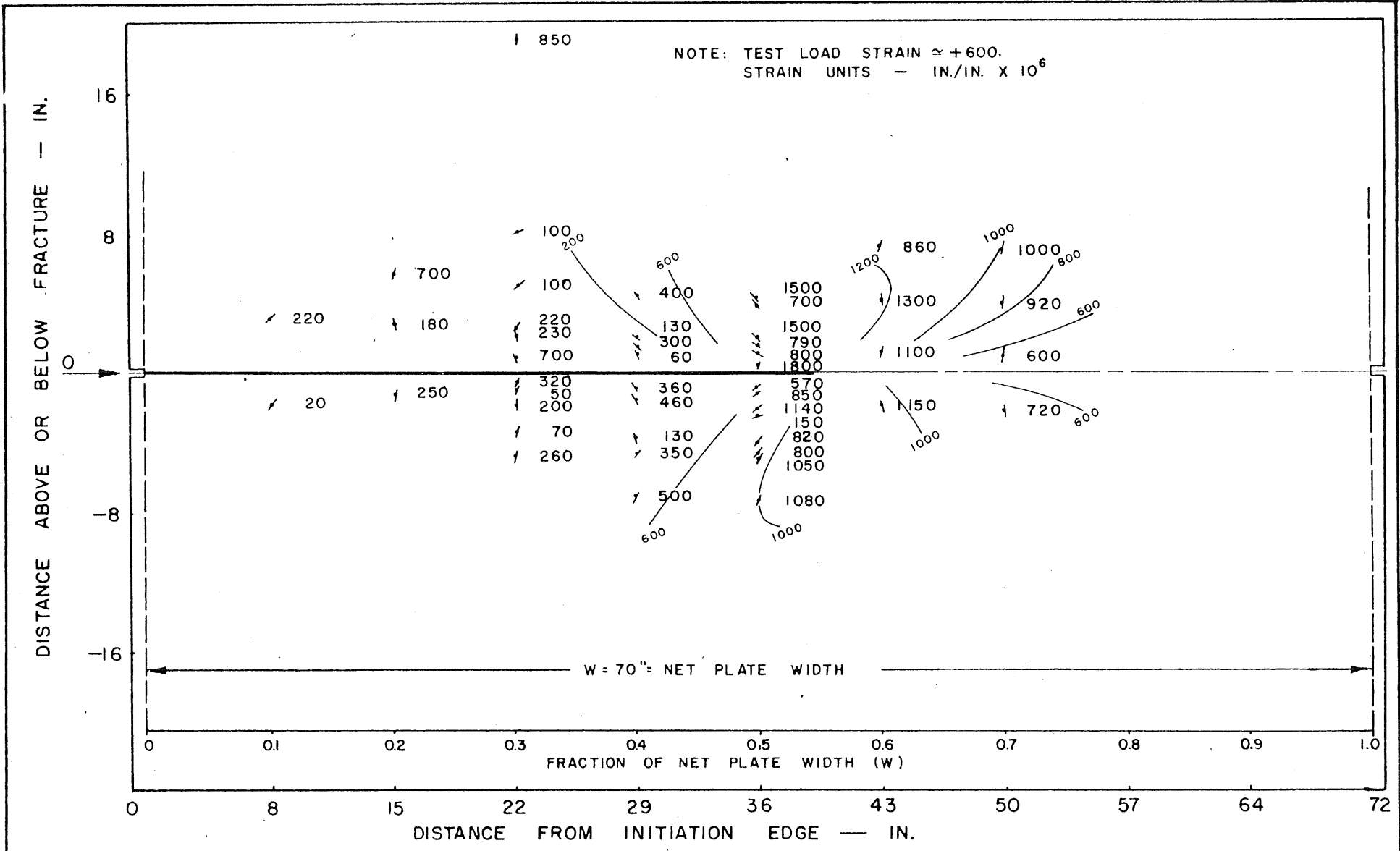
FIG. 103   MAXIMUM PRINCIPAL STRAIN CONTOURS FOR 39.5 — IN. CRACK
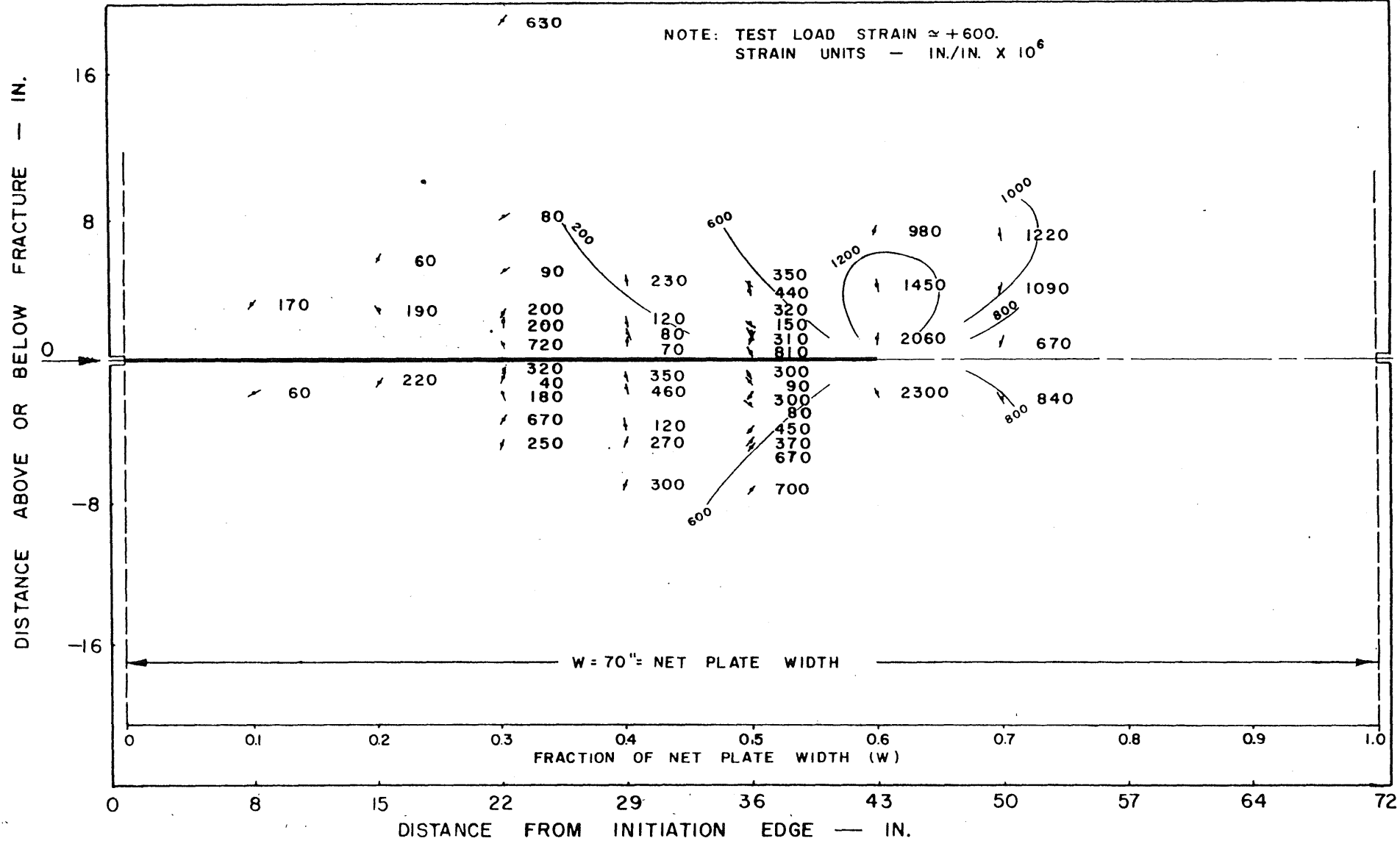
FIG. 104 MAXIMUM PRINCIPAL STRAIN CONTOURS FOR 43 — IN. CRACK
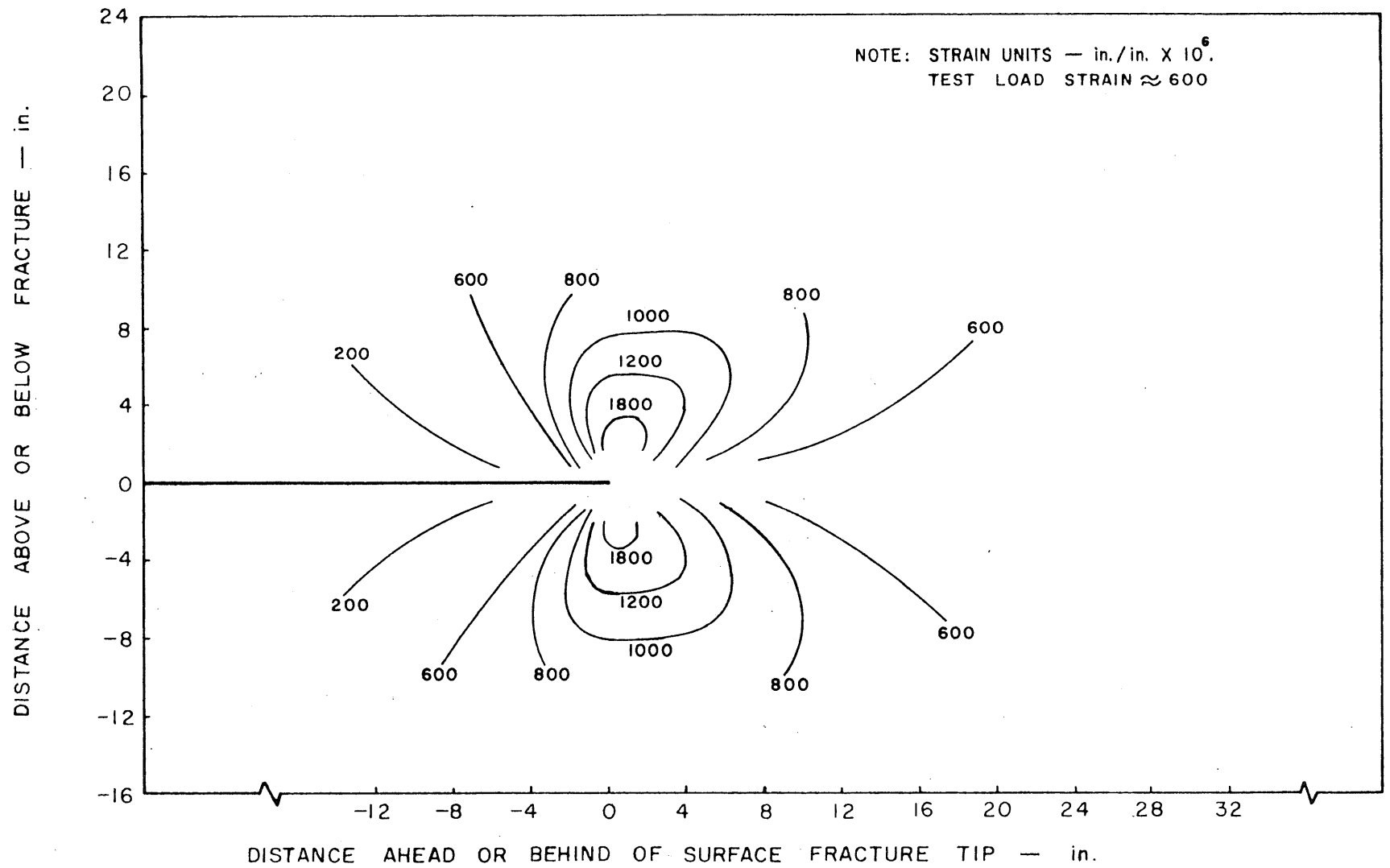
FIG. 105   TYPICAL SET OF PRINCIPAL STRAIN CONTOURS FOR 22-in. TO 50-in. CRACK
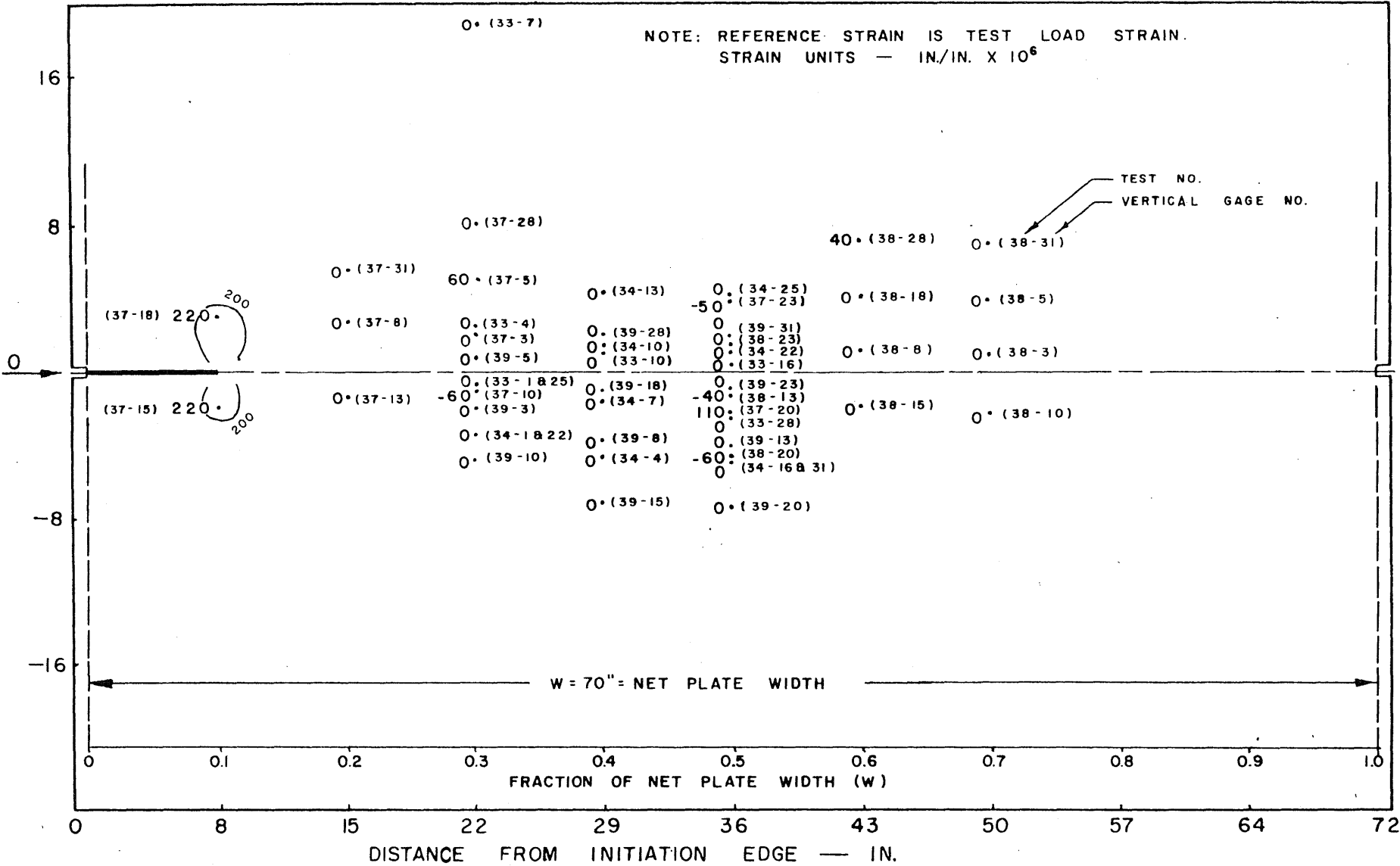
FIG. 106   VERTICAL   STRAIN   CONTOURS   FOR   8   -IN.   CRACK
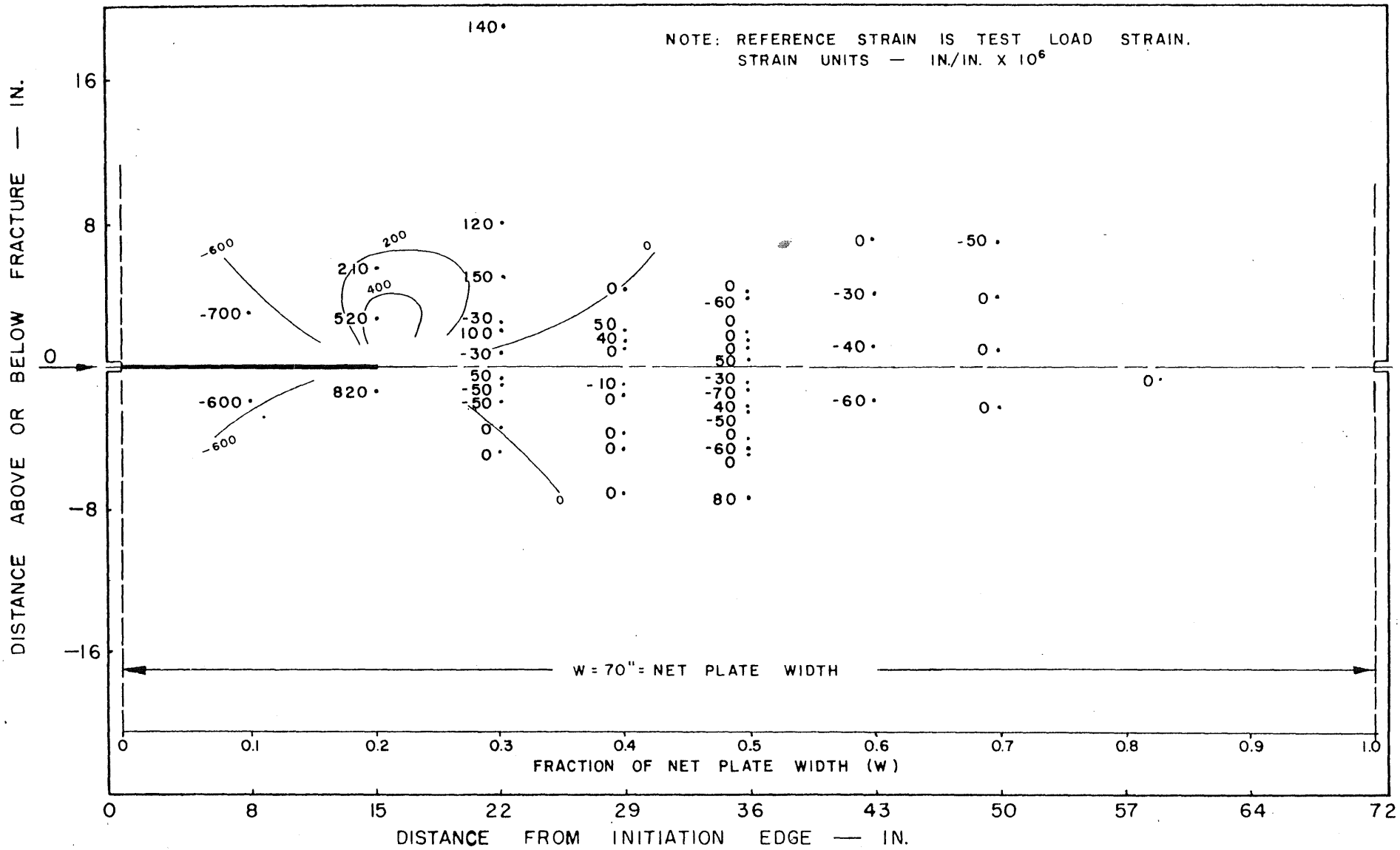
FIG. 107   VERTICAL STRAIN CONTOURS FOR 15 — IN. CRACK
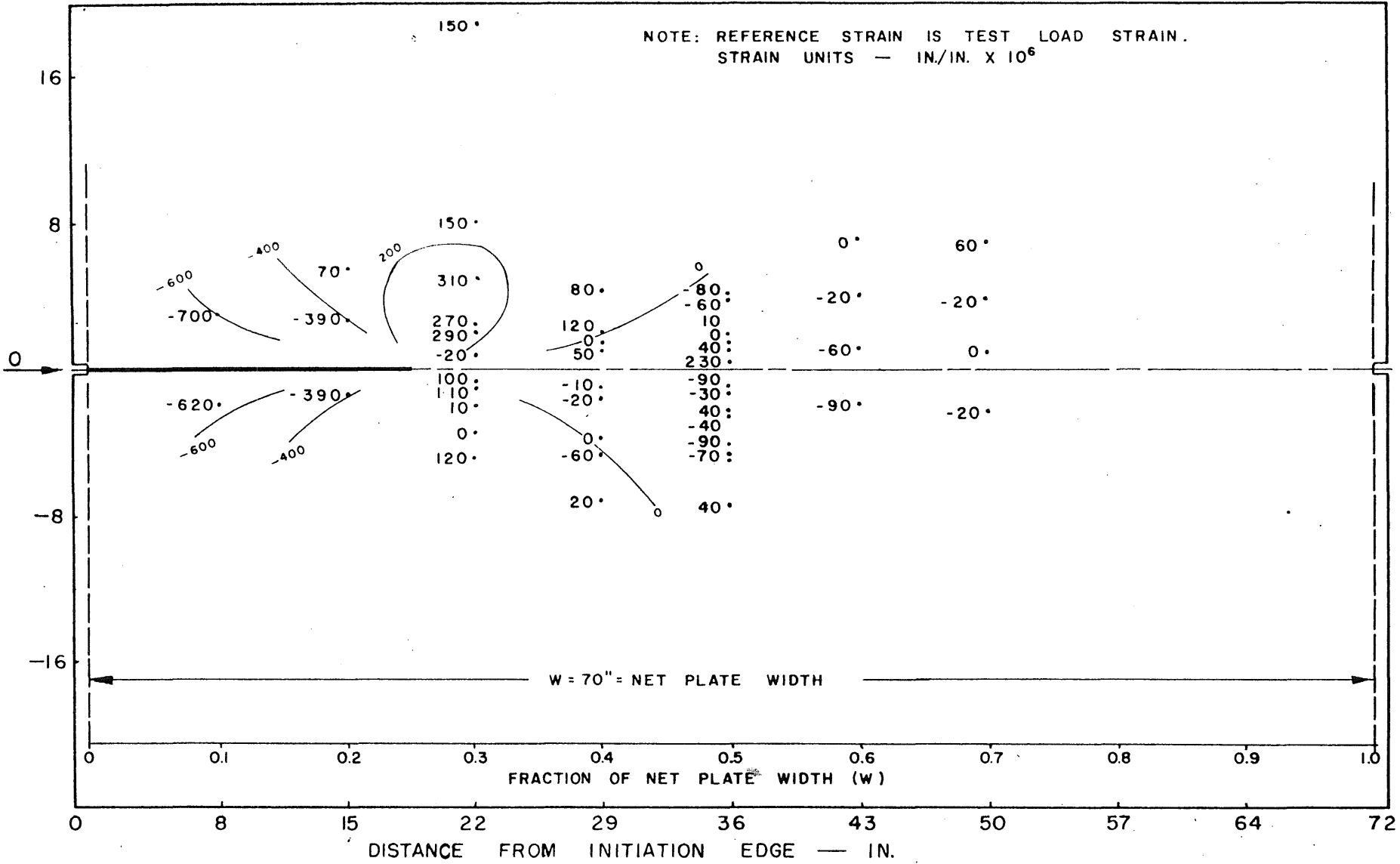
FIG. 108   VERTICAL STRAIN CONTOURS FOR 18.5 — IN. CRACK
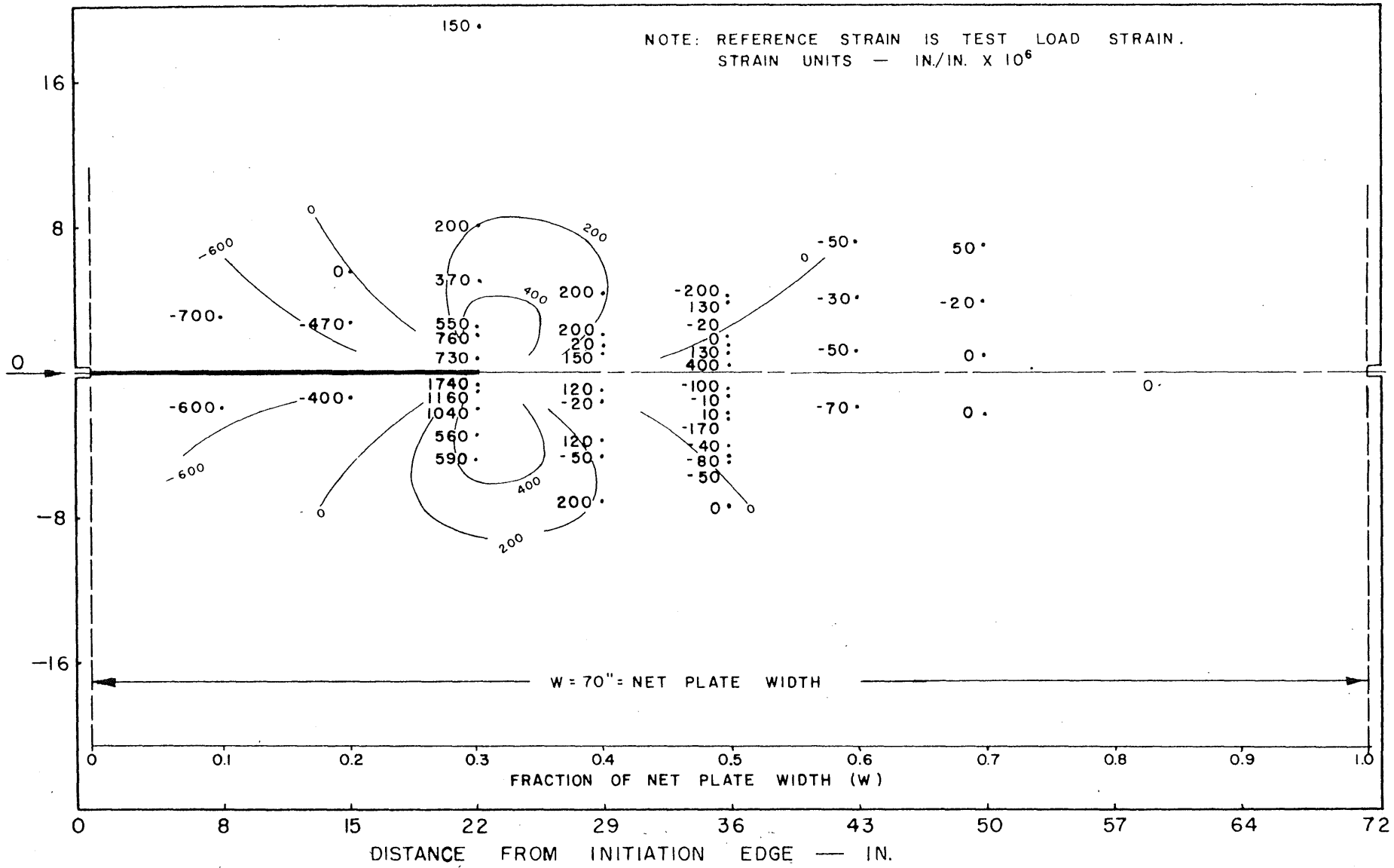
FIG. 109   VERTICAL STRAIN CONTOURS FOR 22 — IN. CRACK

FIG. 110   VERTICAL STRAIN CONTOURS FOR 25.5 — IN. CRACK

FIG. III   VERTICAL STRAIN CONTOURS FOR 29 — IN. CRACK

FIG. 112   VERTICAL STRAIN CONTOURS FOR 32.5 – IN. CRACK

FIG. 113 VERTICAL STRAIN CONTOURS FOR 36 – IN. CRACK

FIG. 114   VERTICAL STRAIN CONTOURS FOR 39.5 – IN. CRACK
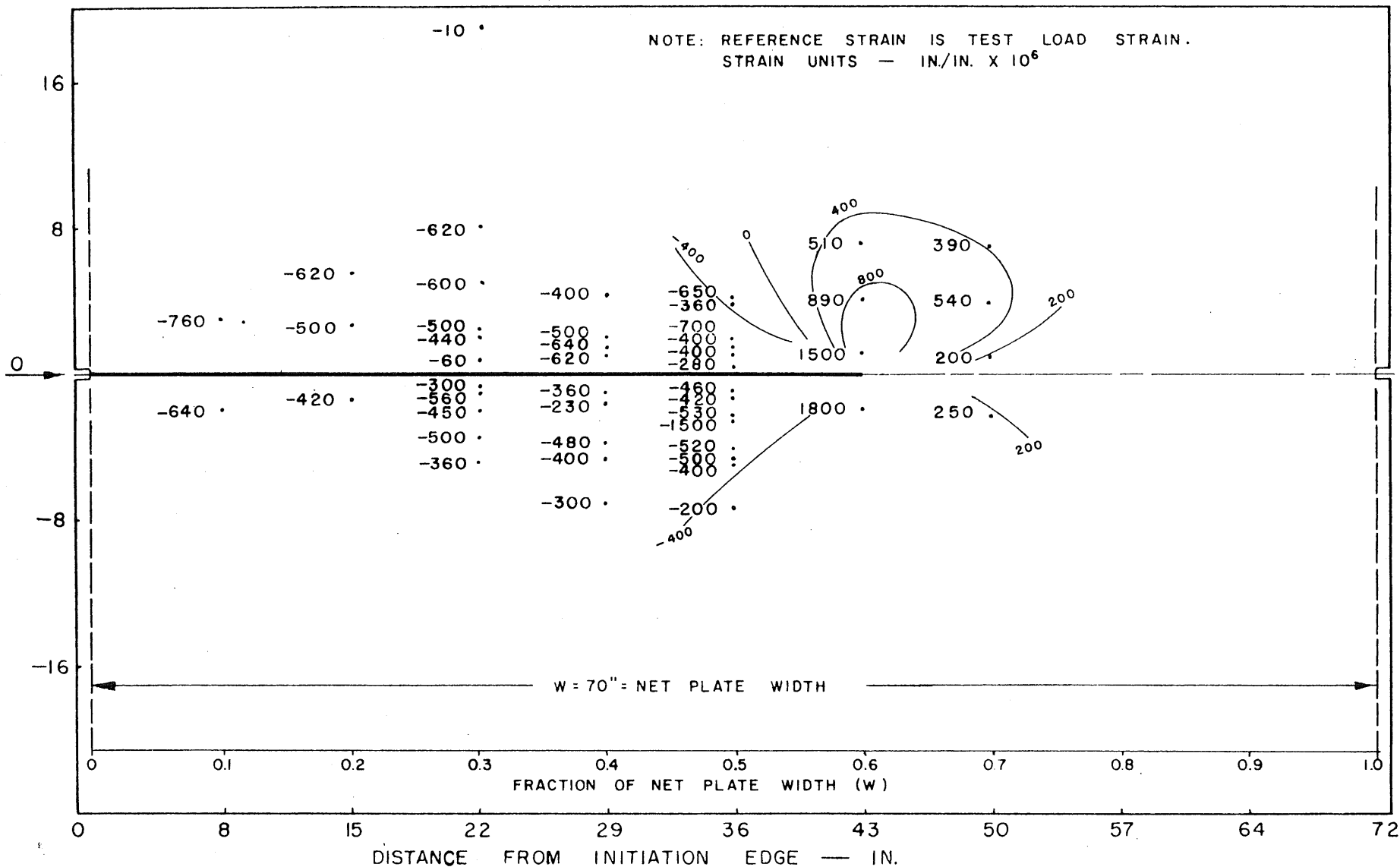
FIG. 115   VERTICAL STRAIN CONTOURS FOR 43 — IN. CRACK
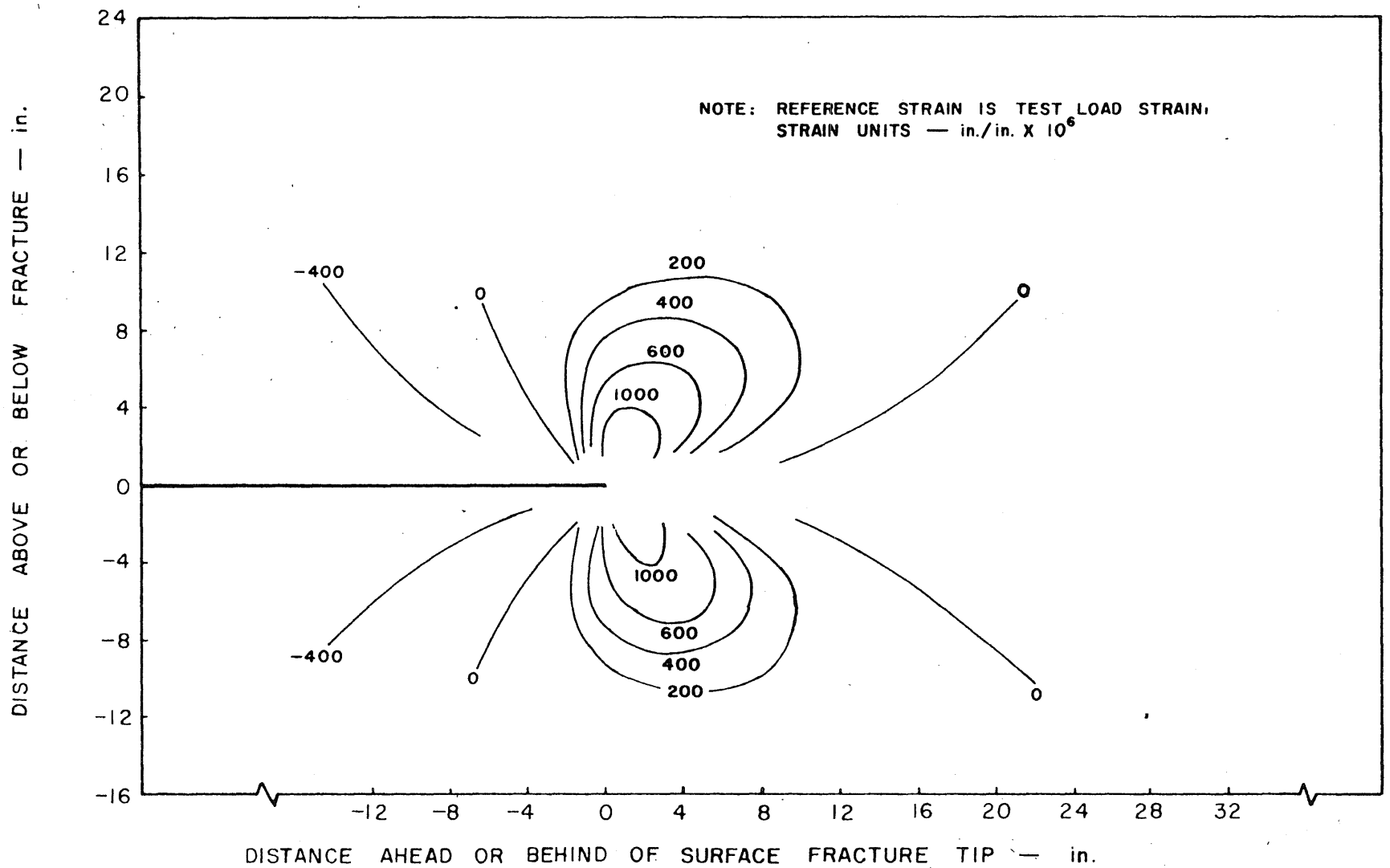
FIG. 116   TYPICAL SET OF VERTICAL STRAIN CONTOURS FOR 22-in. TO 50-in. CRACK
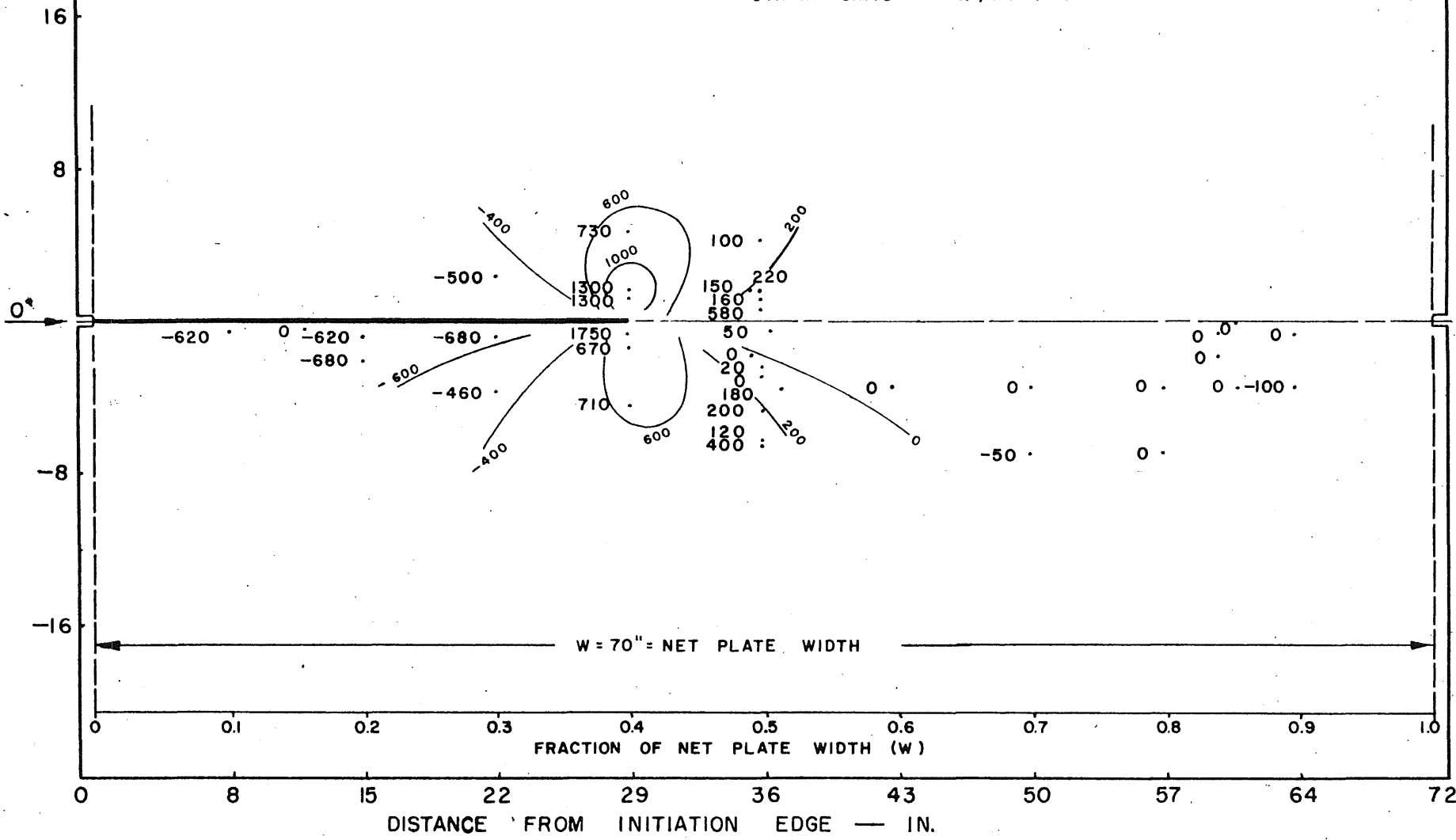
FIG. 117   VERTICAL STRAIN CONTOURS FOR 29 –IN. CRACK— TESTS 13-32
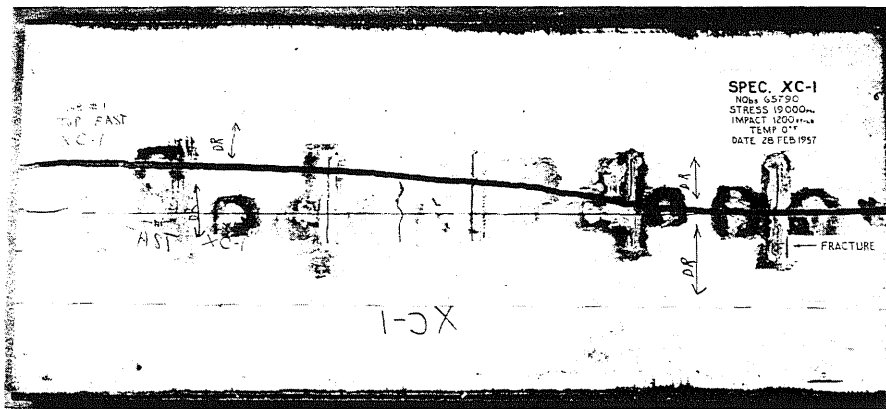
TEST 33
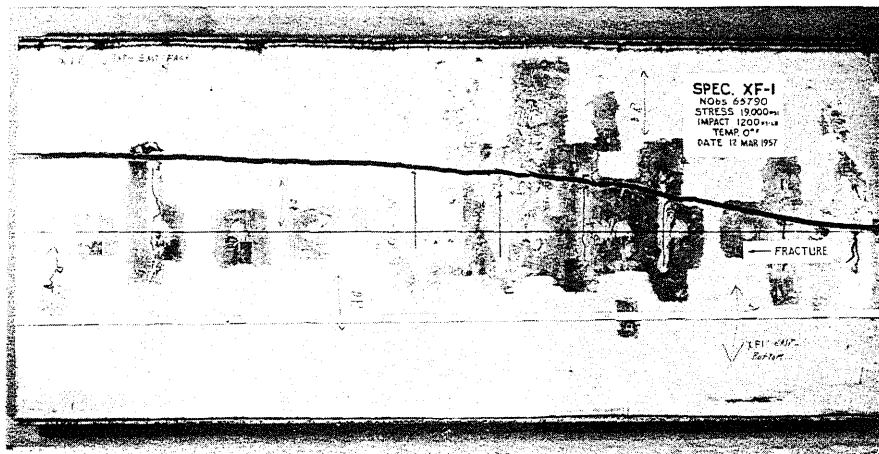
TEST 34
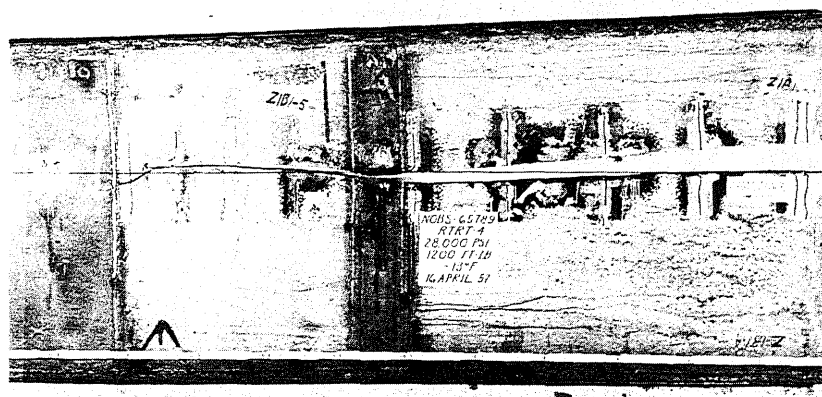
TEST 35

FIG. 118   FRACTURE PATHS — TEST 33, 34, AND 35

FRACTURE PATH

TEST 36

SPECIMEN X2B
NObs 65790

19.0 ksi -12 F.

1200 ft-lb

TESTED 10 OCT. 57
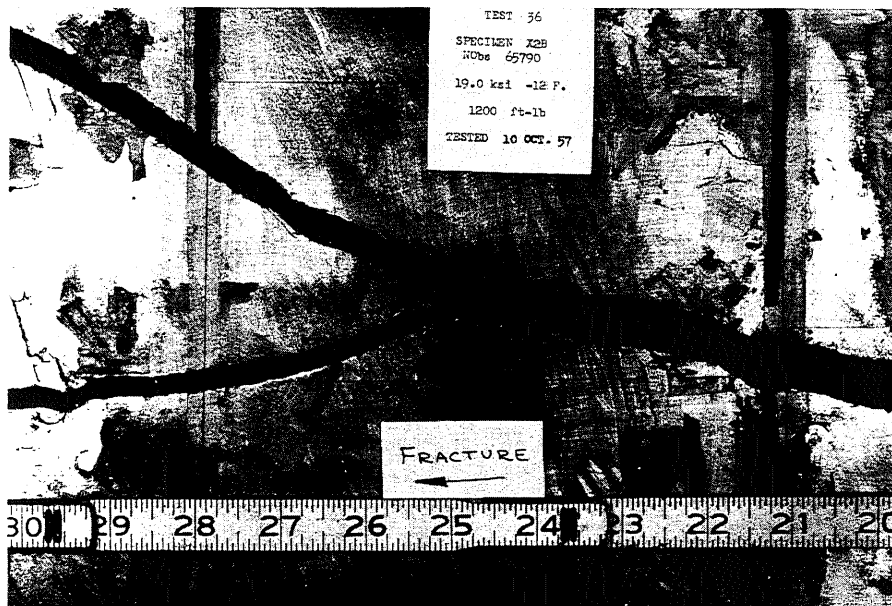
FRACTURE

ORIGIN OF DOUBLE FRACTURE

FIG. 119   FRACTURE PATH — TEST 36
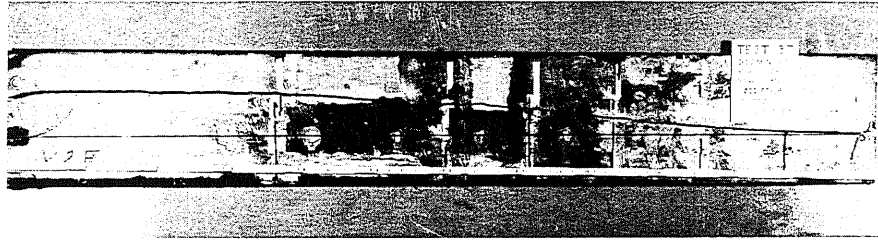
TEST 37
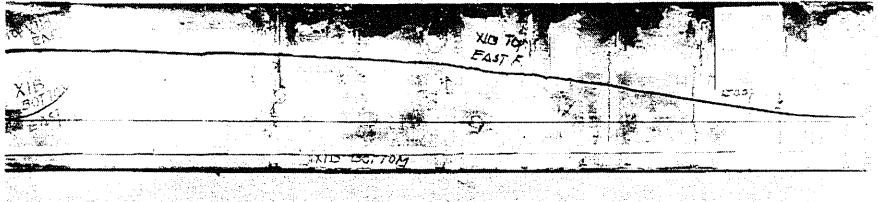
TEST 38
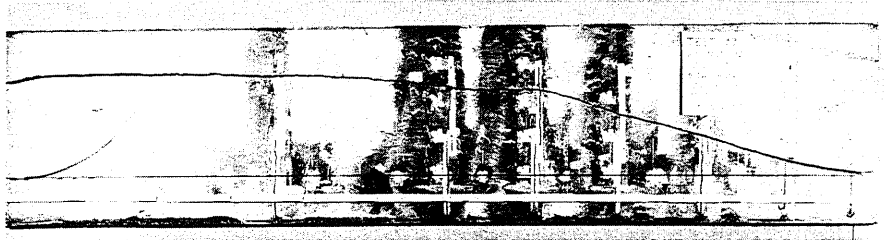
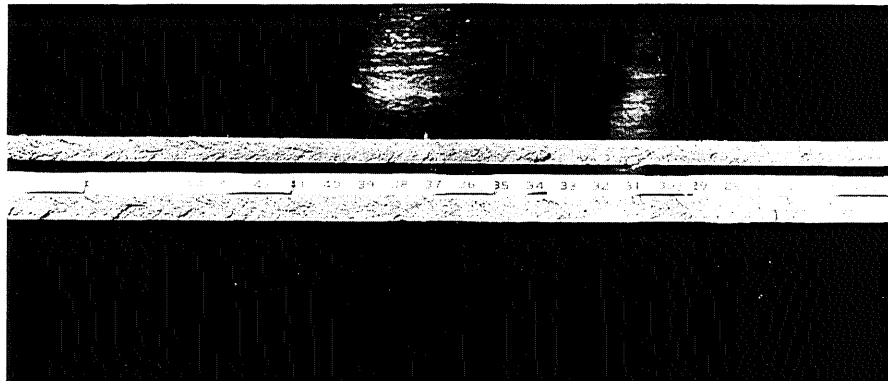
TEST 39

FIG. 120   FRACTURE   PATHS — TEST 37, 38, AND 39

TEST 38
SPECIMEN XIB
NObs 65790
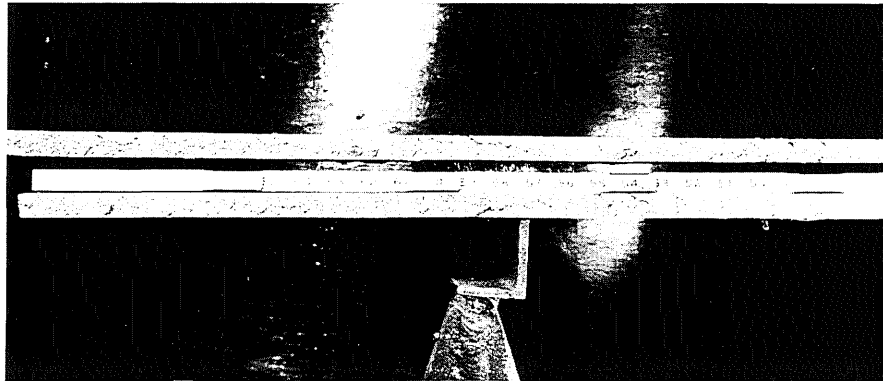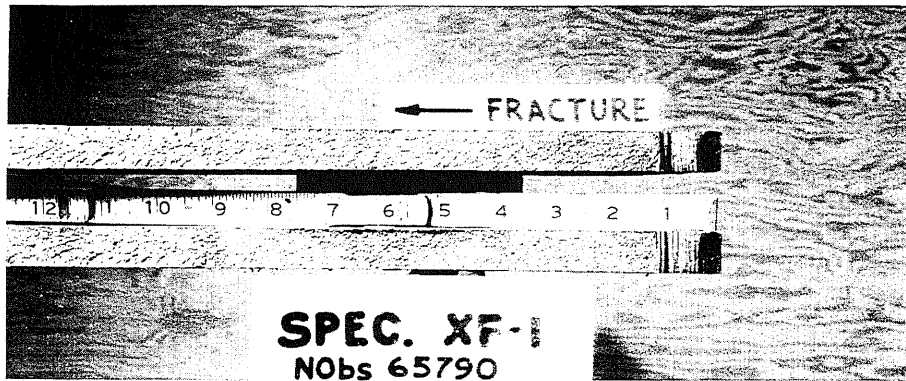19.0 KSI - - 9°F
1200 FT-LB
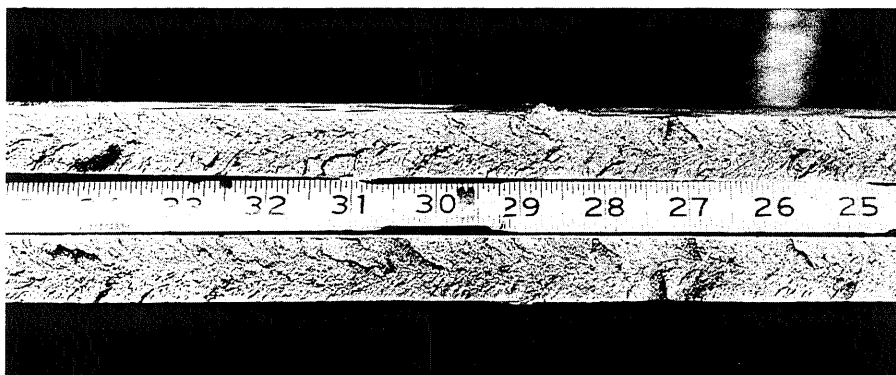TESTED
I NOV '57
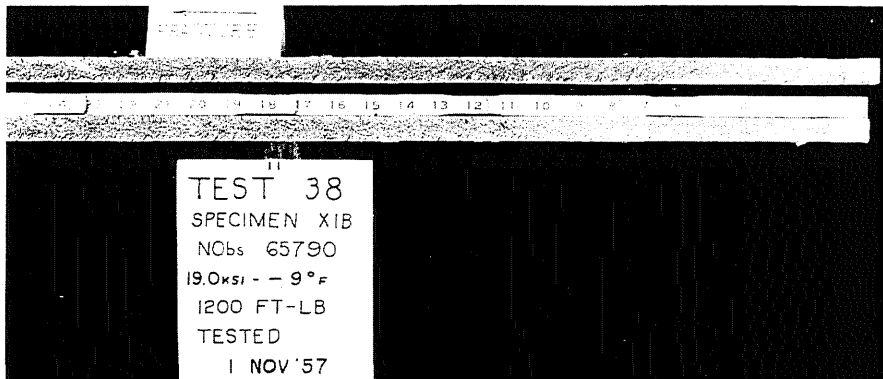
FIG. 121   TYPICAL   FRACTURE   SURFACE

TEST 34

TEST 34

TEST 38

FIG. 122 VIEWS OF PORTIONS OF TYPICAL FRACTURE SURFACES